NINTH INTERNATIONAL WORKSHOP ON MEASUREMENT

TNF 9 WORKSHOP

MONTREAL, CANADA
JULY 31 – AUGUST 2, 2008

& COMPUTATION OF TURBULENT NONPREMIXED FLAMES

NINTH INTERNATIONAL WORKSHOP ON MEASUREMENT & COMPUTATION OF TURBULENT NONPREMIXED FLAMES

TNF WORKSHOP 9

TNF9 Sponsors

SFB 568 | Technical University of Darmstadt

imagination at work

ANSYS®

edgewave

ROLLS ROYCE Rolls-Royce

DANTEC DYNAMICS

LAVISION
WE COUNT ON PHOTONS

NUMECA INTERNATIONAL

Continuum®

Princeton Instruments

Sirah
Tunable Lasers
www.sirah.com

SUMMARY

Ninth International Workshop on Measurement and Computation of Turbulent Nonpremixed Flames

31 July – 2 August 2008
Montreal, Canada

R.S. Barlow, A. Dreizler, J.H. Frank, J. Janicka, A. Kempf,
R.P. Lindstedt, A.R. Masri, J.C. Oefelein, S.B. Pope

INTRODUCTION

The series of workshops on Measurement and Computation of Turbulent Nonpremixed Flames (TNF) is intended to facilitate collaboration and information exchange among experimental and computational researchers in the field of turbulent combustion. The emphasis is on fundamental issues of turbulence-chemistry interaction. In past workshops these issues have been explored through collaborative comparisons of measured and modeled results for a selected set of turbulent nonpremixed and partially premixed target flames burning H_2, CH_4 or CH_4/H_2 mixtures. Several participating research groups have strong interest in applying this same collaborative framework to a broader range of combustion modes and fuels. With the increasing importance of combustion LES as a modeling tool, there has also been discussion of the need to develop a more complete framework for LES validation. With these considerations in mind, TNF9 was organized as a planning process to identify priorities for collaborative research and future workshop activities over a 4-6 year time frame. Background for this planning process was also outlined in the TNF8 Summary, which is available online (http://ca.sandia.gov/TNF/8thWorkshop/TNF8.html).

TNF9 was attended by 82 researchers from 13 countries. Thirty-nine posters were contributed, with abstracts included in the proceedings. The agenda emphasized three challenges facing the turbulent combustion research community:

- Development and validation of modeling approaches which are accurate over a broad range of combustion modes and regimes (nonpremixed, partially premixed, stratified, and premixed).
- Extension of quantitative validation work to include more complex fuels (beyond CH_4) and fuel mixtures that are of practical interest.
- Establishment of a more complete framework for verification and validation of combustion LES, including quality assessment of calculations, as well as development and utilization of approaches which extract knowledge and understanding from comparisons of detailed experimental measurements with detailed simulations.

This summary briefly outlines highlights of presentations and discussion on these central challenges. Comments and conclusions given here are based on the perspectives of the authors and do not necessarily represent consensus opinions of the workshop participants. This summary does not attempt to address all topics discussed at the Workshop or to define all the terms, acronyms, or references. Readers are encouraged to consult the complete TNF9 Proceedings and also the summaries from previous TNF Workshops, because each workshop builds upon what has been done before.

Our overall goal is to accelerate the development of advanced combustion models that are soundly based in fundamental science, rigorously tested against experiments, and capable of predicting the behavior of a wide range of turbulent combustion modes and regimes. Toward this goal, our strategy is to expand the scope of the workshop, while simultaneously refocusing the collaborative process, by selecting a small number new fuels and flames that can serve as future targets for multiple modeling approaches.

The complete TNF9 Proceedings are available for download in pdf format from the Internet at www.ca.sandia.gov/TNF. The pdf file includes materials from the proceedings notebook that was distributed to workshop participants in Montreal, as well as additional materials (such as presentation slides) contributed after the workshop.

Several papers relevant to TNF9 topics and target flames were presented at the 32nd Combustion Symposium. Most of these papers may be found in the sections on turbulent combustion within the *Proceedings of the Combustion Institute*, Vol. 32.

ACKNOWLEDGMENTS

Local arrangements for the TNF9 Workshop were coordinated by Jennifer Bamberger of Sandia. Sponsorship by the German SFB-568 research program, General Electric, ANSYS, Edgewave, Rolls-Royce Canada, Dantec, La Vision, Numeca, Continuum Lasers, Sirah Lasers, and Princeton Instruments is gratefully acknowledged. These contributions allowed for reduction of the registration fees for university faculty and students. Support for Rob Barlow in coordinating TNF Workshop activities is provided by the U. S. Department of Energy, Office of Basic Energy Sciences, Division of Chemical Sciences, Geosciences, and Biosciences. Sandia National Laboratories is a multiprogram laboratory operated by Sandia Corporation, a Lockheed Martin Company, for the United States Department of Energy under contract DE-AC04-94-AL85000.

AN IMPORTANT NOTE OF CAUTION

Results in this and other TNF Workshop proceedings are contributed in the spirit of open scientific collaboration. Some results represent completed work, while others are from work in progress. Readers should keep this in mind when reviewing these materials. It would be inappropriate to quote or reference specific results from these proceedings without first checking with the individual authors for permission and for their latest information on results and references.

HIGHLIGHTS OF PRESENTATIONS AND DISCUSSIONS

Challenges and Strategies for Model Development and Validation across Combustion Modes and Regimes

This session was coordinated by Pope, Masri, Barlow, and Lindstedt. Material to prompt discussion was presented in two parts: an overview of relevant modeling issues (Pope), including a proposed system to characterize general modes of combustion; and an overview of candidate experimental target flames and burners (Barlow). The major points from the presentations and subsequent discussion are summarized below.

As with most combustion research, the investigations of the TNF workshop are motivated by practical applications, such as gas turbines and internal combustion engines. The combustion involved in applications is usually multi-phase, multi-physics, and multi-scale, and always multi-

dimensional. To make progress in this difficult area, both in understanding and modeling, TNF has concentrated on relatively simple flames (i.e., single-phase, non-premixed, statistically axi-symmetric and stationary), so that we can focus on the phenomena of turbulence-chemistry interactions. To the extent that some models have been successful in providing a quantitative description of these phenomena (e.g., in the piloted flames, and lifted flames in vitiated co-flows), it is time to take another step towards the complexity of applications. Accordingly, a challenge addressed at TNF9 was to identify experiments suitable for the development and validation of models which are applicable across modes and regimes of combustion. (Here we use "mode" to differentiate between premixed, non-premixed, etc., whereas the "regime" depends on Reynolds number, Damkohler number, etc.)

The development and validation of models depends crucially on experimental (and increasingly DNS) insights and data, and hence it is appropriate to consider at the outset the experimental configurations which determine the modes of combustion. The two simplest modes of combustion are premixed and non-premixed. In going beyond these extreme modes, two questions that arise are: How to characterize more general modes of combustion? And, how general does a model need to be, in order to be useful in applications?

At TNF9, a system was proposed to characterize general modes of combustion, depending on how many "supplies" (S) are involved, and whether the system is adiabatic (A) or non-adiabatic (N). The idealized premixed flame is formed from a single supply (S=1) formed from the complete mixing of fuel and air, and hence without heat loss it is designated 1A, or with heat loss 1N. Similarly the idealized non-premixed flame is 2A or 2N, with the two supplies being fuel and air. Other 2A flames include: lifted non-premixed jet flames (in which there is partial pre-mixing between the streams prior to combustion); piloted jet flames (in which the pilot originates from the mixing and combustion of a stream formed from the two supplies); and stratified flames (in which there is mixing between to streams that are each within flammability limits). An example of a 3A flame is the piloted premixed jet burner (Dunn, Masri & Bilger 2006), because it requires distinct supplies for the central jet, pilot, and vitiated coflow. The significant difference between a 2A and a 3A flame is that, in a 2A flame, familiar concepts from both non-premixed and premixed combustion can be applied, e.g., reaction progress variable, laminar burning velocity, a single mixture fraction, and scalar dissipation. (In general, S-1 mixture fractions are needed to describe the mixing between the streams.) The significant difference between adiabatic (A) and non-adiabatic (N) is that, in the former, enthalpy does not need to be represented explicitly, since it depends in a known linear way on mixture fraction.

Consensus views at TNF9 were:

- Many practical flames can be approximated as 2N (or sometimes 2A), and given the theoretical simplifications that they afford, 2A/N flames provide good targets for model validation.
- Some applications are 3A/N and hence such flames merit research.
- Few practical flames involve more than 3 streams, and hence 4A/N etc., should not be considered.

A combustion mode diagram was introduced for 2A/N flames (see Fig. 1). In the mixture-fraction-temperature plane, the diagram shows the fuel and oxidant supplies, the inert mixing line, the equilibrium line, and the rich and lean flammability limits, all of which depend solely on the properties of the two supplies. Homogeneous inflowing streams (e.g., fuel jet, pilot stream, air

stream) are shown as points on the plane; whereas a stratified stream is shown as a line. The locations of the inflowing streams on this plot then characterize the mode of combustion.

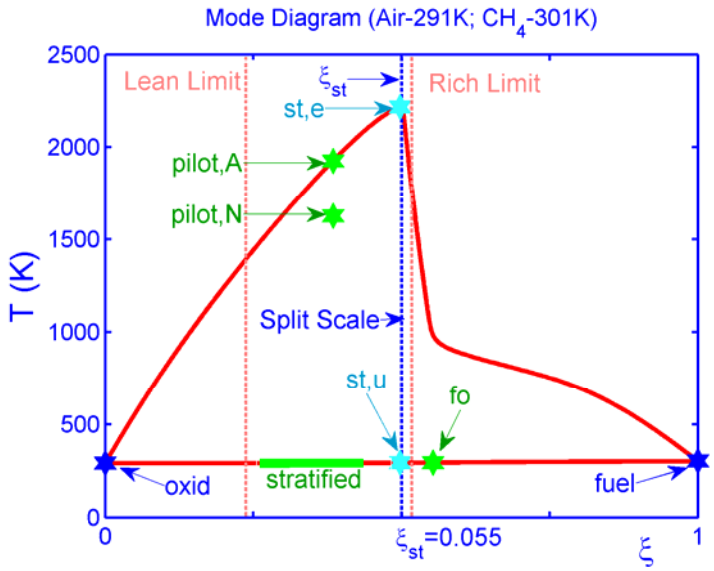

Figure 1. Diagram of 2A and 2N combustion modes.

Some turbulent combustion models are generally applicable, while others are limited in applicability to premixed, non-premixed, or 2A/N flames. In particular, models whose fundamental representations are based on species and enthalpy are generally applicable. ("Applicability" is distinct from, and does not imply, accuracy.) Such generally applicable models include: DNS, PDF, LES/FDF, RANS (with the neglect of species and temperature fluctuations), EDC, LEM and ODT. In contrast, models applicable to 2A flames are usually based on mixture fraction and progress variable; while, for 2N flames, enthalpy is added as a third variable. For general statistical models (e.g., PDF, LES/FDF) the challenges posed by more general modes of combustion are accounting for thin reaction zones and the effect of reaction to augment mixing. Both these challenges already exist in premixed combustion, and have been addressed in previous research – although questions remain. For models based on mixture fraction and progress variable (and possibly enthalpy), some of the challenges are: representing the joint PDF of the variables; consistently modeling the scalar dissipations; incorporating realistic combustion chemistry (beyond one- or two-variable parameterizations); and incorporating the effects of unsteadiness and scalar dissipation.

An overview of various burner configurations and experimental flames from the literature and from known work in progress was presented, and their suitability for use as TNF target cases was discussed. Most of the flames considered are 2A flames, and the discussion emphasized partially premixed and stratified flames. This emphasis was predicated on the assumptions that:

- The TNF Workshop will continue to be centered on issues of turbulence-chemistry interaction in atmospheric pressure flames of relatively simple fuels.
- Work will continue on some of the established nonpremixed target flames and burner geometries. (For example, established flames and burners are expected to be used in the context of LES quality assessment and extension of experiments to more complex fuels.)

For the purpose of this summary, stratified flames are those where the primary mode of combustion is propagation of a turbulent reaction zone through non-uniformly mixed, flammable reactants. Partially premixed flames, such as lifted jet flames, allow for mixing across the full mixture fraction range prior to reaction. Thus, partially premixed flames can admit a combination of combustion modes within one burner, including edge flame propagation, diffusion flame burning, and auto-ignition, if mixed temperatures are sufficiently high.

Figure 2 was used to illustrate qualitatively the combustion modes and regimes represented by existing TNF target flames and other flames that might serve as future targets. Brief descriptions and references are provided in the TNF9 Proceedings. Desirable characteristics of validation target flames were also outlined, as listed in the proceedings. In addition to discussion during the full session on Friday morning of the workshop, additional smaller group discussion took place on Friday afternoon to identify new target flames and action items.

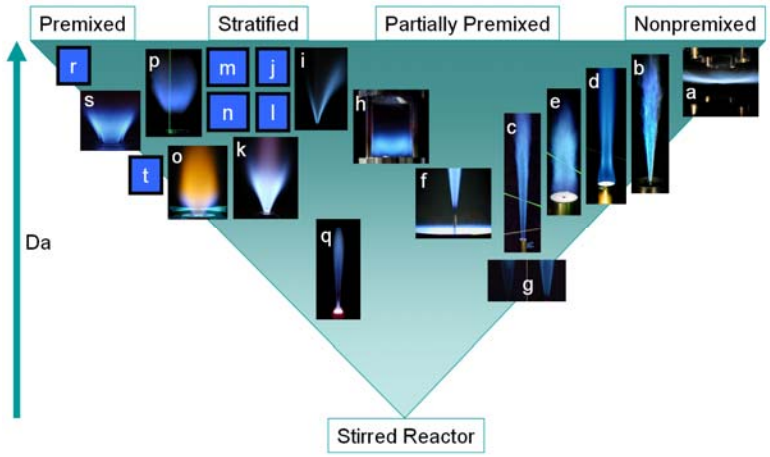

Figure 2. Qualitative map of combustion modes with various laboratory-scale flames investigated by TNF Workshop participants or reported in the literature. Letter designations refer to a table in the full proceedings, which also includes brief descriptions and references for newly considered cases.

Summary of points on partially premixed flames:

1. The DLR model gas turbine combustor has been measured extensively and appears to be a rich problem in terms of combustion modes. However, the complexity of the inflow passages, especially for methane injection, was considered a significant disadvantage, so this burner will not be used as a target case for the next TNF Workshop. Future consideration is possible.
2. There is still significant interest in the lifted jet flames in hot coflow. Data on these flames is still somewhat limited in comparison to the DLR jet flames or the Sandia piloted flames, for example. The Sydney group will review and consolidate their data on these flames, and interested parties will discuss the possibility of generating a ‘standard’ burner design and building multiple copies of that design.
3. Sensitivity of these flames to variations in computational boundary conditions, combined with experimental uncertainty in measured boundary conditions was one item of concern. Coflow composition was identified as a sensitive parameter, in addition to coflow temperature. The Cornell group performed calculations illustrating this sensitivity, and results are included in the proceedings.

4. The suggestion was made that an interesting validation test series would include a parametric progression across the transition from flame propagation to auto-ignition being the main stabilization mechanism.

5. It is hoped that specific cases for collaborative comparisons on this flame geometry will be agreed upon quickly, so that multi-model comparisons may be performed at the next TNF Workshop in 2010.

Summary points on stratified and premixed flames are as follows:

6. Among several stratified burners considered, the TU Darmstadt stratified burner (labeled k in Figure 2) attracted the most interest. Data are not yet available, but velocity measurements have been complete on several flames (see poster abstract by Seffrin et al.), and the group hopes make velocity data and some scalar results available in time for collaborative model comparisons at the TNF10 Workshop.

7. Any stratified flame experiments should include a premixed baseline case or cases, so that particular effects of stratification may be identified and the corresponding models tested. Within the context of the TNF Workshop, it is anticipated that premixed flames will be addressed as baseline cases for stratified burners. Accordingly, no cases of purely premixed combustion were seriously considered.

8. Stratified combustion experiments at low turbulence levels, such as V-flame experiments, were recognized as useful from a fundamental perspective and for comparison with DNS but less interesting for the purpose of turbulent combustion model validation within the TNF framework.

9. The TECFLAM swirl flame and the TU Darmstadt version of the Cheng low-swirl burner (o and p in Figure 2) each burn as premixed flames near the burner center. However, due to air entrainment in these open geometries, the flame propagates through stratified mixtures at the outer edges. The complexity of the inflow geometries of these cases made them less appealing to modelers within this group than the new co-annular burner.

10. A few groups will continue to work with the Sydney Piloted Premixed Jet Burner (q in Figure 2). This is a 3-stream problem (3A) and cannot be addressed by some of the methods of interest.

11. We will stick with methane as the fuel of choice for this first push into stratified combustion.

Another point common to both types of flames is that it will be useful to have some preview calculations performed ahead of the general data release. This should provide insights on various aspects of the problem that may be beneficial to other modelers.

Extension of Validation Work to More Complex Fuels

The session on the extension of validation to more complex fuels was co-ordinated by Lindstedt with contributions made by Barlow, Bourque, Law, Chen (J.H.) and Chen (J.Y.). The topics addressed included practical needs, development directions for simplification methodologies, and an assessment of the ability of both DNS and experimental research to contribute to the process. The further development and application of methods for mechanism construction and reduction are not covered in the current summary. Rather, the focus is on reporting the outcome of the discussions held at the workshop and on making recommendations for a route towards more extensive validation of computational methodologies.

A range of aspects of relevance to the inclusion of more complex fuels (or fuel blends) were discussed in a breakout session. Agreement was reached on several points that form a route towards the gradual introduction of more complex fuels.

1. The introduction of heavier hydrocarbon blended with methane was identified as a key factor in practical applications. The consequences include a direct impact on the auto-ignition limit and hence on the permissible residence time used as part of premixing devices in gas turbines. The allowable amount of heavier hydrocarbons can be expected to depend on the amount of inert material, but is likely to be of order 10%. If the heavier hydrocarbon component is initially treated as a C_2 species, then it can be expected that current reduced chemistry models can be (comparatively) readily adjusted to cover such compositions. The further development of reduced models for heavier hydrocarbons is currently being pursued using a range of methodologies. It is anticipated that accurate detailed and reduced models for fuels such as n-heptane, which exhibit a negative temperature coefficient (NTC) region, will become more generally available in the medium term. The group initially identified the Cabra (jet in hot coflow) and Sandia/Sydney piloted burner geometries as suitable for experimental studies of (i) auto-ignition in a turbulent flow field and (ii) the impact of higher hydrocarbons on local extinction/re-ignition. The latter could, for example, take place in a Flame E/F equivalent. The suggested timescales would be the initial use of C_1/C_2 mixtures over a 1 to 3 year period with the addition of higher hydrocarbons, such as C_3/C_7, over a period of 3 to 6 years.

2. The second item discussed at some length covered the importance of more hydrogen and/or carbon monoxide and/or carbon dioxide rich fuel streams. Specifically, hydrogen rich fuel streams may arise in the context of carbon sequestration technologies and through the use of process gas from chemical industries. The presence of large amounts of carbon dioxide is common in biogas derived from reactors or landfill. It is arguable that such mixtures do not fall into the category of more complex fuels, but rather present an evolution of what is currently being done (or has been done) through the consideration of fuel mixtures of relevance to sustainability driven technologies. From such a point of view, it would make sense to explore the interest of the TNF community to consider such mixtures. A comparatively recent study of localized extinction in high Reynolds number CH_4/H_2 flames has been made at Sandia (Lindstedt *et al.*, Proc. Combust. Inst. 31 (2007) 1551-1558) and a write-up of the experimental data is almost complete (Barlow *et al.*, to be submitted). Other past studies have covered mixtures with carbon dioxide and carbon monoxide, and it is suggested that current data sets be reviewed and that the topic be revisited should a consensus be reached by a group of interested investigators.

3. A strong interest in a comparative study of oxygenated (bio-derived) fuels was recorded. A specific suggestion was made that the different properties of ethanol and dimethyl ether could result in a potentially ideal study of the impact of octane/cetane numbers on auto-ignition and local extinction/re-light in turbulent flames. The flames where such effects could be studied include the jet in hot coflow (Cabra) and piloted jet (Sandia/Sydney) geometries discussed in Item 1 above. Further advantages of this route include a modest extension of the chemical complexities, direct practical relevance, and the anticipated comparatively modest additional experimental difficulties. Given the focus on turbulence-chemistry interactions in the TNF workshop community, it was suggested that the fuels should be pre-vapourized.

4. The issue of moving towards transportation fuels via the blending of increasing amounts of fuels such as n-heptane with methane was also discussed. The experimental challenges that such a step would entail are likely to be significant and it is recommended that a stepwise approach is taken as the quality of the data produced must not be significantly adversely affected.

5. The need for much better data featuring incipient and/or actual soot formation was also discussed at length. The problem is experimentally exceptionally challenging and there is an increasing possibility that DNS studies may provide additional information. The issue of soot formation is, despite the intrinsic difficulties, ideally suited to the TNF community due to the importance of turbulence-chemistry interactions caused by both the slow formation and oxidation chemistries. It is also probable that suitable flames could be formulated by increasing the amount of ethylene in methane along with residence time variations through changes in the Reynolds number.

In addition to the above points, it was emphasised that DNS studies of combusting flows are approaching the point where complex fuels are addressed. Specifically, data may be produced that directly complements experimental studies. The topics that can be covered include flame stabilization mechanisms and the relative roles of auto-ignition and flame propagation at the base of lifted flames. It is also likely that the fuels mentioned above (e.g. hydrogen, ethylene, methane, dimethyl ether, ethanol and n-heptane) will be accessible. A direct consequence is the potential for synergies in submodel development for such fuels.

The following recommendations are made for advancement ahead of TNF10.

6. Study the impact of the gradual addition of heavier hydrocarbons on auto-ignition and extinction/re-light as outlined in Item 1 above.

7. Study the impact of fuel structure through the use of DME and ethanol as outlined in Item 3 above.

Finally, it is recognised that increased levels of partial premixing may have to be used to mitigate experimental difficulties associated with the use of more complex fuels. From a practical perspective, such a development is not likely to be limiting, though it may impact the applicability of more classical modelling approaches. However, it is likely that both recommended items will have direct practical application and as such the use of additional flame geometries would be beneficial.

LES Quality Assessment

Following recommendations from TNF8, Andreas Kempf and Joe Oefelein coordinated a session aimed at formalizing quality assessment techniques for LES in the context of the TNF target flames. The goal was to establish a starting point for the progressive incorporation of quality assessment in future calculations.

The session opened with an invited talk by Bernard Geurts (Universities of Eindhoven and Twente, The Netherlands) on interacting errors in LES. The presentation showed how modeling errors and numerical errors can partially cancel one another, leading to a situation where less numerical error could lead to a less accurate prediction – or alternatively, where better sub-grid models could also lead to a less accurate prediction. The “error-landscape” approach was also presented, where a

single error-quantity is presented as a function of grid-resolution and an independent model parameter. The error landscape shows that an optimum exists for the value of the model parameter, at least for decaying homogenous isotropic turbulence. If the Smagorinsky model is used, the optimum model parameter C_s was shown to decrease with grid refinement to the point where a DNS is obtained with C_s=0.

A comparison of model calculations and experiments for the Sydney Bluff Body Flames was coordinated and presented by Andreas Kempf. Emphasis was placed on LES quality, quality indices, predictability, and sensitivity of the flow. Contributions from ANSYS (Goldin), Darmstadt (Hahn, Olbricht, Janicka) and Imperial College (Kempf) were shown using 625 thousand to 40 million cells. Predictions of velocity and mixture fraction fields varied but were reasonable for all contributions with at least 1-million cells. Comparable results were obtained with a commercial CFD code (ANSYS) on partially unstructured grids with a block-structure research code (FASTEST, Darmstadt), and with a research code using equidistant meshes (PsiPhi, Imperial). The flames were found to be relatively sensitive to boundary conditions, and as a consequence a, discussion evolved about detailed boundary conditions for LES, what level of detail can be realistically expected, and how sensitive a relevant test-flame should (or should not) be. The issue of boundary conditions and the related sensitivities will be an ongoing topic at future workshops.

As part of the analysis of the Sydney Bluff Body Flames, Goldin (ANSYS) and Kempf (Imperial) provided data from LES-quality indicators, like the estimated resolved turbulent kinetic energy or Celik's LESIQ method based on different grids and turbulent viscosity. This was similar to Geurt's approach. Conceptually, these indicators can help quantify the quality of an LES. However, none of the indicators considered provided a suitable measure of a well resolved LES. Indicators based on turbulent viscosity rely on the subgrid-model, which itself is only accurate if the resolution is sufficiently fine and the numerical method is non-dissipative. Otherwise, these models may under-predict the unresolved fluctuation, falsely implying that the simulations resolve most of the fluctuations. A key outcome of the comparisons was that the methods proposed for quantification of LES accuracy are still in their early development. Examples presented demonstrated that the formal development and application of quality assessment techniques has a lot of potential, but will require systematic research over the next several workshops to refine. The recommendation was that we continue to integrate quality assessment techniques with the progression of target flames being considered and work toward using the techniques to assist in quantifying the errors associated with LES and the respective models and numerical methods used.

A talk by M. Ihme examined the sensitivity of LES noise calculations to LES accuracy. Combustion induced noise strongly depends on the instantaneous heat release rate. Thus, this quantity must be modelled very accurately, which is only possible if subgrid-scale mixing and chemical kinetics are well understood. Accurate treatment of combustion noise will ultimately be a very difficult test for LES accuracy.

G. Goldin of ANSYS presented his simulations of the Sydney Bluff Body flames, before presenting a new ANSYS feature to analyse sensitivities. The new version of the code can calculate how changes in any selected parameter would affect the flow at a given point, shedding more light on flow-sensitivity and instability.

Issues and Examples for Comparing Experiments and LES

The development of predictive LES capabilities for a wide range of turbulent combustion conditions requires the development and validation of subgrid scale models and experimental

verification of resolved-scale dynamics. Comparisons between measured and modeled statistics need to be expanded beyond matching mean and rms profiles. To date, the TNF Workshop has primarily focused on using point and line measurements for comparisons with models, and 2-D imaging measurements have remained a largely untapped resource. The coupling of imaging diagnostics and LES enables comparisons between measured and modeled physical structures in turbulent flames. Imaging measurements provide insight into spatial and temporal correlations, which can be compared with LES calculations on a statistical basis. Recent high-resolution 1-D and 2-D measurements can be used to evaluate resolution requirements, provide guidance for LES filter sizing, and develop subgrid scale models. However, a number of fundamental issues must be addressed before quantitative information can be extracted from comparisons of imaging measurements and LES. The TNF Workshop can play a central role in establishing a framework for these comparisons.

Jonathan Frank, Joe Oefelein, and Andreas Dreizler organized a session that highlighted issues for comparing measurements and simulations of spatial structures and temporal evolution of turbulent flames and non-reacting flows. The first section focused on measurements of thermal dissipation structures in flames. Considerations for LES included the variation of turbulence levels and dissipation length scales with temperature, the anisotropy of the dissipation structures, and the relatively sparse sampling of dissipation layers within a typical LES grid cell.

The second section highlighted the effects of LES filter size on modeling the dynamics of scalar mixing in a turbulent non-reacting jet. Comparisons of measurements and LES of non-reacting flows isolate the passive scalar mixing problem from the effects of chemical reactions and heat release in flames. Preliminary results demonstrated that temporal damping and dispersion can significantly alter the spatial evolution and structural similarities of the filtered dissipation structures relative to the actual dissipation field. LES of passive scalar mixing must be better understood in the course of validating LES of flames.

The final section of the presentation described current diagnostic capabilities and sampling requirements for time-series measurements as well as the possibility of using Taylor's hypothesis to convert time-series measurements to pseudo 3-D measurements (see poster abstract by Gamba, Clemens, Ezekoye). Examples included PIV and PLIF measurements in turbulent counterflow and jet flames. Recent advances in high-repetition rate detectors and lasers provide relatively high sampling rates. However, the current state-of-the-art equipment does not meet all of the demands for recording the temporal evolution of TNF flames. The sampling-rate requirements depend on the quantity being measured and the location in the flame. The inclusion of time-history effects in comparisons between measurements and LES presents a number of challenges. The interpretation of 2-D imaging measurements is complicated by out-of-plane motion. Comparisons require conditional sampling of the measurements and simulations. For example, measurements of localized flame extinction could use a coordinate system that is referenced to the location of initial extinction.

Discussion points for comparing experiments and LES:

- Consistency in spatial and temporal averaging of experiments and LES
- Systematic method for choosing LES filter sizes
- Sensitivity of subgrid models to turbulence anisotropy and to low local Reynolds numbers in high-temperature regions
- Extension of results from current TNF flames to higher Reynolds number flames that have less overlap of the energy and dissipation spectra

- Methods for comparing measured and simulated physical structures of turbulent flames on a statistical basis
- Applicability of knowledge from LES of turbulent non-reacting flows to turbulent flames
- Applicability of Taylor's hypothesis for enabling pseudo 3-D measurements
- Limitations of spatial and temporal resolution for measurements at high Reynolds numbers

Priorities and Planning for Future Work and TNF10 (2010)

The 33rd Combustion Symposium will be held at Tsinghua University in Beijing, China, August 1-6. It is likely that TNF10 will be held just before the Symposium in the same part of the world.

There is ongoing work on modeling of existing TNF target flames, using new or improved submodels or new modeling approaches. There will also be ongoing work on LES quality assessment and methods for comparing experiments and LES. Much of this can be done based on experimental data that already exist. Movement into the new challenges of validating models for flames that extend across different modes and regimes of combustion will require new experimental data sets. Highest priorities related to these new directions are:

- Completion of initial experiments on the TU Darmstadt stratified burner and selection of specific target cases. It is hoped that boundary conditions, key experimental results, and initial guidelines for calculations and comparisons will be available for distribution before the end of 2009. Another discussion point was that preliminary calculations may be used to help establish a well posed problem for calculation by multiple groups.
- Completion of exploratory experiments to evaluate the potential to extend current multiscalar measurement techniques to investigate turbulent flames with hydrocarbon fuels more complex than CH_4. TU Darmstadt and Sandia will be conducting collaborative experiments during early 2009. A variety of flows and flames with ethane, ethylene, propane, and dimethyl ether will be considered. Prospects for turbulent flame measurements using the piloted jet burner or the lifted flame in hot coflow will also be evaluated at that time.
- Consolidation by the Sydney University group of data on lifted flames in hot coflow and Joint consideration by several groups of the possible construction of a set of identical burners for collaborative studies on this type of flame.

Discussion of progress and refinement of target flame priorities for TNF10 should take place during the first half of 2009.

Notes

TNF9 Workshop – Table of Contents

TNF9 Workshop – Preface and Acknowledgments

Holiday Inn Midtown Hotel, Montreal, Canada, July 31–August 2, 2008

PREFACE:

The TNF Workshop series has, for more than a decade, facilitated collaboration and information exchange among experimental and computational researchers in the field of turbulent nonpremixed and partially premixed combustion. Our primary focus has been on issues of turbulence-chemistry interaction in flames of relatively simple fuels. Other modeling issues, including radiation, mixing, chemical kinetic mechanisms, turbulence modeling, and boundary conditions, have been addressed to the extent necessary to reduce ambiguity in comparisons of measured and modeled results.

The 1st TNF Workshop was held in Naples, Italy in July 1996. Its objectives were to select experimental data sets for testing combustion models and to establish guidelines for collaborative comparisons of measured and calculated results on those target flames. Subsequent workshops were held in Heppenheim, Germany (1997), Boulder, Colorado (1998), Darmstadt, Germany (1999), Delft, The Netherlands (2000), Sapporo, Japan (2002), Chicago, Illinois (2004), and Heidelberg, Germany (2006). Proceedings are available on the internet at http://www.ca.sandia.gov/TNF.

Over this period of time, the TNF Workshop series has provided an effective framework for comparing multiple combustion modeling approaches, and it has established a set of benchmark experiments and calculations that covers a progression in geometric and chemical kinetic complexity. Collaborative research efforts have expanded the experimental knowledge base for the benchmark flames and lead to a better understanding of the capabilities and limitations of combustion models and experimental methods.

However, for reasons outlined in the Summary of the TNF8 Proceedings, our efforts have become more diffuse in recent years, and the time has come to redefine and refocus this collaborative process. The Organizing Committee decided to use the TNF9 Workshop to step back and take a longer view of challenges and opportunities in turbulent combustion, so that we can attempt to identify research areas where this group can have the greatest impact over the next 4 to 6 years.

The agenda emphasizes three challenges:

- Development and validation of modeling approaches which are accurate over a broad range of combustion modes and regimes (nonpremixed, partially premixed, stratified, and premixed).
- Extension of quantitative validation work to include more complex fuels (beyond CH_4) and fuel mixtures that are of practical interest.
- Establishment of a more complete framework for verification and validation of combustion LES, including quality assessment of calculations, as well as development and utilization of approaches which extract knowledge and understanding from comparisons of detailed experimental measurements with detailed simulations.

Our hope is to engage the TNF9 Workshop participants in an open and lively discussion of research opportunities and priorities related to these challenges, so that we can draft an outline of a strategic plan for collaborative and complementary research that participants want to pursue over the next several years. All participants are encouraged to be active in these discussions, both during scheduled full sessions and in small groups at other times.

We emphasize that this is not a competition, but rather a means of creating a combined research impact that can be significantly greater than the sum of our individual contributions. The TNF Workshop process benefits from contributions by participants having complementary capabilities and areas of expertise, including velocity measurements, scalar measurements, diagnostic development, turbulence modeling, chemical kinetics, mechanism reduction, combustion models, mixing models, radiation, combustion theory, numerical methods, large-scale computing, and data mining. Furthermore, the process extends beyond the meetings themselves to include multiple ongoing collaborations among the active groups.

Global energy issues and concern over climate change amplify the urgency of the need to develop robust and accurate predictive tools for combustion systems. However, current economic and political pressures continue to constrain research funding. The combination of these factors means that collaborative research is even more important now that when this workshop series began.

ACKNOWLEDGEMENTS:

Partial support for organization of the TNF9 Workshop was provided by Sandia National Laboratories, with funding from the United States Department of Energy, Office of Basic Energy Sciences, and by the Technical University of Darmstadt, Germany with funding from SFB-568.

Sponsorship contributions from ANSYS, Continuum, Dantec, Edgewave, GE Aviation, La Vision, NUMECA, Princeton Instruments, Rolls-Royce, the SFB-586 Program, and Sirah Lasers are gratefully acknowledged. Funds are used to significantly reduce registration fees for academic professionals and students and to pay a portion of the fixed costs of the conference facility.

Darlene Spaulding and Jennifer Bamberger of Sandia and Jasmin Krenzer of TU Darmstadt EKT provided administrative support for various aspects of this Workshop.

Cover art by Daniel Strong uses a LES flame “image” provided by Andreas Kempf.

TNF9 ORGANIZING COMMITTEE:

R. S. Barlow, R. W. Bilger, J.-Y. Chen, A. Dreizler, J. Janicka, A. Kempf, R. P. Lindstedt, A. R. Masri, J. C. Oefelein, H. Pitsch, S. B. Pope, D. Roekaerts, and L. Vervisch

TNF9 Workshop – Participants

Holiday Inn Midtown Hotel, Montreal, Canada, July 31–August 2, 2008

	First Name	Last Name	Affiliation	Email
Dr.	Christian	Angelberger	IFP, France	christian.angelberger@ifp.fr
Mr.	Jan	Anker	NUMECA International, Belgium	jan.anker@numeca.be
Prof.	Xue-Song	Bai	Lund Institute of Technology, Sweden	xue-song.bai@energy.lth.se
Dr.	Robert	Barlow	Sandia National Laboratories, USA	barlow@sandia.gov
Dr.	Fabrizio	Bisetti	Stanford University, USA	fbisetti@stanford.edu
Dr.	Gilles	Bourque	Rolls-Royce, Canada	Gilles.Bourque@Rolls-Royce.com
Mr.	Jian	Cai	Clemson University, USA	jcai@clemson.edu
Dr.	Stewart	Cant	University of Cambridge, UK	rsc10@cam.ac.uk
Mr.	Qing	Chan	The University of Adelaide, Australia	schan@chemeng.adelaide.edu.au
Prof.	J.-Y.	Chen	University of California Berkeley, USA	jychen@me.berkeley.edu
Dr.	Jacqueline	Chen	Sandia National Laboratories, USA	jhchen@sandia.gov
Dr.	Matthew	Cleary	University of Queensland, Australia	m.cleary@uq.edu.au
Prof.	Noel	Clemens	The University of Texas at Austin, USA	clemens@mail.utexas.edu
Prof.	Pedro	Coelho	Instituto Superior Tecnico, Portugal	pedro.coelho@ist.utl.pt
Mr.	Bruno	Coriton	Yale University, USA	bruno.coriton@yale.edu
Dr.	Bassam	Dally	The University of Adelaide, Australia	bassam.dally@adelaide.edu.au
Mr.	Reni	De Meester	Ghent University, Belgium	reni.demeester@ugent.be
Dr.	Cecile	Devaud	University of Waterloo, Canada	cdevaud@uvaterloo.ca
Dr.	Andreas	Dreizler	TU Darmstadt – EKT, Germany	dreizler@ekt.tu-darmstadt.de
Mr.	Matthew	Dunn	The University of Sydney, Australia	m.dunn@usyd.edu.au
Prof.	Luis Fernando	Figueira da Silva	Pontificia Universidade Catolica , Brasil	luisfer@esp.puc-rio.br
Dr.	Hendrik	Forkel	ANSYS Germany GmbH, Germany	Hendrik.Forkel@ansys.com
Dr.	Jonathan	Frank	Sandia National Laboratories, USA	jhfrank@sandia.gov
Mr.	Frederik	Fuest	TU Darmstadt – EKT, Germany	fuest@ekt.tu-darmstadt.de
Dr.	Pierre	Gauthier	Rolls-Royce, Canada	Pierre.Gauthier@Rolls-Royce.com
Prof.	Bernard	Geurts	University of Twente, Netherlands	b.j.geurts@utwente.nl
Mr.	Sam	Ghazi-Hesami	Concordia University, Canada	samhessami@yahoo.com
Dr.	Graham	Goldin	ANSYS, USA	graham.goldin@ansys.com
Prof.	Alessandro	Gomez	Yale University, USA	alessandro.gomez@yale.edu
Dr.	Robert	Gordon	TU Darmstadt – EKT, Germany	gordon@ekt.tu-darmstadt.de
Dr.	Evatt	Hawkes	University of New South Wales, Australia	evatt.hawkes@unsw.edu.au
Prof.	Simone	Hochgreb	University of Cambridge, UK	sh372@cam.ac.uk
Prof.	Matthias	Ihme	University of Michigan, USA	mihme@umich.edu
Prof.	Hong	Im	University of Michigan, USA	hgim@umich.edu
Prof.	Johannes	Janicka	TU Darmstadt – EKT, Germany	janicka@ekt.tu-darmstadt.de
Mr.	Sandeep	Jella	Rolls-Royce, Canada	sandeepjella@gmail.com
Prof.	Bill	Jones	Imperial College London, UK	w.jones@imperial.ac.uk
Dr.	Peter	Kalt	University of Adelaide, Australia	pkalt@mecheng.adelaide.edu.au
Dr.	Konstantin	Kemenov	Cornell University, USA	kak262@cornell.edu
Dr.	Andreas	Kempf	Imperial College London, UK	a.kempf@imperial.ac.uk
Prof.	Yongmo	Kim	Hanyang University, Korea	ymkim@hanyang.ac.kr
Dr.	Alex	Klimenko	The University of Queensland, Australia	klimenko@mech.uq.edu.au
Mr.	Heeseok	Koo	University of Texas at Austitn, USA	hkoo@mail.utexas.edu

TNF9 Workshop – Participants

Holiday Inn Midtown Hotel, Montreal, Canada, July 31–August 2, 2008

	First Name	Last Name	Affiliation	Email
Dr.	Andreas	Kronenburg	Imperial College London, UK	a.kronenburg@imperial.ac.uk
Mr.	Jens	Kuehne	TU Darmstadt – EKT, Germany	kuehne@ekt.tu-darmstadt.de
Mr.	Jeongwon	Lee	Hanyang University, Korea	ymkim@hanyang.ac.kr
Dr.	Jeremiah	Lee	United Technologies Research Center, USA	leejc@utrc.utc.com
Prof.	Peter	Lindstedt	Imperial College London, UK	p.lindstedt@imperial.ac.uk
Prof.	Marshall	Long	Yale University, USA	marshall.long@yale.edu
Prof.	Assaad	Masri	The University of Sydney, Australia	masri@aeromech.usyd.edu.au
Dr.	Epaminondas	Mastorakos	University of Cambridge, UK	em257@eng.cam.ac.uk
Dr.	Randall	McDermott	NIST, USA	randall.mcdermott@nist.gov
Dr.	Paul	Medwell	The University of Adelaide, Australia	paul.medwell@adelaide.edu.au
Dr.	Wolfgang	Meier	German Aerospace Center DLR, Germany	wolfgang.meier@dlr.de
Prof.	Bart	Merci	Ghent University, Belgium	Bart.Merci@UGent.be
Mr.	Jean-Baptiste	Michel	IFP, France	J-Baptiste.MICHEL@ifp.fr
Prof.	Graham (Gus)	Nathan	The University of Adelaide, Australia	graham.nathan@adelaide.edu.au
Dr.	Salvador	Navarro-Martinez	Imperial College London, UK	s.navarro@imperial.ac.uk
Dr.	Joseph	Oefelein	Sandia National Laboratories, USA	oefelei@sandia.gov
Prof.	Michael	Pfitzner	Universitaet der Bundeswehr München, Germany	michael.pfitzner@unibw.de
Prof.	Stephen	Pope	Cornell University, USA	s.b.pope@cornell.edu
Mr.	Pavel	Popov	Cornell University, USA	ppp7@cornell.edu
Mr.	Pieter	Rauwoens	Ghent University, Belgium	pieter.rauwoens@ugent.be
Prof.	Michael	Renfro	University of Connecticut, USA	renfro@engr.uconn.edu
Dr.	Edward	Richardson	Sandia National Laboratories, USA	esrich@sandia.gov
Prof.	Dirk	Roekaerts	Delft University of Technology, Netherlands	d.j.e.m.roekaerts@tudelft.nl
Mr.	David	Rowinski	Cornell University, USA	dhr46@cornell.edu
Dr.	Vaidyanathan	Sankaran	Sandia National Laboratories, USA	vsankar@sandia.gov
Mr.	Alan	Sayre	Babcock & Wilcox, USA	ansayre@babcock.com
Mr.	Florian	Seffrin	TU Darmstadt – EKT, Germany	seffrin@ekt.tu-darmstadt.de
Mr.	Baris	Sen	Georgia Tech, USA	baris.sen@gatech.edu
Dr.	Christopher	Shaddix	Sandia National Laboratories, USA	crshadd@sandia.gov
Ms.	Ivana	Stankovic	Ghent University, Belgium	Ivana.Stankovic@Ugent.be
Dr.	Michael	Stoehr	German Aerospace Center DLR, Germany	Michael.Stoehr@dlr.de
Dr.	Peter	Strakey	NETL, USA	peter.strakey@netl.doe.gov
Mr.	Mark	Sweeney	University of Cambridge, UK	marksweeney@cantab.net
Prof.	Chenning	Tong	Clemson University, USA	ctong@ces.clemson.edu
Mr.	Antonios	Triantafyllidis	University of Cambridge, UK	at419@cam.ac.uk
Dr.	Andrew	Wandel	Imperial College London, UK	a.wandel@imperial.ac.uk
Mr.	Haifeng	Wang	Cornell University, USA	hw98@cornell.edu
Prof.	Forman	Williams	UCSD, USA	faw@ucsd.edu
Dr.	Chun Sang	Yoo	Sandia National Laboratories, USA	csyoo@sandia.gov

TNF9 Workshop – Agenda

Holiday Inn Midtown Hotel, Montreal, Canada, July 31–August 2, 2008

(Tentative. Times may be adjusted.)

Thursday July 31, 2008

4:00 – 5:00	Registration and Poster Setup
5:00 – 9:00	Welcome Reception and Poster Session

Friday August 1, 2008

8:30 – 9:00	Introduction and Overview of the TNF Workshop Process (Rob Barlow)
9:00 – 10:30	Challenges and Strategies for Model Development and Validation across Combustion Regimes (Coordinators: Steve Pope, Assaad Masri, Rob Barlow, Peter Lindstedt)
10:30 – 11:00	Coffee Break
11:00 – 12:00	Challenges and Strategies in Addressing more Complex Fuels (Coodinator: Peter Lindstedt)
12:00 – 12:30	Introduction of Topics for Afternoon Focus Groups (Coordinator: Andreas Dreizler)
12:30	Lunch
After lunch	*Meeting of organizers and presenters to readjust the schedule as needed.*
	Focus group meetings (times to be determined).
	Free time for small group discussions and other activities.
17:00 – 18:00	Poster Hour (with refreshments)
18:00 – 19:20	Dinner
19:30 – 21:30	LES Quality Assessment (Coodinators: Andreas Kempf and Joe Oefelein) (Invited speaker: Bernard Geurts)

TNF9 Workshop – Agenda

Holiday Inn Midtown Hotel, Montreal, Canada, July 31–August 2, 2008

(Tentative. Times may be adjusted.)

Saturday August 2, 2008

8:30 – 9:??	LES Quality Assessment (Continued) (Coodinators: Andreas Kempf and Joe Oefelein)
9:?? – 10:30	Issues and Examples for Comparing Experiments and LES (Coordinators: Jonathan Frank, Joe Oefelein, Andreas Dreizler)
10:30 – 10:50	Coffee Break
10:50 – 11:50	Reports from Focus Groups (Coordinator: Andreas Dreizler)
11:50 – 12:30	Highlights from Posters and Recent Developments on TNF Flames (Coordinators: Assaad Masri and Dirk Roekaerts)
12:30	Lunch (Working lunch for the Organizing Committee)
13:30 – 14:30	Proposals and Discussion of Priorities for Future Collaborations and Comparisons (Discussion Leader: Johannes Janicka)
14:30 – 14:45	Closing Remarks (Rob Barlow)
14:45	Adjourn, Remove Posters

TNF9 Workshop – Welcome

Ninth International Workshop on Measurement and Computation of Turbulent Nonpremixed Flames

Montreal, Canada
July 31 – August 2, 2008

Organizing Committee:

Rob Barlow	Sandia
Bob Bilger	Sydney University
J.-Y. Chen	UC Berkeley
Andreas Dreizler	TU Darmstadt
Johannes Janicka	TU Darmstadt
Andreas Kempf	Imperial College
Peter Lindstedt	Imperial College
Assaad Masri	Sydney University
Joe Oefelein	Sandia
Heinz Pitsch	Stanford
Steve Pope	Cornell
Dirk Roekaerts	TU Delft
Luc Vervisch	INSA de Rouen

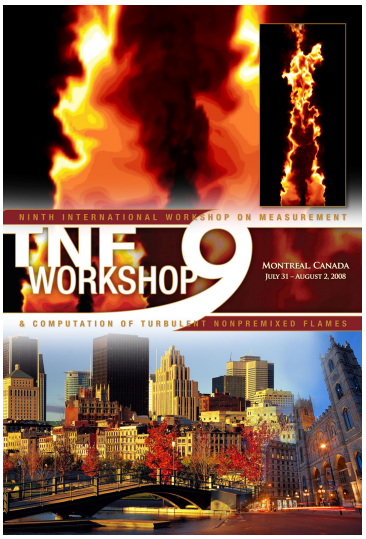

Acknowledgments

- Sponsors
  - Funds used mainly to reduce fees for faculty and students
- Administrative support
  - Jennifer Bamberger (Sandia)
  - Jasmin Krenzer (TU Darmstadt)
- US DOE and German SFB
- Session coordinators & contributors

Agenda – Friday, August 1

8:30 – 9:00	Overview of the TNF Workshop Process (Rob Barlow)
9:00 – 10:30	Challenges and Strategies for Model Development and Validation across Combustion Modes and Regimes (Coordinators: Steve Pope, Assaad Masri, Rob Barlow, Peter Lindstedt)
10:30 – 11:00	Coffee Break
11:00 – 12:00	Challenges and Strategies in Addressing more Complex Fuels (Coodinator: Peter Lindstedt)
12:00 – 12:30	Introduction of Topics for Afternoon Focus Groups (Coordinator: Andreas Dreizler)
12:30	Lunch
After lunch	*Meeting of organizers and presenters* *Focus group meetings (times to be determined)* *Free time for small group discussions and other activities*
17:00 – 18:00	Poster Hour (with refreshments)
18:00 – 19:20	Dinner
19:30 – 21:30	LES Quality Assessment (Coodinators: Andreas Kempf and Joe Oefelein) (Invited speaker: Bernard Geurts)

Overview of the TNF Workshop Process

- Brief history
- Accomplishments
- Problems
- TNF9 Objectives

Genesis of the Workshop Series

- Observations during early 1990's
  - Incomplete data sets
  - Poorly defined comparisons
  - Normal publication loop too slow
  - Good examples from turbulent fluid mechanics community
- Opportunities
  - Good connections from previous Sandia "working groups" and visitor program
  - Internet offered rapid communication, data sharing
  - Concept floated at 25th Combustion Symposium, Irvine 1994
- TNF1 in Naples before the 26th Combustion Symposium (1996)
  - Selected flames, data format, common submodels
  - Established ground rules
  - Planned to compare results for simple H_2 jet flames at TNF2

A Partial Timeline

Naples	Heppenheim	Boulder	Darmstadt	Delft	Sapporo	Chicago	Heidelberg
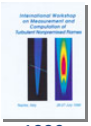		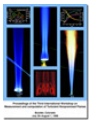					
1996	1997	1998	1999	2000	2002	2004	2006

- **TNF1 -** Initial selections for target flame library. Ground rules established for comparisons on H_2 jet flames
  - LDV measurements of Sandia H_2 and $CO/H_2/N_2$ jet flames at ETH Zurich
    - Piloted CH_4/air jet flames measured at Sandia (Sydney burner)
    - Delft piloted burner measured at Sandia
      - **TNF2 -** Comparisons on H_2 jet flames
        - "Extra" measurements at to resolve NO discrepancy in H_2 flames
          - LDV measurements of Sandia piloted flames and DLR flame at TU Darmstadt
            - **TNF3 -** Comparisons on DLR flames, Sandia & Delft piloted flames, Sydney BB flames
            - **Significant differences among models, lots of questions!**

TNF3 Workshop (1998) – "Classic" Results for Flame D

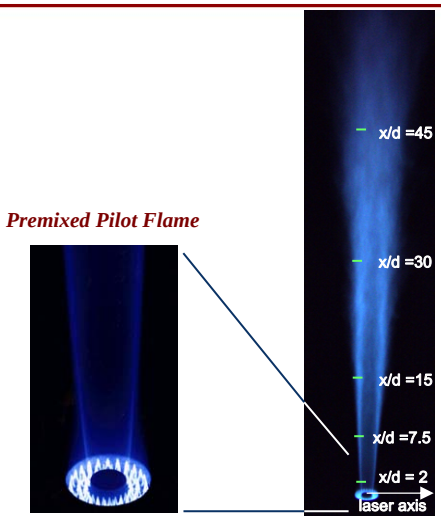

Premixed Pilot Flame

PDF, CMC, steady flamelet

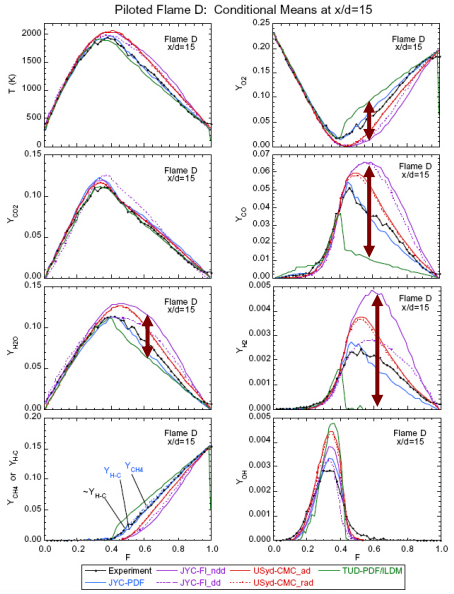

Partial Time Line

- **TNF1 -** Initial selection for target flame library. Ground rules established for comparisons on H_2 jet flames
  - LDV measurements of Sandia H_2 and $CO/H_2/N_2$ jet flames at ETH Zurich
    - Piloted CH_4/air jet flames measured at Sandia
    - Delft piloted burner visits Sandia
      - **TNF2 -** Comparisons on H_2 jet flames
        - "Extra" measurements to resolve NO discrepancy in H_2 flames
          - LDV measurements of Sandia piloted flames and DLR flame at TU Darmstadt
            - **TNF3 -** Comparisons on Sandia & Delft piloted flames, DLR flames, Sydney BB flames
            - **Significant differences among models, lots of questions!**
              - "Extra" measurements of radiant fraction for several flames
                - **TNF4 -** Expanded comparisons of Sandia piloted flames D,E,F
                  - DLR jet flames measured at Sandia
                    - "Extra" measurements and calculations of laminar CH_4/air flames
                      - **TNF5 -** Focus on radiation, chemistry, and mixing models
                      - LES included in comparisons on piloted flames
                        - Sydney swirl burner visits Sandia
                        - Berkeley vitiated coflow burner visits Sandia
                        - Adelaide MILD combustion burner visits Sandia
                        - Darmstadt turbulent opposed jet burner visits Sandia
                          - Move into new Turbulent Combustion Lab, 2001
                            - **TNF6 -** Begin to target scalar dissipation

TDF Lab configuration 1995-2001

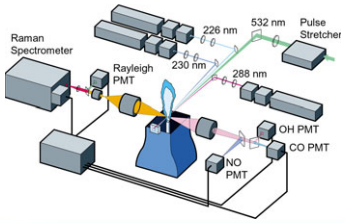

Toward Validation of Predictive Combustion Models

- Focus on turbulence-chemistry interaction in nonpremixed and partially premixed flames of simple fuels

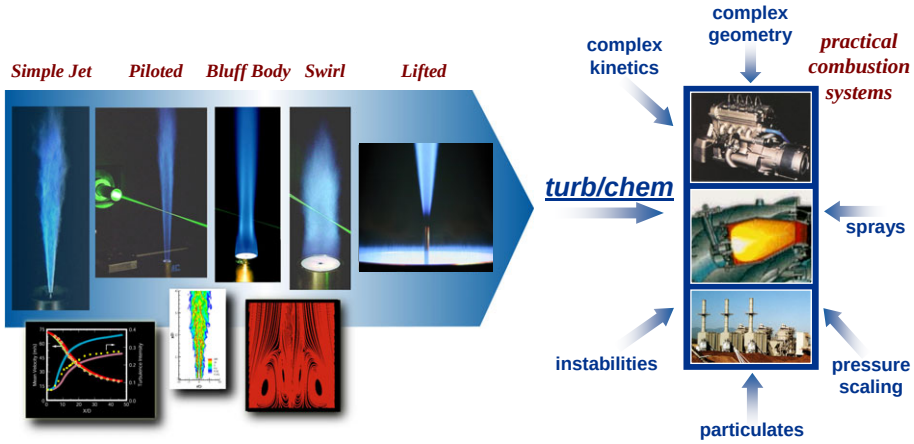

- Progression of well documented cases that address the fundamental issues of turbulent flow, transport, and chemistry

TNF Flames as Targets for New Diagnostics and Analysis

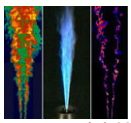
Bergmann et al. (1998)
DLR-Stuttgart
Schneider et al. (2003)
TU Darmstadt


DLR Flames
$CH_4/H_2/N_2$

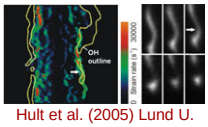
Hult et al. (2005) Lund U.

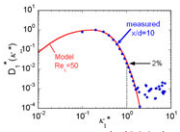
Wang et al. (2007)

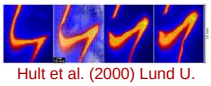
Hult et al. (2000) Lund U.

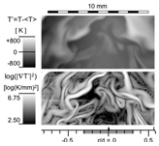
Kaiser & Frank (2007)

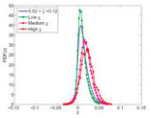
Barlow et al. (2007)

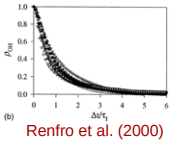
Renfro et al. (2000)
Purdue

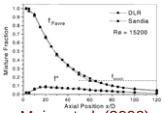
Meier et al. (2000)
Sandia/DLR

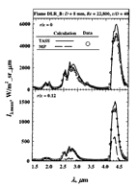
Yuan et al. (2003)
Purdue/Sandia

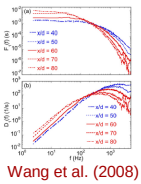
Wang et al. (2008)
UT Austin/Sandia

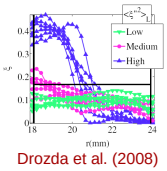
Drozda et al. (2008)

Accomplishments

- Improved quality, completeness, and availability of experimental data
  - Detailed scalar and velocity data on several types of flames
  - New diagnostics applied to “standard” flames
  - Validation experiments → rich source of fundamental insight
- Significant progress in understanding of turbulence-chemistry interaction in nonpremixed and partially-premixed flames
  - Collaborative comparison of experiment and computation
  - Systematic progression and iteration
- A few flames are very well understood and accurately modeled
  - Widely used by academia, CFD houses, and industry to test models
  - Parametric studies on sensitivities of submodels (RANS/PDF)

Problems

- Loss of focus (see TNF8 Summary online)
- LES
  - Combustion subgrid models have not really been tested within the workshop
  - Quality assessment is a priority
- Comparisons limited to point statistics
- Other modes and regimes of combustion

This Workshop: More like TNF1

- Use the TNF framework to address three challenges:
  1. Develop and validate models which are accurate across a broad range of combustion modes and regimes
  2. Extend quantitative validation work to include more complex fuels (beyond CH_4)
  3. Establish a more complete framework for verification and validation of combustion LES

- What do we want to accomplish over the next 4-6 years?
- What are the best opportunities and priorities for collaborative research?

TNF Workshop – Philosophy

- "We emphasize that this is not a competition…."
- "This collaborative process benefits from contributions by participants having different areas of expertise…."

Challenges and Strategies for Model Development and Validation Across Combustion Modes and Regimes

Steve Pope, Rob Barlow, Assaad Masri, Peter Lindstedt

9th International Workshop on Measurement & Computation of Turbulent Non-premixed Flames

Montreal
July 31-August 2, 2008

Overview of Presentation

Challenges and Strategies for Model Development and Validation Across Combustion Modes and Regimes

- Combustion technologies and TNF
- Status of modeling (TNF8): achievements and challenges
- Modes of combustion: premixed, non-premixed, and beyond
- Categorization of flames; mode diagram
- Models: applicability and challenges
- Candidate experiments (Rob Barlow)

2

Combustion Technologies

- Driver for combustion research
- Complexity
  - Multi-phase – spray, particles, gas, soot, …
  - Multi-physics – reaction, diffusion, radiation, phase change, compressibility, …
  - Multi-dimensional – complex geometry, unsteady, …
  - Multi-scale – device-scale, reaction zone, turbulence, …

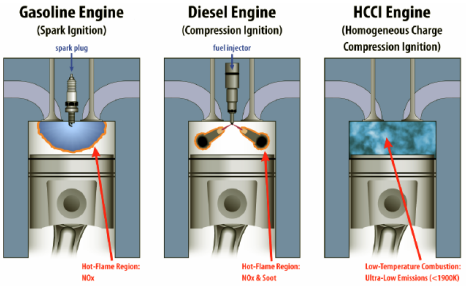

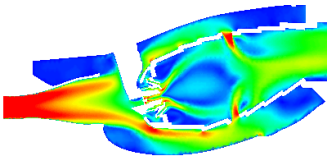

3

Combustion Research (TNF)

- Extract simpler, idealized problems to study
- Focus on particular phenomena
  - Turbulence-chemistry interactions
- Towards tractable, accurate, validated, predictive models

4

Focus of TNF

- Simplifications
  - Gas phase
  - Statistically stationary
  - Statistically axisymmetric
  - Atmospheric pressure
  - Homogeneous, non-premixed streams
  - Simple fuels

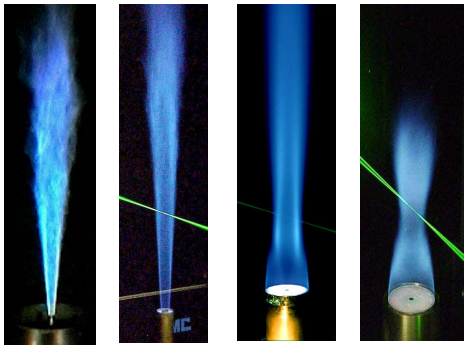

DLR flame | Sandia piloted jet flame | Sydney bluff-body flame | Sydney Swirling flame

5

TNF: Adding Complexity

- Flow
  - from simple jets to swirling recirculating flows
- Chemistry
  - more complex fuels
  - e.g., instabilities in H_2-rich fuels
- Combustion modes
  - multiple and inhomogeneous streams (including premixed)
- (Not being considered)
  - Sprays
  - High pressure

TECFLAM premixed swirl burner

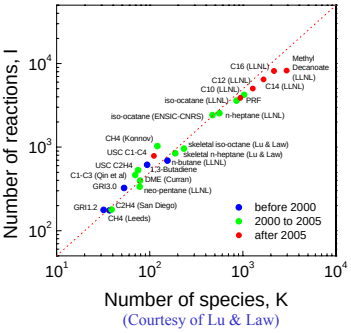

(Courtesy of Lu & Law)

Sydney piloted premixed jet flame

6

TNF 8: Modeling Achievements and Remaining Challenges (1/5)

- Achievement: Piloted jet flames
  - Local extinction & re-ignition
    - PDF methods (Cornell, Imperial)
    - CMC (Kronenburg & Kostas 2005)
    - Flamelet (Ihme & Pitsch 2008)
    - LES/FDF (Raman & Pitsch 2007)

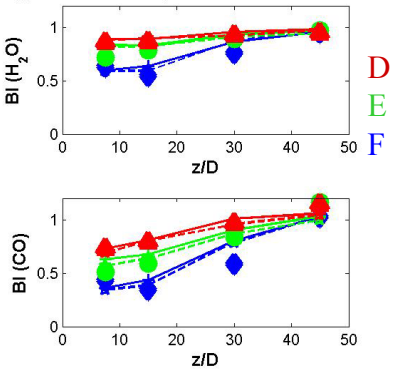

D
E
F

Barlow & Frank (1998); Cao & Pope (2005), solid GRI3.0, dashed GRI2.11

7

TNF 8: Modeling Achievements and Remaining Challenges (2/5)

- Achievement: Bluff body flames
  - Calculation of velocity and mixing fields

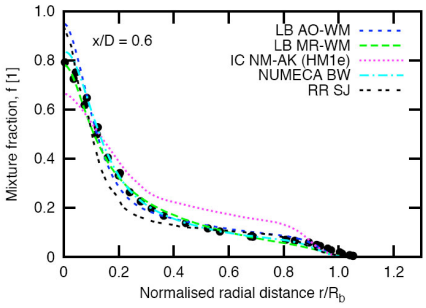

8

TNF 8: Modeling Achievements and Remaining Challenges (3/5)

- Achievement: Swirling flames
  - Calculation of velocity and mixing fields
  - Calculations of reactive scalar fields
  - Preliminary calculations of flow instabilities using LES

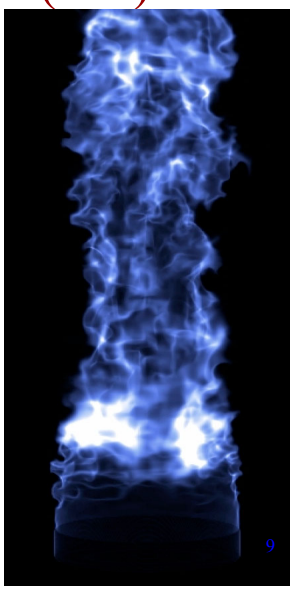

OH chemiluminescence rendered from LES of swirling flame SMH1 (Kempf et al., 2007, Imperial College)

9

TNF 8: Modeling Achievements and Remaining Challenges (4/5)

- Achievement: Lifted flames in vitiated co-flows
  - Sensitivity to co-flow temperature
    - PDF methods
    - LES/CMC

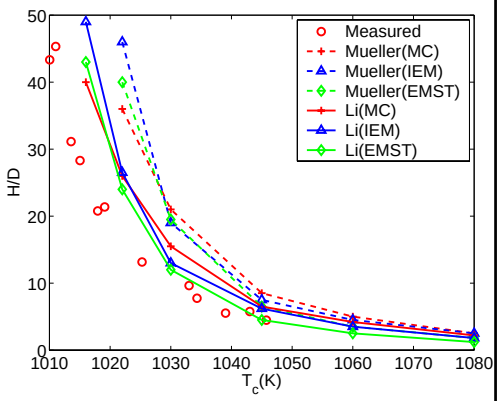

Expt.: Kent (2003)
Calc: Cao et al. (2005)
Note: 36 computations

10

TNF 8: Modeling Achievements and Remaining Challenges (5/5)

- Modeling challenges:
  - Comprehensive study of jet flames using LES
  - Study of turbulence-chemistry interactions in bluff-body and swirling flames
  - Flow instabilities in swirling flames
  - Adding further complexity
    - Different modes of combustion
    - More complex chemistry

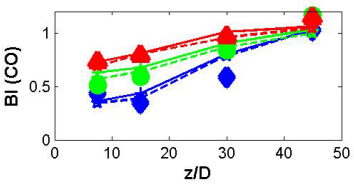

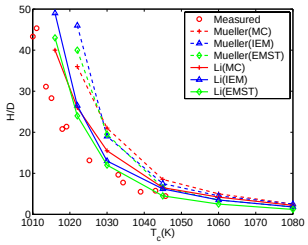

11

TNF 9: Adding Complexity

- When simple idealized problems are "solved", consider more general problems motivated by applications
- Beyond non-premixed
  - Other modes of combustion
- One objective of TNF 9: **To identify experiments suitable for the development and validation of models which are applicable across modes and regimes of combustion**
- Models for simple idealized problems
  - Applicable only to simple idealized case?
  - Can be applied (or extended) to general case?
    - Incorporated in CFD codes?

12

Combustion Modes: Two Simple Extremes

- Premixed
  - Single, homogeneous, flammable stream
  - Regimes: *Da*, *Re* (or u'/S_L and δ_L/L)
  - Particular concepts:
    - Laminar flame speed (s_L), progress variable (c), surface density (Σ), level set (G), scalar dissipation (χ_c) …
- Non-premixed
  - Two homogeneous non-flammable streams (fuel and oxidizer)
  - Regimes: *Da*, *Re*
  - Particular concepts:
    - Mixture fraction (Z), scalar dissipation (χ), …

13

Other Modes

- Multiple homogeneous streams
  - e.g., PPJB, Dunn et al. (2007), 4 streams
- Partial mixing of streams prior to combustion
  - partially-premixed combustion
  - e.g., Cabra et al.
- Inhomogeneous, flammable streams
  - Stratified combustion
  - e.g., Robin et al.
- Other …
- Categorization and mode diagrams

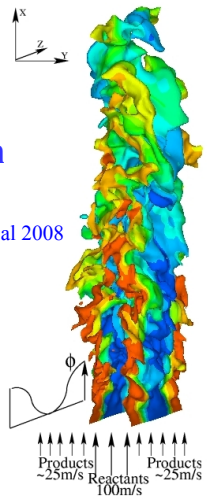

Chen et al 2008

14

Application Drivers

- GT aircraft engines
  - Spray inevitably leads to partial premixing
  - Multiple streams
  - Augmentors – stratified; multiple streams
- GT for power generation
  - Almost premixed
  - Small mixture inhomogeneities can influence performance
  - Differential diffusion can cause de-mixing in H_2-rich mixtures
- IC engines
  - Diesel – spray, stratified
  - Stratified charge - stratified
  - HCCI - Small mixture inhomogeneities can influence performance
- Furnaces
  - Low NO_x burners, fuel and air staging; dilution of products

15

Categorization of Flames: Adiabatic Two-Supply (A2) Flames

- Simplest idealization
  - Beyond pure premixed and non-premixed (but includes them)
- Fuel supply (T_F); Oxidant supply (T_O)
  - Supply may be inert blend, e.g., CH_4/H_2, H_2/N_2
- Inflowing streams formed by adiabatic mixing of supplies
  - Inert mixing
  - Fully burnt (equilibrium)
- Significance
  - Mixing characterized by a single mixture fraction
- Examples:
  - Two-stream lifted non-premixed flames
  - All flames with 1 or 2 homogeneous streams
  - Piloted non-premixed flames (with adiabatic pilot)
  - Stratified combustion

16

Categorization of Flames: A(S) and N(S) Flames

- (S) – number of supplies (S > 1)
- Mixing charcterized by *S-1* mixture fractions
- A/N:
  - A – adiabatic
  - N – non-adiabatic (heat loss from inflowing streams)
- Examples
  - Barlow & Frank flames D, E, F:
    - A2/N2 – (enthalpy deficit of pilot, "pilot error")
  - Dunn et al. PPJB
    - A3/N3 – four inflowing streams
    - Supplies
      - Methane (jet)
      - Hydrogen (for vitiated co-flow burner)
      - Air

17

Categorization of TNF Flames

	Case	Type	Supplies
A	TUD turbulent opposed jet burner	A2	CH_4, Air
B	DLR jet flames	A2	$CH_4/H_2/N_2$, Air
C	Sandia piloted jet flames	N2	CH_4, Air
D	Sydney bluff body flames	A2	CH_4/H_2, Air
E	Sydney swirl/bluff body flames	A2	CH_4 or CH_4/Air or CH_4/H_2, Air
F	Berkeley/Sydney nonpremixed jet flames in vitiated coflow	A2/A3	H_2/N_2, H_2/Air, Air
G	Adelaide nonpremixed jet flames in vitiated coflow	A2/A3	CH_4/H_2, $CH_4/H_2/N_2$/Air, Air
H	DLR model gas turbine combustor	A2	CH_4, Air
I	Cambridge stratified slot burner	A2	CH_4, Air
J	CORIA-INSA stratified V-flame	A2	C_3H_8 or CH_4, Air
K	TUD piloted annular stratified burner		
L	ORACLES burner	A2	C_3H_8, Air
M	Cambridge stratified swirl burner		
N	Twente stratified swirl combustor	A2	CH_4, Air
O	TECFLAM premixed swirl burner	A2	CNG, Air
P	TUD premixed low-swirl burner	A2	CH_4, Air
Q	Sydney piloted premixed jet in vitiated coflow	A3	CNG, H_2, Air
R			
S	Sandia premixed swirling dump combustor		CH_4, Air
T			

18

Mode Diagram for A2 and N2 Flames

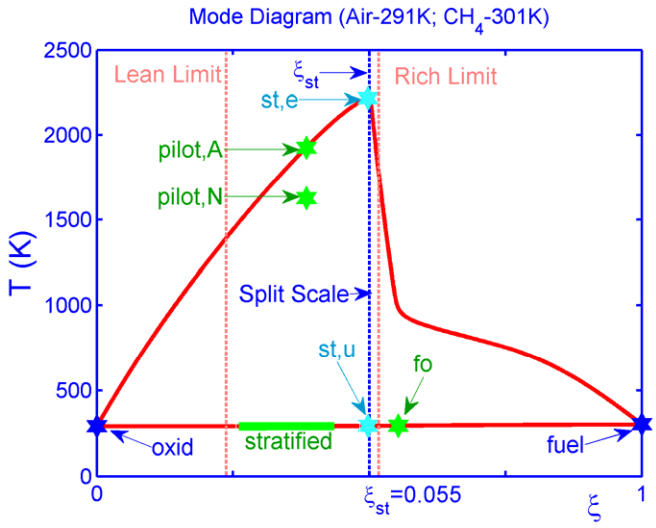

19

Mode Diagrams for Two-Stream TNF Flames

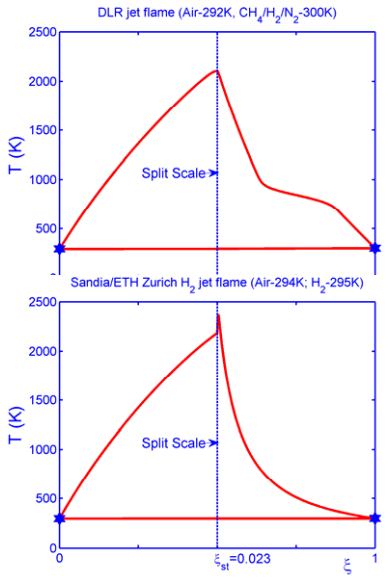

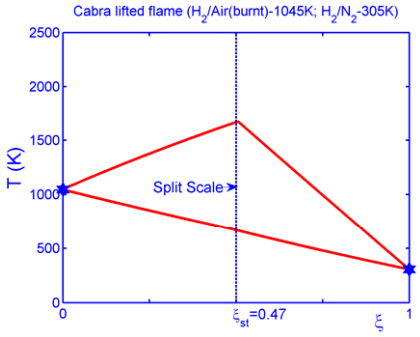

20

Mode Diagram for A2 and N2 Flames

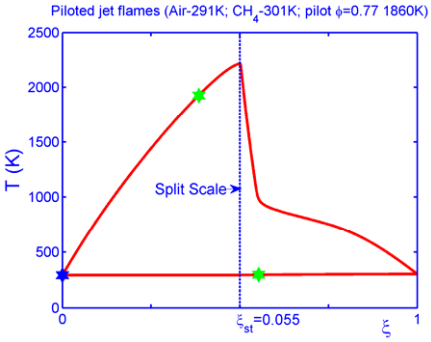

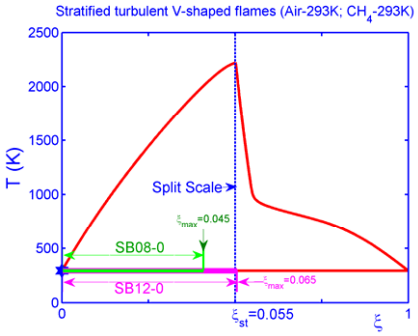

21

Models for All Modes of Combustion: Applicability and Accuracy

- A model may be applicable, but not accurate
- Applicability of a model to a flow
  - Can boundary conditions be applied and equations solved?
  - Can the thermochemical composition of inflowing streams be represented?
- Boundary-layer equations are NOT applicable to general flows
- The k-ε model IS applicable to complex, swirling, recirculating flows, but it is NOT accurate (for these flows)

22

Models Applicable to All Modes of Combustion

- Based on full composition (e.g., species mass fractions and enthalpy)
  - DNS
  - PDF and LES/FDF
  - RANS (with neglect of fluctuations, "laminar chemistry")
  - Thickened flame front
  - Eddy break-up models
  - Eddy dissipation concept (EDC)
  - LEM, ODT, others

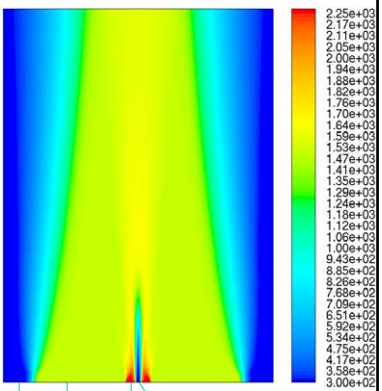

Mean temperature in PPJB: Composition PDF calculations (Fluent), Rowinski & Pope (2008)

Challenges for Models Applicable to All Modes of Combustion

- PDF and LES/FDF:
  - Accounting for thin reaction zones
  - Accounting for the effects of reaction to augment mixing
  - (Both challenges already present in premixed flames)

- PDF calculations of premixed
  - Pope & Anand (1985)
  - Anand & Pope (1987)
  - …..
  - Lindstedt & Vaos (2006)

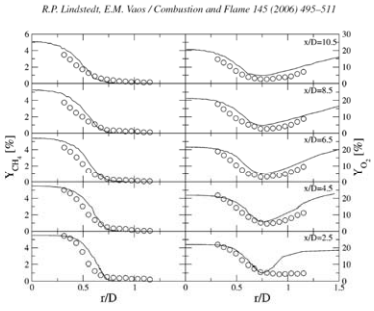

Fig. 17. Mean CH_4 and O_2 mass fractions for a stoichiometric CH_4/air mixture at Re = 52,500 (flame F1). Transported PDF calculations with modified Curl's model [35] and Eq. (8) with $C_\phi^* = 1.2$, $C_\phi = 4$ (—), and $T_\mathrm{P} = 1785$ K. Experimental data (○) from Chen et al. [37].

Models Applicable to Two-Supply (A2/N2) Flames

- Adiabatic (A2):
  - Z, c (or Y_F, or…)
    - Janicka & Kollman (1978), Correa & Pope (1986), Bradley et al. (1990,…), Libby & Williams (2000), Pierce & Moin (2004), Robin et al. (2008), Vreman et al. (2008), Ihme & Pitsch (2008), Fluent/CFX ("partially-premixed)
  - Z, G – Muller et al. (1994)
- Non-adiabatic (N2):
  - Z, c, h – Fluent/CFX "partially-premixed"
  - Z, G, h – Chen, Herrmann & Peters (2000)

25

Challenges for Models Applicable to Two-Supply Flames

- Choice of progress variable
  - Statistical independence

$$p_{Zc} = p_Z\, p_{c|Z} \approx p_Z\, p_c$$

- Assumed shape of PDF of c
  - SMLD - Pope (1979), Ihme & Pitsch(2008)
- Consistent modeling of scalar dissipations
- Beyond 1-step or simply-parameterized chemistry (FGM)
- Effects of scalar dissipation; unsteady effects
- Heat loss, diff-diff, non-unity *Le*

26

What Modes for TNF?

- To what extent are A2 (or N2) models applicable to practical combustion problems?
- Are there inherent limitations in these models (e.g. simple/flame-based chemistry)?
- Should TNF focus on generally-applicable models?
- Should TNF experiments and DNS be limited to A2 (or N2)?

27

Closing Remarks

- In applications, "partially-premixed" is the rule:
  - purely premixed or non-premixed combustion are the exceptions
- Different modes of "partially-premixed" combustion
  - Multiple, inhomogeneous streams
  - Mixing prior to combustion
  - Stratified mixtures
  - Categorization (A(S) and N(S)) and mode diagrams
- Model development relies heavily on TNF-quality experimental data
  - More use of DNS in the future
- Important to be in interesting mode/regime
- Some candidate burners/configurations….

28

Overview of Flame Experiments **(R. Barlow, A. Masri)**

One of the objectives of the TNF9 Workshop is to review and discuss the characteristics of potential future target flames with respect to their appropriateness for collaborative model validation efforts that address a broader range of combustion modes and regimes than the TNF Workshop has considered in the past. The figure below is a qualitative map of modes and regimes of gas phase, atmospheric pressure combustion with various flames place approximately. Many are already known to the TNF community. Flames with high Damköhler are across the top of the inverted triangle, and the various modes merge to a perfectly stirred reactor in the limit of Da << 1. (Damköhler number is used here only conceptually and without specific definition.) The boundaries between combustion modes and regimes are not always obvious, so placement details and inclusiveness are not important for this illustration. The point is that there are already flames in the literature or under current investigation that spread across this map. The brief overview which follows does not list the nonpremixed jet flames that have been the main focus of previous TNF Workshops. However, it is expected that work will continue on these flames and that some of the same burners will be used with new fuels.

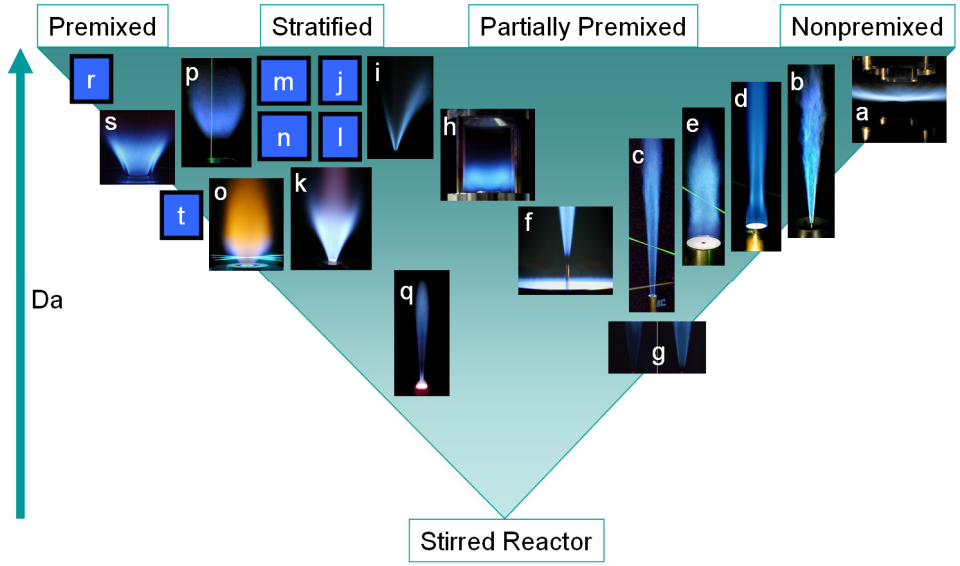

Fig. 1. Qualitative map of combustion modes and regimes for various laboratory-scale flames. Letter designations refer to Table 1.

Generally, as we expand the scope of TNF to extend across a range of combustion regimes, we should maintain an emphasis on turbulence-chemistry interaction in gas phase combustion of relatively simple fuels. This is where the TNF process can be most effective over the next few years. It should also be kept in mind that a desirable long-term outcome is the development and validation of robust combustion models that can accurately address all regimes of combustion. However, that is not an exclusive goal because some models may be used effectively within a limited range of regimes. As we have done from the beginning of this workshop series, we want to systematically evaluate the capabilities and limitations of a variety of modeling approaches, so that overall capabilities may be advanced.

Table 1 List of experimental flames in shown in Fig. 1, the approximate regime map for gas-phase, atmospheric pressure flames. (Reference list is not complete, so suggestions for additions are welcome.)

a	TUD turbulent opposed jet burner.	Geyer2005, Böhm2006
b	DLR simple jet flames of $CH_4/H_2/N_2$ in air	Bergmann1998, Meier2000, Hult2005, Wang2007, Wang2008, Frank2008,
c	Sandia piloted CH_4/air air jet flames	Barlow1998, Schneider2005, Barlow2005, Karpetis2005, Wang2007
d	Sydney bluff-body flames of CH_4/H_2	Dally1998, Dally2003
e	Sydney swirl/bluff-body flames	Kalt2002, Al-Abdeli2003, Masri2004
f	Berkeley/Sydney nonpremixed lifted jet flames in vitiated H_2/air coflow	Cabra2002, Cabra2005, Gordon2007
g	Adelaide nonpremixed jet flames in vitiated coflow (low O_2 levels)	Dally2002, Medwell2007
h	DLR model gas turbine combustor (steady and unsteady cases)	Duan2005, Gizendanner2005, Meier2005, Weigand2005, Weigand2006, Meier2006, Meier2007
i	Cambridge stratified slot burner, CH_4/air V-flame	Anselmo-Filho2008, Barlow2008
j	CORIA-INSA stratified V-flame	Renou2004, Robin2008
k	TUD piloted annular stratified burner	Work in progress
l	ORACLES burner	Nguyen2003, Domingo2005, Robin2006, Duwig2007
m	Cambridge stratified swirl burner	Work in progress
n	Twente stratified swirl combustor (steady and oscillating cases)	Sengissen2007
o	TECFLAM premixed swirl burner	Schneider2005, Freitag2005, Freitag2007, Schneider2008,
p	TUD premixed low-swirl burner	Nogenmyr2007,
q	Sydney piloted premixed jet in vitiated coflow	Dunn2007, Dunn2008
r	Place holder for various premixed flames with low u'/S_L	
s	Sandia premixed swirling dump combustor	Oefelein2006
t	Place holder for premixed flames, higher u'/S_L	

Desirable burner/flame characteristics:

1. Well defined boundary conditions that serve to minimize ambiguity in results.
2. Easy optical access.
3. Steady flow (depending on current and future modeling interest in unsteady cases).
4. Turbulence parameters at appropriate levels (Re, u'/S_L, etc.). What 'appropriate' means is open for discussion.
5. Velocity and scalar measurements with good statistical sample size. (Other measurements to be discussed.)
6. Variation of one or more parameters to which the flames are sensitive (particularly with respect to turbulence-chemistry interaction or a transition between combustion regimes).
7. Portable and repeatable. Investigation of a burner using a broad range of diagnostics in different labs can be very informative. If this is to be done, then it must be possible to run flames reliably and repeatably in different labs.

Some things to consider in evaluating potential target flames:

1. It may be useful to identify burners that allow transition from one combustion mode to another (lateral movement in the diagram, Fig. 1) as well as variation in Damköhler number or other relevant parameter. For example, running stratified burners in a fully premixed mode will help to isolate the effects of stratification and will serve to anchor any validation process that extends premixed models into stratified conditions.
2. Some burners have complex internal flows that are difficult or impossible to measure. It may be appropriate to carry out detailed simulations of the internal flows (nonreacting) and provide results to others as inflow conditions for model calculations. This can be useful even with fully developed pipe or channel flows.
3. With the primary emphasis of this group being on validation of robust models for turbulence-chemistry interaction, the selection of preferred models or assumptions for other aspects of the problem (chemical mechanisms, radiation models, turbulence model parameters, details of boundary conditions, etc.) should be discussed, and recommended models should be made available. This has been and important function of the TNF Workshop in the past.
4. Turbulence generation: There are many premixed and stratified flame experiments that rely on grid-generated turbulence. Should we focus more on shear-generated turbulence? Fully developed inflows? Does it matter?
5. If possible, we should identify a modest number of flames (preferably with parameter variation for each case) that are seen as be appropriate targets for systematic collaborative comparisons over the next 4-6 years.
6. Target cases should be prioritized based on relevance (in the judgment of the Workshop participants), interest from multiple modeling groups, and the quality and completeness of experimental data or the schedule for availability of data on experiments that have not yet been published. Primary coordinators for each case should be identified and schedules for data distribution and eventual comparisons should be discussed.

Potential Target Flames for Partially Premixed and Stratified Combustion:

There are at least three general classes of burners that should be considered. One class is represented by 'Cabra' burner [see Table 1 for references], which has already had some attention at past workshops, and the DLR model gas turbine combustor [see Table 1], which has been measured in both steady and unsteady modes. These burners inject fuel directly, but there is significant mixing before combustion because the flame is not attached to the fuel nozzle. Figure 2 shows the burner diagrams along with scatter data for mixture fraction vs. temperature. Measurements are from the flame stabilization region in both cases, and it is apparent in both cases that a significant fraction of samples have been mixed to conditions within the flammability limits before reaction progresses. In the Cabra flame, because of the elevated temperature along the mixing line, the flame is stabilized by some combination of auto-ignition and flame propagation. In the DLR combustor, there is a cold ~300 K mixing line (between fuel and air), but there is also mixing of cold reactants with hot products from the inner and outer recirculation zones. Both burners apparently involve multiple combustion modes.

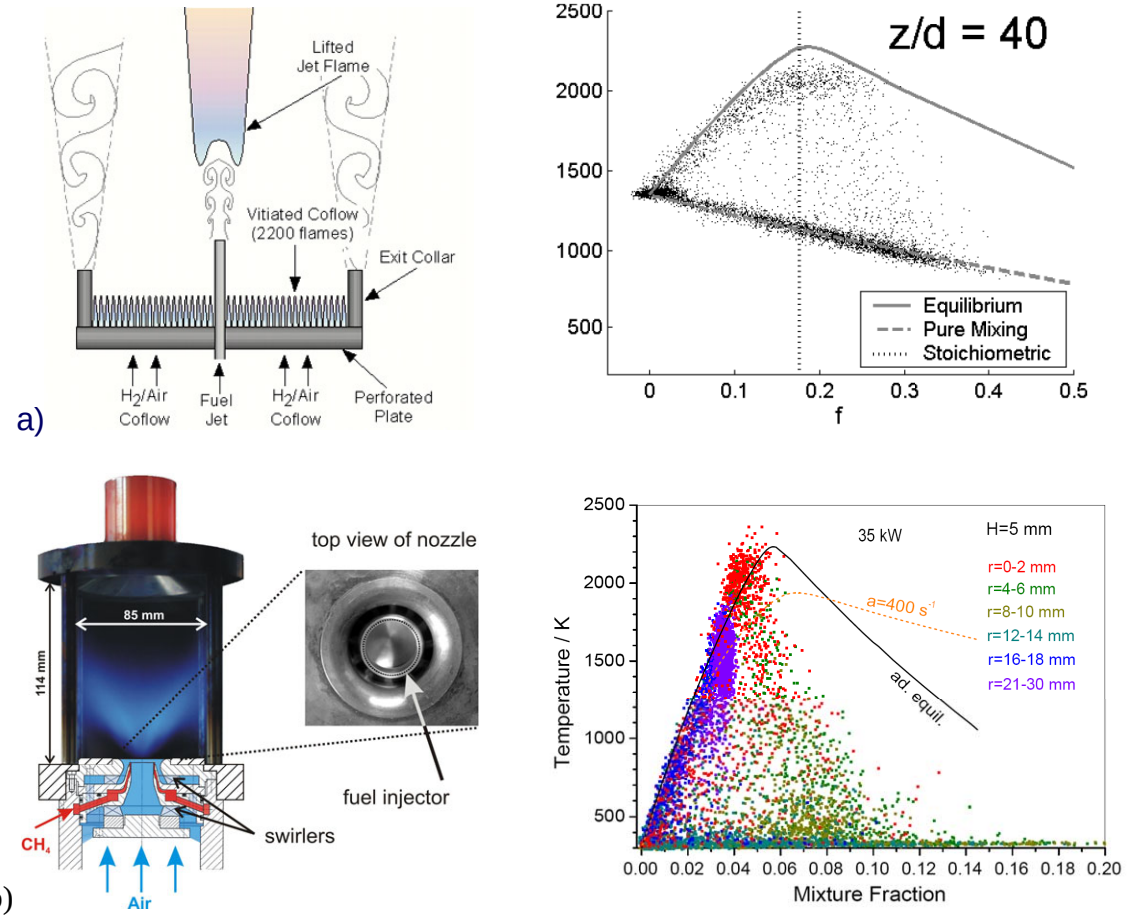

Fig. 2. Burner diagrams and scatter data for temperature vs. mixture fraction in the Cabra lifted CH_4/air jet flame in vitiated H_2/air coflow.

The second class of burners that should be considered includes those designed specifically to investigate stratified flames, where the primary mode of combustion is propagation of a turbulent reaction zone through non-uniformly mixed, flammable reactants. The stratified mixture is produced by injecting two or more streams of premixed and flammable reactants in relatively simple geometric configurations. There are several burners of this type described in the literature or under current study, and examples are shown in Fig. 3. The two V-flame burners use grid generated turbulence and have low levels of u'/S_L. The annular burners have long development sections to attain well developed internal turbulent channel flows, and there can also be shear between streams. Two additional stratified combustors have been reported that have more complex flow fields and are enclosed. These are the ORACLES combustor, which has a two-dimensional dump combustor geometry with a splitter plate upstream of the dump plane, and an annular swirling dump combustor with a main premixed flow and extra fuel injection upstream of the dump plane. These are shown in Fig. 4.

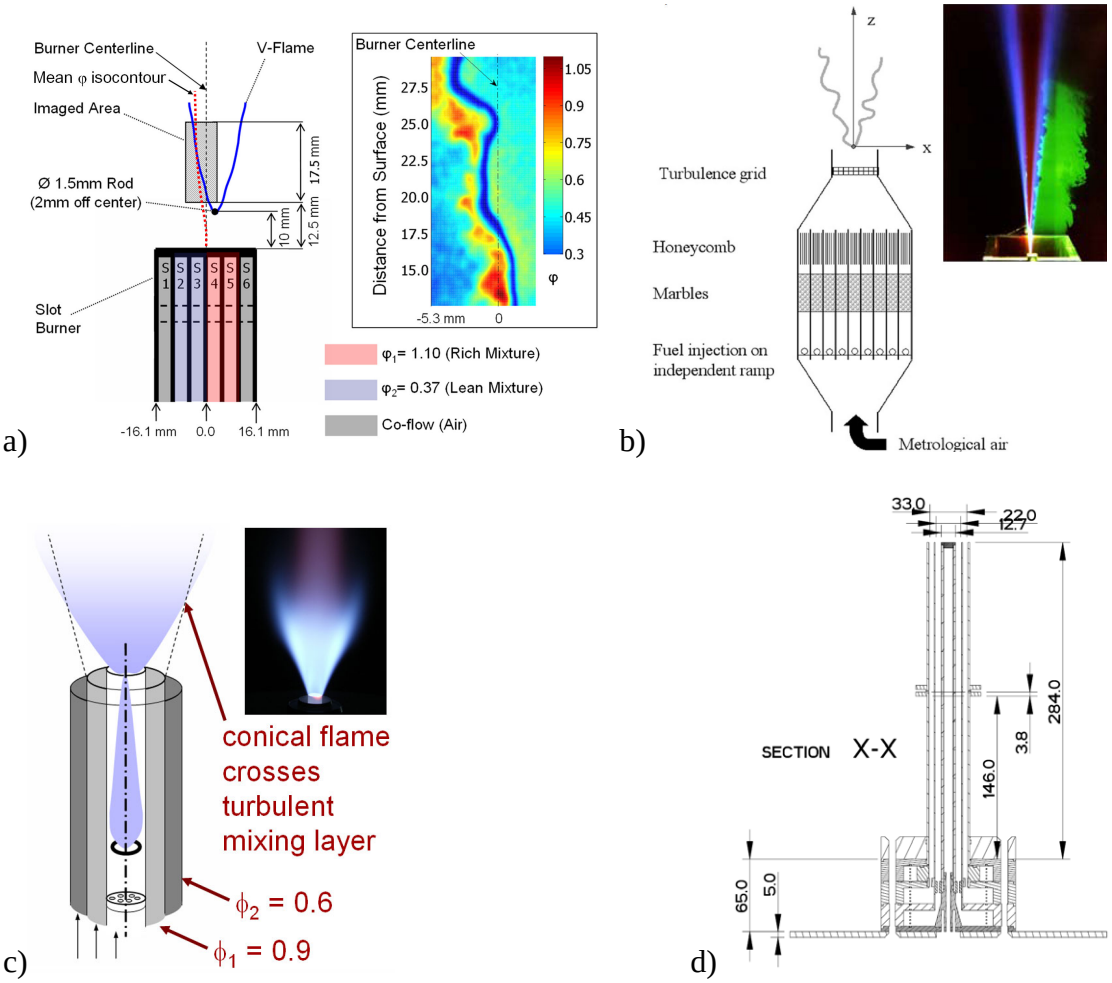

Fig. 3. Stratified combustion burners (see Table 1 for references): a) Cambridge V-flame with single mixing layer. b) CORIA-INSA V-flames with multiple reactant streams. c) TUD Conical flame with central pilot and two annular reactant flows. d) Central bluff body and two annular flows with swirling outer annular flow (under development at Cambridge).

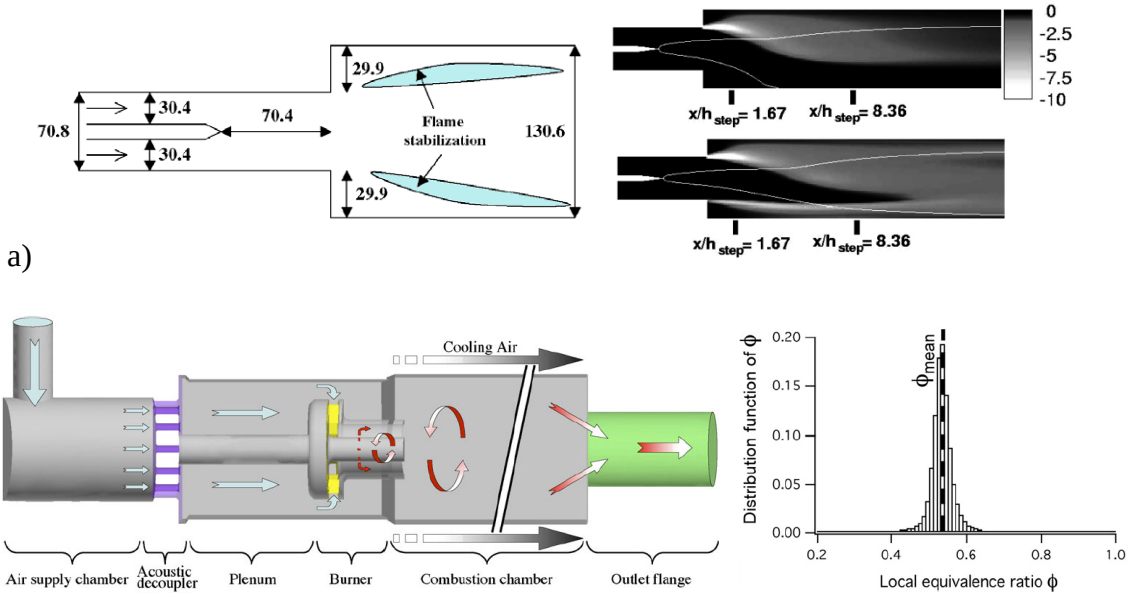

Fig. 4. a) ORACLES combustor sketch and calculated heat release for two stratified cases [Robin2006]. b) Twente University stratified swirling dump combustor and modeled pdf of equivalence ratio along the flame front [Sengissen2007].

A third class of flames is that of open premixed flames that have mixture stratification at the edges due to mixing with air. These flames burn primarily in a premixed mode, but models have had to account for the stratified regions. Two examples are shown in Fig. 5. One is a low swirl burner constructed by TU Darmstadt and based on the concept developed by Cheng and coworkers. The other is the TECFLAM premixed swirl flame.

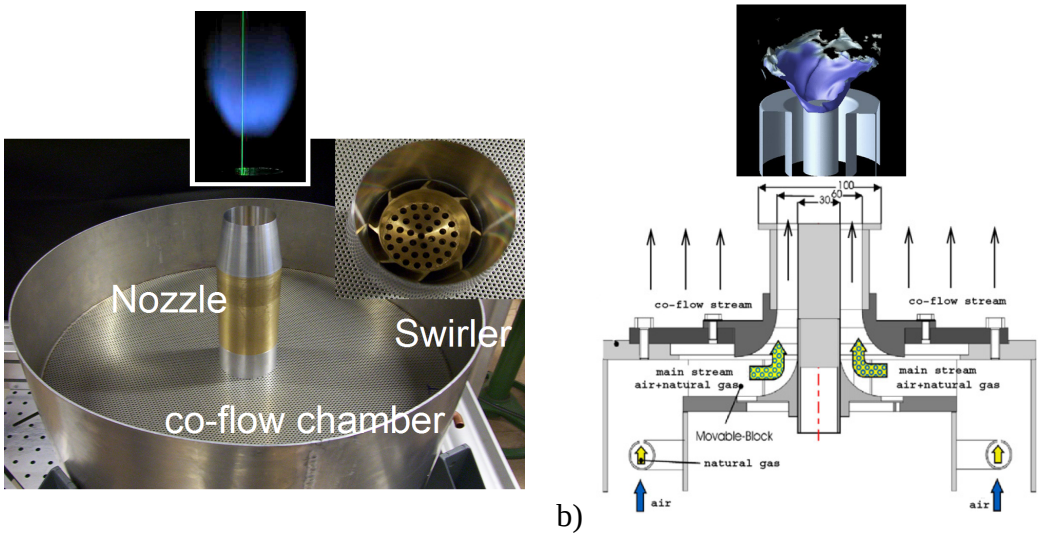

Fig. 5. Nominally premixed flames with stratified combustion at the boundary where reactants mix with air: a) TU Darmstadt low-swirl burner, b) TECFLAM premixed swirl burner. See Table 1 for references.

An additional burner that should be considered but does not fit easily into the previous groups is the Sydney piloted premixed jet burner (Fig. 6), which injects a high velocity jet (up to 250 m/s) of lean premixed CH_4/air into a large coflow of lean H_2/air combustion products, with a small stoichiometric CH_4/air pilot flame around the jet exit. Mixing rates are very high, such that significant entrainment of the pilot and coflow fluids occurs simultaneously with reaction in the highest velocity cases.

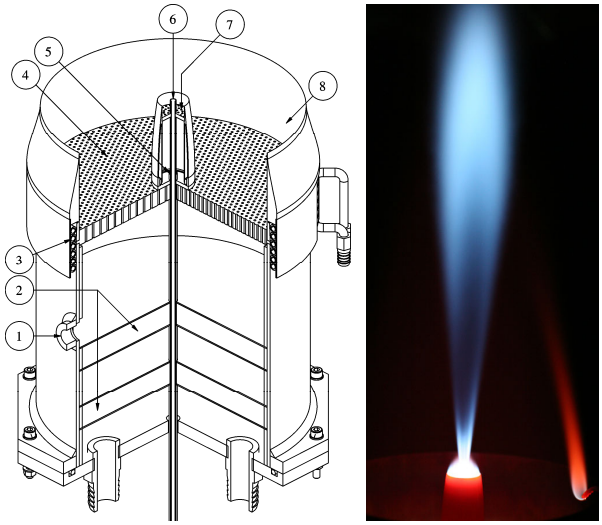

Fig. 6. Sydney Piloted premixed jet burner [Dunn2007, Dunn2008].

Some other cases of possible interest:

Purely premixed flames: There are many examples of premixed turbulent flames in the literature, including V-flames, Bunsen flames, low-swirl flames, and bluff-body stabilized flames, and dump combustors. Only a few examples have been included above, and those are cases were a burner has been operated with both premixed and stratified flames or where the nominally premixed flames has air mixing at the edges, so that a part of the flame propagates through a stratified mixture. Discussion of purely premixed cases is welcome.

Lifted jet flames in air: Lifted jet flames in air have been targets for many experimental and computational studies, including LES and DNS. However, they have not attracted more than passing attention in past TNF Workshop discussions of possible target flames for collaborative model validation efforts. The absence of a heated coflow greatly simplifies the experiments, with respect to burner operation, application of laser diagnostics, and specification of boundary conditions for model calculations. Comments on lifted flames are welcome.

Jets and Jet Flames in Cross Flow: There is industry interest in the mixing characteristics of jets in cross flow. The Twente burner in Fig. 4b includes fuel injection by jets that feed into the swirling annular flow upstream of the dump plane, as an example. There has also significant work done on jets in cross flow in the context of high speed combustion. Is this an area that groups participating in the TNF process are interested in pursuing?

Other jet flames in hot coflow: Lifted flames in vitiated coflow (Cabra burner) have received significant attention from groups involved in this Workshop. There are other experiments involving jet flames in high-temperature coflow that might be of interest. These include burners shown in Fig. 7, which are designed to investigate flameless oxidation or MIND combustion conditions.

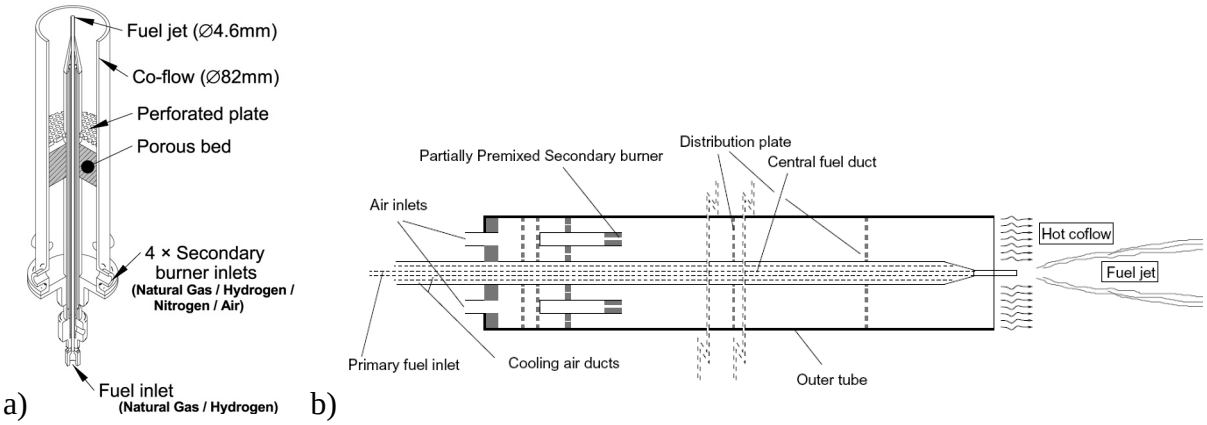

Fig. 7. Burner configurations for jets in hot coflow: a) Adelaide MILD combustion burner [Dally2002], b) Delft jet in hot coflow [work in progress, see poster by Oldenhof].

Forced ignition experiments*:* Spark ignition and subsequent flame propagation through stratified fuel-air mixtures is important for many applications. Significant work has been done on this topic by the IC engine research community. However, the IC engine literature is not considered here. There have been several recent experiments on forced ignition and flame development in stratified or partially premixed turbulent flows. Spark ignition followed by PIV/PLIF imaging was used to study structure and propagation of turbulent stratified flames in a constant volume chamber [Pasquier2007]. These are single shot experiments that must be run many times to gain statistical significance. There has also been significant recent work on forced ignition and the light-up process of nonpremixed or partially premixed configurations, which are relevant to such things as fire safety, gas turbine startup, and altitude relight. Ignition and flame growth (or extinction) occurs in partially premixed turbulent flows and can involve a range of combustion regimes, including edge flames or triple flames, flame propagation through lean or rich stratified mixtures, and diffusion flames. A TNF9 poster from Ahmed and Mastorakos describes several of these experiments using various geometries.

Auto-ignition experiments and simulations: In addition to work on the Cabra burner configuration (lifted jet flame in vitiated coflow) there have been experiments and detailed simulations on auto-ignition of preheated, turbulent mixing flows. Depending on the specific conditions (temperatures, turbulence parameters, fuels and mixture characteristics) these cases can involve multiple combustion regimes, so they may be of interest at targets for collaborative comparisons. There are TNF9 posters by (listing first authors only) Jones, Stankovic, and Yoo that deal with auto-ignition.

Other enclosed flames and elevated pressure: At some stage, consideration should be given to model validation cases at elevated pressure. Ability to obtain detailed measurements at elevated pressure is obviously more limited. For example, complications associated with Raman measurements in a model gas turbine combustor at elevated pressure were informatively described [Wehr2007]. The burner used for those experiments was geometrically similar to a larger burner (see Fig. 2b) that has been studied extensively at atmospheric pressure. Figure 8 shows one example of a burner that has been measured at modestly elevated pressure as part of the MOLECULES project.

Combustor pressure p (bar)	2	4	6
Combustion air temperature T_{air} (K)	623	623	623
Fuel temperature T_{fuel} (K)	373	373	373
Combustion air mass flow rate $\dot{m}$ (g/s)	30	60	90
Equivalence ratio ϕ	0.8	0.8	0.8
Re_{air}	46,000	92,000	138,000
Re_{fuel}	33,000	67,000	100,000

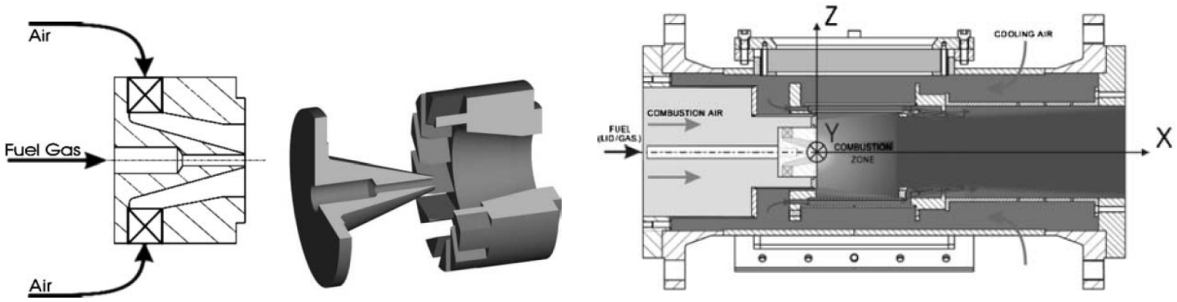

Fig. 8. TURBOMECA burner, test conditions, and combustion chamber for TU Darmstadt experiments on lifted swirl flames at elevated pressure [Janus2005].

References:

Al-Abdeli, YM, Masri, AR, *Exp. Thermal Fluid Sci.,* 27 (2003) 655–665.

Anselmo-Filho, P, Hochgreb, S, Cant, RS, Barlow, RS, "Experimental measurements of geometric properties of turbulent stratified flames," *Proc. Combust. Inst.* (2008, accepted).

Barlow, RS, Frank, JH, *Proc. Combust. Inst*. 27 (1998) 1087–1095.

Barlow, RS, Frank, JH, Karpetis, AN, Chen, JY, *Combust. Flame* 143 (2005) 433–449.

Barlow, RS, *Proc. Combust. Inst*. 31 (2007) 49–75.

Barlow, RS, Wang, GH, Anselmo-Filho, P, Sweeney, M, Hochgreb, S, "Application of Raman/Rayleigh/LIF diagnostics in turbulent stratified flames," *Proc. Combust. Inst.* (2008, accepted).

Bergmann, V, Meier, W, Wolff, W, Stricker, W, *Appl. Phys. B* 66 (1998) 489–502.

Bilger, RW, Pope, SB, Bray, KNC, Driscoll, JF, *Proc. Combust. Inst.* 30 (2005) 21–42.

Böhm, B, Geyer, D, Dreizler, A, Venkatesan, KK, Laurendeau, NM, Renfro, MW, *Proc. Combust. Inst*. 31 (2007) .709–717.

Cabra, R, Myhrvold, T, Chen, JY, Dibble, RW, Karpetis, AN, Barlow, RS, *Proc. Combust. Inst*. 29 (2002) 1881–1888.

Cabra, R, Chen, JY, Dibble, RW, Karpetis, AN, Barlow, RS, *Combust. Flame* 143 (2005) 491–506.

Dally, BB, Masri, AR, Barlow, RS, Fiechtner, GJ, *Combust. Flame* 114 (1998) 119–148.

Dally, BB, Masri, AR, Barlow, RS, Fiechtner, GJ, *Combust. Flame* 132 (2003) 272–274.

Dally, BB, Karpetis, AN, Barlow, RS, *Proc. Combust. Inst.* 29 (2002) 1147–1154.

Domingo, P, Vervisch, L, Payet, S, Hauguel, R, *Combust. Flame* 143 (2005) 566–586.

Duan, XR, Meier, W, Weigand, P, Lehmann, B, *Appl. Phys. B* 80 (2005) 389–396.

Dunn, MJ, Masri, AR, Bilger, RW, *Combust. Flame* 151 (2007) 46–60.

Duwig, C, Fureby, C, *Combust. Flame* 151 (2007) 85–103.

Frank, JH, Kaiser, SA, *Exp. Fluids* 44 (2008) 221–233.

Freitag, M, Klein, K, *Flow Turb. Combust.*75 (2005) 51–66.

Freitag, M, Janicka, J, *Proc. Combust. Inst*. 31 (2007) 1477–1485.

Geyer, D, Kempf, A, Dreizler, A, Janicka, J, *Proc. Combust. Inst*. 30 (2005) 681–689.

Gizendanner-Thoben, R, Meier, U, Meier, W, Aigner, M, *Flow Turb. Combust.* 75 (2005) 317–333.

Gordon, RL, Masri, AR, Pope, SB, Goldin, GM, *Combust. Flame* 151 (2007) 495–511.

Hult, J, Meier, U, Meier, W, Harvey, A, Kaminski, CF, *Proc. Combust. Inst*. 30 (2005) 701–709.

Janicka, J, Sadiki, A, *Proc. Combust. Inst*. 30 (2005) 537–547.

Janus, B, Dreizler, A, Janicka, J, *Flow Turb. Combust.* 75 (2005) 293–315.

Kalt, PAM, Al-Abdeli, YM, Masri, AR, Barlow, RS, *Proc. Combust. Inst*. 29 (2002) 1913–1919.

Karpetis, AN, Barlow, RS, *Proc. Combust. Inst*. 30 (2005) 665–672.

Masri, AR, Kalt, PAM, Barlow, RS, *Combust. Flame* 137 (2004) 1–37.

Medwell, PR, Kalt, PAM, Dally, BB, *Combust. Flame* 148 (2007) 48–61.

Meier, W, Barlow, RS, Chen, YL, Chen, JY, *Combust. Flame* 123 (2000) 326–

Meier, W, Duan, XR, Weigand, P, *Proc. Combust. Inst*. 30 (2005) 835–842.

Meier, W, Duan, XR, Weigand, P, *Combust. Flame* 144 (2006) 225–236.

Meier, W, Weigand, P, Duan, XR, Giezendanner-Thoben, R, *Combust. Flame* 150 (2007) 2–26.

Nguyen, PD, Bruel, P, "Turbulent Reacting Flow in a Dump Combustor: Experimental Determination of the Influence of the Inlet Equivalence Ratio Difference on the Contribution of the Coherent and Stochastic Motions to the Velocity Field Dynamics," 41st Aerospace Sciences Meeting and Exhibit, Reno, January 2003, Paper 2003-0958.

Nogenmyr, KN, Petersson, P, Bai, XS, Nauert, A, Olofsson, J, Brackman, C, Seyfried, H, Zetterberg, J, Li, ZS, Richter, M, Dreizler, A, Linne, M, Alden, M, *Proc. Combust. Inst.* 31 (2007) 1467–1475.

Oefelein, JC, Schefer, RW, Barlow, RS, AIAA Journal 44 (2006) 418–433.

Pasquier, N, Lecordier, B, Trinité, M, Cessou, A, *Proc. Combust. Inst.* 31 (2007) 1567–1574.

Renou, B, Samson, E, Boukhalfa, A, *Combust. Sci. and Tech.* 176 (2004) 1867–1890.

Robin, V, Mura, A, Champion, M, Plion, P, *Combust. Sci. Tech*., 178 (2006) 1843-1880.

Robin, V, Mura, A, Champion, M, Degardin, O, Renou, B, Boukhalfa, M, *Combust. Flame* 153 (2008) 288–315.

Schneider, C, Dreizler, A, Janicka, J, *Flow, Turb. Combust*. 74 (2005) 103–127.

Schneider, E, Maltsev, EA, Sadiki, A, Janicka, J, *Combust. Flame* 152 (2008) 548–572.

Sengissen, AX, Van Kampenb, JF, Huls, RA, Stoffels, GGM, Kok, JBW., Poinsot, TJ, *Combust. Flame* 150 (2007) 40–53.

Wang, GH, Karpetis, AN, Barlow, RS, *Combust. Flame* 148 (2007) 62–75.

Wang, GH, Clemens, NT, Varghese, PL, Barlow, RS, *Combust. Flame* 152 (2008) 317–335.

Weigand, P, Meier, W, Duan, XR, Gizendanner-Thoben, R, Meier, U, *Flow Turb. Combust.* 75 (2005) 275–292.

Wehr, L, Meier, W, Kunte, P, Hassa, C, *Proc. Combust. Inst.* 31 (2007) 3099–3106.

Weigand, P, Meier, W, Duan, XR, Stricker, W, Aigner, M, *Combust. Flame* 144 (2006) 205–224.

Overview of Experimental Flames: Potential Validation Targets for Challenge 1

Rob Barlow and Assaad Masri

Assumptions behind this talk

- TNF Workshop will continue to be centered around:
  - Turbulence-chemistry interaction
  - Gas phase, atmospheric pressure flame
  - Relatively simple fuels
- Work will continue on some of the nonpremixed target flames and burners
  - DLR jet flames
  - Piloted jet flames
  - Sydney bluff-body (and swirl) flames
- Consider possible targets for partially-premixed and stratified modes
  - Published experiments
  - Work in progress

Laboratory-Scale Turbulent Flames

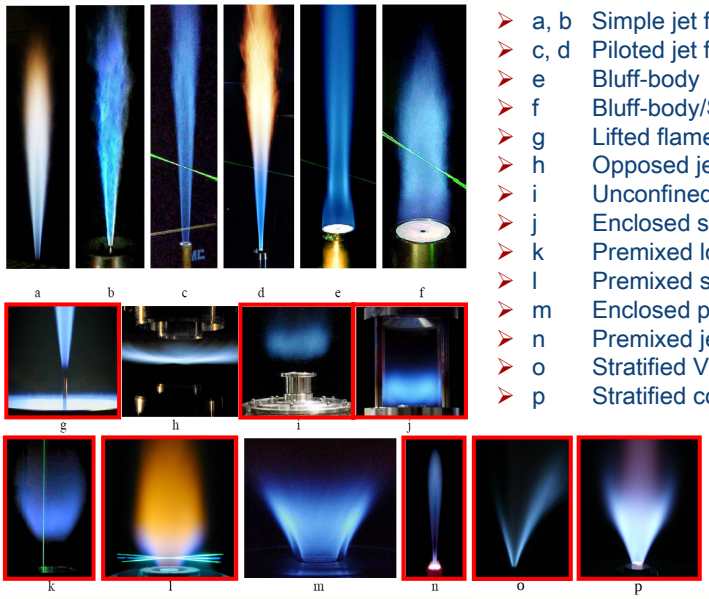

- a, b Simple jet flames
- c, d Piloted jet flames
- e Bluff-body
- f Bluff-body/Swirl
- g Lifted flame in vitiated coflow
- h Opposed jet flame
- i Unconfined swirl flame
- j Enclosed swirl flame
- k Premixed low-swirl flame
- l Premixed swirl, bluff-body
- m Enclosed premixed swirl flame
- n Premixed jet in vitiated coflow
- o Stratified V-flame
- p Stratified coaxial flame

Cambridge
Darmstadt TU
Delft TU
DLR-Stuttgart
Sandia
Sydney Univ.

TNF9 Workshop, Montreal 2008

Simple Map: Combustion Modes & Regimes of Some Available Flames

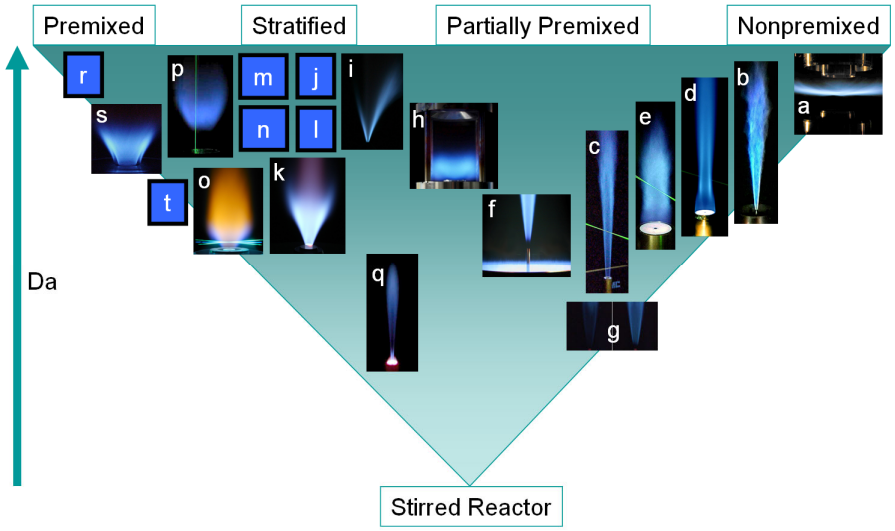

TNF9 Workshop, Montreal 2008

Desirable Burner/Flame Characteristics

- Well defined boundary conditions
- Easy optical access → more complete data
- Turbulence parameters at appropriate levels (Re, Da, u'/S_L, etc.)
  (what 'appropriate' means is open for discussion)
- Portable and repeatable
  (apply diagnostics in different labs)
- Velocity and scalar measurements with good statistical sample size
  (other measurements to be discussed)
- Variation of one or more parameters to which the flames are sensitive
  (particularly with respect to turbulence-chemistry interaction or a transition between combustion regimes)
- Steady flow (depending on modeling interest in unsteady cases)

Considerations

- Complex inflows: use detailed simulation to augment measurements?
- Turbulence generation: shear vs. grids?
- Selection based on:
  - Relevance (to this validation process)
  - Data quality, completeness, and availability (when?)
  - Interest from modelers (multiple groups and methods)
  - Willing victims (people who will coordinate comparisons)
- Use prescribed or preferred submodels in common

Potential Target Flames: Partially Premixed (Detached)

- Lifted jet flame in hot coflow (Sydney/Berkeley/Sandia)

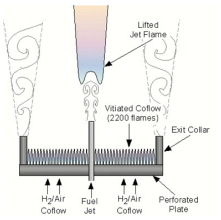

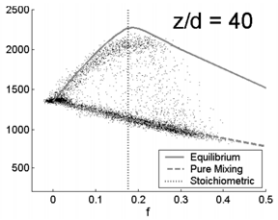

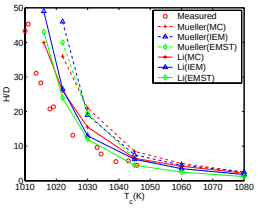

- Model Gas Turbine Combustor (DLR-Stuttgart)

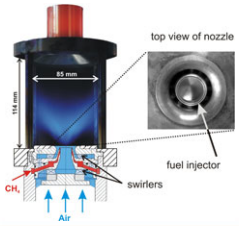

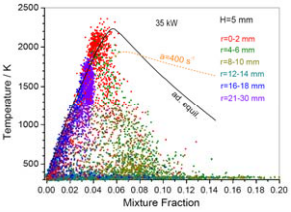

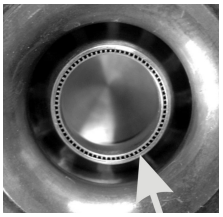

TNF9 Workshop, Montreal 2008

Potential Target Flames: Stratified Burners (1)

- V-Flames in stratified mixing layers (low u'/S_L, no mean shear)

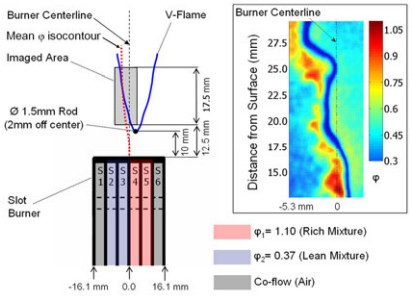

Cambridge
(poster – Sweeney)

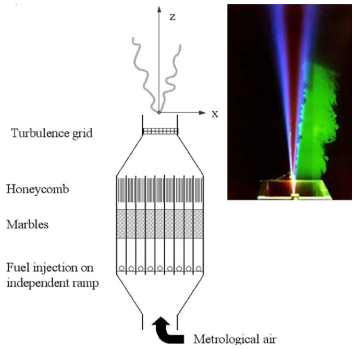

CORIA-INSA

TNF9 Workshop, Montreal 2008

Potential Target Flames: Stratified Burners (2)

- Conical flames in stratified mixing layers (higher u'/S_L, mean shear)

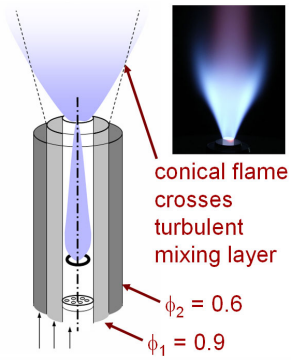

TU Darmstadt
(poster – Sefrin)

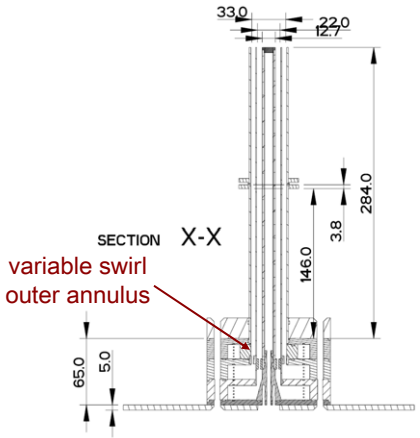

Cambridge
(work in progress)

Potential Target Flames: Stratified Burners (3)

- Enclosed flames

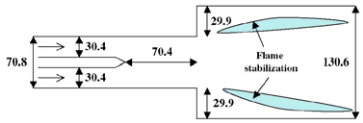

ORACLES

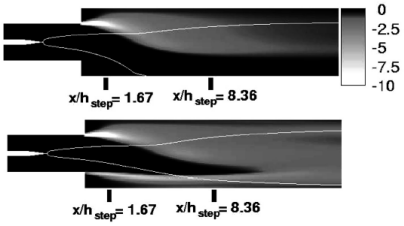

Robin 2006

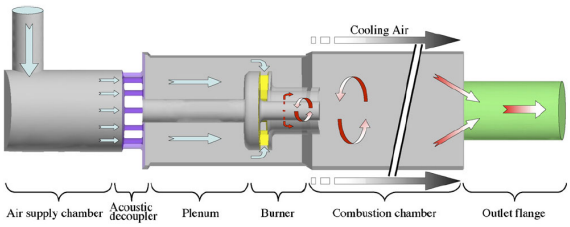

Twente University

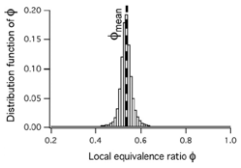

Sengissen 2007

Potential Target Flames: "Premixed" with Stratified Edges

- Nominally premixed flames that are not enclosed

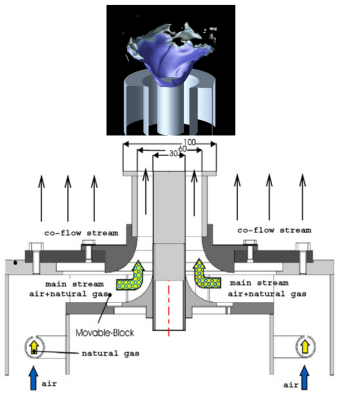

TECFLAM Premixed
TU Darmstadt

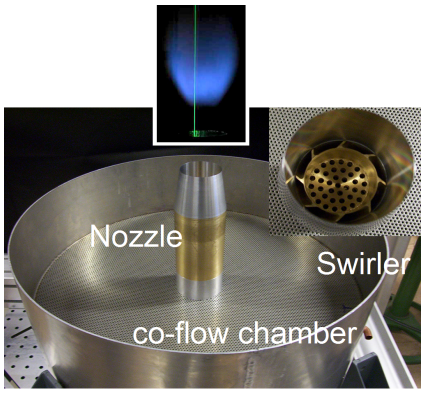

Low-Swirl (Cheng et al.)
TU Darmstadt

Potential Target Flames: Piloted Premixed Jet Burner

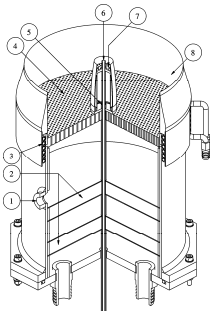

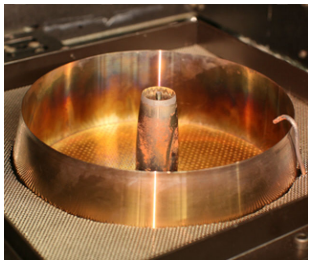

Sydney University
(Dunn – poster)

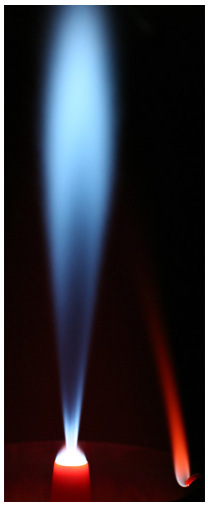

High jet velocity,
very rapid 3 stream mixing

Others Cases of Possible Interest (Comments Welcome)

- Purely premixed flames
- Lifted jet flames in air
- Jets and jet flames in cross flow (Angelberger proposal)
- Other jets in hot coflow, MILD (posters by Dally; Oldenhof)
- Forced ignition in turbulent flow (poster by Ahmed)
- Auto-ignition exp. and simulation (posters by Jones; Stankovic; Yoo)
- Elevated pressure (TU Darmstadt, DLR-Stuttgart)

TNF9 Workshop, Montreal 2008

Simple Map: Combustion Modes & Regimes of Some Available Flames

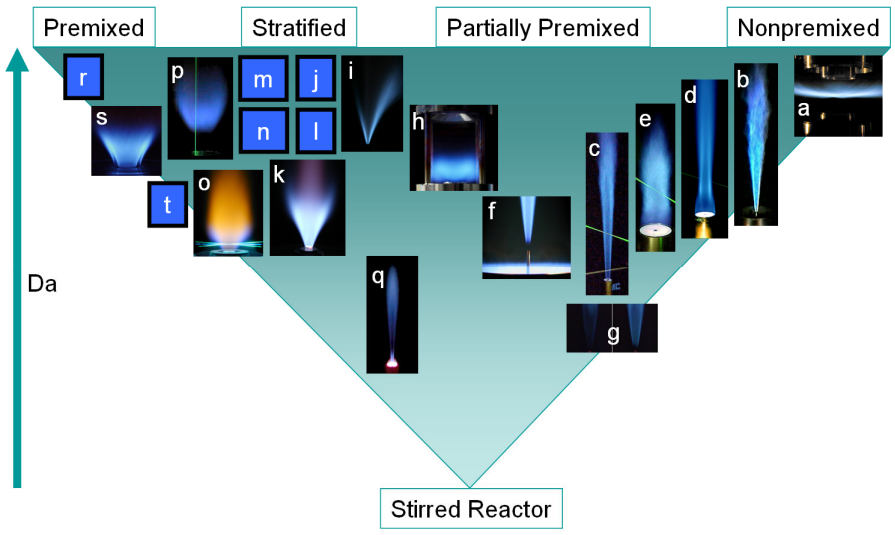

TNF9 Workshop, Montreal 2008

Discussion:

- Pros and Cons
- Insights from people who have measured or modeled particular flames
- Appropriate tests for models?
- Data completeness and availability (schedule?)
- Are there obvious near-term and longer term targets

Discussion:

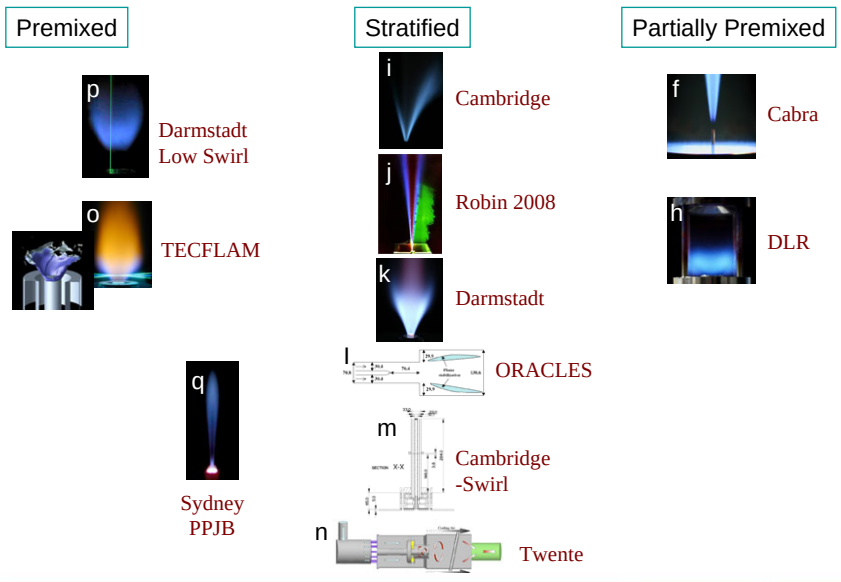

Challenges and Strategies in Addressing more Complex Fuels

Rob Barlow, Gilles Bourque, Jackie Chen,
J.-Y. Chen, Andreas Dreizler, Ed Law and
Peter Lindstedt

9th International Workshop on Measurement & Computation of Turbulent Non-premixed Flames

Montreal
July 31-August 2, 2008

Purpose of Session

Objective

Provide a broad view of the motivation and possibilities for extending fuels beyond methane.

Goals

Tentative priorities on fuels and some targets for what can be achieved in the next 4 to 6 years.

Linkage to combustion modes and burner configurations.

Outline of Talk

Background

Focus on turbulence chemistry interactions (TCI) for a wider range of fuels.

Industrial perspectives

Gas turbines for power/transport and automotive related.

How?

Reduced and detailed chemical mechanisms for new fuels.

Supporting experimental work.

Supporting DNS studies.

Combustion Modes and TCI

Practical Technical Challenges.

The auto-ignition in a turbulent flow field and the formation of pollutants. Ignition issues come to light in UNIBUS, HCCI and many other new combustion technologies such as Flameless Oxidation.

Pollutants include **carbon monoxide**, **particulates**, **oxides of nitrogen** and **oxygenated species**. Of these, oxygenated species represent a potentially new challenge.

Lower temperatures will also favour a different set of pathways for the formation and inter-conversion of **aromatics** and poly-aromatic hydrocarbons which may affect **nano-particle** properties.

What should our focus be?

Background to Fuels

Must understand how the fuel structure impacts practical behaviour in a quantitative manner.

A greater diversity of fuels will be used in the future: Bio-derived alcohols or ethers, FT generated fuels along with greater variations for fossil fuels including “awkward” compositions.

Increased fuel variability – more mixtures – some may make simple base fuels such as methane more difficult to handle.

What about our priorities?

Practical Fuels for Aviation and Ground Transport

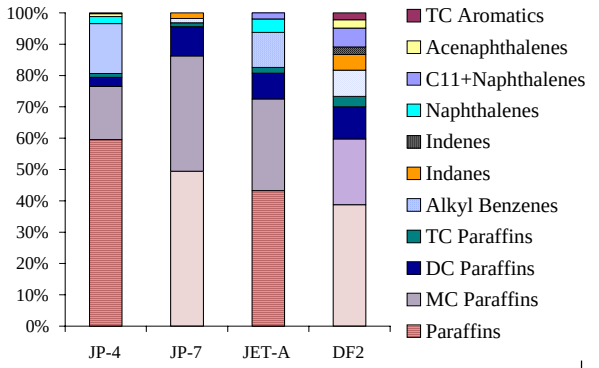

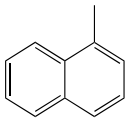

1-methyl naphthalene

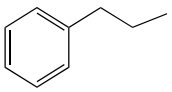

n-propyl benzene

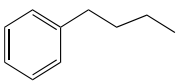

n-butyl benzene

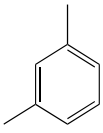

1,3-dimethyl benzene

C_nH_{2n+2}

alkanes

Some Surrogate Fuel Model Issues

(i) The accuracy of the surrogate fuel model wrt to selected key features (direct experimental tests possible).

(ii) The accuracy of the detailed chemical kinetic model (comparisons with relevant experimental data).

(iii) The accuracy of the reduced model (assessed by comparison with both experimental data and the starting mechanism).

(iv) The ability of the chosen turbulent calculation procedure (e.g. LES/FMDF) to include direct chemistry effects.

Too complicated for TNF in the 4-6 year time period?

Progress is being made, e.g. through AFOSR initiatives, and individual components (e.g. n-heptane. iso-octane and/or toluene) may well be possible.

Auto Ignition of Toluene in Turbulent Flows

Toluene/Air Flame
Pressure: P = 1 atm
Nozzle Diameter: D = 4.57 mm

Central Fuel Jet
U_{bulk} = 100 m/s , Re = 28000, T = 450 K
Fuel stoichiometry: Φ=1.0-2.0

Vitiated Co-flow
U = 5.4 m/s , Re = 23300, T = 1350-1500 K

Calculation Details
Number Particles/Cell = 100
Number of Cells in Radial Direction = 70
Number of Time Steps = ~3000

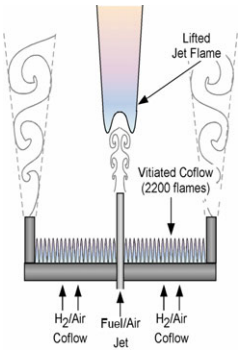

Applied Chemistry
164 Species and 951 reactions

Impact of Stoichiometry and Pressure on Auto-ignition: Axial Profiles

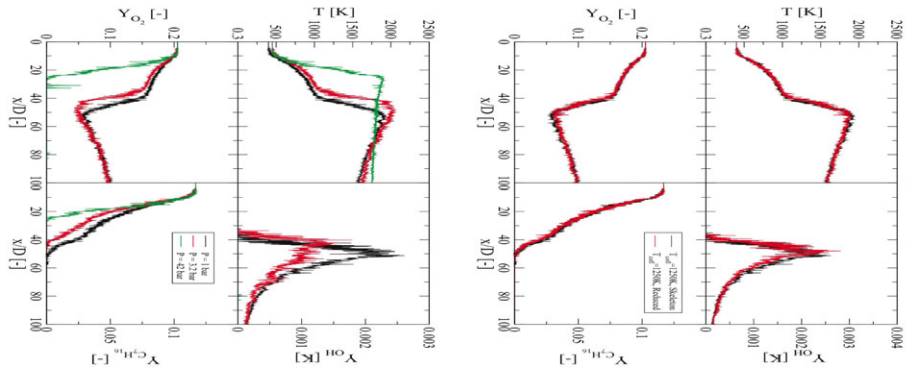

Practical challenges

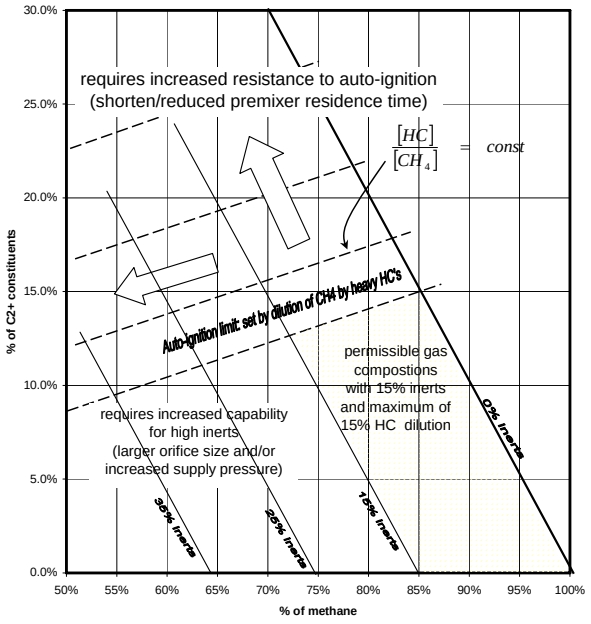

Natural Gas Composition Envelopes: Including the effects of inerts and heavy hydrocarbons

Rolls-Royce

Fuel Flexibility Issues

- Combustion operability:
  - Flashback/Autoignition in premixer
  - Flame anchoring/placement; Thermo-acoustic
  - Accel/Decel; Lean blow off, Blow-out
- Emission compliance
  - NOx, CO, UHCs, VOC, etc…
  - Smoke, Soot, PM-10, etc…
- Hot end Component life:
  - Flame placement
  - Fuel impurity effect on materials
  - Fuel compatibility with supply system

RPL: Can a suitable "model" fuel be agreed?

Rolls-Royce

Oxygenated Fuels

Fuels with oxygen content are likely to feature much more strongly in some sectors.

Such fuels are likely to have beneficial sooting tendencies so should be amenable to experimentation.

Possible choices include ethanol and dimethyl ether.

Is this a fruitful avenue?

It could, for example, potentially allow the studies of oxygenated pollutants (e.g. caused by incomplete combustion).

13

Interim Summary

Plenty of applications with TCI and new fuels. Possibilities for the latter include:

- Enrichment of methane with LPG components.
- Oxygenated fuels.
- Steps towards practical transportation fuels.

14

Reduced and detailed chemical mechanisms related to transportation fuels

Typical Sizes of Detailed Mechanisms

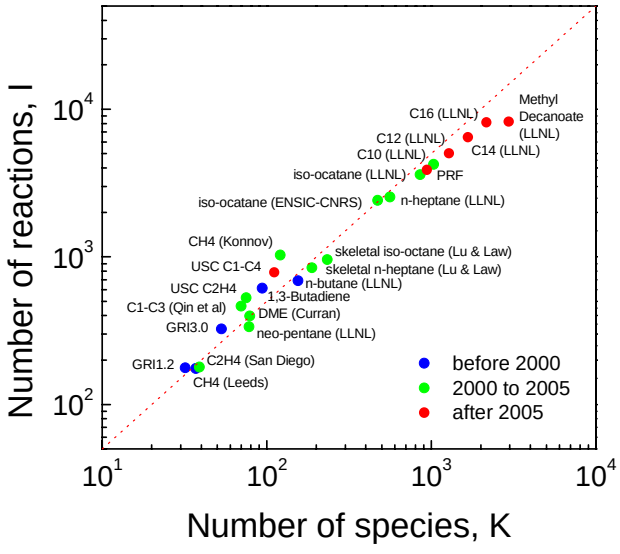

Conventional Approach for Development of Reduced Mechanisms (J.Y.)

Detailed

(# of species) 857

Skeletal

Rate of production Analysis & Sensitivity analysis, DRG, Lumping, ...

215

Automatic Selection & Testing

Reduced

Reduced w/ QSSA
Search Algorithm for search QSSA species
New Algorithm for QSSA

63

Auto-ignition Chemistry

2nd ignition
~1000K

1st ignition

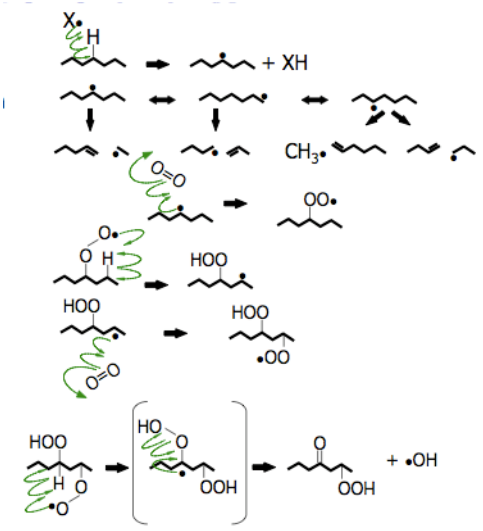

Faravelli et al. (2005).

Development of Skeletal and Reduced Mechanisms (J.Y.)

Challenge

Low temperature chemistry at high pressure is complex involving many isomers & pathways.

Status

Various methods are available, such as sensitivity, rate analysis, DRG & its variants, chemical lumping……

Some observations

None of methods can give the optimal mechanism for given a regime. Iterative trial & error approach can be used but not efficient when size is large.

Significant computational time is required for large mechanisms and only limited bench tests can be performed.

Example: Identification of QSS Species by targeted conditions to represent engine operation states

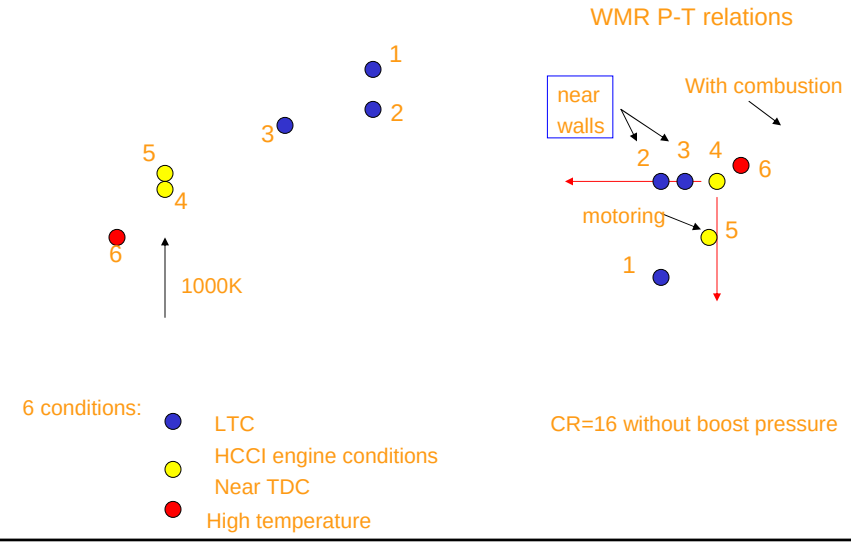

Example: a 63-species reduced chemistry derived from a large iso-octane mechanism (857 species)

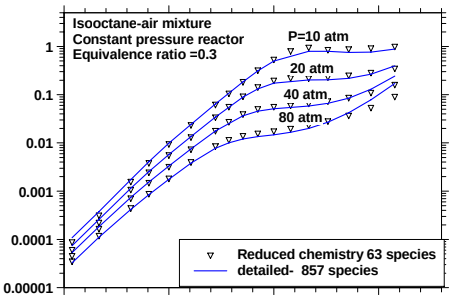

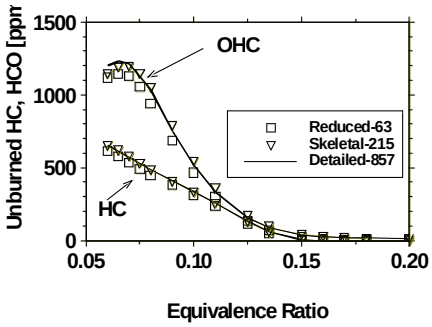

Good agreement is achieved for both auto-ignition & emissions

Example: Ignition Delay Times

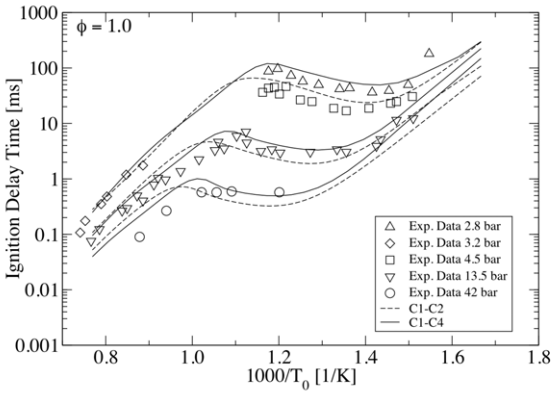

Ignition delay times obtained with simplified chemistry for n-heptane coupled with C_1-C_2 and C_1-C_4 sub-mechanisms for a stoichiometric mixture.

Shock tube data from Ciezki and Adomeit (1993) with Φ = 0.5 - 2.0 in Air, T = 625 - 1250 K and P = 3.2 - 42 bar among others.

Application to a Cabra Burner

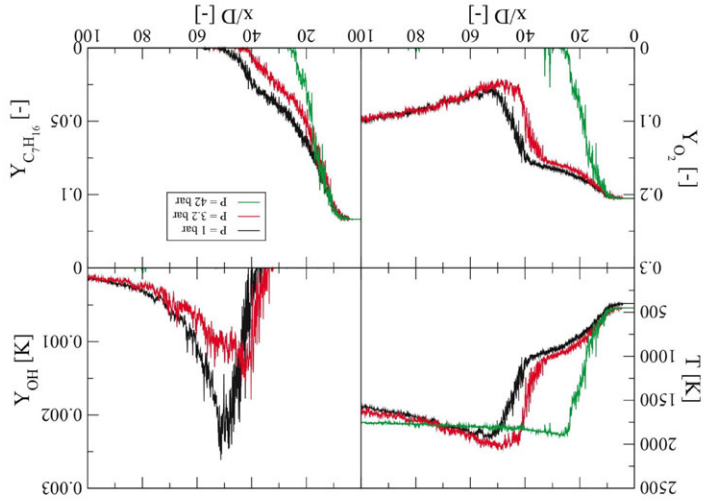

Related Topics (J.Y.)

Development

Existing approaches are not adequate for generation of optimal skeletal & reduced chemistry due to strong nonlinear systems.

Validation

Bench-mark test flames are limited to those can be computed by detailed chemistry, such as auto-ignition, PSR (0-d), flame speed, extinction (1-D); no representations of turbulent flames under strong turbulence-chemistry interactions, such flame extinction & re-ignition.

Implementation in simulations

Numerical techniques for reduction of stiffness, speed storage & retrieval,…

Explicit Versus Implicit Solvers for Large Mechanisms

- Cost of implicit solvers ~ O(K^3)
  - Evaluation of analytic Jacobian, O(K)
  - LU decomposition of Jacobian, O(K^3)
  - …
- Cost of explicit solvers, O(K)
  - Chemical rates, synchronization & misc., O(K)
  - Detailed diffusion, O(K^2, or K^3), eliminable with diffusive species bundling (Lu & Law 2007)
- Explicit solver is asymptotically optimal in efficiency for large mechanisms, provided stiffness can be removed

Average CPU Time for3-D DNS (S3D) with explicit RK

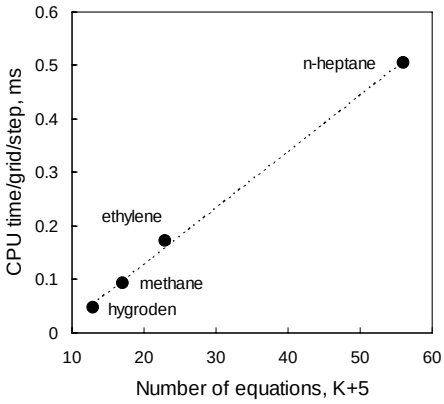

A Systematic Procedure for Dimension Reduction & Stiffness Removal

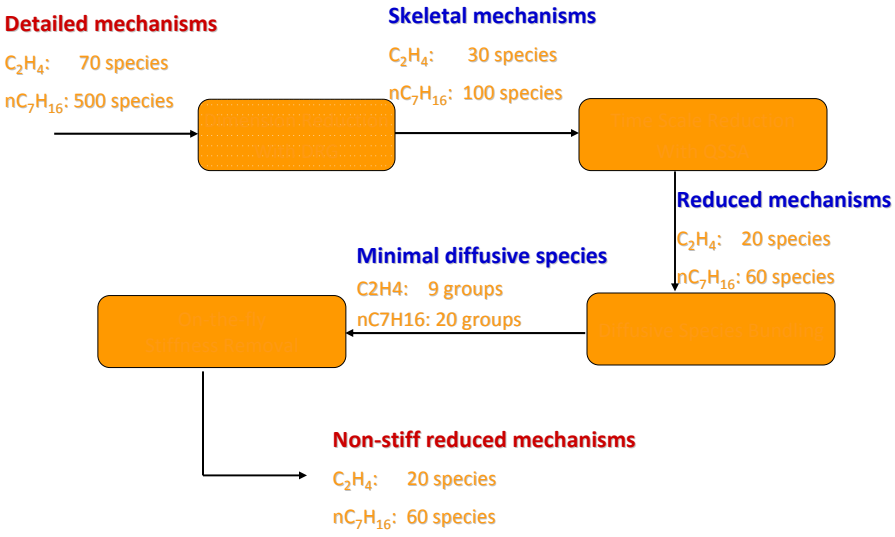

Chemistry Models for DNS

- Usual CH_4-Air mechanisms are not suitable for DNS
- Custom chemistry for DNS
  - By T. Lu and C.K. Law (Princeton U.)

- Starting with GRI1.2
  - 32 species, 177 reactions
- Identify species for elimination
  - Directed relation graph (DRG)
  - Sensitivity analysis
- Eliminate unimportant species
- Quasi-steady state assumption for CH_2OH, CH_2, $CH_2(s)$, HCO
  - Explicit algebraic relations
  - No costly iterations
- Ethylene-air and n-heptane-air (high pressure, low temperature)

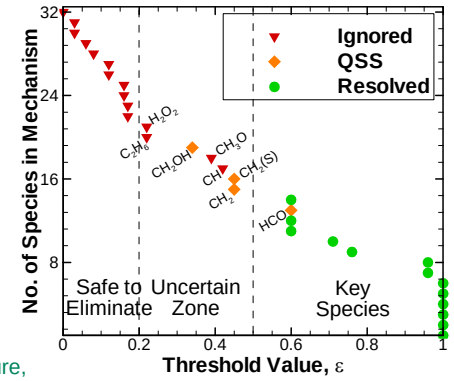

DNS simulations

3D Planar Jet Flames in Heated Coflow

- Hydrogen/air case
  - 3D slot burner configuration: $L_x \times L_y \times L_z = 24 \times 32 \times 6.4\text{mm}^3$ with 940M grid points
  - High fuel jet velocity (347m/s)
  - Nozzle size for fuel jet, H = 1.92mm
  - Re_{jet} = 11,000; τ_j = 0.07ms
  - Cold fuel jet (65% H_2 + 35% N_2) at 400K
    - Stoichiometric mixture fraction, $\xi_{st} \approx 0.2$
  - Hot coflow air at 1,100K
- Ethylene/air case
  - 3D slot burner configuration: $L_x \times L_y \times L_z = 30 \times 40 \times 6\ \text{mm}^3$ with 1.28B grid points
  - High fuel jet velocity (204m/s)
  - Nozzle size for fuel jet, H = 2.0mm
  - Re_{jet} = 10,000; τ_j = 0.15ms
  - Cold fuel jet (18% C_2H_4 + 82% N_2) at 550K
    - Stoichiometric mixture fraction, $\xi_{st} \approx 0.27$
  - Hot coflow air at 1,550K

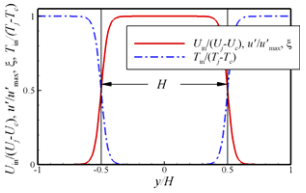

Inlet boundary conditions for temperature, species and velocity

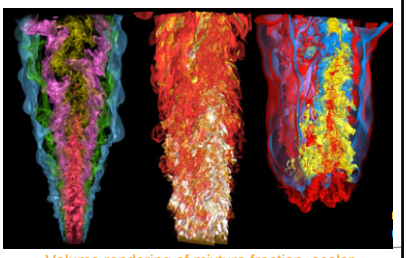

Volume rendering of mixture fraction, scalar dissipation rate and mass fraction of OH an HO_2 of hydrogen/air lifted jet flame in a heated coflow

Sandia National Laboratories

CRF

Hydrogen/Air Lifted Jet Flame

(C.S. Yoo, R. Sankaran, J.H. Chen, submitted to *J. Fluid Mech.*, 2008,
T. Lu, C.S. Yoo, J.H. Chen, C.K. Law, submitted to *J. Fluid Mech.*, 2008)

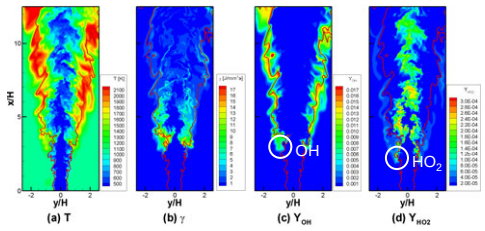

Isocontours of temperature, heat release rate, Y_{OH} and Y_{HO2}. The red line represents the stoichiometric mixture fraction iso-lines

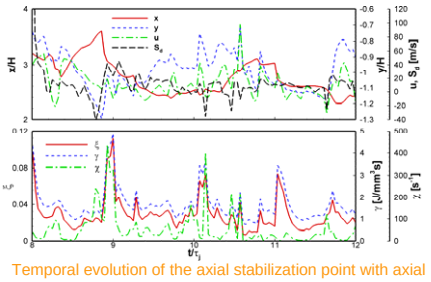

Temporal evolution of the axial stabilization point with axial velocity, S_d (top) and mixture fraction, heat release rate, and scalar dissipation rate (bottom)

- Flame base stabilizes in lean mixture
- HO_2 radical in auto-ignition
  - Builds up upstream of OH and other intermediate radicals (H, H_2O_2)
  - Precursor of auto-ignition in hydrogen-air chemistry
  - Auto-ignition occurs at the flame base
- Stabilization mechanism
  - Ignition occurs in lean mixtures with low χ
  - Stabilization point correlation with jet:
    - The stabilization point propagates upstream following a coherent jet structure
    - Local extinction occurs by high χ and the point moves downstream
    - Ignition occurs in another coherent jet structure

Sandia National Laboratories

CRF

Ethylene/Air Lifted Jet Flame

(C.S. Yoo, E. Richardson, R. Sankaran, J.H. Chen, presented at the TNF9 poster session)

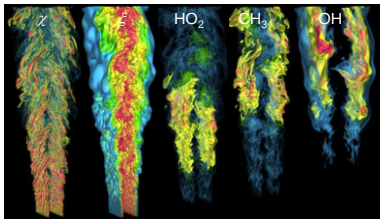

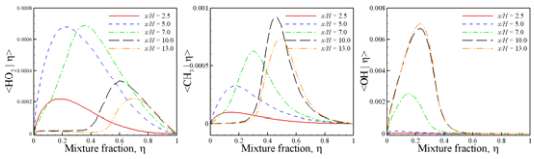

Conditional mean of mass fraction of HO_2, CH_3, and OH

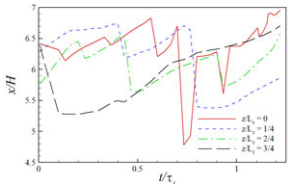

Temporal evolution of stabilization points at different spanwise locations

- Flame base dynamics
  - Similar to the flame base movement of hydrogen/air lifted jet flame

- Upstream of the flame base: HO_2 and CH_3 accumulate in hot, fuel-lean mixtures
  - $C_2H_4 + O \rightarrow CH_3 + HCO$
  - $HCO + O_2 \rightarrow HO_2 + CO$
- Near the flame base: radical explosion induces thermal run-away
  - $CH_3 + HO_2 \rightarrow CH_3O + OH$
  - $CH_3O \rightarrow CH_2O \rightarrow HCO \rightarrow (H, CO, HO_2)$
- Downstream of the flame base: high-temperature diffusion flame develops at ξ_{st}
  - $H + O_2 \rightarrow O + OH$

Sandia National Laboratories

CRF

Stratified Bunsen DNS: Configuration

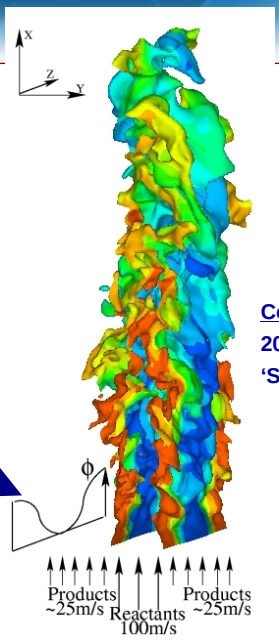

Planar Bunsen flame

Reactant Temperature=800K

Jet Velocity = 100m/s

Slot jet width, h_j = 1.8mm

Domain = 13x12x4h_j

Mean φ = 0.7

Tan*h* φ Variation along z axis

Computational approach

20μm grid, 4ns time step

'S3D' DNS: Compressible N-S

4th order R-K in time

8th order spatially

MPI ~ 10,000 cores

Sandia National Laboratories

CRF

Stratified Bunsen DNS: Configuration

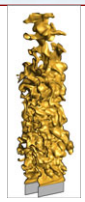
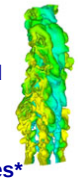
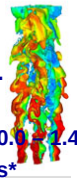

	Premixed	Low Strat.	High Strat.	
Φ variation	0.7	0.41 - 1.0	0.0 – 2.46	
Chemistry	13 species*	13 species*	28 species**	
S_L variation (m/s)	1.8	0.6-2.5	0.0-2.5	[PREMIX]
δl variation (mm)	0.29	0.46-0.26	inf-0.26	
Turbulence intensity (u'/S_L)	10	32 - 7.3	inf – 7.3	
Integral length scale (l_t/δ_L)	1.5	0.98 – 1.8	0.0 – 1.8	TRZ***
Karlovitz Number $(\alpha/S_L l_k)^2$	5.2	47 – 2.5	inf – 2.5	BRZ ?
$Ka^*(\delta_H/\delta_L)^2$	1.9	17.7 – 1.0	inf – 1.0	

* R. Sankaran et al. ProCI 31 (2007) 1291-1298

** T. Lu and C.K. Law. 5th US Combustion Meeting, San Diego (2007)

*** R. Sankaran et al. 5th US Combustion Meeting, San Diego (2007)

Sandia National Laboratories

CRF

Summary

Three options on fuels: (i) Augmented methane, (ii) oxygenated fuels and (iii) start on transportation fuels.

Relevant experimental and DNS studies are probably possible, but must be strongly targeted.

The choice of fuel is likely to be influenced by the combustion regime (e.g. partially premixed will reduce soot).

The choice of burner geometries is likely to be influenced by the above and, possibly, considerations related to physical parameters related to modes/regimes.

Notes

Aspects of LES Quality

For the Sydney Bluff Body Flames &
Darmstadt IC Engine Simulations

Imperial College London

1

Motivation

- Sydney Bluff-Body Flames have proven to be sensitive
- LES may get correct predictions
- Focus on prediction of flow-field first
- Assess error and use techniques to ensure quality
- Return to turbulence-chemistry interaction afterwards

Imperial College London

2

Overview

- The Sydney Flames
- Used LES Codes
- Classical results
- Attempt to assess qualities
  - Algebraic error indicators
  - Behaviour of indicators
  - Indicators for Darmstadt IC engines
- Conclusions

Imperial College London

TNF WORKSHOP 9

3

Application: Sydney Flames

- Cylindrical bluff-body
- Homogeneous air coflow
- Fuel jet from centre of bluff-body
- Rich recirculation zone
- Flame outside recirculation zone
- Fine grid for outer shear layer

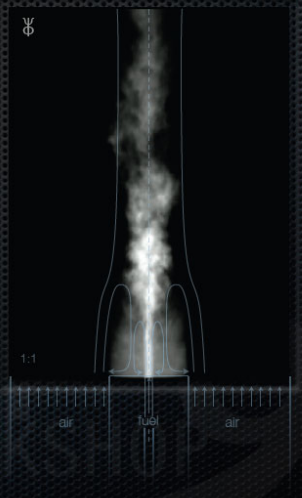

Imperial College London

4

Contributions

- ANSYS-CFX/Fluent, G. Goldin
- TU-Darmstadt, F. Hahn, C. Olbricht
- Imperial College London, A. Kempf

Imperial College London

5

ANSYS

- Finite-Volume unstructured grid
- Coupled and Segregated (SIMPLE) algorithms
- Spatial: 2nd-order Bounded Central Differences (BCD) (momentum) and various upwind schemes (scalars)
- Temporal: Second-order implicit (Euler) and explicit
- Written in C, parallelized with MPI
- Models for combustion, spray, radiation, ...

Imperial College London

6

FASTEST-ECL Code

- Geometry flexible, block-structured, boundary fitted
- Parallel (Domain Decomposition)
- Generally 2nd order (TVD for scalars)
- Projection Based Pressure Correction
- Explicit Fractional Step Method
- Steady Flamelets, FGM,
  Stochastic Fields, Droplet Tracking

Imperial College London

7

ΨΦ-Code

- Transport any scalar Φ, calculate any scalar Ψ
- Simple, modular, easy to develop, maintain, learn
- F-2003, vector, parallel → future streaming hardware
- Generally 2nd order (TVD for scalars)
- Robust pressure correction based on flowsi (TUD)
- Particles, Steady Flamelets, FSD

Imperial College London

8

Cases

NRBB
air, 20 m/s, 61 m/s
velocity measurements

HM1e
fuel, 35 m/s, 108 m/s
velocity measurements

HM1
fuel, 40 m/s, 118 m/s
scalar measurements

Imperial College London

9

Grid Variation

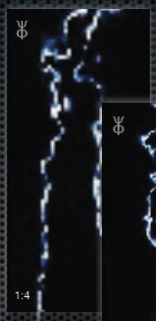

Coarse
$0.6 \cdot 10^6$
0.5^3 mm^3, 40h (50h)

Medium
$5.0 \cdot 10^6$
1.0^3 mm^3, 250h (350h)

Fine
$40.0 \cdot 10^6$
2.0^3 mm^3, 2100 h (2700h)

Imperial College London

10

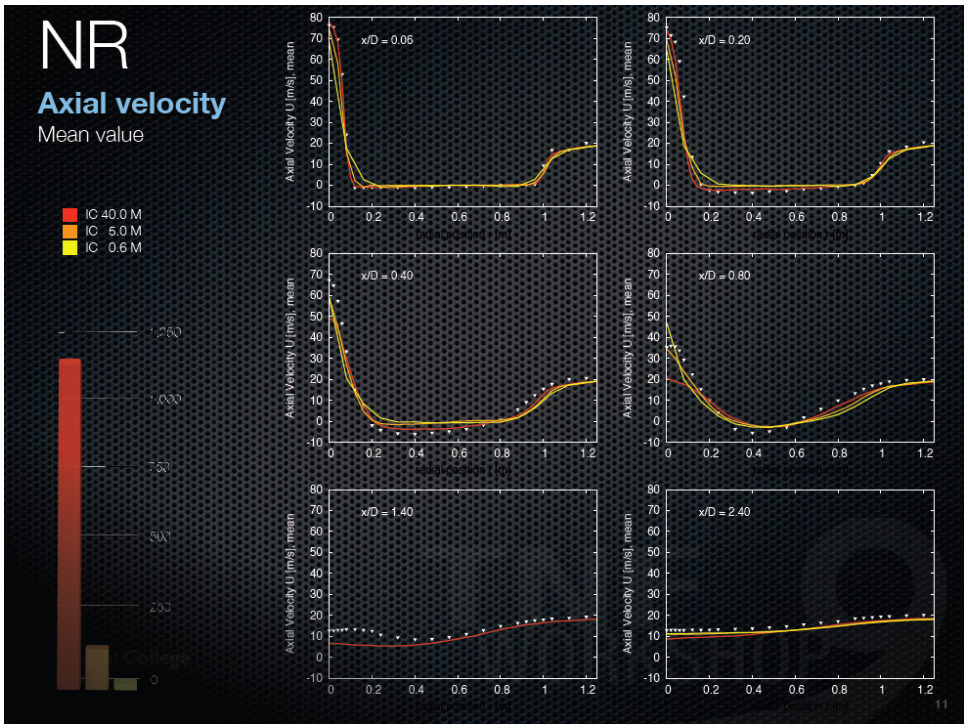
NR
Axial velocity
Mean value
IC 40.0 M
IC 5.0 M
IC 0.6 M
x/D = 0.06
x/D = 0.20
x/D = 0.40
x/D = 0.80
x/D = 1.40
x/D = 2.40
Axial Velocity U [m/s], mean
11

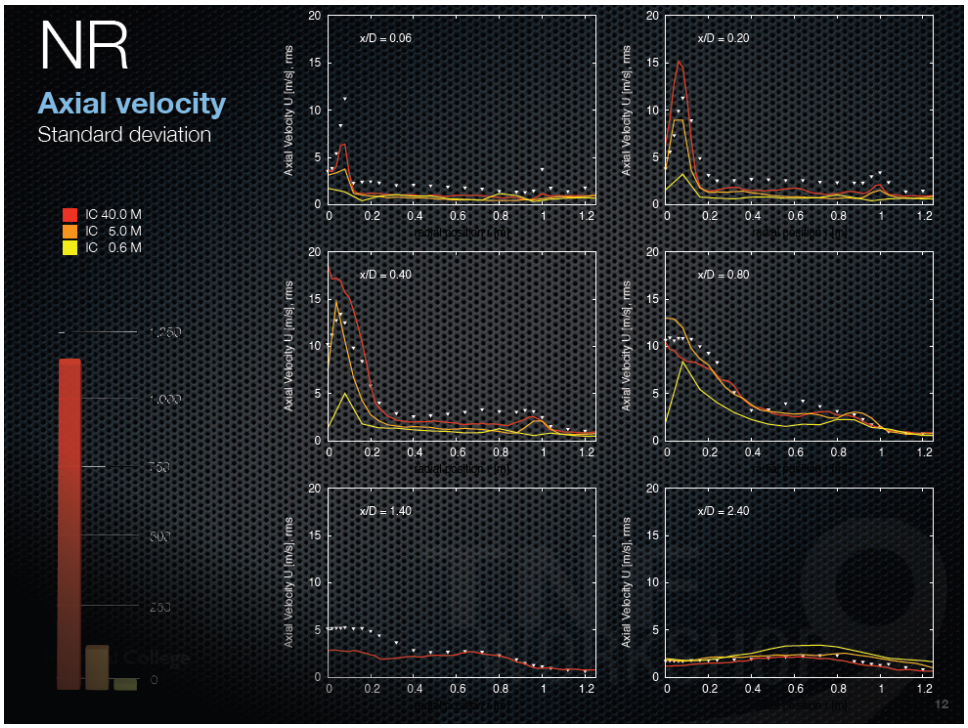
NR
Axial velocity
Standard deviation
IC 40.0 M
IC 5.0 M
IC 0.6 M
x/D = 0.06
x/D = 0.20
x/D = 0.40
x/D = 0.80
x/D = 1.40
x/D = 2.40
Axial Velocity U [m/s], rms
12

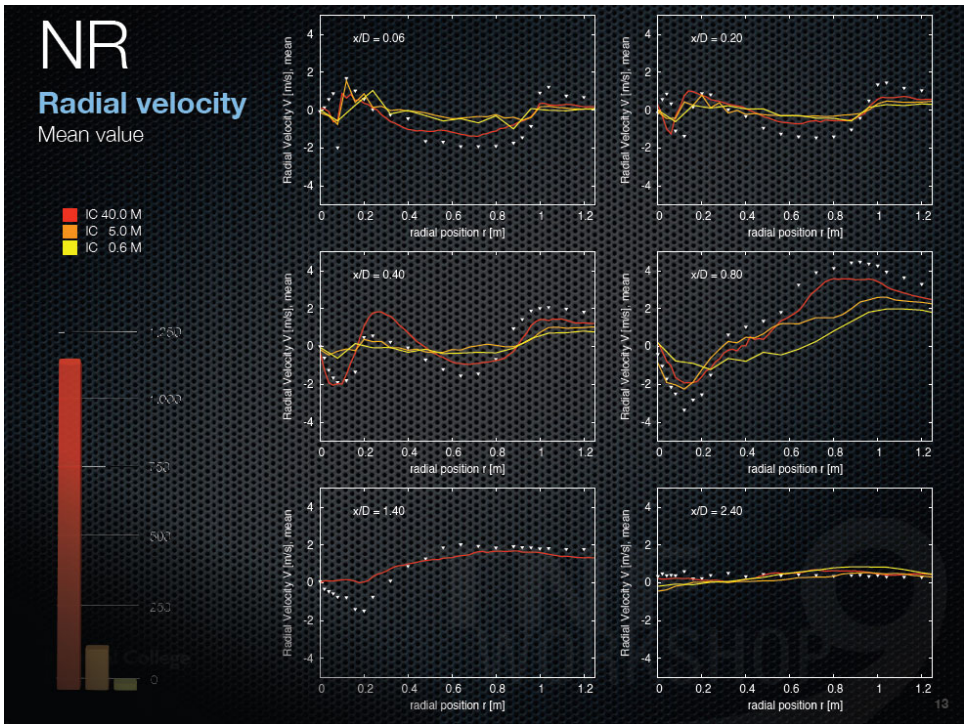
NR
Radial velocity
Mean value
IC 40.0 M
IC 5.0 M
IC 0.6 M
x/D = 0.06
x/D = 0.20
x/D = 0.40
x/D = 0.80
x/D = 1.40
x/D = 2.40
Radial Velocity V [m/s], mean
radial position r [m]
13

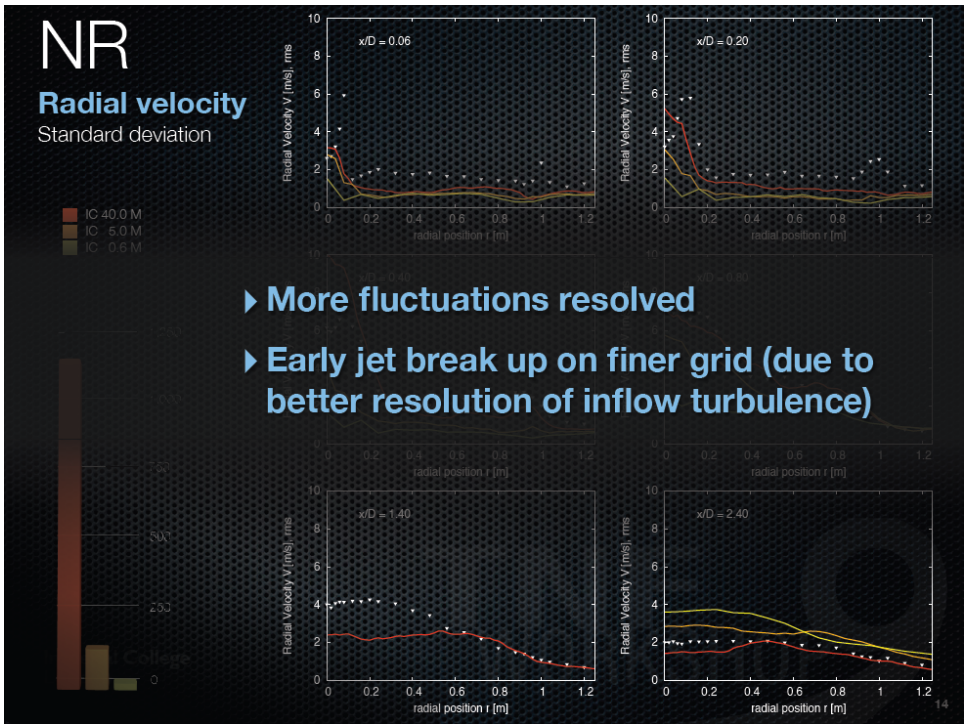
NR
Radial velocity
Standard deviation
IC 40.0 M
IC 5.0 M
IC 0.6 M
x/D = 0.06
x/D = 0.20
x/D = 1.40
x/D = 2.40
Radial Velocity V [m/s], rms
radial position r [m]
More fluctuations resolved
Early jet break up on finer grid (due to better resolution of inflow turbulence)
14

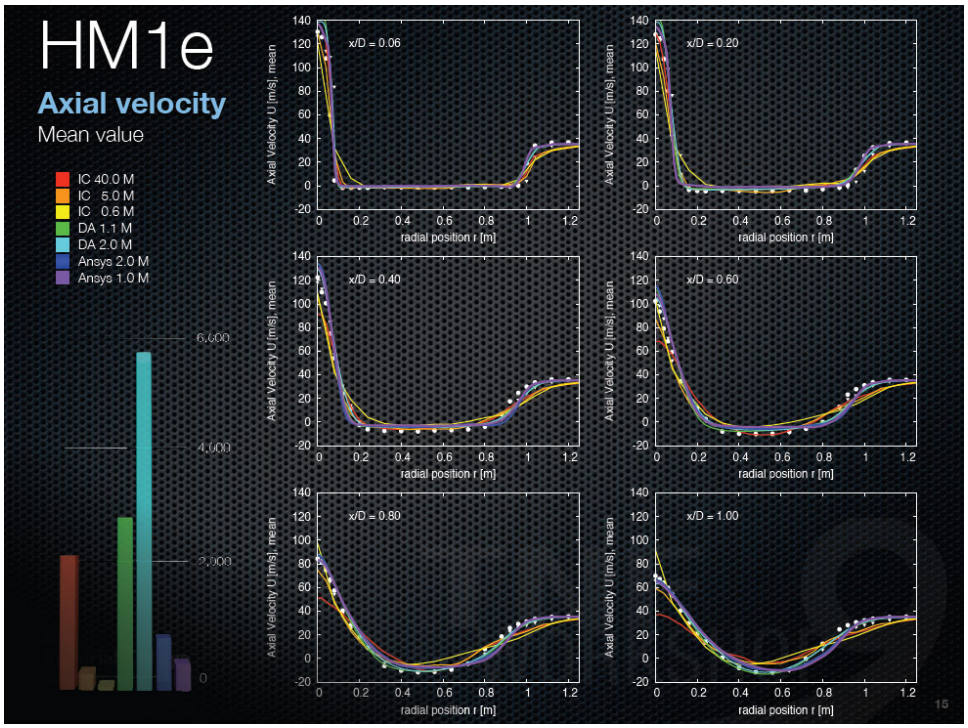
HM1e
Axial velocity
Mean value
IC 40.0 M
IC 5.0 M
IC 0.6 M
DA 1.1 M
DA 2.0 M
Ansys 2.0 M
Ansys 1.0 M
6,000
4,000
2,000
0
x/D = 0.06
x/D = 0.20
x/D = 0.40
x/D = 0.60
x/D = 0.80
x/D = 1.00
Axial Velocity U [m/s], mean
radial position r [m]
15

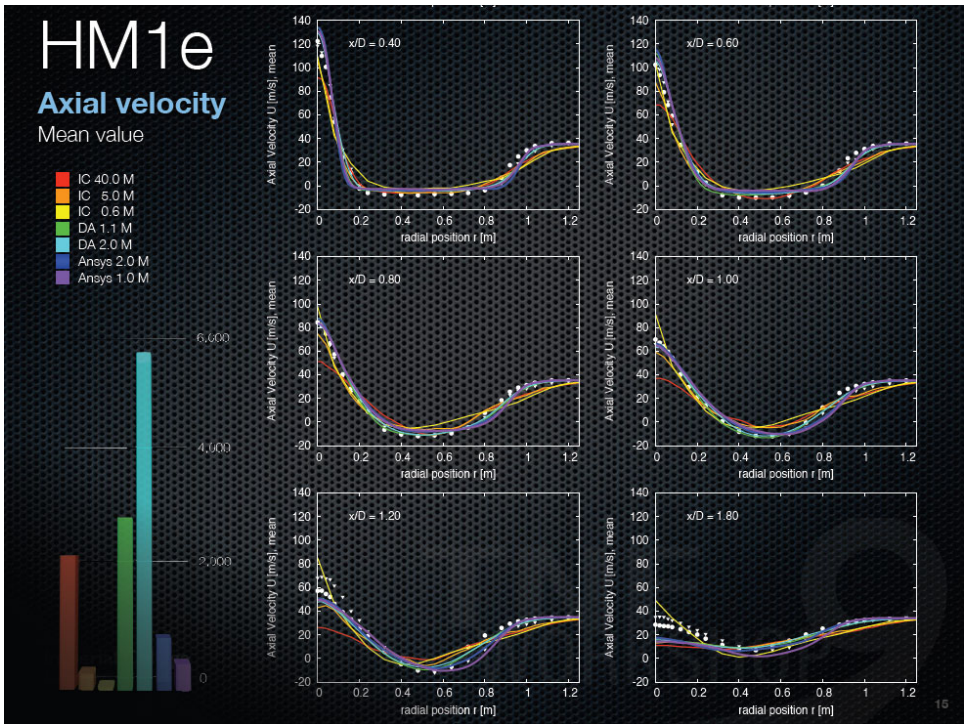
HM1e
Axial velocity
Mean value
IC 40.0 M
IC 5.0 M
IC 0.6 M
DA 1.1 M
DA 2.0 M
Ansys 2.0 M
Ansys 1.0 M
6,000
4,000
2,000
0
x/D = 0.40
x/D = 0.60
x/D = 0.80
x/D = 1.00
x/D = 1.20
x/D = 1.80
Axial Velocity U [m/s], mean
radial position r [m]
15

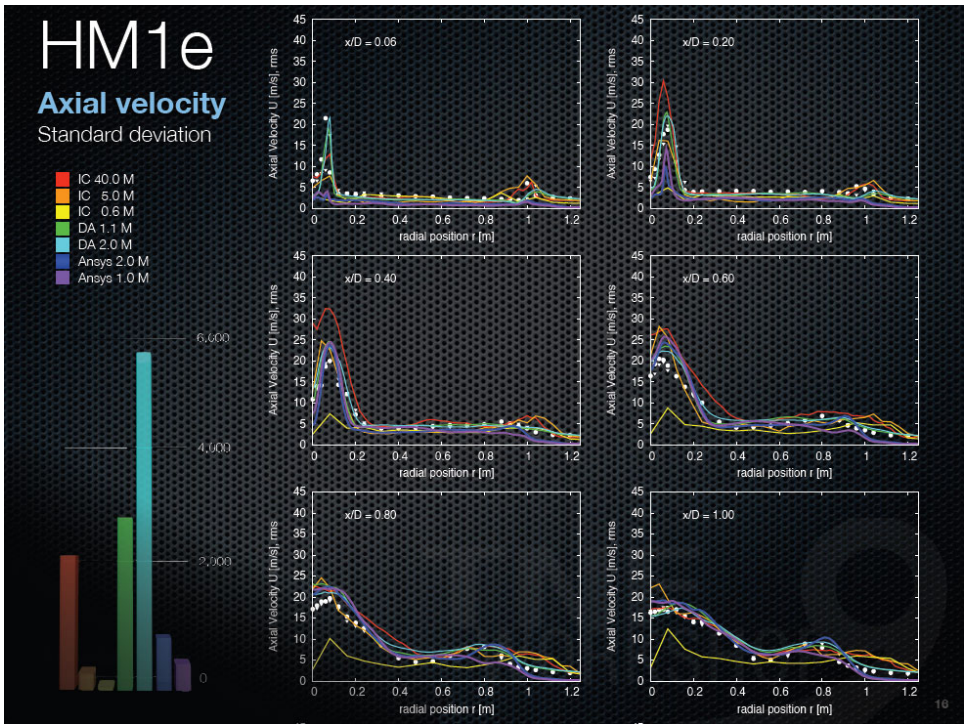
HM1e
Axial velocity
Standard deviation
IC 40.0 M
IC 5.0 M
IC 0.6 M
DA 1.1 M
DA 2.0 M
Ansys 2.0 M
Ansys 1.0 M
6,000
4,000
2,000
0
x/D = 0.06
x/D = 0.20
x/D = 0.40
x/D = 0.60
x/D = 0.80
x/D = 1.00
Axial Velocity U [m/s], rms
radial position r [m]

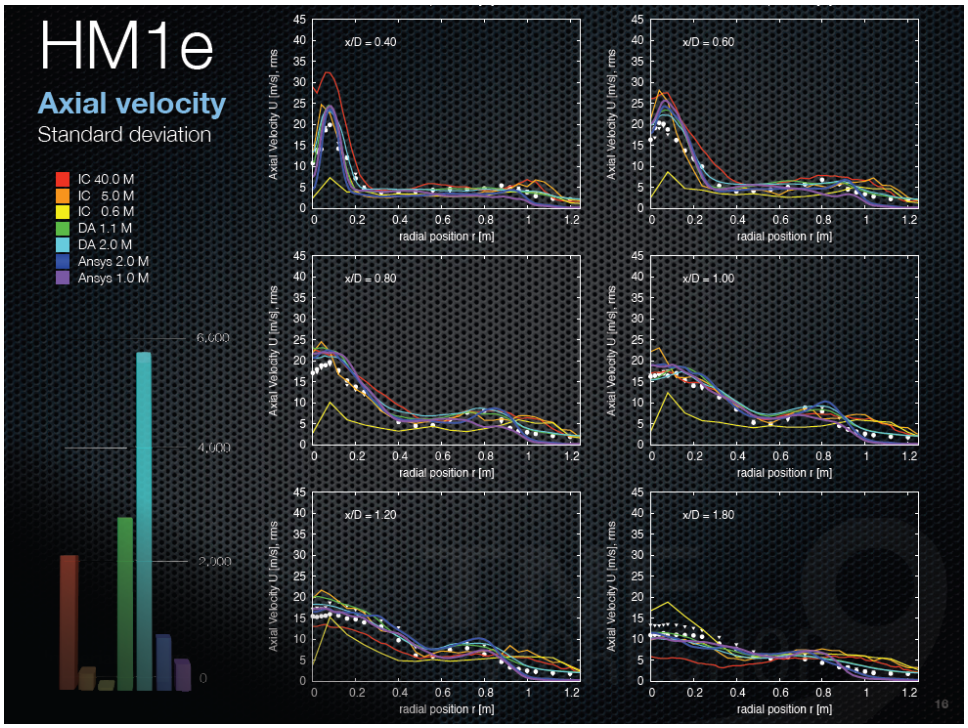
HM1e
Axial velocity
Standard deviation
IC 40.0 M
IC 5.0 M
IC 0.6 M
DA 1.1 M
DA 2.0 M
Ansys 2.0 M
Ansys 1.0 M
6,000
4,000
2,000
0
x/D = 0.40
x/D = 0.60
x/D = 0.80
x/D = 1.00
x/D = 1.20
x/D = 1.80
Axial Velocity U [m/s], rms
radial position r [m]

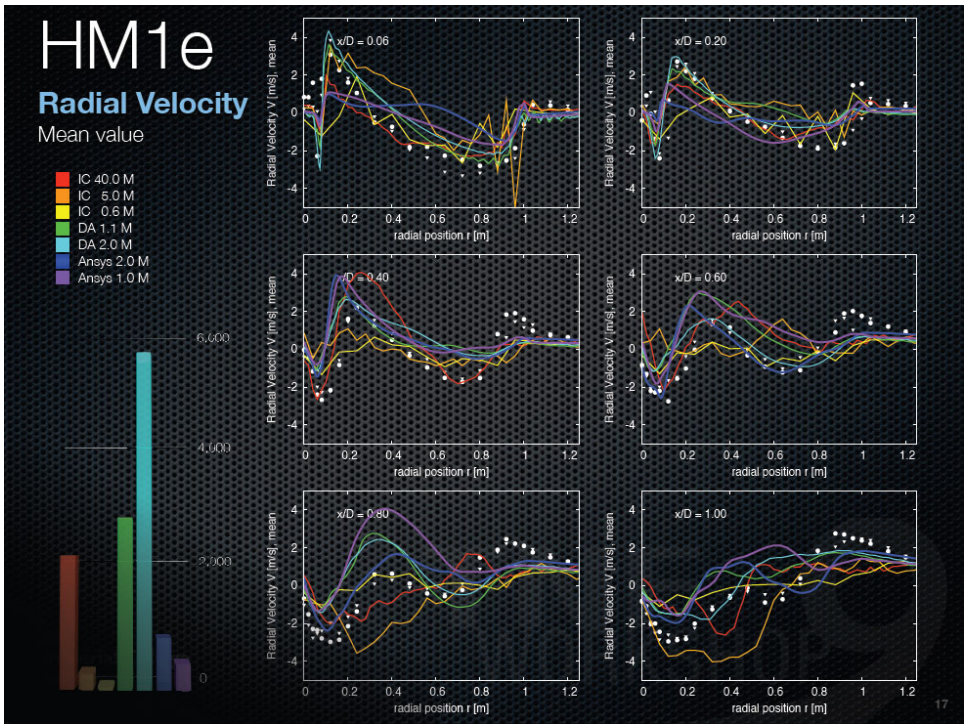
HM1e
Radial Velocity
Mean value
IC 40.0 M
IC 5.0 M
IC 0.6 M
DA 1.1 M
DA 2.0 M
Ansys 2.0 M
Ansys 1.0 M
6,000
4,000
2,000
0
x/D = 0.06
x/D = 0.20
x/D = 0.40
x/D = 0.60
x/D = 0.80
x/D = 1.00
Radial Velocity V [m/s], mean
radial position r [m]
17

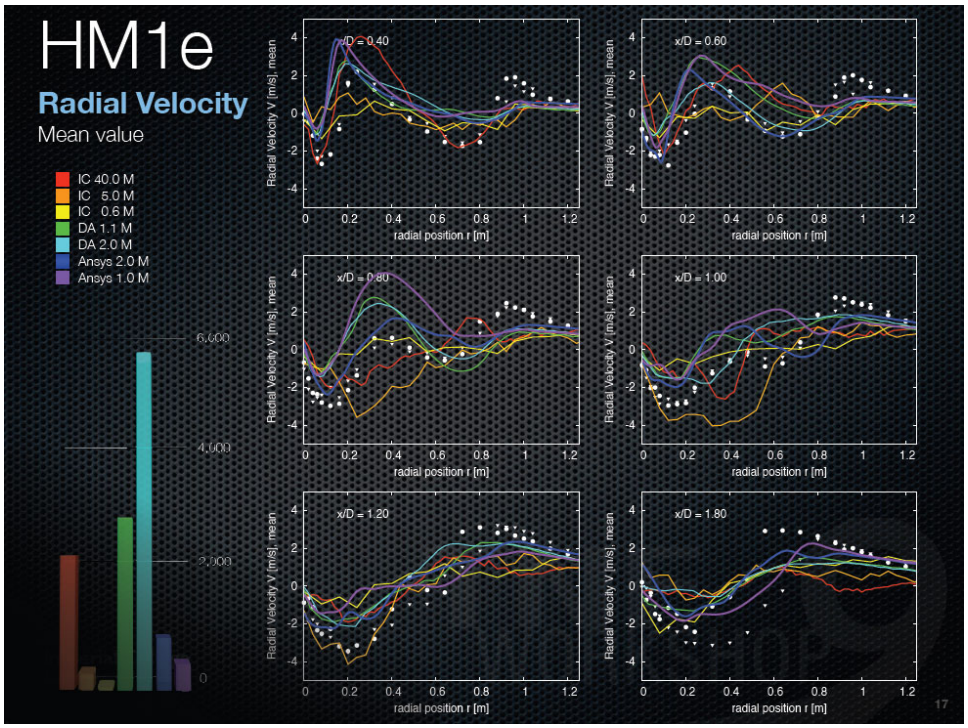
HM1e
Radial Velocity
Mean value
IC 40.0 M
IC 5.0 M
IC 0.6 M
DA 1.1 M
DA 2.0 M
Ansys 2.0 M
Ansys 1.0 M
6,000
4,000
2,000
0
x/D = 0.40
x/D = 0.60
x/D = 0.80
x/D = 1.00
x/D = 1.20
x/D = 1.80
Radial Velocity V [m/s], mean
radial position r [m]
17

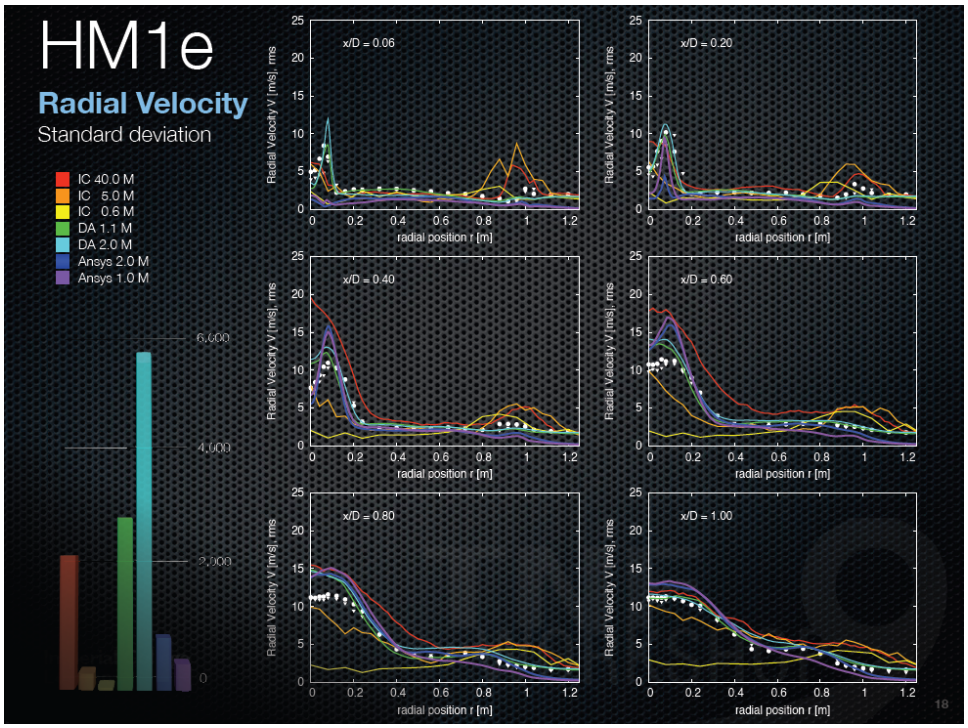
HM1e
Radial Velocity
Standard deviation
IC 40.0 M
IC 6.0 M
IC 0.6 M
DA 1.1 M
DA 2.0 M
Ansys 2.0 M
Ansys 1.0 M
6,000
4,000
2,000
0
x/D = 0.06
x/D = 0.20
x/D = 0.40
x/D = 0.60
x/D = 0.80
x/D = 1.00
Radial Velocity V [m/s], rms
radial position r [m]
18

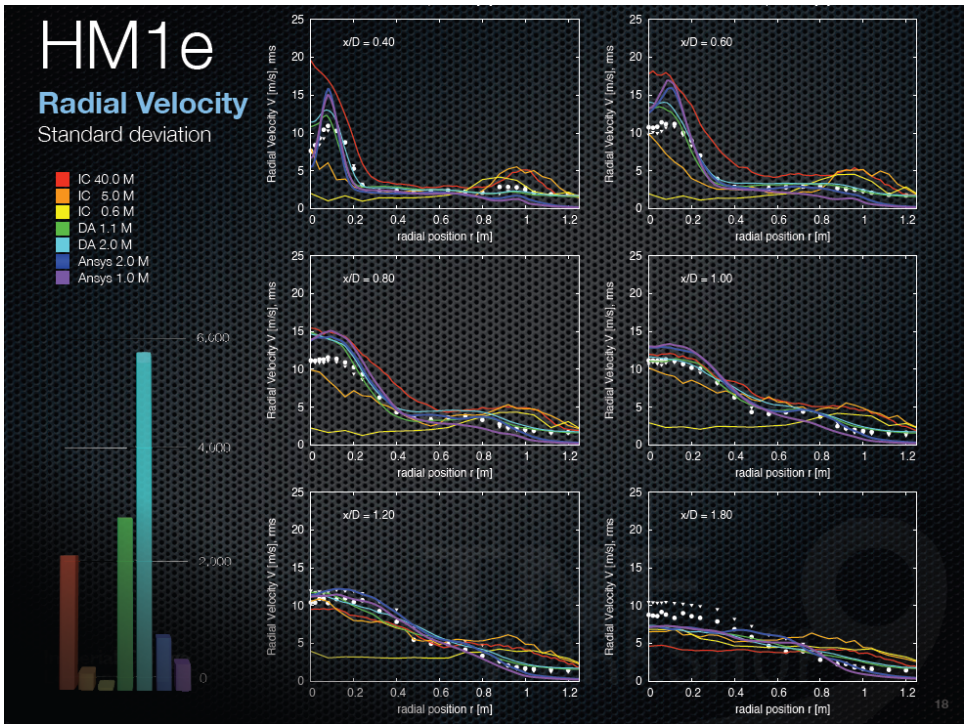
HM1e
Radial Velocity
Standard deviation
IC 40.0 M
IC 6.0 M
IC 0.6 M
DA 1.1 M
DA 2.0 M
Ansys 2.0 M
Ansys 1.0 M
6,000
4,000
2,000
0
x/D = 0.40
x/D = 0.60
x/D = 0.80
x/D = 1.00
x/D = 1.20
x/D = 1.80
Radial Velocity V [m/s], rms
radial position r [m]
18

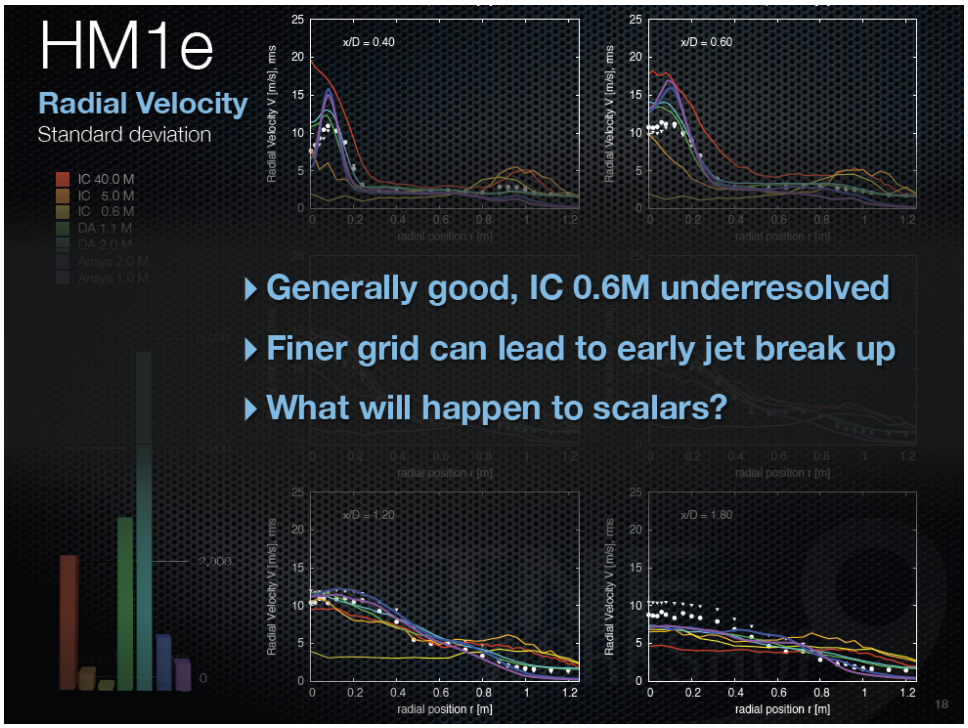

HM1 BC Variation

Different Inflow Conditions

- Case BC1
  - Boundary layer thickness: 8 mm
    - ➡ Less coflow dominated: rich downstream
  - Turbulence level in jet: 10 %
    - ➡ Jet breaks up too early
- Case BC2
  - Boundary layer thickness: 5 mm
    - ➡ More coflow dominated: lean downstream
  - Turbulence level in jet: 4 %
    - ➡ Jet breaks up too late

...no curve-fitting...

19

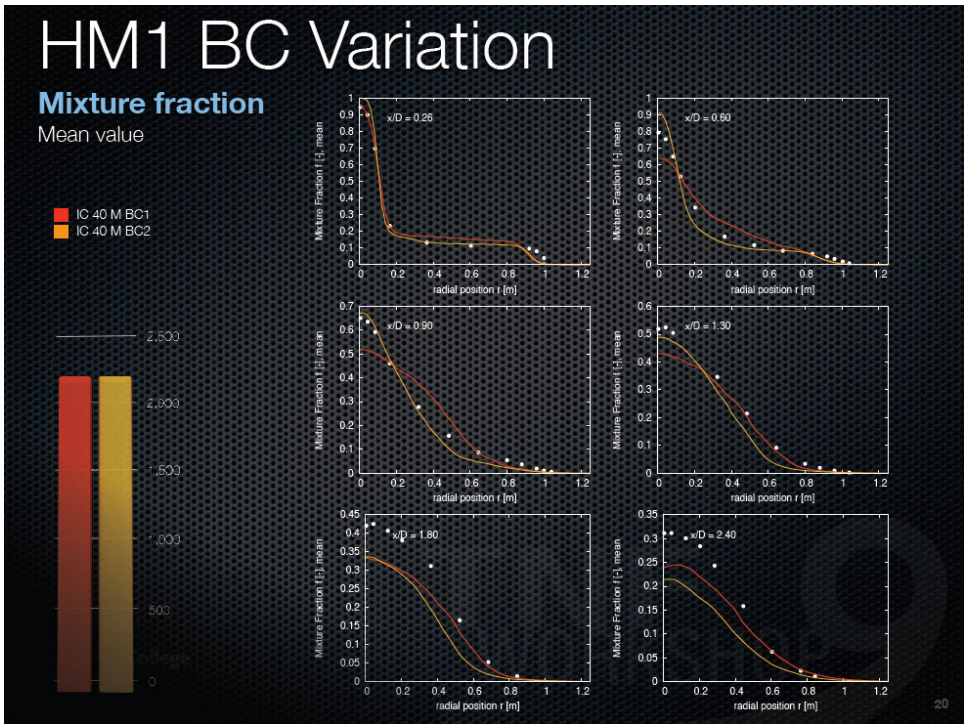
HM1 BC Variation
Mixture fraction
Mean value
IC 40 M BC1
IC 40 M BC2
x/D = 0.26
x/D = 0.60
x/D = 0.90
x/D = 1.30
x/D = 1.80
x/D = 2.40
Mixture Fraction f [-], mean
radial position r [m]
20

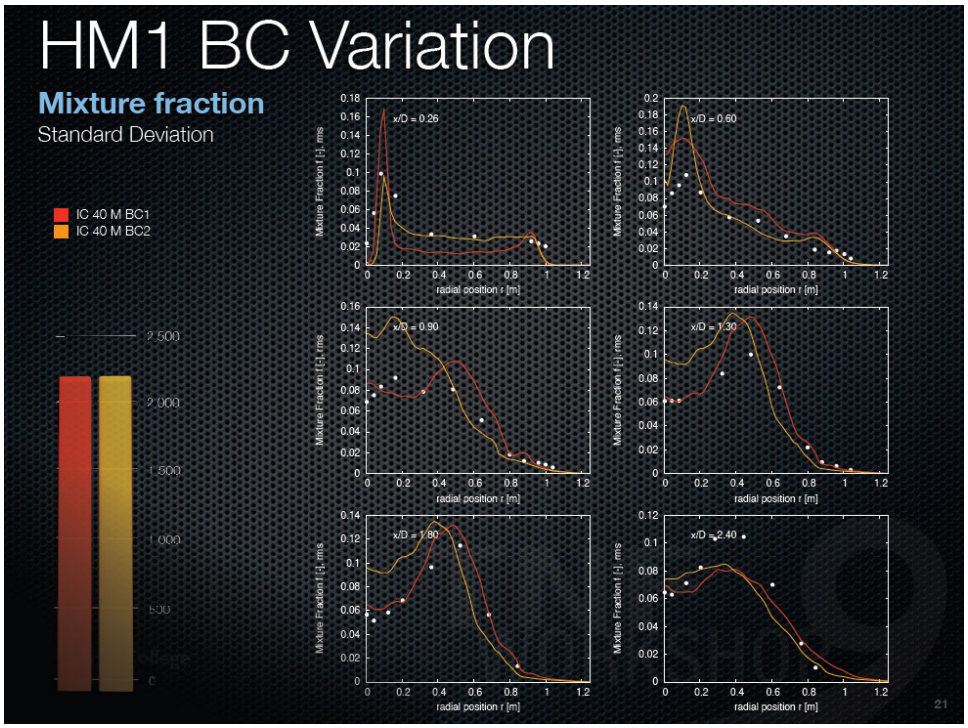
HM1 BC Variation
Mixture fraction
Standard Deviation
IC 40 M BC1
IC 40 M BC2
x/D = 0.26
x/D = 0.60
x/D = 0.90
x/D = 1.30
x/D = 1.80
x/D = 2.40
Mixture Fraction f [-], rms
radial position r [m]
21

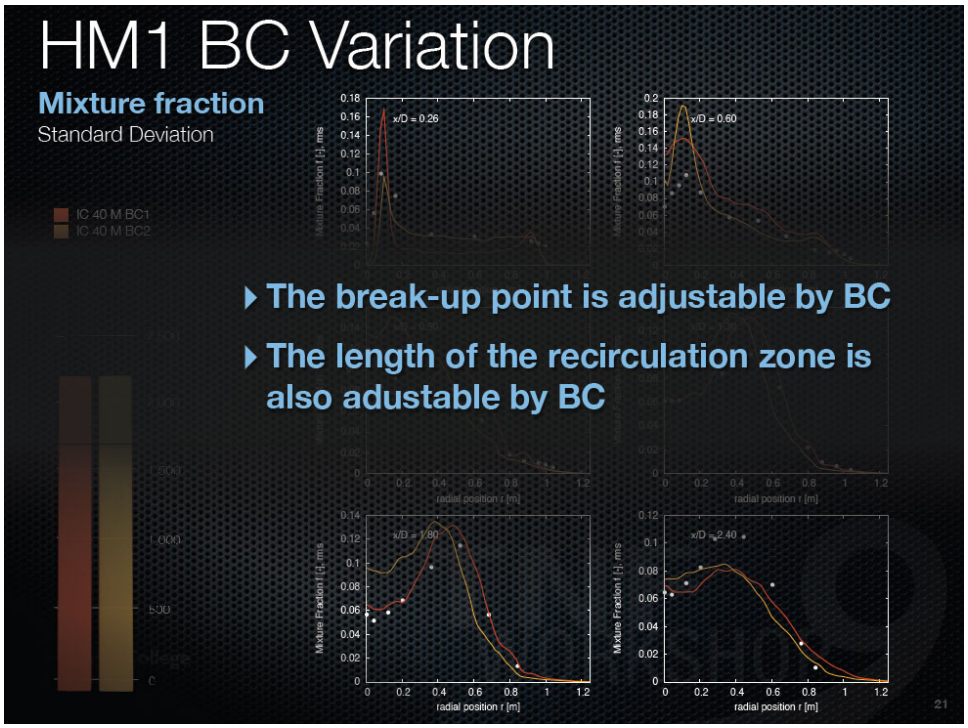
HM1 BC Variation
Mixture fraction
Standard Deviation
IC 40 M BC1
IC 40 M BC2
x/D = 0.26
x/D = 0.60
x/D = 1.80
x/D = 2.40
Mixture Fraction f [-], rms
radial position r [m]
The break-up point is adjustable by BC
The length of the recirculation zone is also adustable by BC
21

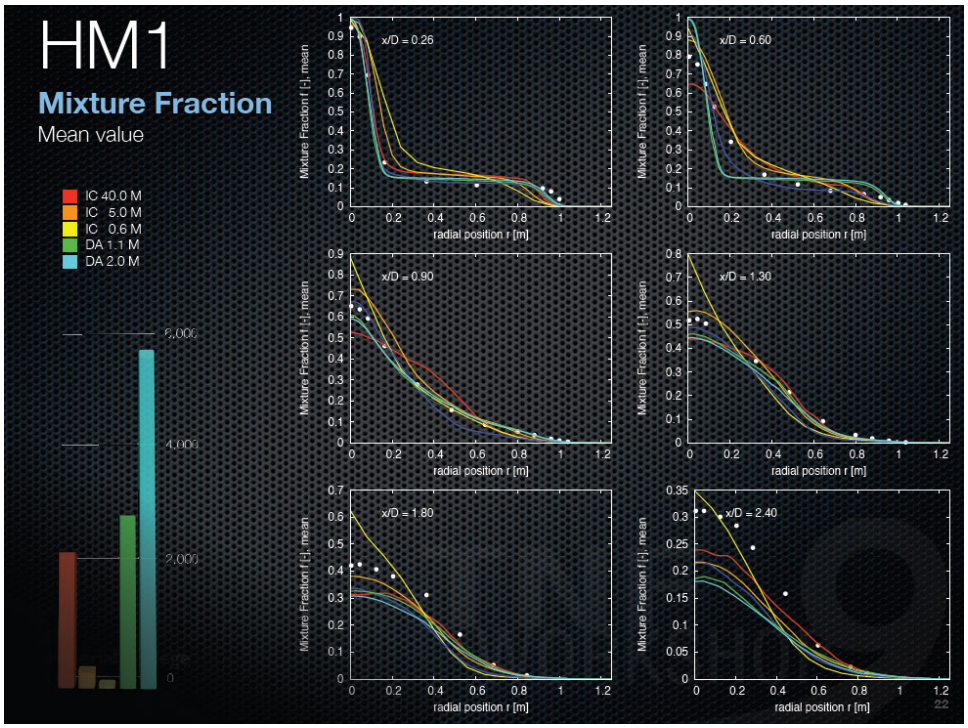
HM1
Mixture Fraction
Mean value
IC 40.0 M
IC 5.0 M
IC 0.6 M
DA 1.1 M
DA 2.0 M
x/D = 0.26
x/D = 0.60
x/D = 0.90
x/D = 1.30
x/D = 1.80
x/D = 2.40
Mixture Fraction f [-], mean
radial position r [m]
22

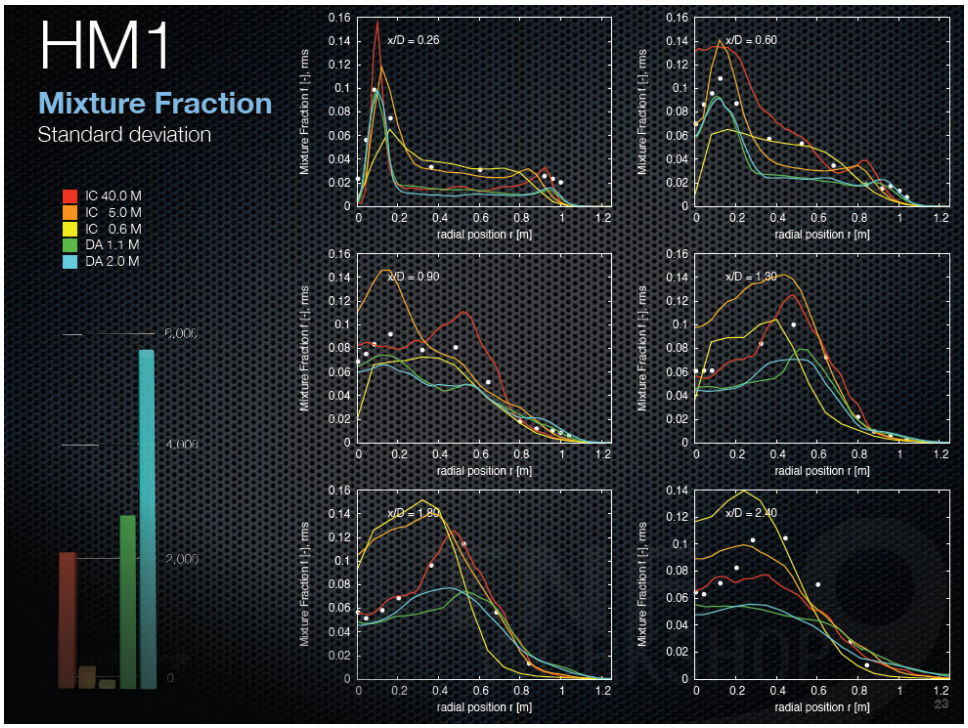
HM1
Mixture Fraction
Standard deviation
IC 40.0 M
IC 5.0 M
IC 0.6 M
DA 1.1 M
DA 2.0 M
6,000
4,000
2,000
0
x/D = 0.26
x/D = 0.60
x/D = 0.90
x/D = 1.30
x/D = 1.80
x/D = 2.40
Mixture Fraction f [-], rms
radial position r [m]
23

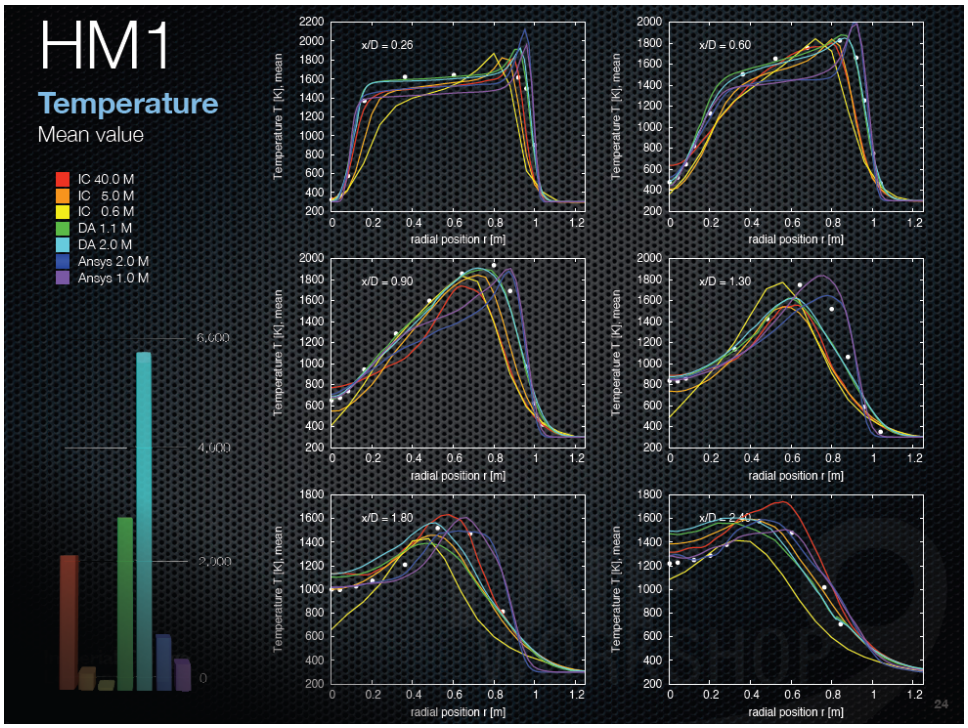
HM1
Temperature
Mean value
IC 40.0 M
IC 5.0 M
IC 0.6 M
DA 1.1 M
DA 2.0 M
Ansys 2.0 M
Ansys 1.0 M
6,000
4,000
2,000
0
x/D = 0.26
x/D = 0.60
x/D = 0.90
x/D = 1.30
x/D = 1.80
x/D = 2.40
Temperature T [K], mean
radial position r [m]
24

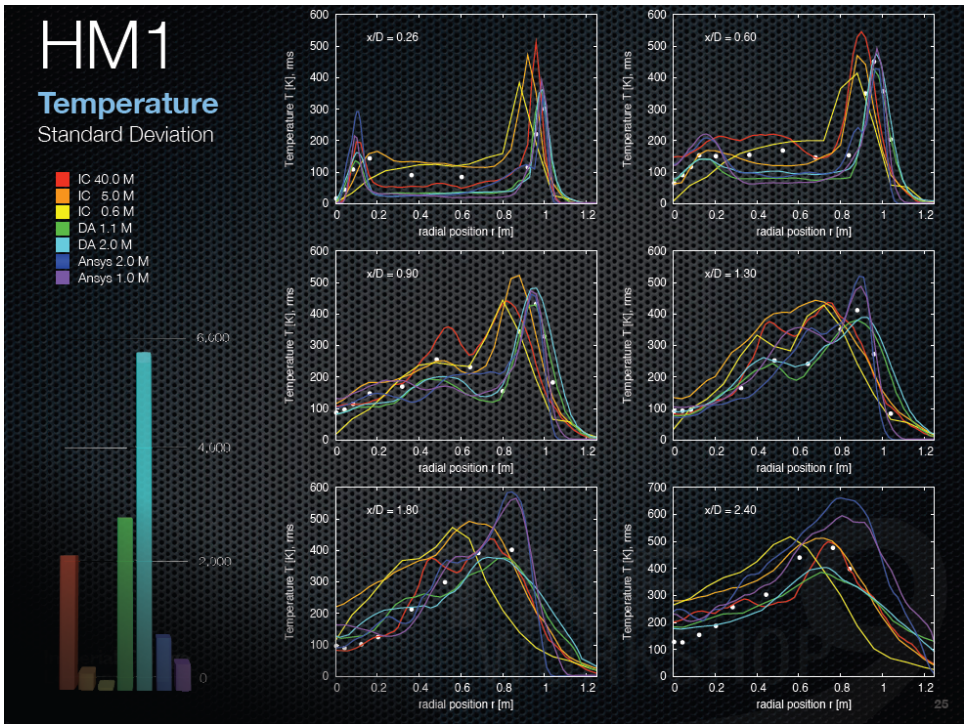
HM1
Temperature
Standard Deviation
IC 40.0 M
IC 6.0 M
IC 0.6 M
DA 1.1 M
DA 2.0 M
Ansys 2.0 M
Ansys 1.0 M
6,000
4,000
2,000
0
x/D = 0.26
x/D = 0.60
x/D = 0.90
x/D = 1.30
x/D = 1.80
x/D = 2.40
Temperature T [K], rms
radial position r [m]
25

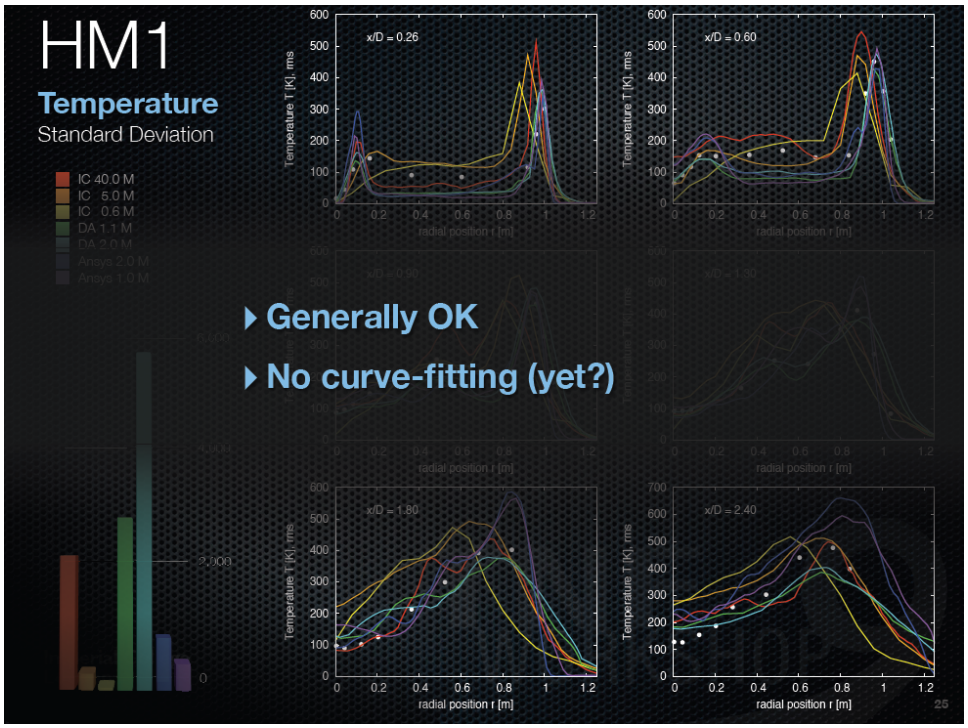
HM1
Temperature
Standard Deviation
IC 40.0 M
IC 6.0 M
IC 0.6 M
DA 1.1 M
DA 2.0 M
Ansys 2.0 M
Ansys 1.0 M
Generally OK
No curve-fitting (yet?)
2,000
0
x/D = 0.26
x/D = 0.60
x/D = 1.80
x/D = 2.40
Temperature T [K], rms
radial position r [m]
25

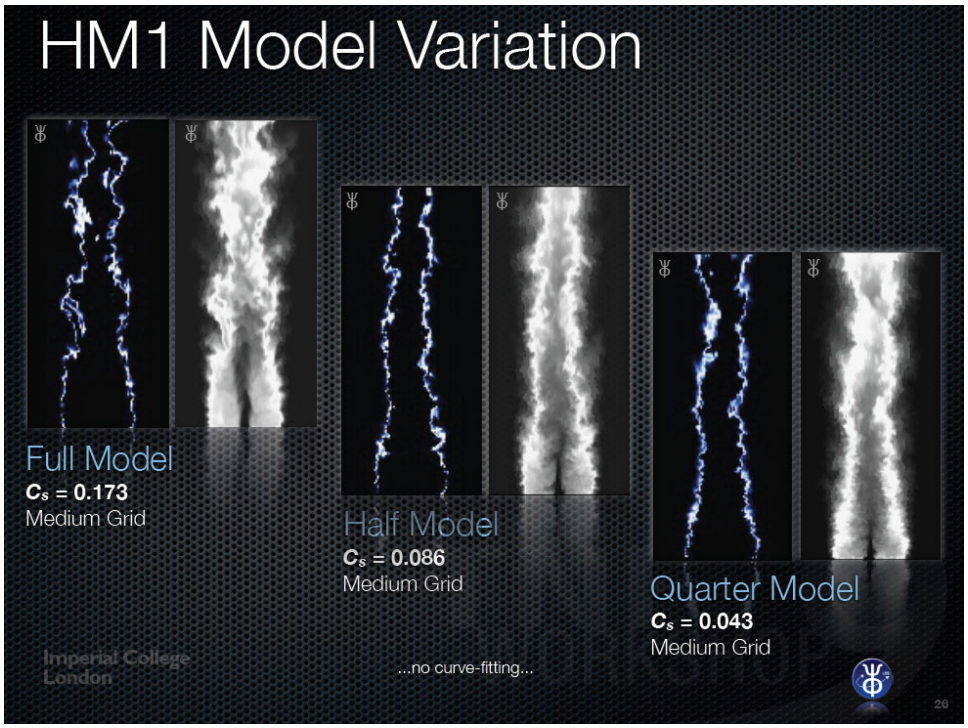
HM1 Model Variation
Full Model
C_s = 0.173
Medium Grid
Half Model
C_s = 0.086
Medium Grid
Quarter Model
C_s = 0.043
Medium Grid
...no curve-fitting...
Imperial College London
28

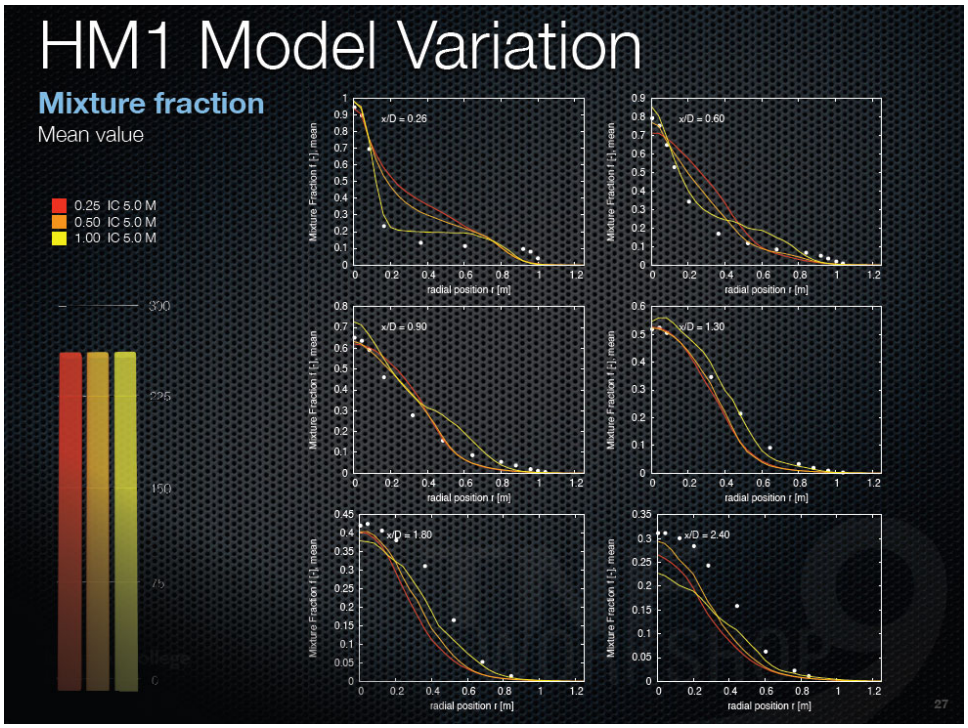
HM1 Model Variation
Mixture fraction
Mean value
0.25 IC 5.0 M
0.50 IC 5.0 M
1.00 IC 5.0 M
300
225
150
75
0
x/D = 0.26
x/D = 0.60
x/D = 0.90
x/D = 1.30
x/D = 1.80
x/D = 2.40
Mixture Fraction f [-], mean
radial position r [m]
27

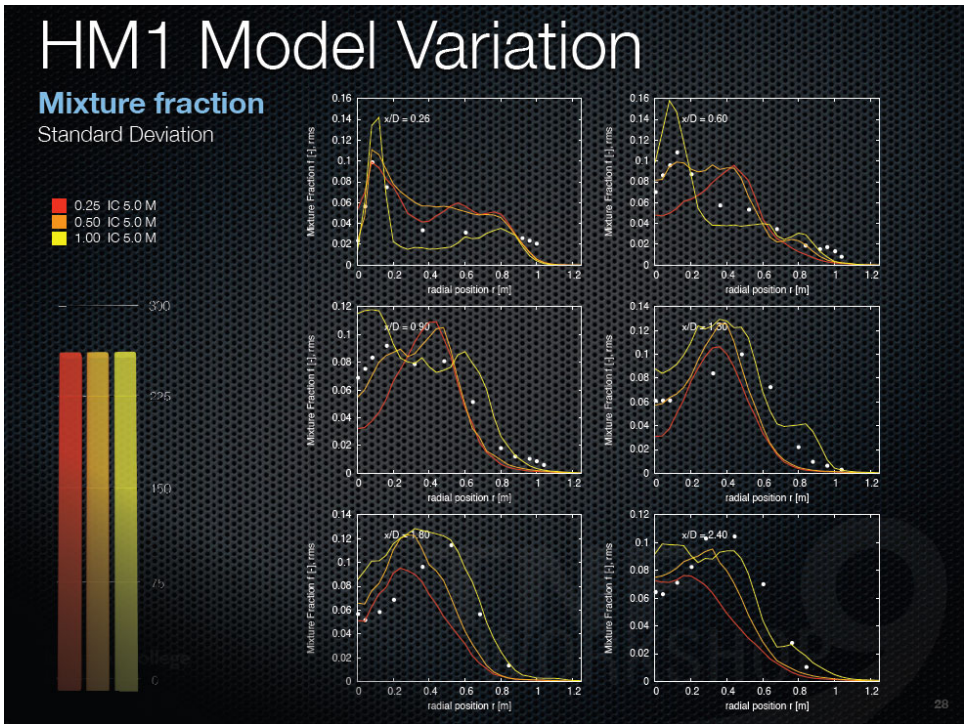
HM1 Model Variation
Mixture fraction
Standard Deviation
0.25 IC 5.0 M
0.50 IC 5.0 M
1.00 IC 5.0 M
300
225
150
75
0
x/D = 0.26
x/D = 0.60
x/D = 0.90
x/D = 1.20
x/D = 1.80
x/D = 2.40
Mixture Fraction f [-], rms
radial position r [m]
28

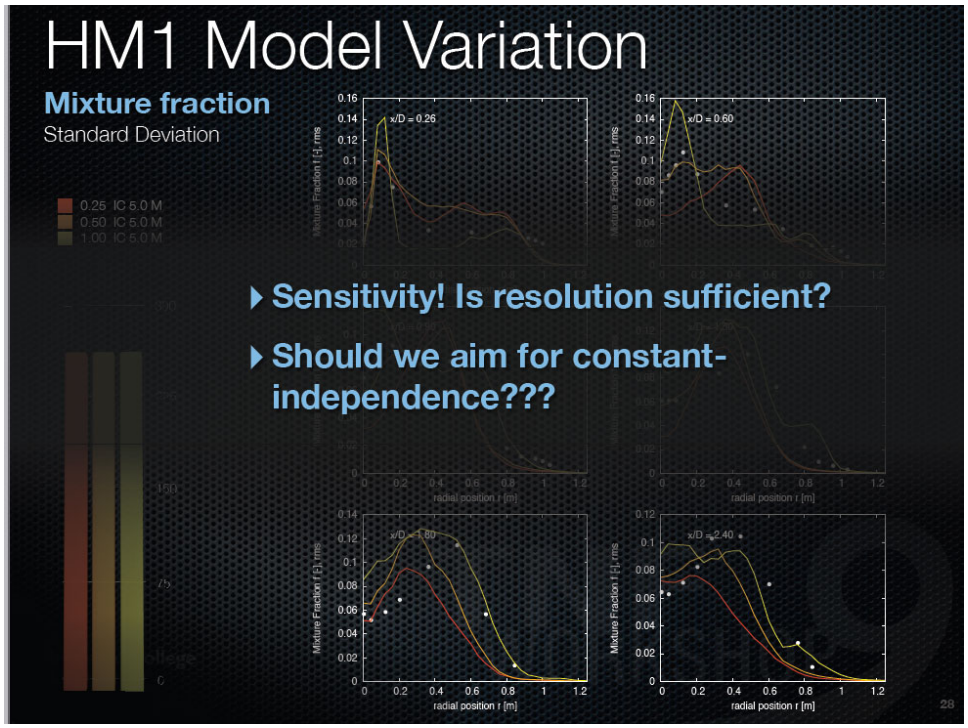
HM1 Model Variation
Mixture fraction
Standard Deviation
0.25 IC 5.0 M
0.50 IC 5.0 M
1.00 IC 5.0 M
Sensitivity! Is resolution sufficient?
Should we aim for constant-independence???
x/D = 0.26
x/D = 0.60
x/D = 1.80
x/D = 2.40
Mixture Fraction f [-], rms
radial position r [m]
28

Klein, Meyers, Geurts, Assessment of LES quality measures using the error landscape approach, Q-LES 2007

Algebraic Error Indicators

- Viscosity ratio

$$VR = \frac{\mu_t}{\mu_{lam}}$$

- Energy ratio ('Pope criterion' with Lilly model)

$$ER \approx \frac{E_{res}}{E_{res} + <E_{sgs}>} \; ; \quad <E_{sgs}> = \left(\frac{<\nu_t>}{c\Delta}\right)^2 \; ; \quad c = 0.094$$

- LES-IQ (Celik, based on viscosity)

$$LESIQ_\nu = \frac{1}{1 + 0.05\left(\frac{\langle\nu+\nu_t\rangle}{\langle\nu\rangle}\right)^{0.53}}$$

- LES-IQ (Celik, based on grids)

$$LESIQ_\epsilon(x) = \left(1 + \left(1 - \frac{K^\epsilon}{K^f}\right) \Big/ \left(\left(\frac{\Delta^c}{\Delta^f}\right)^p - 1\right)\right)^{-1}$$

- Systematic Grid and Model Variation (Klein)

$$ER = \frac{E_{res}}{E_{DNS}} \approx \frac{E_{res}}{E_{res} + E_{sgs}} \qquad E_{sgs}^{Klein} = \left|\frac{E_3 - E_1}{1 - \alpha}\right| + \left|\frac{(E_2 - E_1) - (E_3 - E_1)\frac{1-\beta^m}{1-\alpha}}{1 - \beta^n}\right|$$

Imperial College London

29

HM1e

Viscosity Ratio

$$VR = \frac{\mu_t}{\mu_{lam}}$$

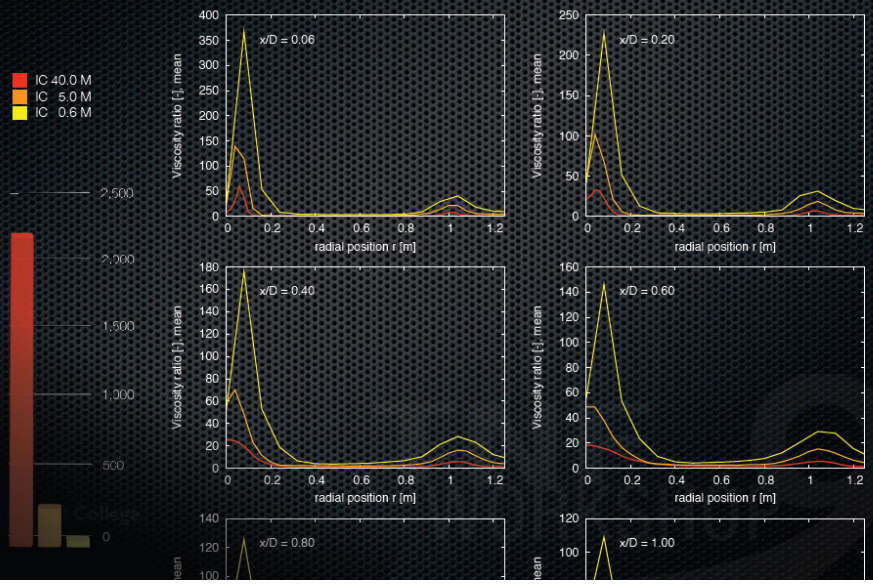

30

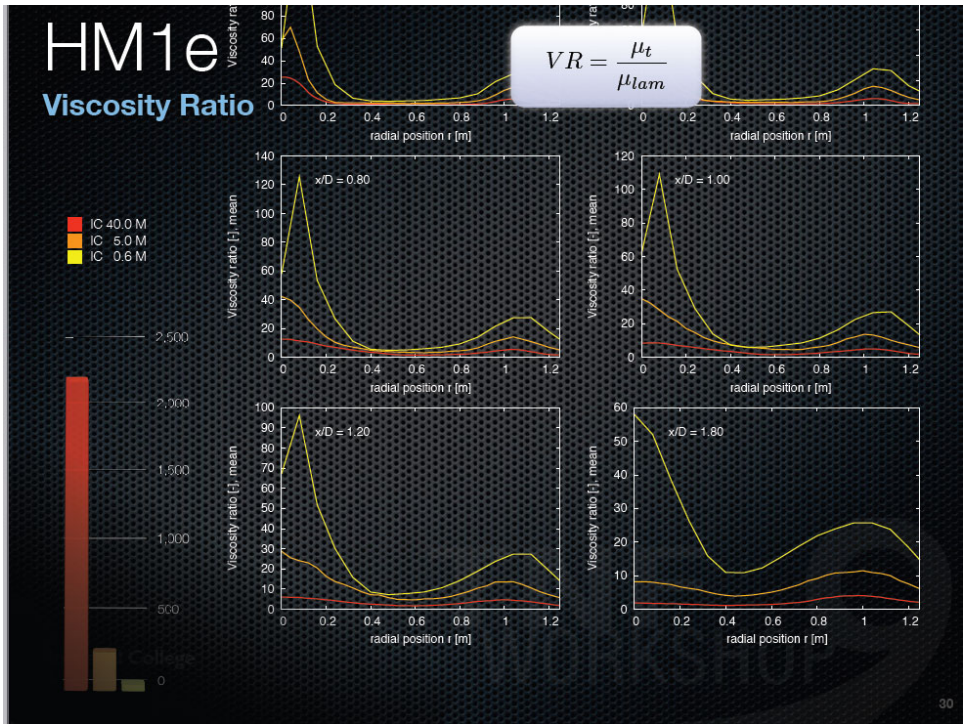
HM1e
Viscosity Ratio
$VR = \frac{\mu_t}{\mu_{lam}}$
IC 40.0 M
IC 5.0 M
IC 0.6 M
x/D = 0.80
x/D = 1.00
x/D = 1.20
x/D = 1.80
Viscosity ratio [-], mean
radial position r [m]
30

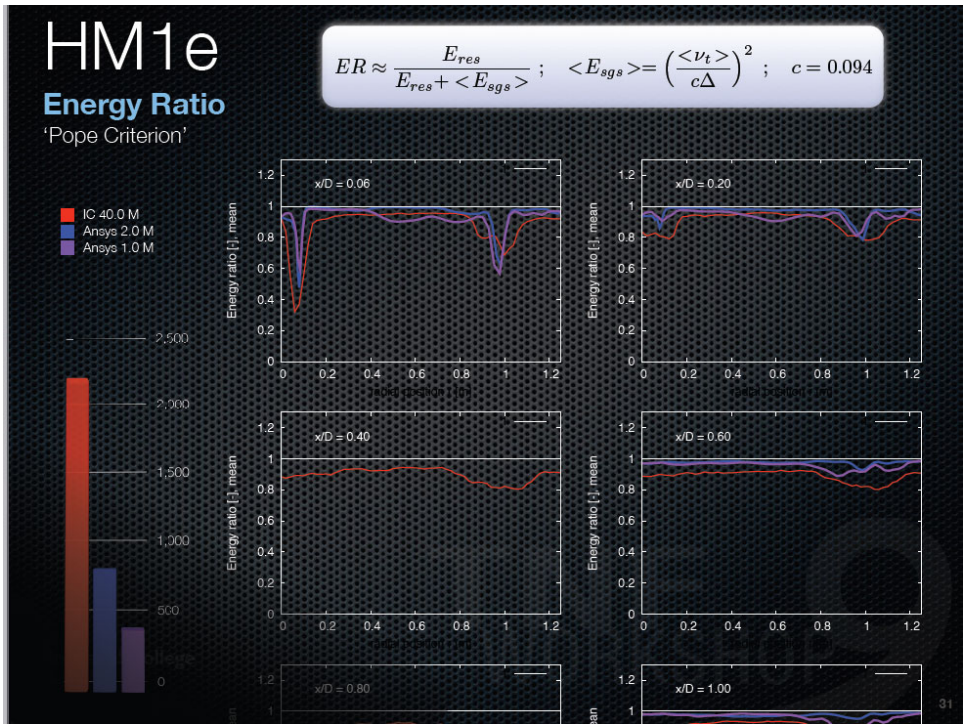
HM1e
Energy Ratio
'Pope Criterion'
$ER \approx \frac{E_{res}}{E_{res} + < E_{sgs} >}$; $< E_{sgs} >= \left(\frac{< \nu_t >}{c\Delta}\right)^2$; $c = 0.094$
IC 40.0 M
Ansys 2.0 M
Ansys 1.0 M
x/D = 0.06
x/D = 0.20
x/D = 0.40
x/D = 0.60
x/D = 0.80
x/D = 1.00
Energy ratio [-], mean
31

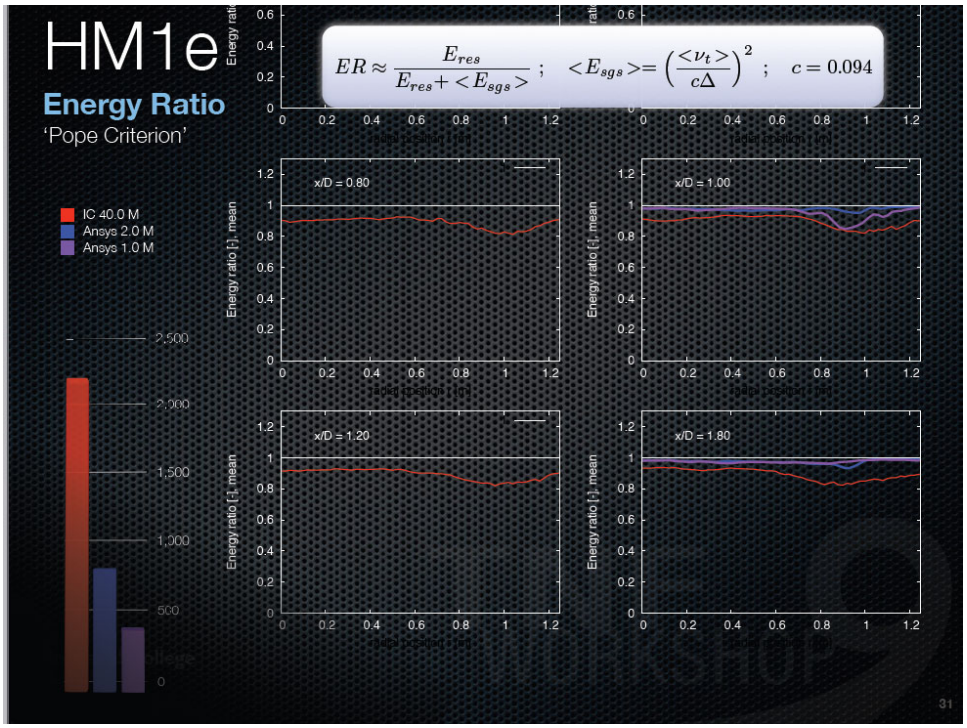
HM1e
Energy Ratio
'Pope Criterion'
$ER \approx \frac{E_{res}}{E_{res} + < E_{sgs} >} \; ; \quad < E_{sgs} >= \left(\frac{< \nu_t >}{c\Delta} \right)^2 \; ; \quad c = 0.094$
IC 40.0 M
Ansys 2.0 M
Ansys 1.0 M
x/D = 0.80
x/D = 1.00
x/D = 1.20
x/D = 1.80
Energy ratio [-], mean
Radial position [m]
2,500
2,000
1,500
1,000
500
0
31

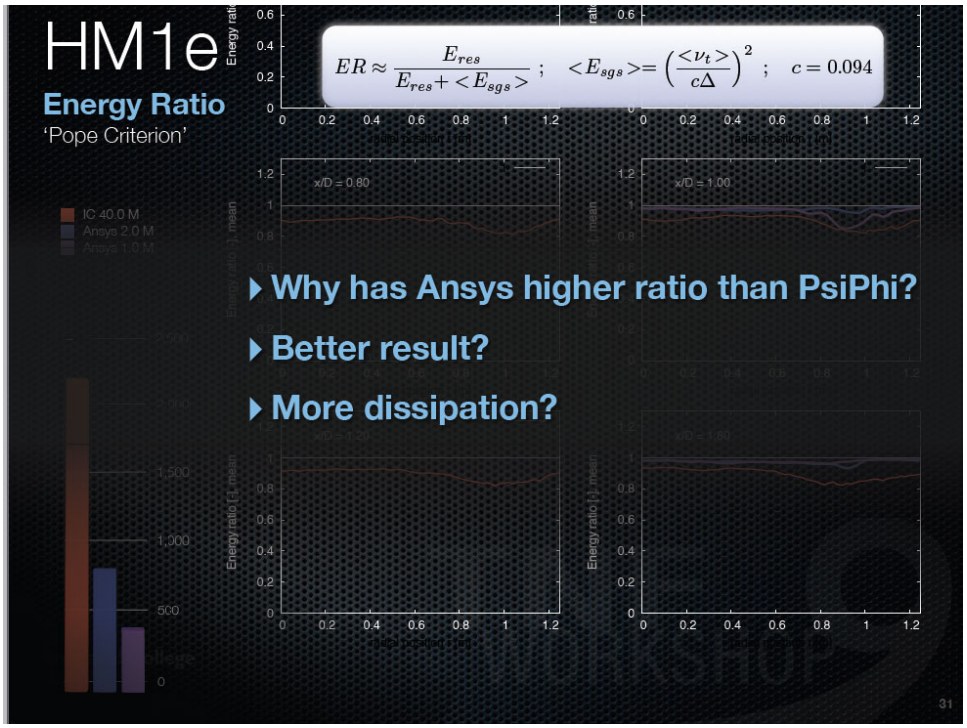
HM1e
Energy Ratio
'Pope Criterion'
$ER \approx \frac{E_{res}}{E_{res} + < E_{sgs} >} \; ; \quad < E_{sgs} >= \left(\frac{< \nu_t >}{c\Delta} \right)^2 \; ; \quad c = 0.094$
IC 40.0 M
Ansys 2.0 M
Ansys 1.0 M
x/D = 0.80
x/D = 1.00
Why has Ansys higher ratio than PsiPhi?
Better result?
More dissipation?
Energy ratio [-], mean
Radial position [m]
1,500
1,000
500
0
31

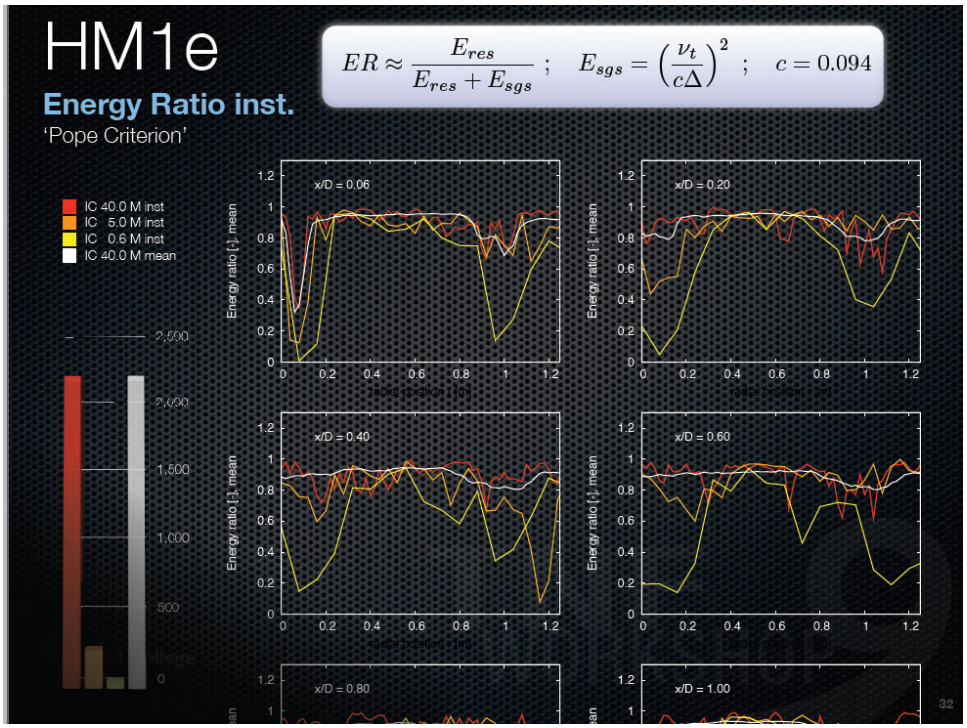
HM1e
Energy Ratio inst.
'Pope Criterion'
$ER \approx \frac{E_{res}}{E_{res}+E_{sgs}}$; $E_{sgs} = \left(\frac{\nu_t}{c\Delta}\right)^2$; $c = 0.094$
IC 40.0 M inst
IC 5.0 M inst
IC 0.6 M inst
IC 40.0 M mean
x/D = 0.06
x/D = 0.20
x/D = 0.40
x/D = 0.60
x/D = 0.80
x/D = 1.00
Energy ratio [-], mean
Radial position [m]
2,500
2,000
1,500
1,000
500
0
32

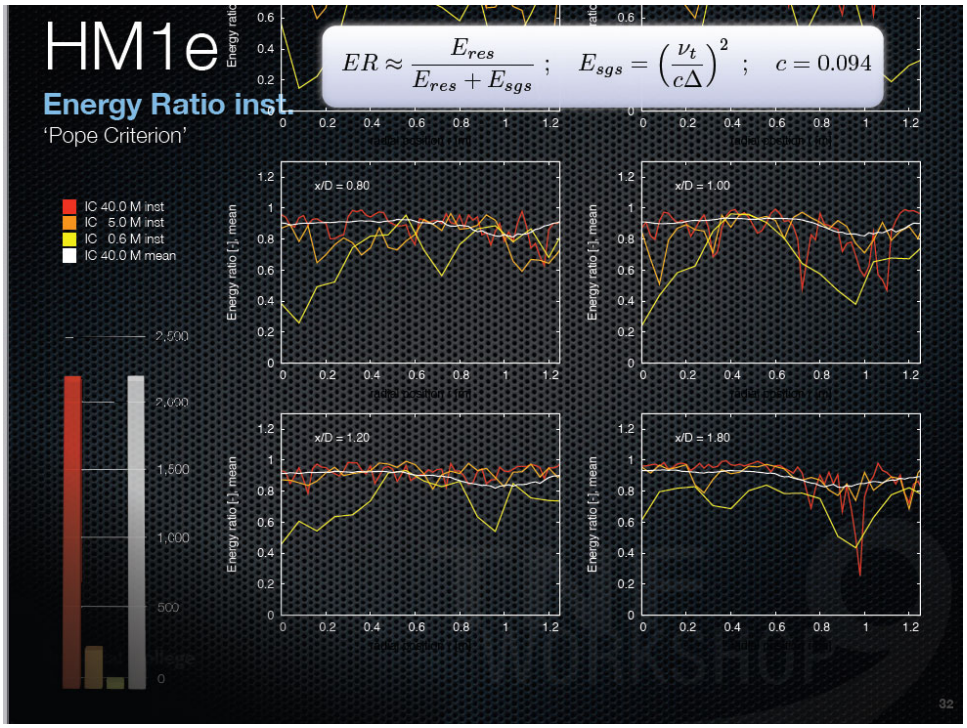
HM1e
Energy Ratio inst.
'Pope Criterion'
$ER \approx \frac{E_{res}}{E_{res}+E_{sgs}}$; $E_{sgs} = \left(\frac{\nu_t}{c\Delta}\right)^2$; $c = 0.094$
IC 40.0 M inst
IC 5.0 M inst
IC 0.6 M inst
IC 40.0 M mean
x/D = 0.80
x/D = 1.00
x/D = 1.20
x/D = 1.80
Energy ratio [-], mean
Radial position [m]
2,500
2,000
1,500
1,000
500
0
32

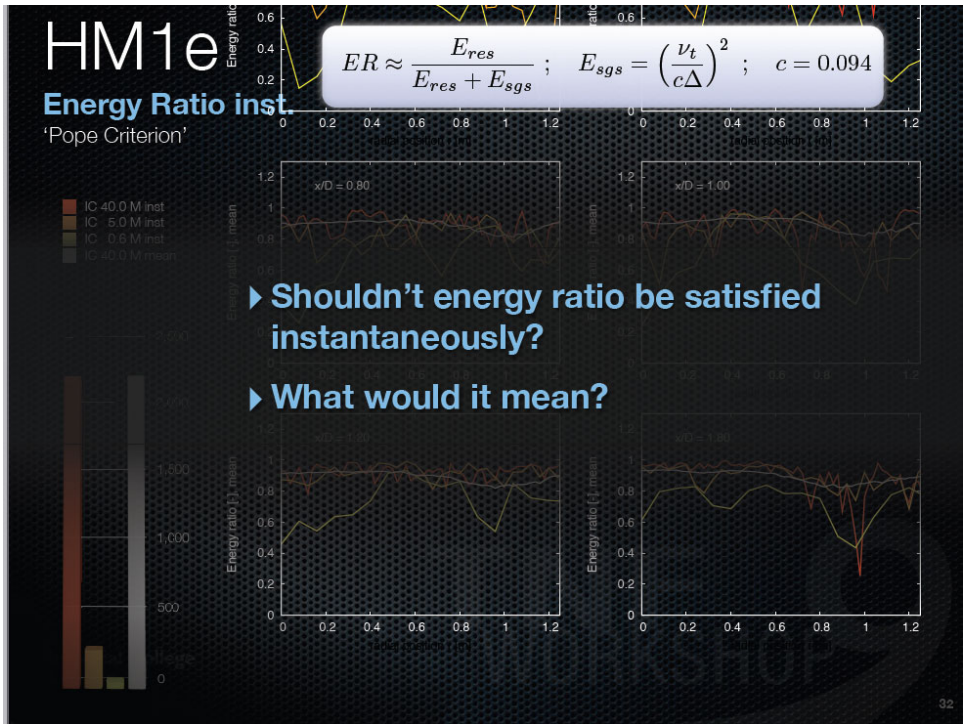
HM1e
Energy Ratio inst.
'Pope Criterion'
$ER \approx \frac{E_{res}}{E_{res}+E_{sgs}}$; $E_{sgs} = \left(\frac{\nu_t}{c\Delta}\right)^2$; $c = 0.094$
IC 40.0 M inst
IC 5.0 M inst
IC 0.6 M inst
IC 40.0 M mean
x/D = 0.80
x/D = 1.00
Shouldn't energy ratio be satisfied instantaneously?
What would it mean?
Energy ratio [-], mean
Radial position [m]
32

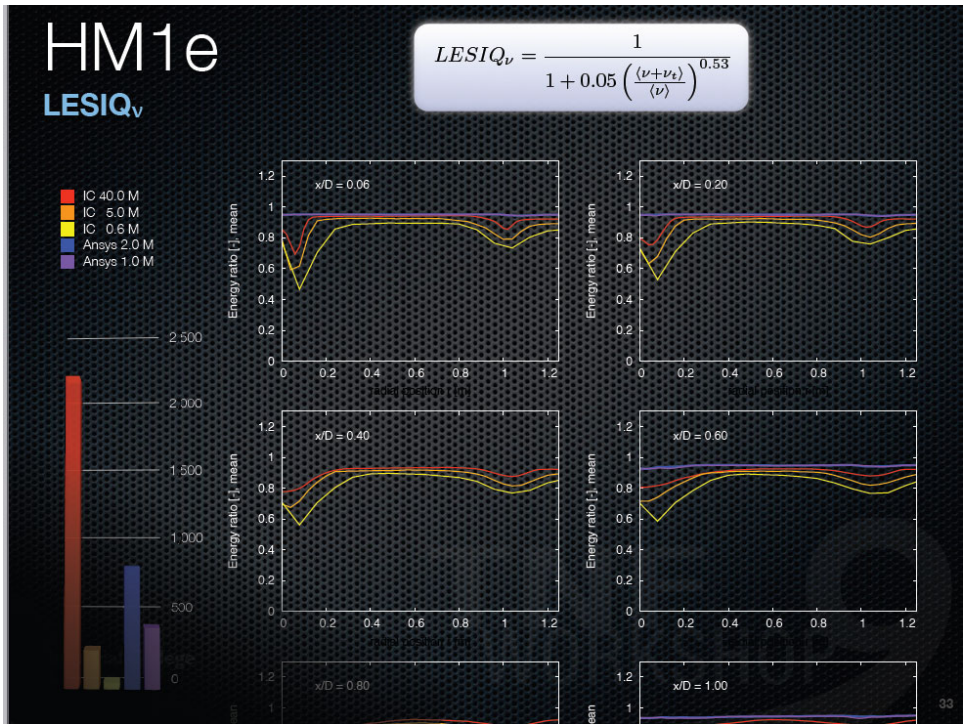
HM1e
LESIQν
$LESIQ_\nu = \frac{1}{1+0.05\left(\frac{\langle\nu+\nu_t\rangle}{\langle\nu\rangle}\right)^{0.53}}$
IC 40.0 M
IC 5.0 M
IC 0.6 M
Ansys 2.0 M
Ansys 1.0 M
x/D = 0.06
x/D = 0.20
x/D = 0.40
x/D = 0.60
x/D = 0.80
x/D = 1.00
Energy ratio [-], mean
Radial position [m]
33

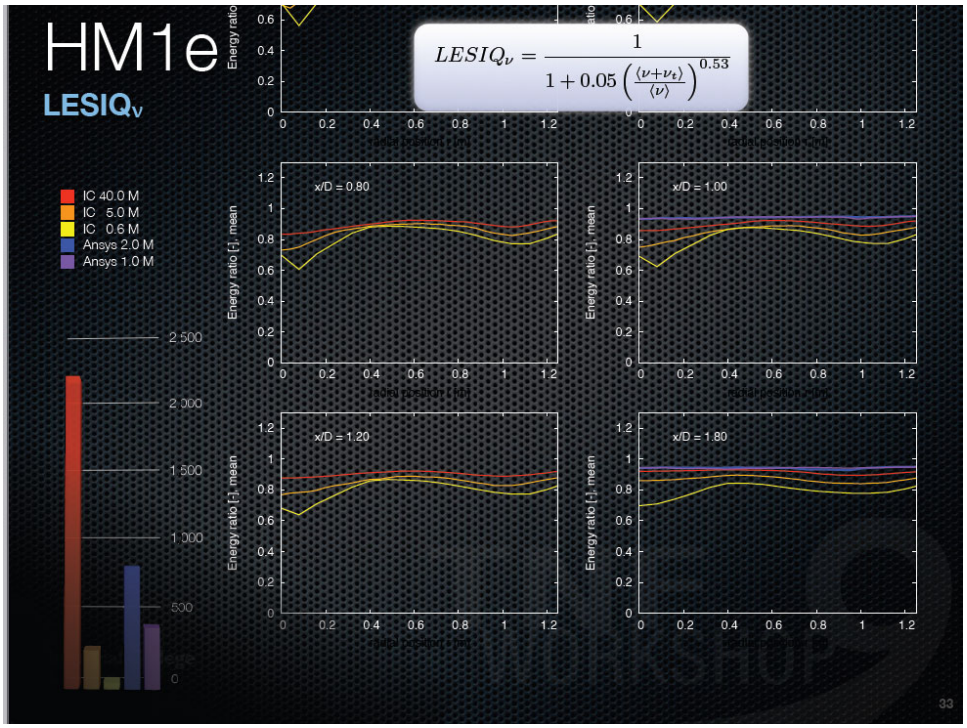
HM1e
LESIQv
$LESIQ_\nu = \frac{1}{1+0.05\left(\frac{\langle\nu+\nu_t\rangle}{\langle\nu\rangle}\right)^{0.53}}$
IC 40.0 M
IC 5.0 M
IC 0.6 M
Ansys 2.0 M
Ansys 1.0 M
x/D = 0.80
x/D = 1.00
x/D = 1.20
x/D = 1.80
Energy ratio [-], mean
2 500
2 000
1 500
1 000
500
0
33


HM1e
LESIQv
$LESIQ_\nu = \frac{1}{1+0.05\left(\frac{\langle\nu+\nu_t\rangle}{\langle\nu\rangle}\right)^{0.53}}$
IC 40.0 M
IC 5.0 M
IC 0.6 M
x/D = 0.80
x/D = 1.00
Good, useful convergence
Ansys looks better again.
Why?
1 000
500
0
33

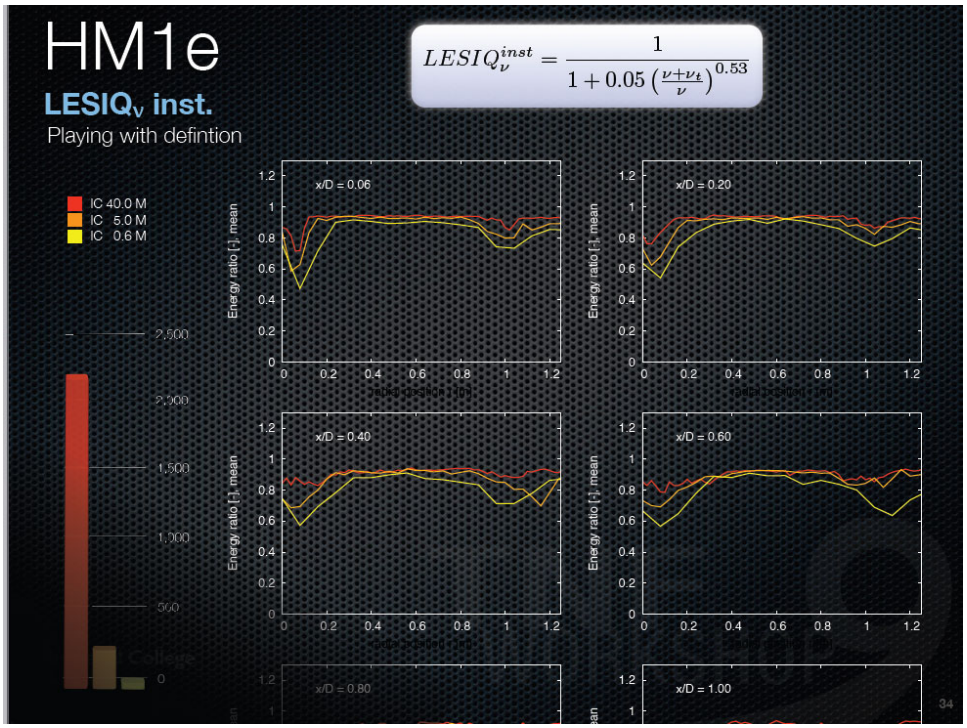
HM1e
LESIQv inst.
Playing with defintion
$LESIQ_\nu^{inst} = \frac{1}{1+0.05\left(\frac{\nu+\nu_t}{\nu}\right)^{0.53}}$
IC 40.0 M
IC 5.0 M
IC 0.6 M
x/D = 0.06
x/D = 0.20
x/D = 0.40
x/D = 0.60
x/D = 0.80
x/D = 1.00
Energy ratio [-], mean
34

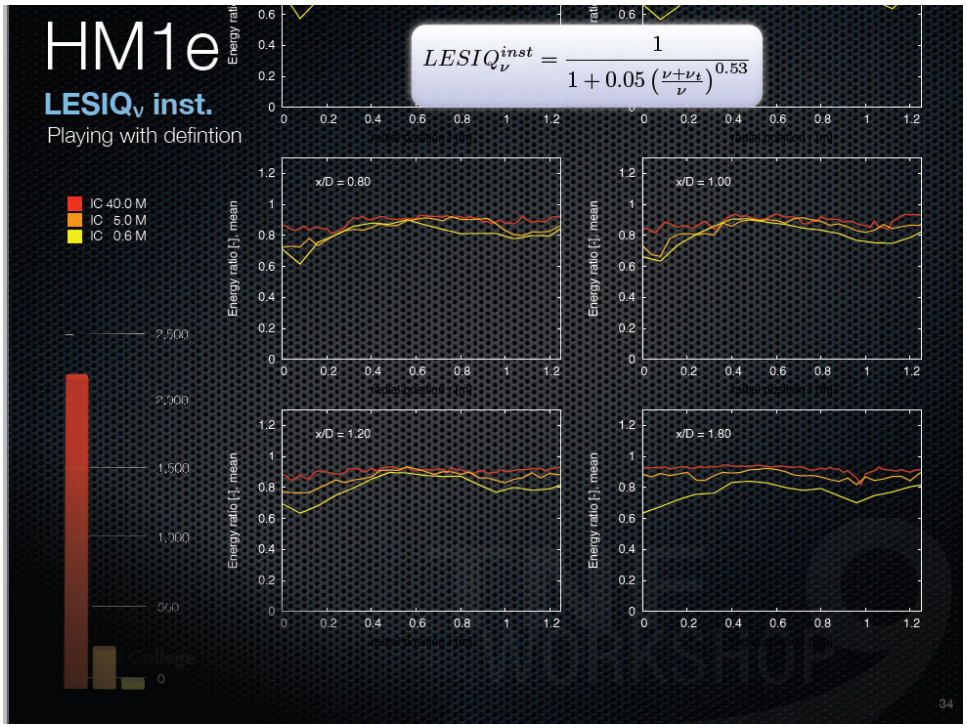
HM1e
LESIQv inst.
Playing with defintion
$LESIQ_\nu^{inst} = \frac{1}{1+0.05\left(\frac{\nu+\nu_t}{\nu}\right)^{0.53}}$
IC 40.0 M
IC 5.0 M
IC 0.6 M
x/D = 0.80
x/D = 1.00
x/D = 1.20
x/D = 1.80
Energy ratio [-], mean
34

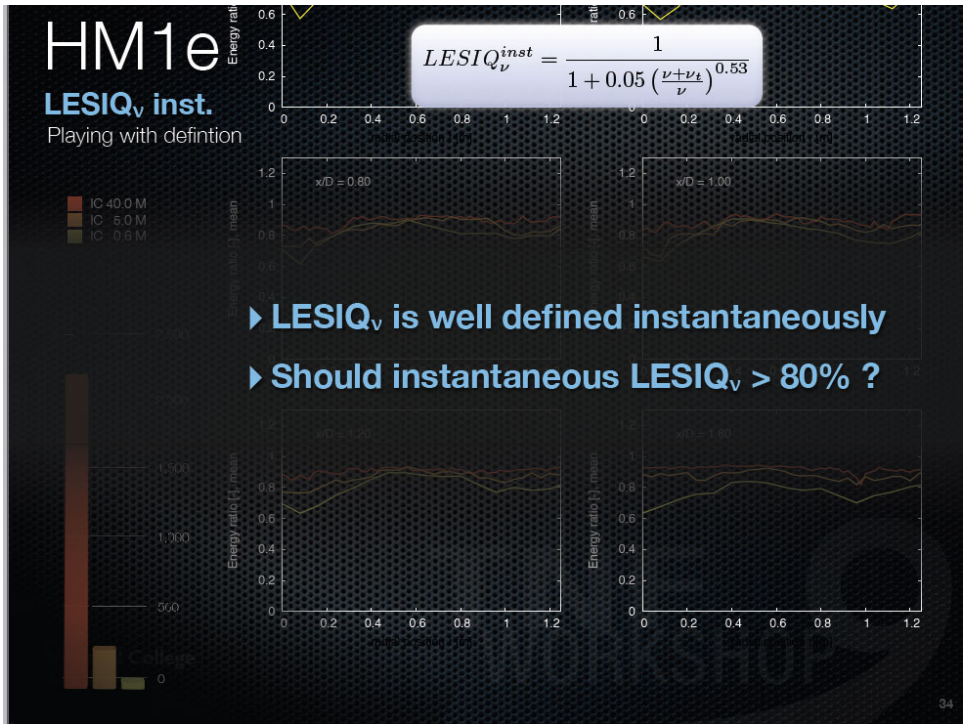
HM1e
LESIQv inst.
Playing with defintion
$LESIQ_{\nu}^{inst} = \frac{1}{1 + 0.05\left(\frac{\nu+\nu_t}{\nu}\right)^{0.53}}$
IC 40.0 M
IC 5.0 M
IC 0.6 M
x/D = 0.80
x/D = 1.00
LESIQv is well defined instantaneously
Should instantaneous LESIQv > 80% ?
Energy ratio [-], mean
34

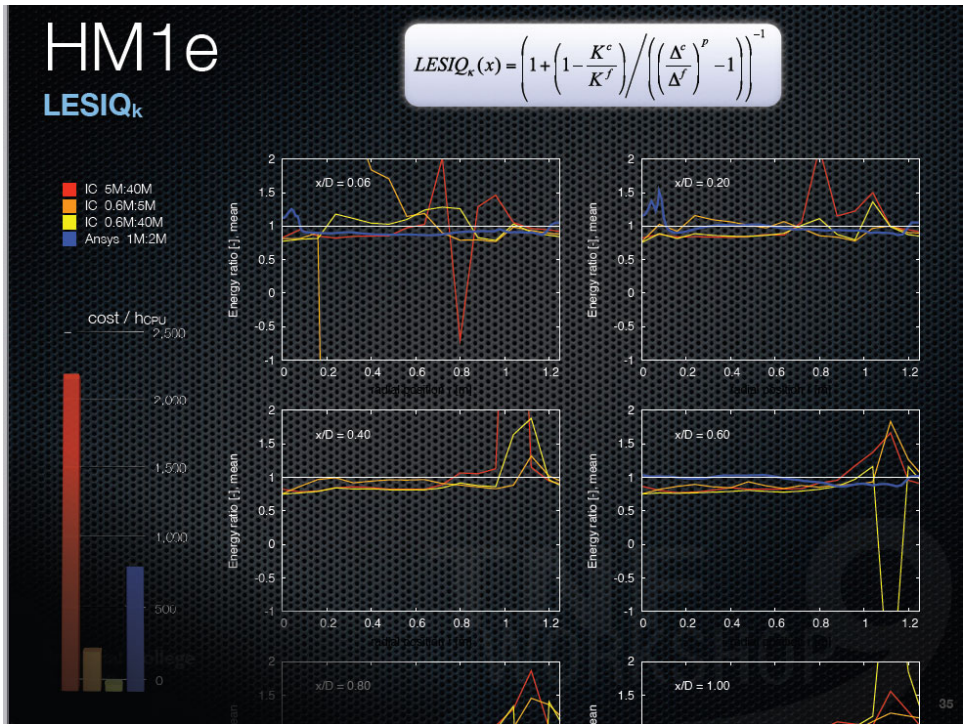
HM1e
LESIQk
$LESIQ_{\kappa}(x) = \left(1 + \left(1 - \frac{K^c}{K^f}\right) \Big/ \left(\left(\frac{\Delta^c}{\Delta^f}\right)^p - 1\right)\right)^{-1}$
IC 5M:40M
IC 0.6M:5M
IC 0.6M:40M
Ansys 1M:2M
cost / hCPU
2,500
2,000
1,500
1,000
500
0
x/D = 0.06
x/D = 0.20
x/D = 0.40
x/D = 0.60
x/D = 0.80
x/D = 1.00
Energy ratio [-], mean
35

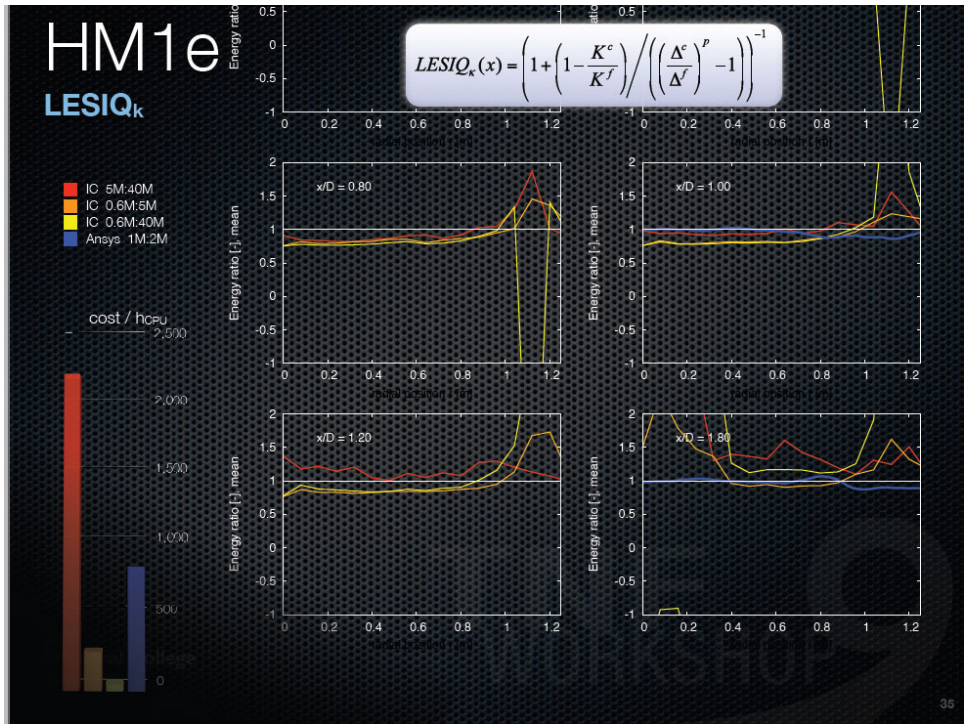
HM1e
LESIQk
$LESIQ_\kappa(x) = \left(1+\left(1-\frac{K^c}{K^f}\right)\Big/\left(\left(\frac{\Delta^c}{\Delta^f}\right)^p - 1\right)\right)^{-1}$
IC 5M:40M
IC 0.6M:5M
IC 0.6M:40M
Ansys 1M:2M
cost / hCPU
2,500
2,000
1,500
1,000
500
0
x/D = 0.80
x/D = 1.00
x/D = 1.20
x/D = 1.80
Energy ratio [-], mean
Radial position [-]
35

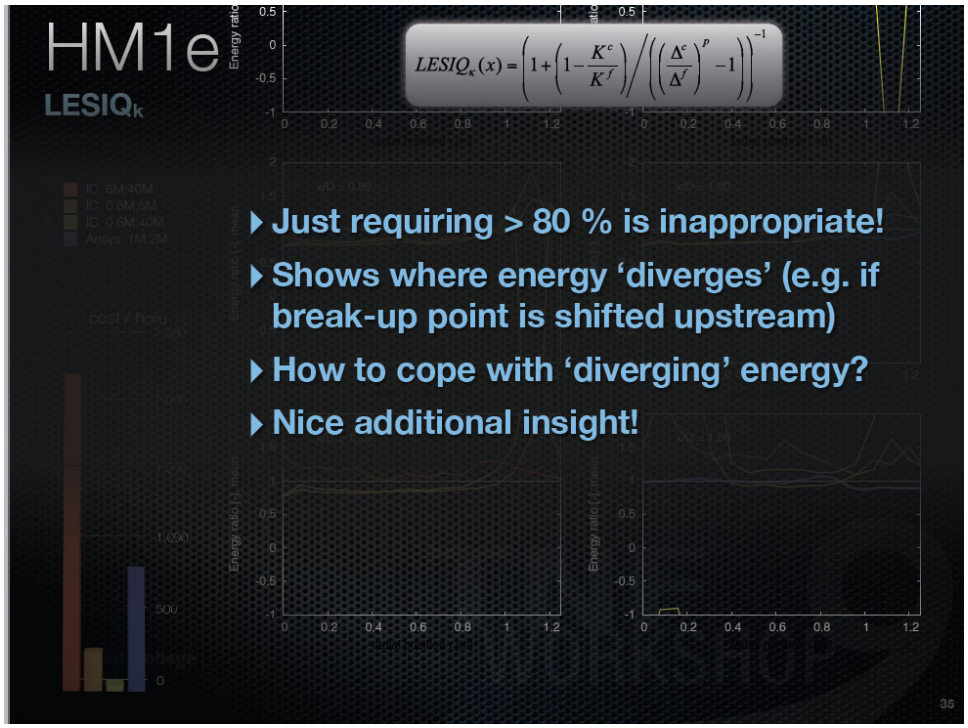
HM1e
LESIQk
$LESIQ_\kappa(x) = \left(1+\left(1-\frac{K^c}{K^f}\right)\Big/\left(\left(\frac{\Delta^c}{\Delta^f}\right)^p - 1\right)\right)^{-1}$
Just requiring > 80 % is inappropriate!
Shows where energy 'diverges' (e.g. if break-up point is shifted upstream)
How to cope with 'diverging' energy?
Nice additional insight!
35

TNF 9

August 2008

TECHNISCHE UNIVERSITÄT DARMSTADT

Quality Assessment for Internal Combustion Engines

D. Goryntsev, M. Klein, J. Janicka

Institute for Energy and Powerplant Technology

Estimation of modeling and numerical errors Theoretical background

TECHNISCHE UNIVERSITÄT DARMSTADT

- **The verification and validation (V&V)of LES is difficult: both the subgrid scale model contribution and numerical discretization errors are functions of the grid resolution;**
- **LES index of quality E_{LESIQ} (by Celik et al.):** $E_{LESIQ} = \frac{|u_3 - u_1|}{1 - \beta^n}$
- **A systematic grid and model variation procedure E_{SGMV} (by Klein);**

$$E_{SGMV} = \left| \frac{u_2 - u_3}{\beta^m (1-\alpha)} \right| + \left| \frac{(u_2 - u_1) - (u_2 - u_3)(1 - \alpha\beta^m) / [(1-\alpha)\beta^m]}{(1 - \beta^n)} \right|$$

1. **Fine grid with standard SGS model (u_1);**
2. **Coarse grid with modified SGS model (u_2);**
3. **Coarse grid with standard SGS model (u_3);**

A grid refinement factor: ß = 1.6;
A model variation factor: α = 4;

$$C^2_{S,2} = \alpha \times C^2_{S,1} \qquad \begin{matrix} n = 2 \\ m = 2/3 \end{matrix}$$

Estimation of modeling and numerical errors Validation

TECHNISCHE UNIVERSITÄT DARMSTADT

- **Validation of the methode by comparison of non reacting flows**
  - **DNS, LES, experiments**
  - **Channel, jet, swirling flow (Re = 5000)**
  - **Shown: LES 4 mill. CV´s, DNS 50 mill. CV´s**

Klein, Flow, Turb, Comb (2005)
Freitag & Klein et. al., J. Turb. (2006)

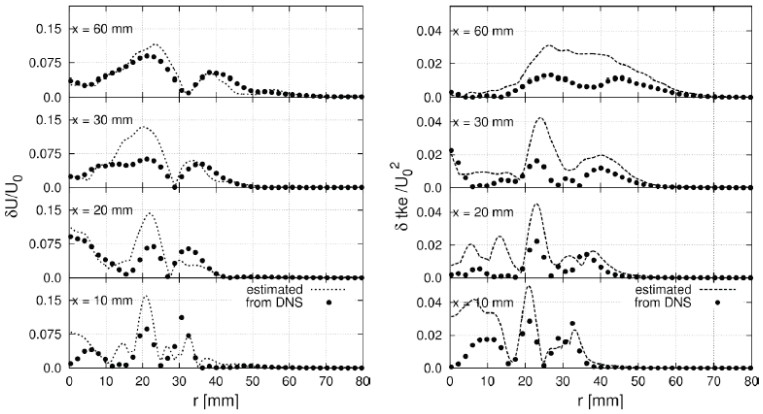

Geometry of "BMBF" IC-Engine

TECHNISCHE UNIVERSITÄT DARMSTADT

Side view

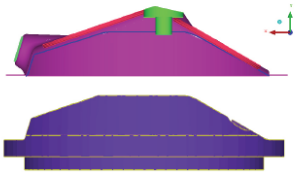

Definition of Valves motion

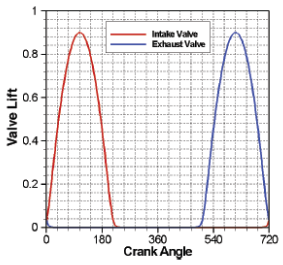

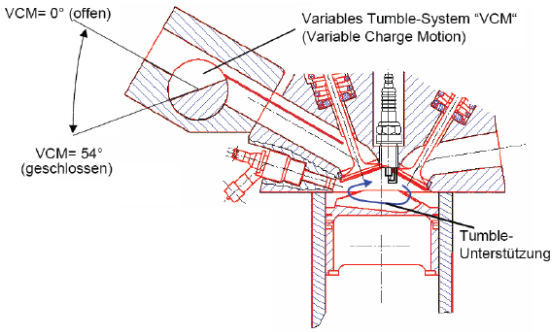

Cylinder head

Piston crown

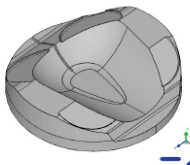

Computational Grids / LES Modeling

TECHNISCHE UNIVERSITÄT DARMSTADT

The engine cycle begins with CA = 0°, (TDC)

Intake: CA = 0° - 180°;

Compression: CA = 180° - 360°;
320 000 CV´s

LES Modeling:

LES, based on the Smagorinsky model, has been implemented in the KIVA-3V code:

$$\nu_t = (C_S\Delta)^2 \left|\overline{S}_{ij}\right|, \quad \left|\overline{S}_{ij}\right| = \sqrt{2\overline{S}_{ij}\overline{S}_{ij}},$$

$$\Delta = (\Delta_1\Delta_2\Delta_3)^{1/3}, \quad C_S \approx 0.1 - 0.12$$

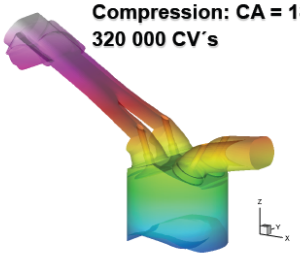

Connecting road length:	**14.1 cm**
Stroke:	**8.5 cm**
Bore:	**8.5 cm**
Engine speed:	**2000 rpm**
Compression Ratio:	**10.5**

Cycle-to-Cycle Fluctuations, CA: 105°, 255°, 450°

(2000/min, VCM: 54°, Cold Flow, 50 Engine Cycles, Fine Grid)

TECHNISCHE UNIVERSITÄT DARMSTADT

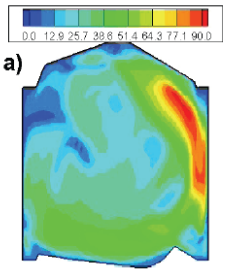

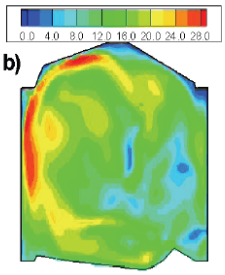

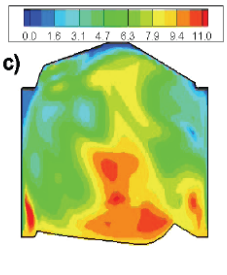

a). CA: 105°

b). CA: 255°

c). CA: 450°

Z = 0.05 m

Estimation of statistical errors
(2000/min, VCM: 54 °, Fine Grid, CA: 270°)

TECHNISCHE UNIVERSITÄT DARMSTADT

Mean velocity (a) and normalized velocity fluctuations (b) averaged over 5, 10, 20, 40 cycles for crank angle 270° at Z = 0.069 m

a).

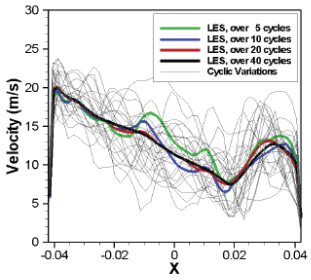

b).

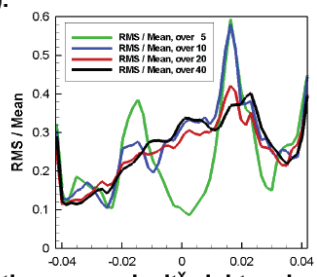

20 samples are needed to get the mean velocity right and 40 samples to determine the fluctuations properly

Accepting a 5% statistical error for mean velocity and 10% for rms of velocity yield 25 and 50 samples respectively (confidence level: 68.3%)

Estimation of modeling and numerical errors
(2000/min, VCM: 54 °, Compression stroke, CA: 255°, z = 0.05 m, 40 engine cycles)

TECHNISCHE UNIVERSITÄT DARMSTADT

Estimated relative velocity error

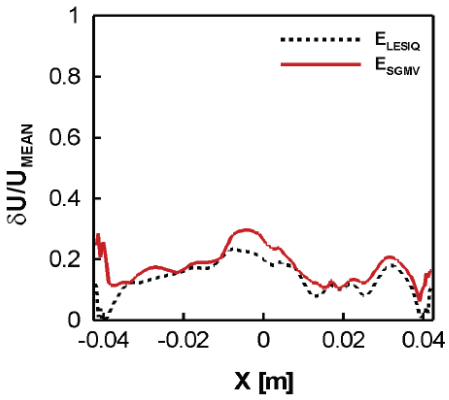

Estimation of modeling and numerical errors

(2000/min, VCM: 54 °, Cold Flow, z = 0.05 m, 40 engine cycles)

TECHNISCHE UNIVERSITÄT DARMSTADT

Estimated ratio of resolved to total TKE

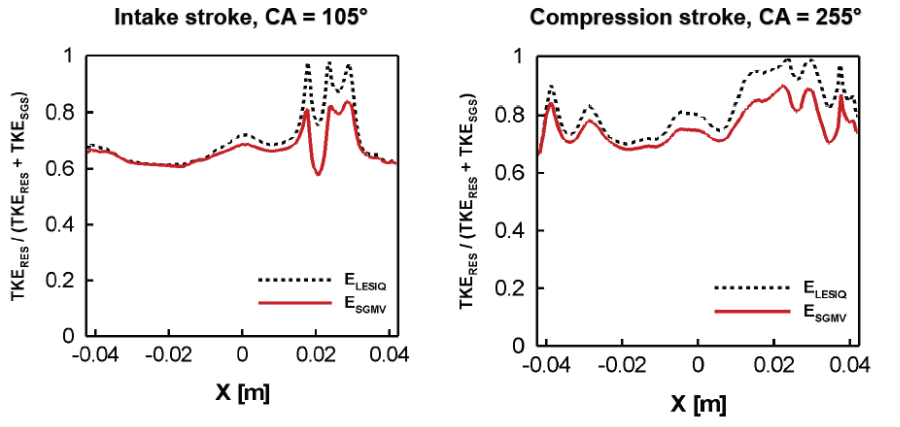

EKT

Conclusions

- LES can achieve excellent results
- Appropriate testcase: realistic & robust or simple & sensitive?
- Tools for quality managment are needed
- Algebraic error-indicators provide useful, additional information
- Meaning/behaviour of these error-indicators is not completely clear yet
- More work on quality management needed!

Imperial College London

45

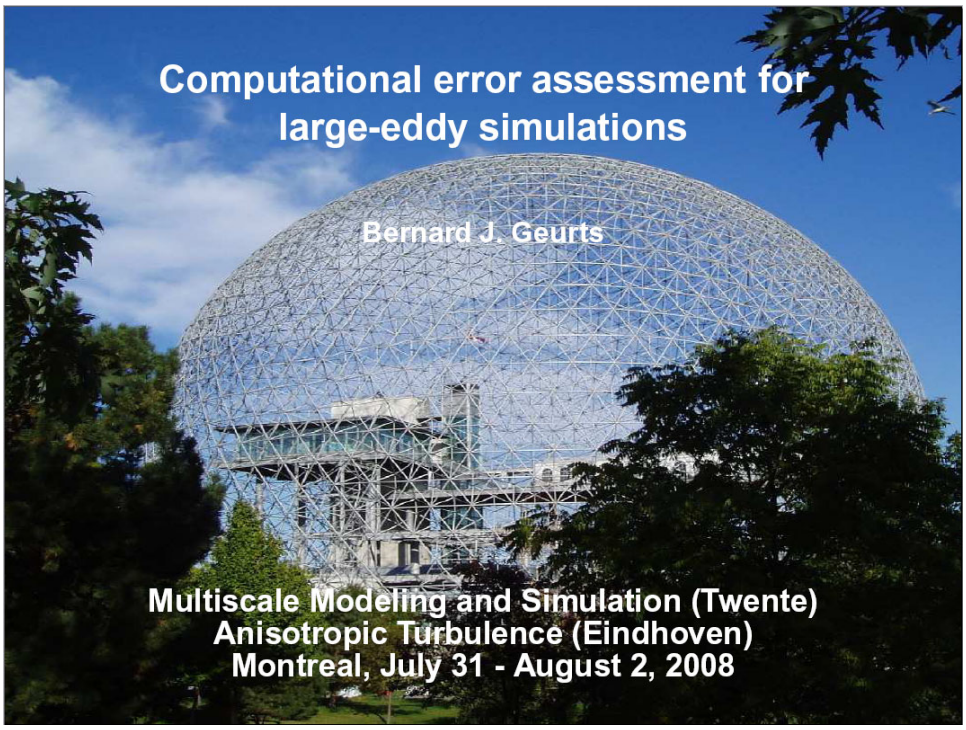

Everyday flows: Wake-Vortex Hazard

Airport throughput limitations: separation up to 10 km

Bernard J. Geurts: Computational error assessment for large-eddy simulations

TU/e

Flow over delta wing

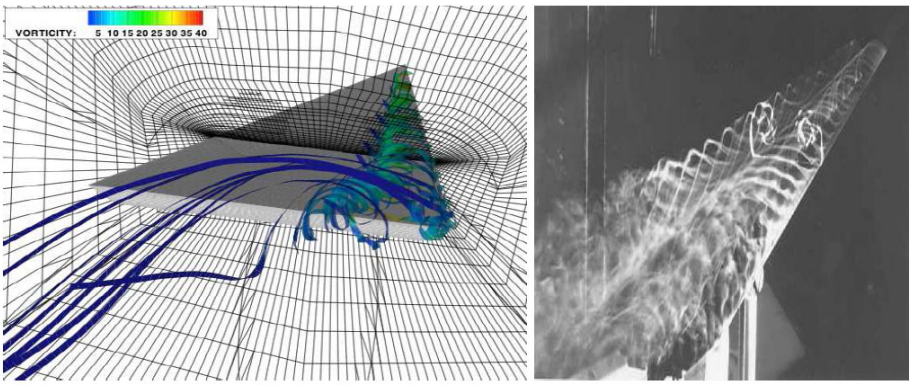

Grid dependence

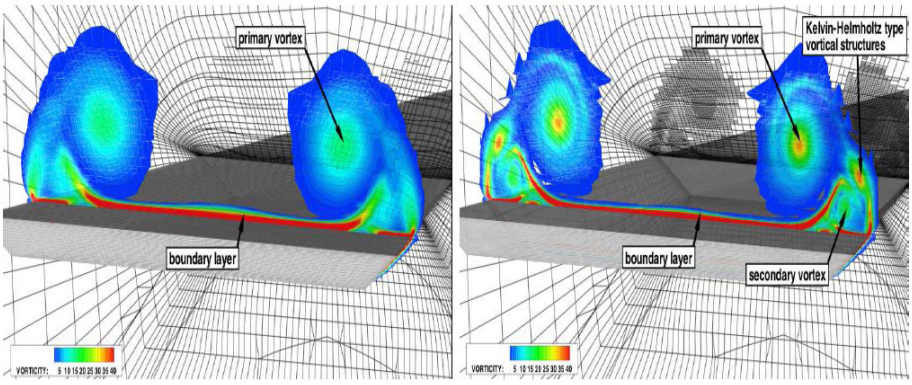

Reliability - Error-bounds - Computational costs?

Combustion-modulated turbulence

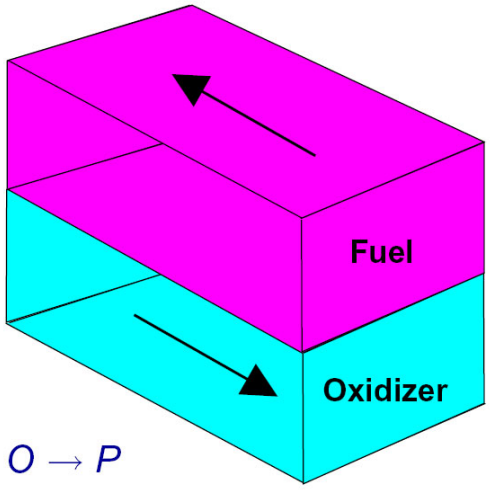

$F + O \rightarrow P$

Developing turbulent $F + O \rightarrow P$ flame

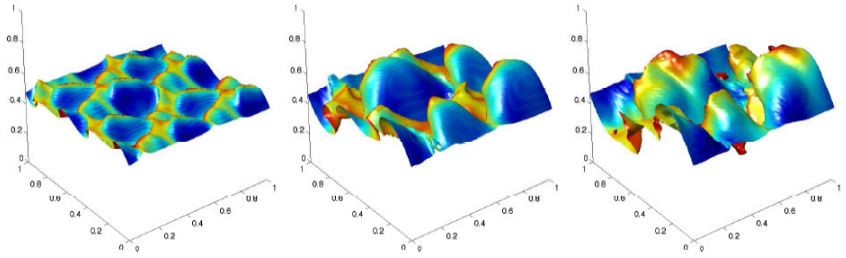

Stoichiometric surface at $t = 20, 40, 60$. Colors denote combustion product (P).

Surface-area and wrinkling

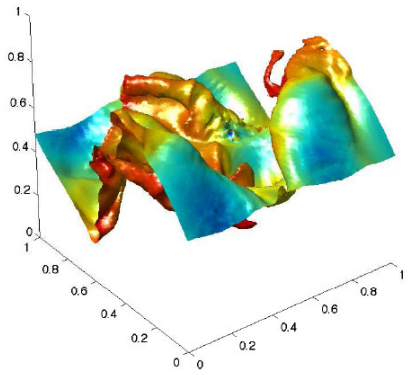

Integral properties, e.g.,

- surface-area A: integrate over $S = \{x \in \mathbb{R} \mid c_F = c_O\}$
- 'wrinkling' W: integrate $|\nabla \cdot \mathbf{n}|$ over S with $\mathbf{n}$ unit normal

DNS-LES: wrinkling at $Q = -100$

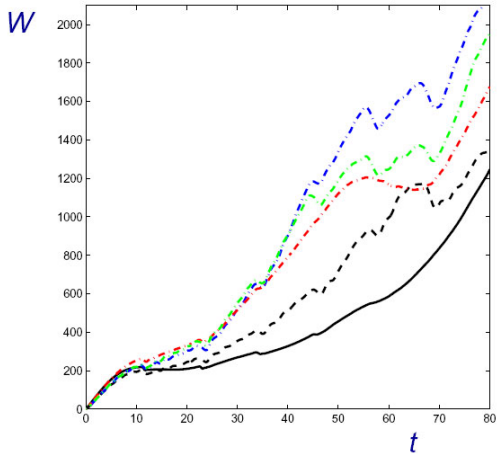

- DNS at 32^3, $\mathbf{128^3}$; dynamic, Leray (32^3, 64^3)
- $W_{LES} > W_{DNS}$: exaggerated small scales in LES

Error contributions from:

- sub filter-scale model: turbulence and combustion
- numerical method: discretization and resolution
- nonlinear interactions/accumulation

How to assess/disentangle this?

Outline

1. Role of numerics in LES
2. Pragmatic LES: error-landscapes
3. Multiple objectives: extensions
4. Concluding remarks

Filtering Navier-Stokes equations

$$\partial_j u_j = 0 \quad ; \quad \partial_t u_i + \partial_j (u_i u_j) + \partial_i p - \frac{1}{Re}\partial_{jj} u_i = 0$$

Convolution-Filtering: *filter-kernel G*

$$\overline{u}_i = L(u_i) = \int G(x-\xi) u(\xi)\, d\xi \quad ; \quad L(1) = 1$$

Large-eddy equations:

$$\partial_j \overline{u}_j = 0$$

$$\partial_t \overline{u}_i + \partial_j (\overline{u}_i \overline{u}_j) + \partial_i \overline{p} - \frac{1}{Re}\partial_{jj} \overline{u}_i = -\partial_j (\overline{u_i u_j} - \overline{u}_i \overline{u}_j)$$

Sub-filter stress tensor

$$\tau_{ij} = \overline{u_i u_j} - \overline{u}_i \overline{u}_j$$

Spatial filtering, closure problem

Shorthand notation:

$$NS(\mathbf{u}) = 0 \quad \Rightarrow \quad NS(\overline{\mathbf{u}}) = -\nabla \cdot \tau(\mathbf{u}, \overline{\mathbf{u}}) \quad \Leftarrow \quad -\nabla \cdot M(\overline{\mathbf{u}})$$

Basic LES formulation

$$\textit{Find } \mathbf{v}: \quad NS(\mathbf{v}) = -\nabla \cdot M(\mathbf{v})$$

After closure system of PDE's results:

- dynamic range restricted primarily to scales $> \Delta$
- does solution $\mathbf{v}$ of closed system resemble $\overline{\mathbf{u}}$?

Goal in LES: *determine the unique solution to system of PDE's that results after adopting explicit closure model*

Numerics in academic LES setting

Goal: *approximate the unique solution to system of PDE's resulting after adopting explicit closure model*

General (textbook) reasoning:

- Filter separates scales $> \Delta$ from scales $< \Delta$
- Computational grid provides additional length-scale h
- Require Δ/h to be sufficiently large ($\Delta/h \to \infty$)
- Good numerics: $v(x,t:\Delta,h) \to v(x,t:\Delta,0)$ rapidly

However:

- computational costs $\sim N^4$: implies modest Δ/h
- potentially large role of numerical method in computational dynamics because of marginal resolution

LES treatment of convective term

Discretization and modeling introduce errors:

$$\begin{aligned}\partial_j(\overline{u_i u_j}) &= \Big[\delta_j(\overline{u}_i\overline{u}_j) + \mathcal{D}_i\Big] + \partial_j\tau_{ij} \\ &= \Big[\delta_j(\overline{u}_i\overline{u}_j) + \mathcal{D}_i\Big] + \Big\{\partial_j m_{ij} + \mathcal{R}_i\Big\} \\ &= \delta_j(\overline{u}_i\overline{u}_j) + \delta_j m_{ij} + \Big(\mathcal{D}_i + \mathcal{R}_i + \mathcal{D}_i^{(m)}\Big)\end{aligned}$$

Distinguish:

- $\mathcal{D}_i$: discretization error from using method δ_j
- $\mathcal{R}_i = \partial_j(\tau_{ij} - m_{ij})$: total 'model-residue'
- $\mathcal{D}_i^{(m)}$: error when treating model m_{ij}, e.g., filtering

Q1: Justified to ignore $\mathcal{D}_i$? Grid-(in)-dependent LES ?

Q2: Interacting errors? Error-decomposition? Dominance?

Total error decomposition

Total (ε_t)=Discretization (ε_d) + Modeling (ε_m)

Decomposition requires: DNS and LES at various $r = \Delta/h$

- Reference via (filtered) DNS data
- LES without discretization errors: fixed Δ, $r \to \infty$
- LES with both types of errors

Provides a posteriori decomposition:

$$\varepsilon_d(E) = E_{\mathrm{LES}}(\Delta, r) - E_{\mathrm{LES}}(\Delta, \infty)$$
$$\varepsilon_m(E) = E_{\mathrm{LES}}(\Delta, \infty) - E_{\overline{\mathrm{DNS}}}(\Delta, r)$$
$$\varepsilon_t(E) = \varepsilon_d(E) + \varepsilon_m(E) = E_{\mathrm{LES}}(\Delta, r) - E_{\overline{\mathrm{DNS}}}(\Delta, r)$$

Requires number of LES: various Δ, h, models, schemes ...

Counter-acting errors: LES-paradoxes

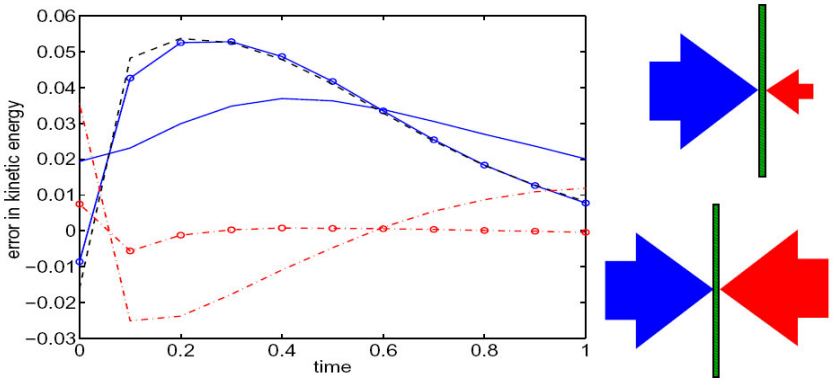

Decaying turbulence: discretization, modeling and total-error

Counter-acting errors: LES-paradoxes

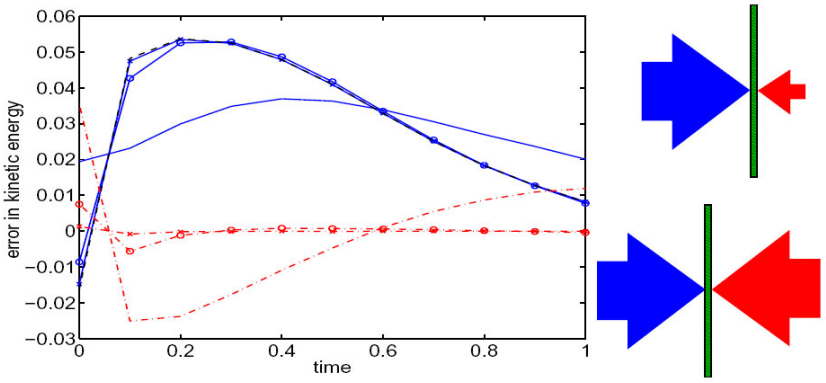

Decaying turbulence: discretization, modeling and total-error

- better model may result in worse predictions
- better numerics may result in worse predictions

Numerics or modeling or both ?

Observe:

- At marginal resolution the numerics strongly modifies the equations that should be solved
- Likewise, the introduction of a subgrid model modifies these equations

Dilemma: which is to be preferred?

- Pragmatic guideline: minimal total error at given computational costs
- NOT: simply combine best numerics and best model

Outline

Grid-dependencies and computational resources

How to use your computer 'wisely'?

A: Δ constant, Δ/h increasing:
- convergence to grid-independent LES is feasible
- grid-independent solution still has model-deficiencies

B: Δ/h constant, Δ decreasing:
- convergence to grid-independent DNS, if feasible
- refinement changes both model-influence and discretization

C: Other refinement strategy ...

Large collection of 'raw' data from simulations: systematic variation to assess influence

Testing ground: turbulent mixing

Three-dimensional impression: vertical velocity

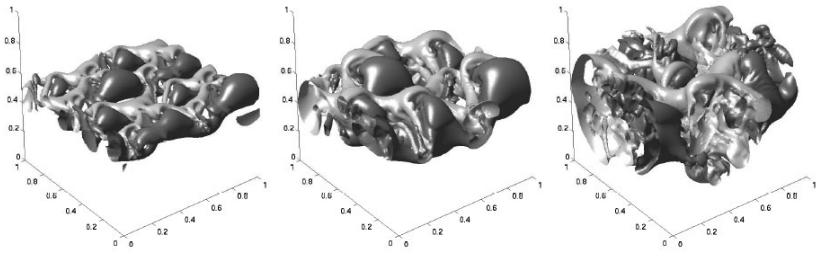

Snapshots at $t = 20$, $t = 40$ and $t = 80$

Option A: Δ constant, Δ/h increasing

Velocity variations: $\langle (u_i - \langle u_i \rangle)^2 \rangle$

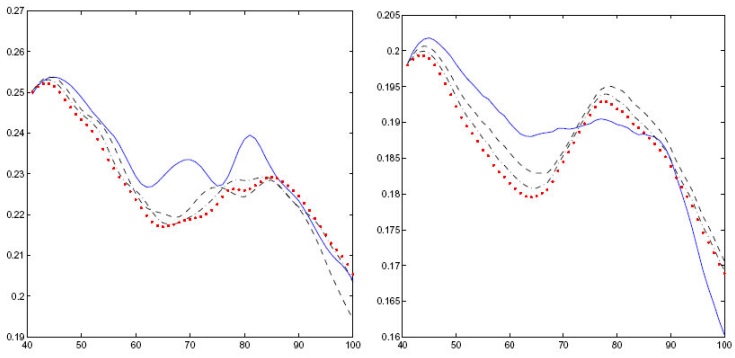

Left:$\Delta = \ell/32$ and Right: $\Delta = \ell/16$ using different resolutions:
$n = 32,\ 48,\ 64,\ 96$

Option A: Δ constant, Δ/h increasing

Kinetic energy spectrum:

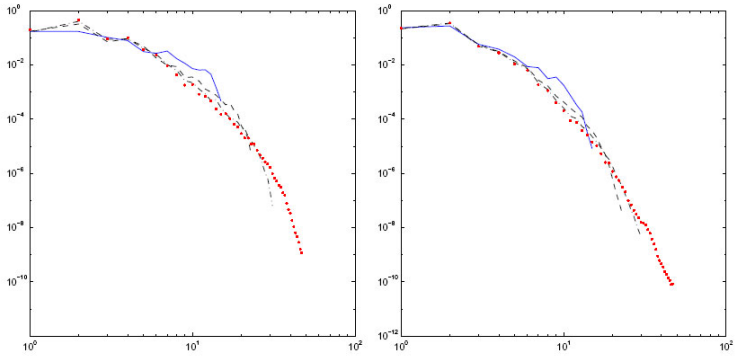

Left: $\Delta = \ell/32$ and Right: $\Delta = \ell/16$ using different resolutions:
$n = 32,\ 48,\ 64,\ 96$

Option B: Δ/h constant, Δ decreasing

Decay of kinetic energy:

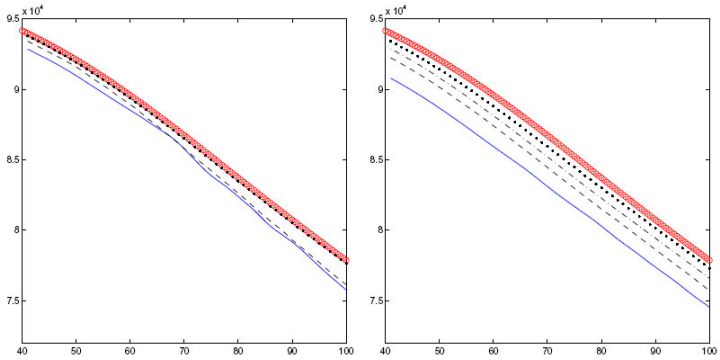

Left: $\Delta/h = 1$ and Right: $\Delta/h = 2$ using different resolutions:
$n = 32,\ 48,\ 64,\ 96$, markers $\circ$: DNS-results

Option B: Δ/h constant, Δ decreasing

Velocity variations: $\langle (u_i - \langle u_i \rangle)^2 \rangle$

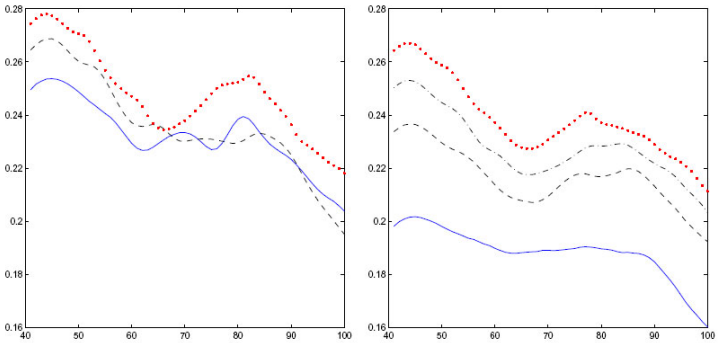

Left: $\Delta/h = 1$ and Right: $\Delta/h = 2$ using different resolutions:

$n = 32,\ 48,\ 64,\ 96$

CPU-time $\sim N^4$ and memory $\sim N^3$

How to put 'raw'-data into helpful framework?

Smagorinsky fluid

Homogeneous decaying turbulence at $Re_\lambda = 50,\ 100$

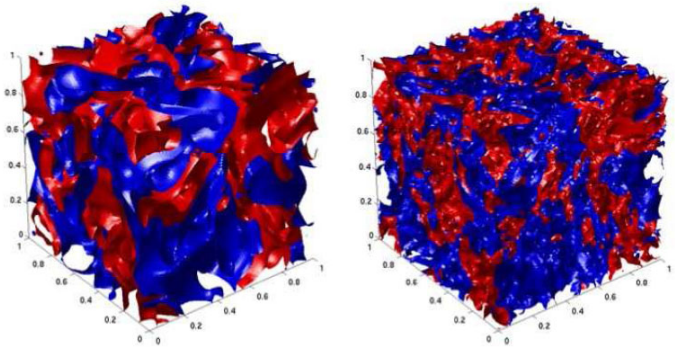

- Smagorinsky fluid — subgrid model:

$$m_{ij}^S = -2(C_S\overline{\Delta})^2|\overline{S}|\overline{S}_{ij} = -2\ell_S^2|\overline{S}|\overline{S}_{ij}$$

introduces Smagorinsky-length ℓ_S

Accuracy measures

Monitor resolved kinetic energy

$$E = \frac{1}{|\Omega|}\int_\Omega \frac{1}{2}\overline{\mathbf{u}}\cdot\overline{\mathbf{u}}\,d\mathbf{x} = \frac{1}{2}\langle\overline{\mathbf{u}}\cdot\overline{\mathbf{u}}\rangle$$

Measure relative error: top-hat filter Δ, grid $h = \Delta/r$

$$\delta_E(\Delta, r) = \left\| \frac{E_{LES}(\Delta, r) - E_{\overline{DNS}}(\Delta, r)}{E_{\overline{DNS}}(\Delta, r)} \right\|$$

with error integrated over time

$$\|f\|^2 = \frac{1}{t_1 - t_0}\int_{t_0}^{t_1} f^2(t)dt$$

- each simulation represented by **single** number
- concise representation facilitates comparison

Error-landscape: Definition

Framework for collecting error information:

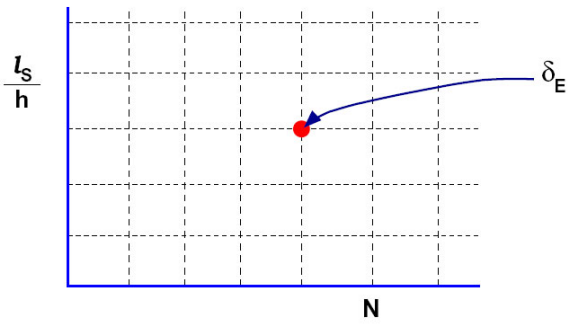

Each Smagorinsky LES corresponds to single point:

$$\left(N, \frac{\ell_S}{h}\right) \quad ; \quad error: \quad \delta_E$$

Contours of δ_E — fingerprint of LES

Total error-landscape

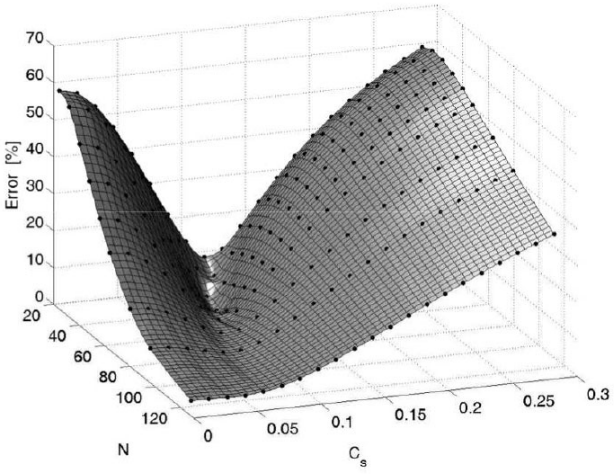

- combination of central discretization and Smagorinsky
- optimum at $C_S > 0$: SGS modeling is viable here

Error-landscape: optimal refinement

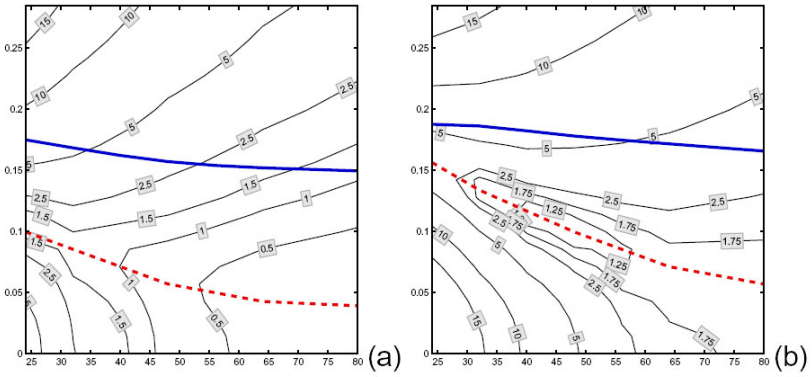

Optimal trajectory for $Re_\lambda = 50$ (a) and $Re_\lambda = 100$ (b)

- Under-resolution leads to strong error-increase
- Dynamic procedure over-estimates viscosity

Finding the optimum: SIPI

Goal: minimize total error at given N

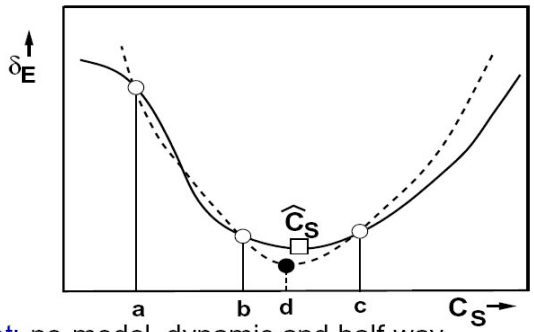

Initial triplet: no-model, dynamic and half-way

New iterand

$$d = b - \frac{1}{2}\frac{(b-a)^2[\delta_E(b)-\delta_E(c)] - (b-c)^2[\delta_E(b)-\delta_E(a)]}{(b-a)[\delta_E(b)-\delta_E(c)] - (b-c)[\delta_E(b)-\delta_E(a)]}$$

SIPI applied to homogeneous turbulence

Each iteration = separate simulation

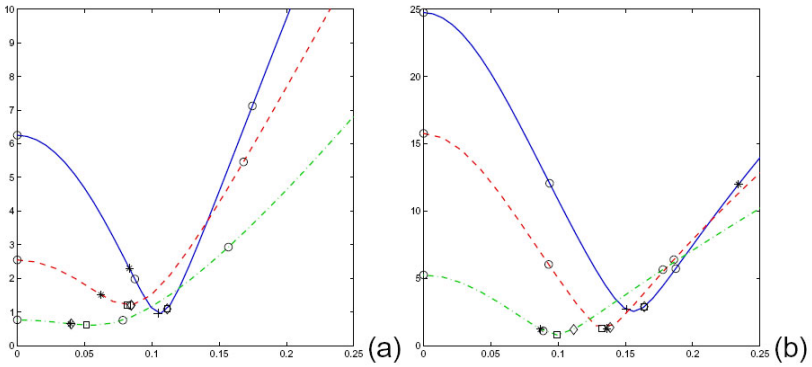

$Re_\lambda = 50$ (a) and $Re_\lambda = 100$ (b). Resolutions $N = 24$ (solid), $N = 32$ (dashed) and $N = 48$ (dash-dotted)

Iterations: $\circ \rightarrow * \rightarrow \diamond \rightarrow \square \rightarrow +$

Convergence example

	$Re_\lambda = 50$		$Re_\lambda = 100$	
n	$C_S^{(n)}(24)$	$C_S^{(n)}(48)$	$C_S^{(n)}(24)$	$C_S^{(n)}(48)$
2	0.17470000	0.15690000	0.18740000	0.17780000
3	0.08735000	0.07845000	0.09370000	0.08890000
4	0.08330619	0.03959082	0.23399921	0.08686309
5	0.11142326	0.04010420	0.16404443	0.11154788
6	0.11156545	0.05141628	0.16400079	0.09935076
7	0.10461386	0.05283713	0.15068033	0.09947629
8	0.10508422	0.05468589	0.15445586	0.09926872
9	0.10602797	0.05504089	0.15600828	0.09938967

- Computational overhead SIPI: CPU-time $T \sim N^4$ implies approximate optimization at N can be (almost) completed within cost of one simulation at $3N/2$

MILES philosophy

Observation:

- practical LES implies marginal resolution
- which implies large role of specific numerical discretization
- next to dynamics due to subgrid model
- and leads to strong interactions and complex error-accumulation

Proposal:

- obtain smoothing via appropriate numerical method alone
- accept that there is no grid-independent solution, other than DNS
- accept that predictions become discretization dependent

Is 'no-model/just numerics' option optimal/viable ?

Consider example: DG-FEM and homogeneous turbulence

DG-FEM of homogeneous turbulence

Discretization: Approximate Riemann solver

$$F = F_{central} + \gamma F_{dissipative} \quad ; \quad HLLC - flux$$

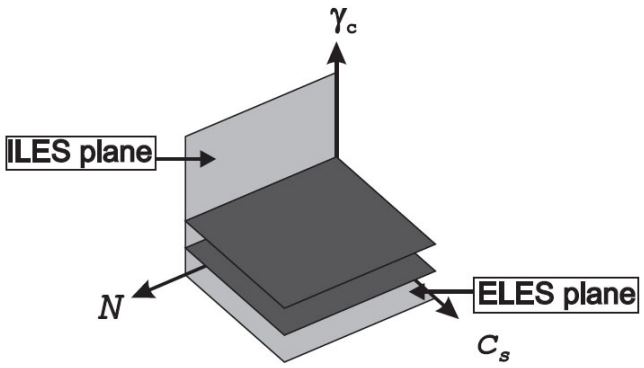

Three-dimensional accuracy charts

LES with DG-FEM: dissipative numerics

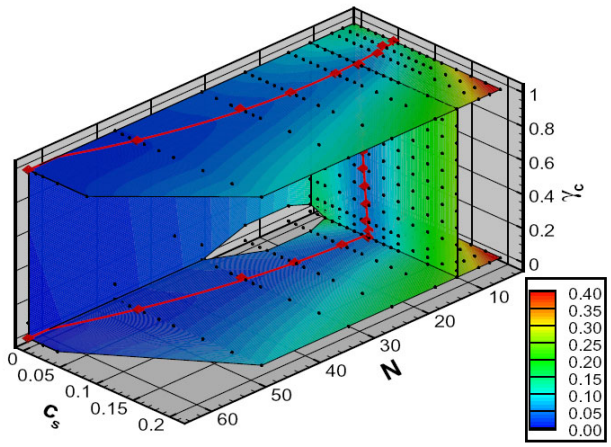

Third order DG-FEM at $Re_\lambda = 100$

Optimal refinement strategies: 2nd order

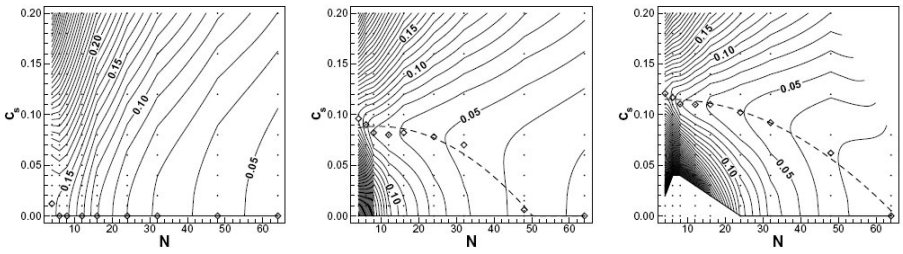

- left-to-right: $\gamma_c = 1$, $\gamma_c = 0.1$, $\gamma_c = 0.01$
- $C_S^* = 0$ at $\gamma_c = 1$: MILES best option
- $\gamma_c < 1$ implies $C_S^* \geq 0$: MILES sub-optimal
- decrease γ_c implies increase C_S^*: exchange of dissipation?

Optimal refinement strategies: 3rd order

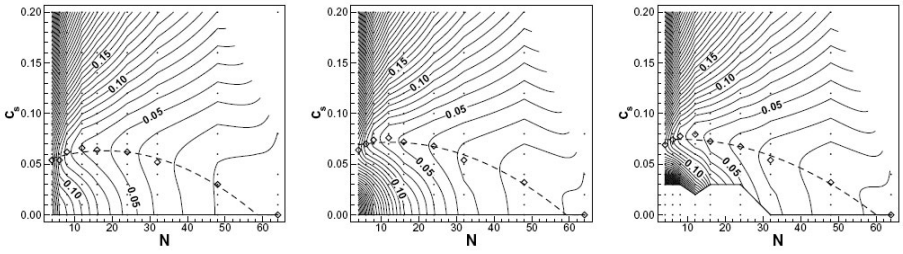

- left-to-right: $\gamma_c = 1$, $\gamma_c = 0.1$, $\gamma_c = 0.01$
- for all $\gamma_c \in [0, 1]$ find $C_S^* \geq 0$: MILES sub-optimal
- optimal C_S is less sensitive to γ_c value than 2nd order

Optimality of MILES ?

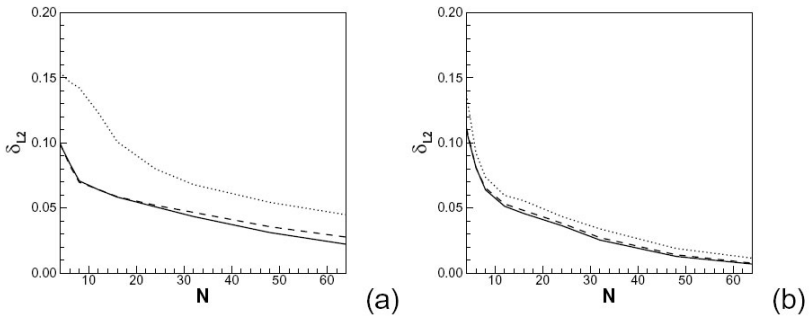

- (a): 2nd order ; (b): 3rd order
- $\gamma_c = 1.00$ (dot), $\gamma_c = 0.10$ (dash) and $\gamma_c = 0.01$ (–)
- 2nd: MILES-error larger than with explicit SGS model
- 3rd: optimum requires explicit SGS model

Outline

Simultaneous error-landscapes

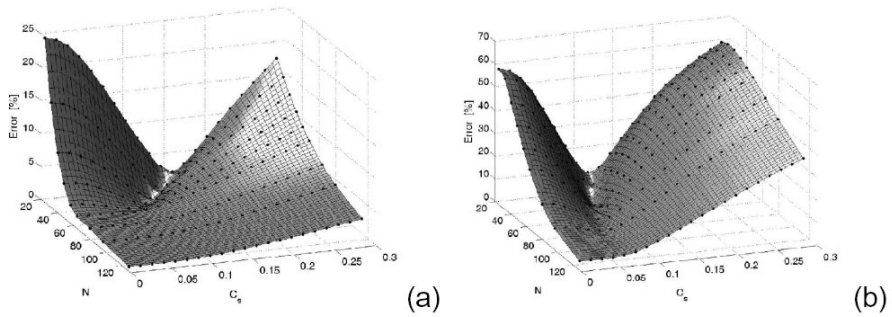

Error pattern in Energy (a) and Enstrophy (b)

Near optimal parameter region: 20%

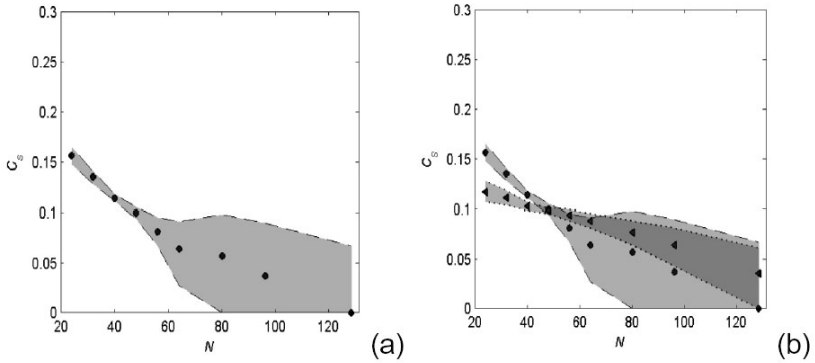

(a) energy, (b) energy and enstrophy: in overlap both accurate.

- connected, overlapping region $N \geq 48$
- weighing of errors leads to 'multi-objective near optimum'

Physics-based or mathematical errors?

Physics-based errors: (option 'a')

$$\varepsilon_p^a = \frac{\int_0^T dt \left[\int_0^{k_c} dk\ k^p \left(E_{LES}(k) - E_{\overline{DNS}}(k) \right) \right]^2}{\int_0^T dt \left[\int_0^{k_c} dk\ k^p E_{\overline{DNS}}(k) \right]^2}$$

Notice: large and small scales included

$$p = -1: \quad \varepsilon_{-1}^a = \varepsilon_{\mathcal{L}} \quad ; \quad p = 0: \quad \varepsilon_0^a = \varepsilon_E \quad ; \quad p = 2: \quad \varepsilon_2^a = \varepsilon_{\mathcal{E}}$$

Mathematical norm: (option 'b')

$$\varepsilon_p^b = \frac{\int_0^T dt \int_0^{k_c} dk\ k^p \left(E_{LES}(k) - E_{\overline{DNS}}(k) \right)^2}{\int_0^T dt \int_0^{k_c} dk\ k^p E_{\overline{DNS}}(k)^2}$$

No direct physical interpretation

Multi-objective regions: type a & b

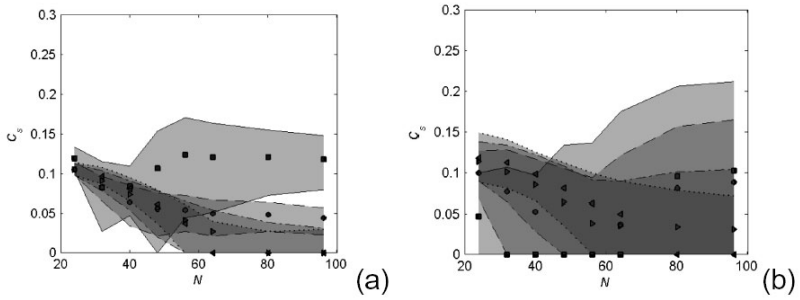

$Re_\lambda = 50$: in (a) physics-based error measure and in (b) mathematical norm

Multi-objective regions: Re-dependence

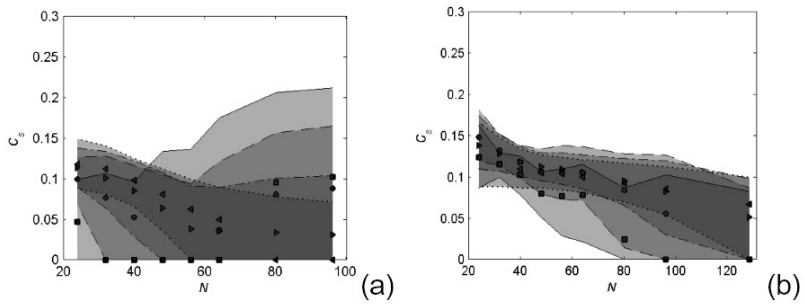

Mathematical norm error at $Re_\lambda = 50$ (a) and $Re_\lambda = 100$ (b)

Combine large and small scale errors

What if we want it all? Weighted error - multi-objective optimal

$$\widetilde{\varepsilon}^a(N, C_S) = \sum_{p=-1}^{2} \varepsilon_p^a(N, C_S)/\varepsilon_p^a(N, \widehat{C}_S)$$

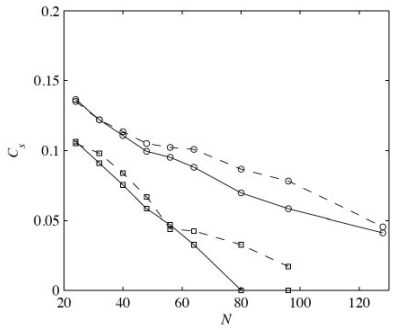

$Re_\lambda = 50$ (□), $Re_\lambda = 100$ (○) for option 'a' (solid) and 'b' (dash)

Quite robust MO optimal lines (option a vs b)

Head or tail? Nudging spectra

Optimum corresponding to ε_0^a (○) or ε_2^a (△)

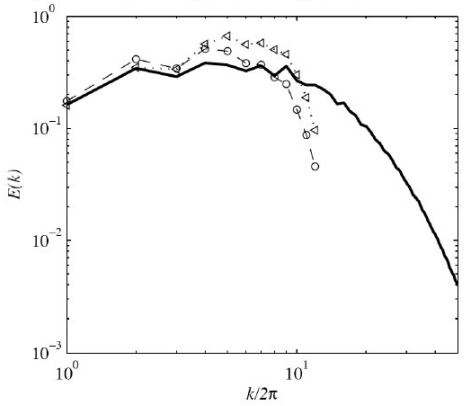

Accuracy desired for head or tail of spectrum?
(use error-measure $p = 0$ or $p = 2$ respectively)

Numerics and optimality - 1

Spatial discretization: Convective (2-4) and Viscous (2-4)

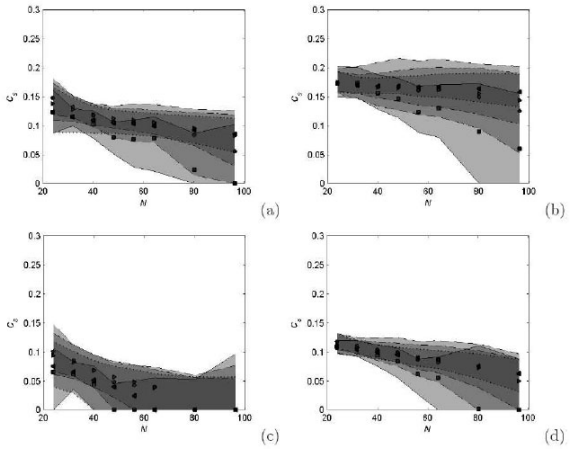

(a): 2-2, (b): 4-2, (c): 2-4, (d): 4-4

Numerics and optimality - 2

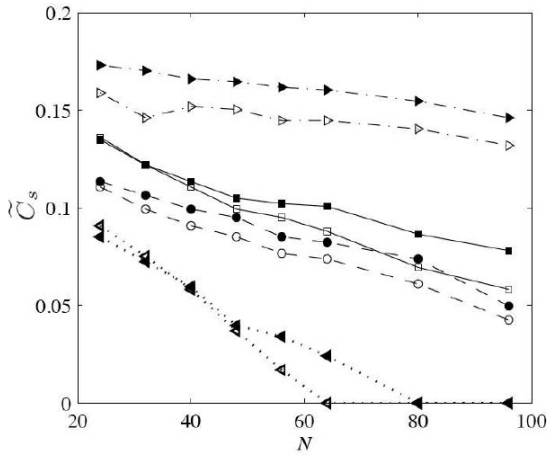

(a): 2-2 (□), (b): 4-2 (right-△), (c): 2-4 (left-△), (d): 4-4 (○)

Open issues ...

Database analysis for HIT only:

- What if no DNS is available? (compare with experiment, theory, ...: "if one can 'grade' solution, one can optimize it")
- What if flow is inhomogeneous? (ongoing study, e.g., mixing layer: assessment based on "cost function" and SIPI - application specific)
- What if flow-physics is complex? (e.g., combustion: defines "its" cost-function, include numerical and physical 'wish list', adjoint optimization?)
- ...

Concluding remarks

- error-decomposition: modeling, discretization effects
- LES-paradoxes and interacting errors: better models/numerics may not lead to better predictions
- error-landscape – optimal refinement strategy
- multiple objectives – include mathematical norm, weigh 'large' and 'small' scale properties
- landscape: effective tool, MILES, numerical method, SGS model, ...

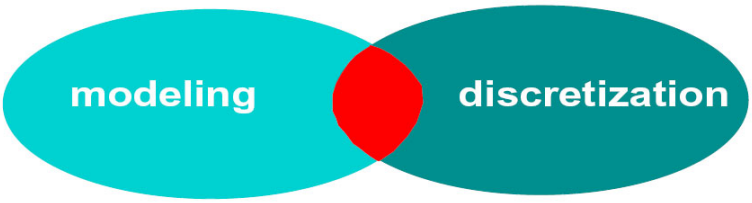

LES Quality Assessment in the Context of Combustion Noise Predictions

Presented by: Matthias Ihme

With contributions from: Heinz Pitsch,
Phong Bui, Wolfgang Schroeder,
and Manfred Kaltenbacher

LES Combustion Modeling

- Key aspects in combustion LES
  - Modeling of combustion modes (diffusion, premixed, and partially premixed flames)
  - Prediction of complex combustion phenomena
    - Flame dynamics (extinction, auto-ignition, lifted flames)
    - Finite rate chemistry effects, complex fuels
    - Geometrical complexity (swirl, recirculation, confined flames)
- Current LES validation practice
  - Time-averaged data (mean, RMS, Reynolds stresses, scalar profiles, conditional data, PDFs, and burning indices)

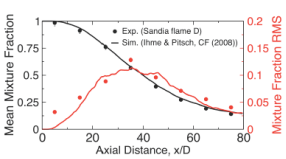

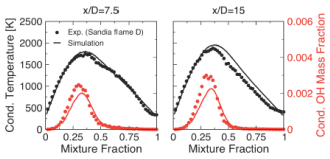

LES Combustion Modeling

- LES provides space-time resolved information about turbulent flows
  - Turbulence length scales
  - Space-time correlations
  - Energy and scalar spectra
- Use this information for validation and development of combustion LES models

LES Combustion Modeling

- DLR Flame A
  - OH frequency- and integral time scales (Renfro et al. 2004)
  - Temperature spectra (Wang et al. 2008)

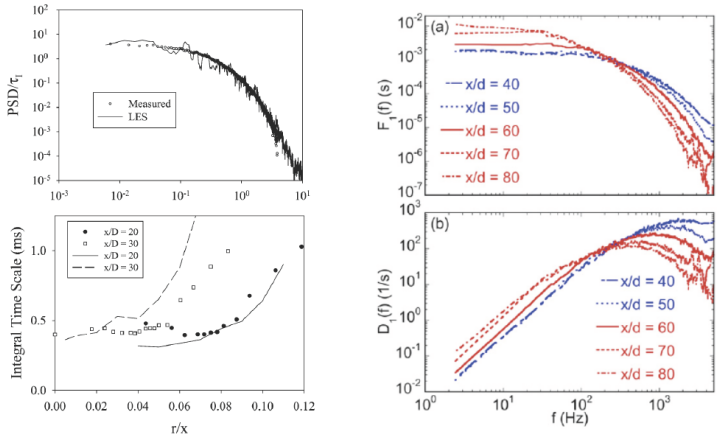

LES Combustion Modeling

- DLR Flame A
  - OH two-point correlation length (Zhang et al. 2005)

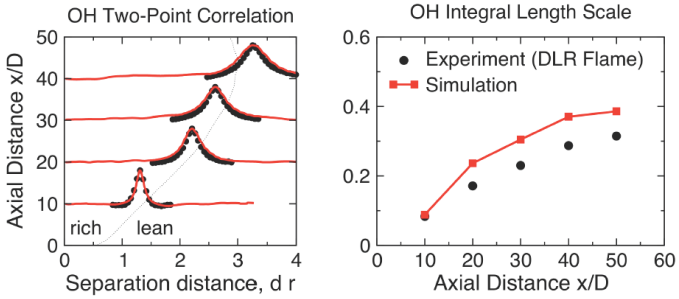

LES Combustion Modeling

- Two-point correlation and spectral data are currently not fully utilized for LES validation and QA
  - Lack of experimental data
  - Engineering relevance
- Space-time correlations and energy spectra are crucial in aeroacoustics applications and for prediction of combustion noise
  - Acoustic source term characteristics
  - Sound pressure level
- Objective: LES validation and QA in context of combustion noise

LES Combustion Modeling

- Technical relevance of combustion noise
  - Significant noise source in aircraft and auxiliary power units
  - Acoustic radiation in turbulent flames (swirling flames, PVC)
  - Potential precursor for acoustic instabilities in confined combustors
- Challenges in predicting combustion noise
  - Unsteady process
  - Acoustic inefficiency
    - Small fraction of total (kinetic and thermo-chemical) energy is converted in acoustic power
  - Discrepancy between characteristic length scales

Turbulence/Chemistry Interaction

$$\underbrace{\mathrm{M}\lambda \sim l_t \sim \mathrm{Re}_t^{3/4}\eta}_{\text{Turbulence/Acoustic Coupling}} \sim \mathrm{Re}_t^{1/2}\mathrm{Da}^{1/3} l_r$$

  - Reliable characterization of noise-generation and transmission mechanisms

Overview

- Physics of Combustion Noise
- Mathematical modeling
- LES Quality Assessment for Combustion Noise
  - Numerical Issues
  - Modeling Issues
  - Physical Issues
- Validation Data
- Summary and Conclusions
- Discussion

Physics of Combustion Noise

Physics of Combustion Noise

- Combustion noise ≠ thermo-acoustic instabilities
- Two-modes of combustion noise
- Indirect combustion noise:
  - Interaction of entropy inhomogeneities with strong pressure gradients

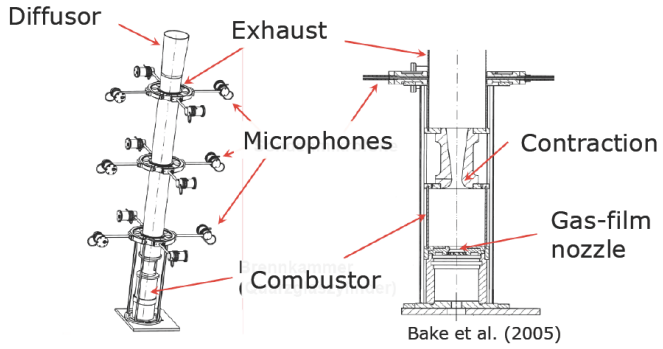

Bake et al. (2005)

Physics of Combustion Noise

- Direction combustion noise
  - Expansion of gas volume by unsteady heat release at ambient pressure

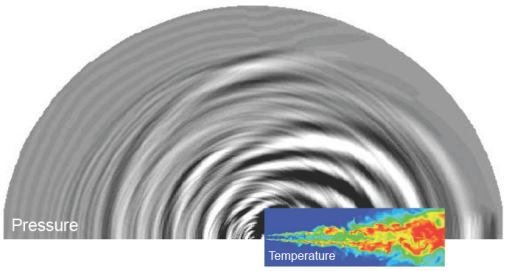

Physics of Combustion Noise: Jet Flames

- Broadband spectra with random phase and amplitude
- Overall sound pressure depends on fuel composition, fuel mass flow rate
- Nearly universal spectra (dependency on burner diameter and turbulence velocity) with peak at low frequencies
- Weak/no coupling between pressure perturbations and heat release rate

Measurements of Sound Pressure Level in Partially Premixed Flame (Singh et al. (2005))

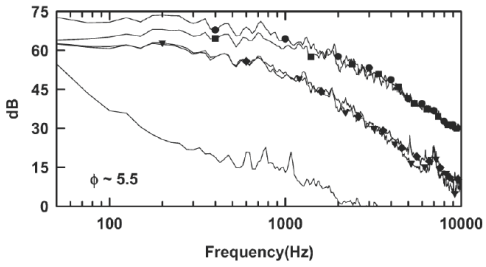

Combustion Noise Modeling

Mathematical Modeling

- Direct computation of sound (DNS, LES)

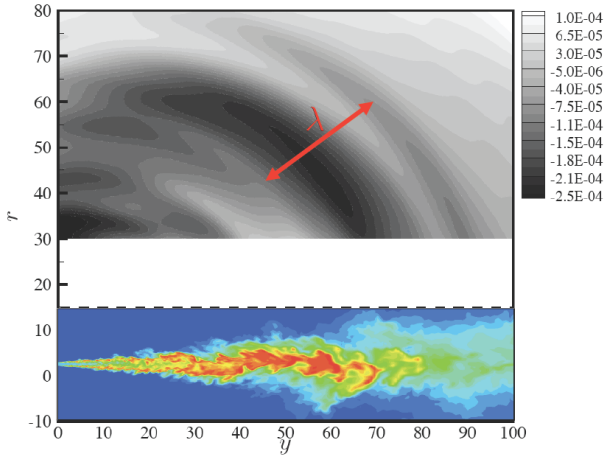

Mathematical Modeling

- Direct computation of sound (DNS, LES)
  - Integrated computation of flow field and acoustic radiation; computational domain includes noise-generating flow region and acoustic region
  - Challenges for direct sound computation
    - Spatial resolution: $\lambda/l_r \sim \mathrm{Re}_t^{1/2}\mathrm{Da}^{1/3}\mathrm{M}^{-1} \Rightarrow \lambda \gg l_r$
    - Minimize grid stretching artifacts, high-order numerical methods

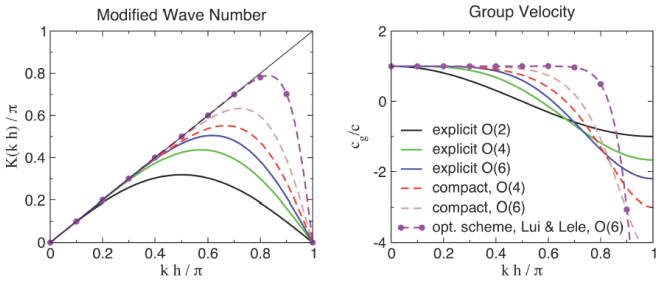

Mathematical Modeling

- Hybrid approach
  - Couple flow field simulation (LES, URANS) with acoustic analogy (Lighthill, Phillips, APE, …)
  - Identify and represent acoustic sources by equivalent source term distribution
  - Extract acoustic source terms form turbulent reacting flow
  - Interpolation of acoustic sources onto acoustic-grid

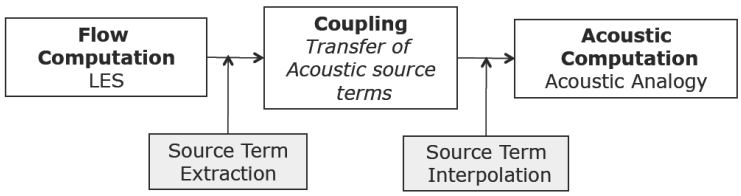

LES Quality Assessment for Combustion Noise

LES Quality Assessment for Combustion Noise

- Challenges in hybrid LES/CAA approach for prediction of combustion noise

Modeling Errors
- Turbulent subgrid models
- Combustion model (characterization of acoustic sources: unsteady heat release, extinction and reignition, …)

Numerical Errors
- Spatial and temporal discretization in flow and acoustic domains, high-frequency filters for numerical stability
- Interpolation of acoustic sources between flow and acoustic domains

Physical/Eng. Challenges
- Spatial extend of acoustic source region
- Acoustic frequency-range
- Geometrical complexity
- Acoustic/chemical coupling mechanisms

LES Quality Assessment for Combustion Noise

- Employ hybrid LES/CAA formulation
  - Combustion model: Flamelet/progress variable model
  - Acoustic model:
    - (1) Acoustic perturbation equations
    - (2) Lighthill's acoustic analogy

$$\left\{\mathrm{M}^2\partial_\tau^2 - \Delta\right\} p' = \nabla\cdot\nabla\cdot\left(\overline{\rho}\widetilde{\boldsymbol{u}}\widetilde{\boldsymbol{u}}\right) - \partial_\tau\nabla\cdot\left((1-\overline{\rho})\widetilde{\boldsymbol{u}}\right) - \mathrm{Da}\partial_\tau\left(\widetilde{\overline{\rho}\frac{\omega_C}{\rho^2}\partial_C\rho}\right)$$

Wave Operator | Acoustic sources, extracted from LES

- LES application and validation
  - DLR flame A
- Quality assessment
  - Validation of combustion LES
  - Acoustic validation

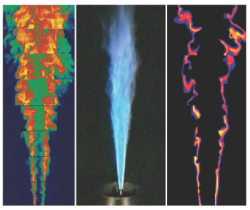

LES Quality Assessment for Combustion Noise

- Modeling Error:

  (1) Acoustic contributions from residual stresses and fluxes are typically neglected
  - Source terms are of quadrupole/octupole nature with rapid decay (potentially only second order effects)
  - Mostly relevant at high frequencies/wave length (f_{LES}~20 kHz) , but combustion noise is dominant around f_{CN}~500 Hz

  (2) Combustion Model and Chemistry Tabulation
  - Combustion modeling errors (PDF, flamelet, …)
  - LES combustion models often employ tabulation techniques for efficient chemistry representation (flamelet model, FPI, FGM, ISAT, PRISM)
  - Data-retrieval using multi-linear table interpolation, polynomial expansion, Taylor series, …
  - Table resolution and interpolation errors not systematically addressed ➔ Convergence study

LES Quality Assessment for Combustion Noise

- Modeling Error:
  (2) Combustion Model and Chemistry Tabulation

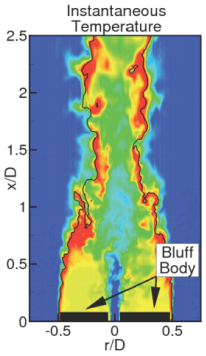

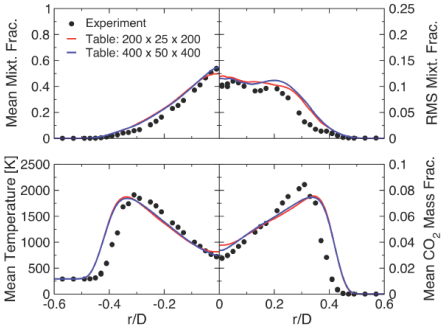

- Table resolution and interpolation error have often only insignificant effect on flow-field statistics (mean, RMS, conditional data)

LES Quality Assessment for Combustion Noise

- Modeling Error:
  (2) Combustion Model and Chemistry Tabulation
  - Table interpolation introduces errors that are reflected in frequency spectra and will be represented as spurious noise

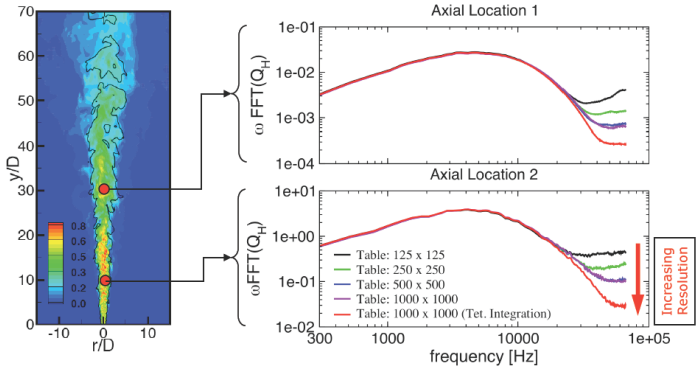

LES Quality Assessment for Combustion Noise

- Modeling Error:
  - (2) Combustion Model and Chemistry Tabulation
    - Table interpolation introduces errors that are reflected in frequency spectra and will be represented as spurious noise sources

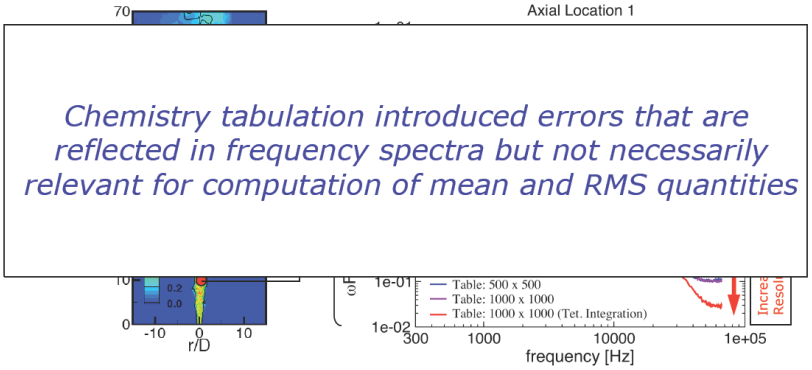

Chemistry tabulation introduced errors that are reflected in frequency spectra but not necessarily relevant for computation of mean and RMS quantities

LES Quality Assessment for Combustion Noise

- Numerical errors: Interpolation of acoustic sources from LES-grid onto acoustic grid
  - Unsteady heat release rate is dominant acoustic source term in direct noise
    - Confined to narrow region around $\widetilde{Z} = Z_{st}$
    - Typically not fully resolved in LES

$$\overline{Q}_H = \overline{\rho}\widetilde{\frac{\omega_C}{\rho^2}\frac{\partial \rho}{\partial C}}$$

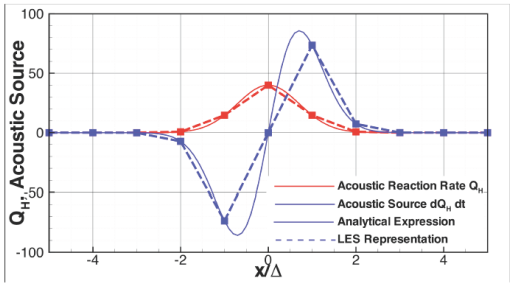

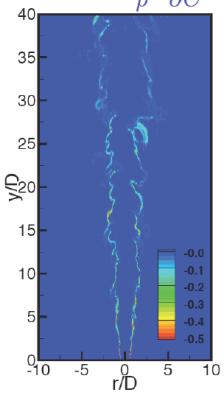

LES Quality Assessment for Combustion Noise

- Numerical errors: Interpolation of acoustic source from LES grid onto acoustic grid introduced spurious noise
  - Example: Convection of density inhomogeneity through constant mean flow ➔ no sound generation

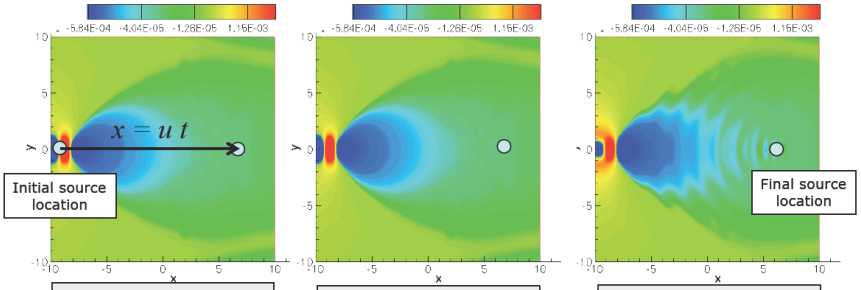

Analytical solution generates no sound

LES-CAA fine-fine grid interpolation: no sound generation

LES-CAA coarse-fine grid interpolation: spurious noise

LES Quality Assessment for Combustion Noise

- Numerical errors: Interpolation of acoustic source from LES grid onto acoustic grid introduced spurious noise
  - Example: Convection of density inhomogeneity through constant mean flow ➔ no sound generation

Interpolation of acoustic sources from LES to acoustic grid introduced spurious noise

sound generation

spurious noise

LES Quality Assessment for Combustion Noise

- Physical/Engineering Challenges: Spatial Extend of Acoustic Source Domain

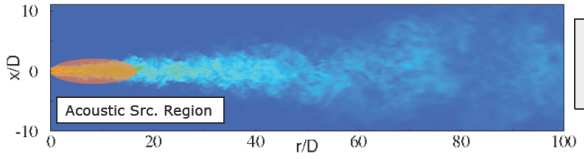

Isothermal Jets:
-Acoustic source region confined to shear layer region

LES Quality Assessment for Combustion Noise

- Physical/Engineering Challenges: Spatial Extend of Acoustic Source Domain

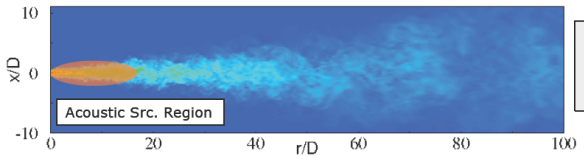

Isothermal Jets:
-Acoustic source region confined to shear layer region

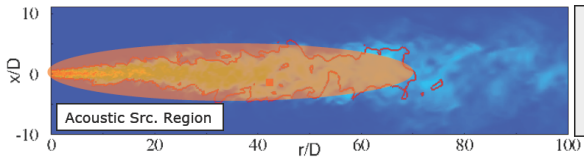

Jet Flames:
-Heat release is most significant noise source
-Confined to Z_{st}
-Acoustic source region confined to flame region

LES Grid Stretching →

LES Quality Assessment for Combustion Noise

- Physical/Engineering Challenges: Spatial Extend of acoustic domain
  - Convection of acoustic sources
  - Temporal resolution of acoustic signal is limited by convective cut-off frequency

$$f_c = \frac{\langle \widetilde{u} \rangle}{2\Delta x}$$

  - For jets: $\langle \widetilde{u} \rangle \propto x^{-1}$
  - LES grid: $\Delta x \propto x$

$$\Big\} f_c \propto x^{-2}$$

  - Spatio-temporal resolution of acoustic source region in diffusion flames require extremely large computational grids

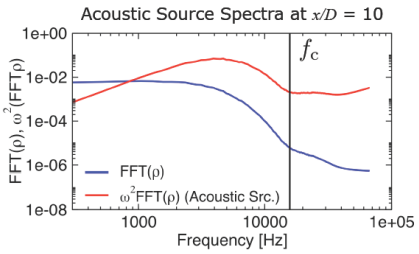

  - Recommendation: Consider partially premixed flames as acoustic benchmark flame configurations

Summary and Conclusions

- Combustion noise prediction present novel challenges for LES/CAA
  - Additional length scale disparity
  - Acoustic inefficiency and resulting difference in amplitudes between pressure perturbation and turbulence fluctuations
  - Strong dependence of acoustic signal on space-time correlation and frequency spectra
- LES quality assessment
  - Spurious noise source contaminate acoustic results due to
    - Numerical errors
    - Combustion model
    - Insufficient resolution of extensive acoustic source region
- Other challenges:
  - Characterization of acoustic source terms in LES
  - Ambiguities in identification of acoustic and non-acoustic quantities
  - Acoustic transmission effects (refraction, scattering effects)
- LES/CAA modeling
  - Requires difference set of validation data, including spectral, correlation information

Notes

ANSYS®

Quality Assessment of hm1 and hm1e

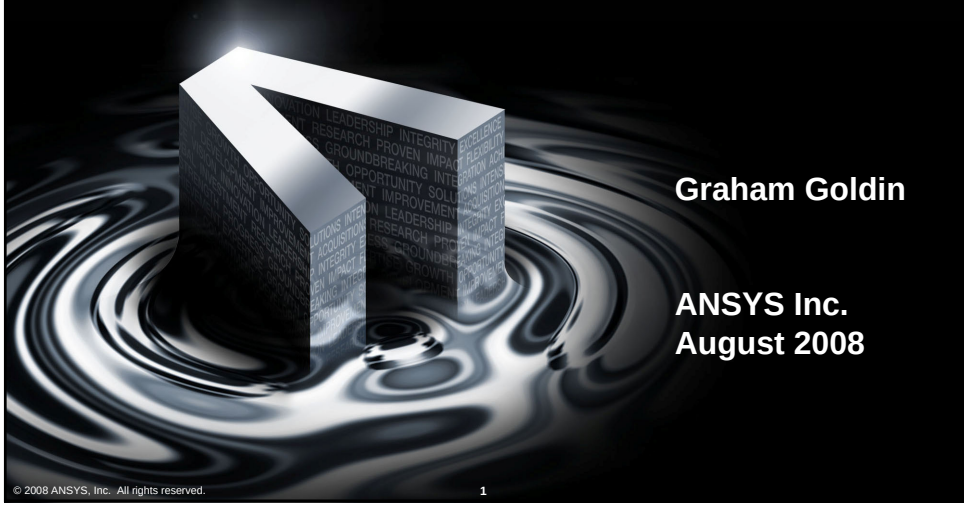

Graham Goldin

ANSYS Inc.
August 2008

Summary

ANSYS®

- **LES of Sydney Bluff flames hm1e and hm1**
  - Models and Discretization
  - Boundary Conditions
  - Results
- **Results of LES Quality Indices**

LES of Sydney Bluff flame

- **Models**
  - Dynamic Smagorinsky
  - Steady Laminar Flamelet (GRI2.11 chemistry)
    - Dynamic Sc_t
- **Discretization**
  - 2nd order Bounded Central (BCD) for momentum
  - 2nd order QUICK for all other scalars
  - Unstructured hex-mesh
    - 1M and 2M cells
  - 2nd order implicit Euler: time-step = 5e-6s

LES of Sydney Bluff flame

- **1M cell mesh**

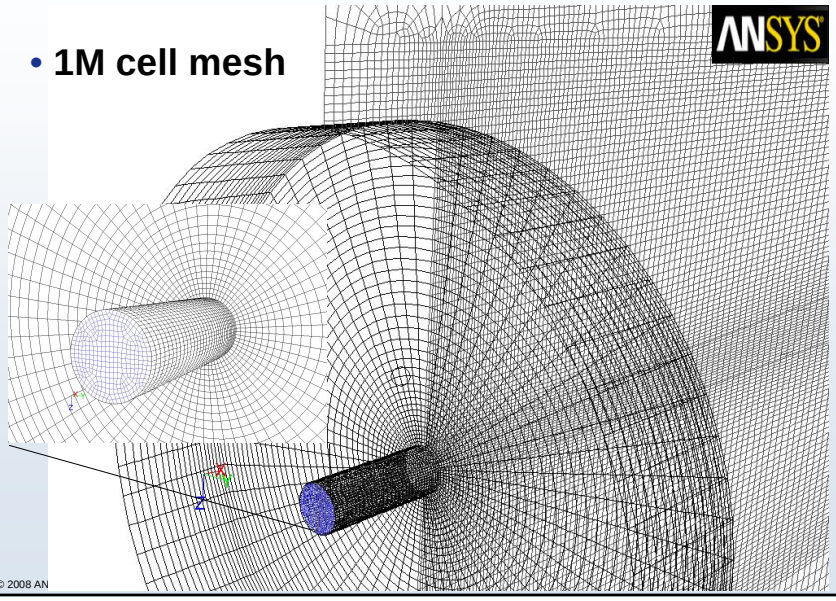

Boundary Conditions

- **Jet inlet**
  - Vortex method for turbulent fluctuations
  - 10% turbulence intensity
  - x-velocity (SI units): U_{jet} + *26.25 – 22000r*
- **Co-flow inlet**
  - ~ following Pitsch&Raman, x-velocity (SI units):

    $U_{co\text{-}flow}$ *-5 + 5*MIN(1, MAX(0, (r-0.025)/0.003))*
    +20(1-2*ξ) MAX(0, (0.030-r)/0. 005)*
    - where ξ is a uniform random number
- **Bluff body**
  - Adiabatic, no-slip

Boundary Conditions

- **Results very sensitive to inlet BCs**

Small vortices in co-flow inlet cause small vortices at shear layer edge and increase air entrainment. Large vortices in co-flow cause large scale unsteadiness down-stream

Penetration of central jet depends on specified jet intensity

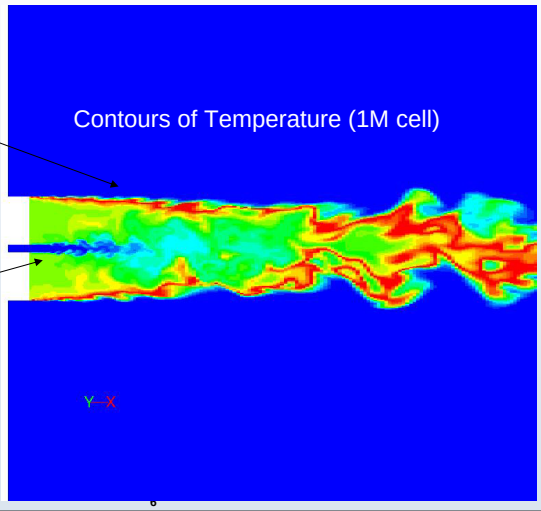

Results: hm1e

- ***Ujet = 108 m/s***
- **Uco-flow = *35 m/s***
- **Velocity measurements only**
- **LES statistics collected over 6 flow throughs**

Results: Mean axial velocity hm1e

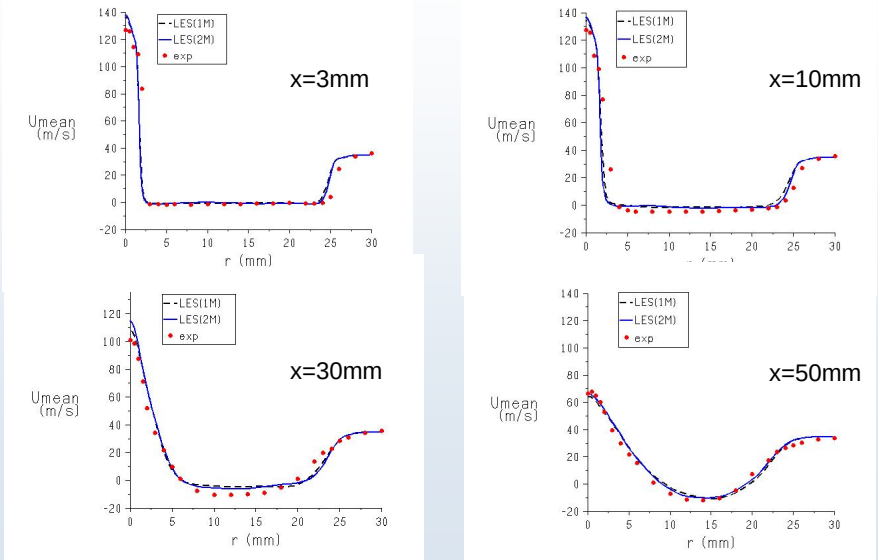

Results: Mean axial velocity hm1e

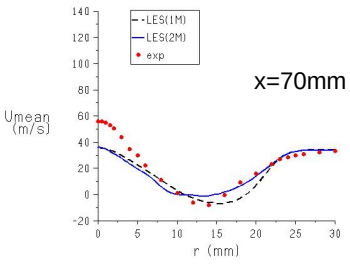

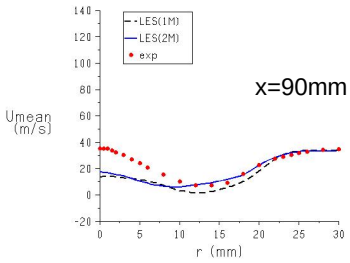

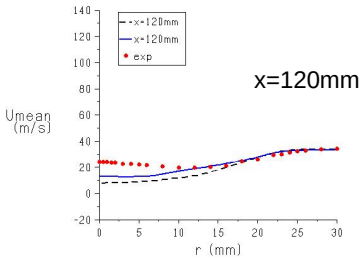

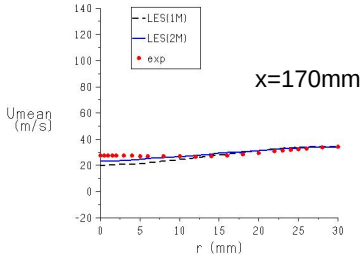

© 200 9

Results: Mean radial velocity hm1e

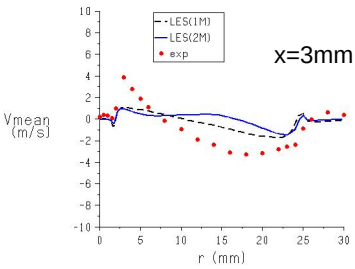

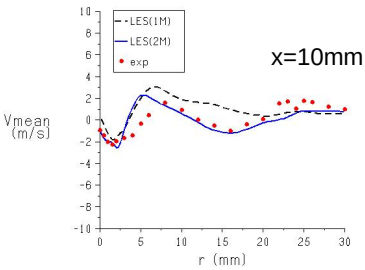

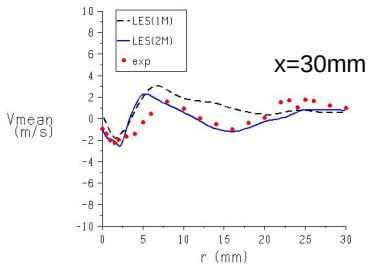

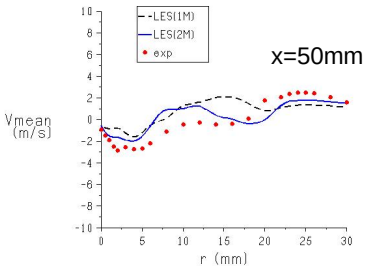

© 10

Results: Mean radial velocity hm1e

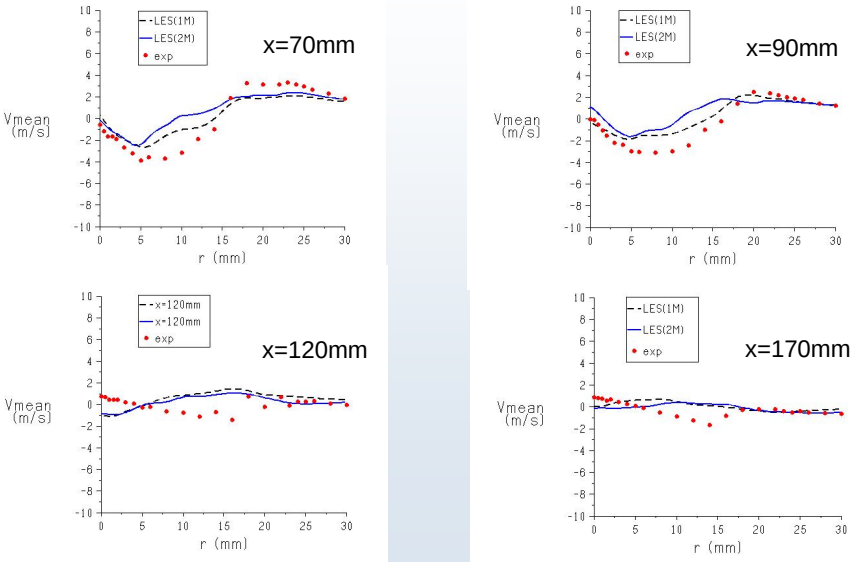

Results: RMS axial velocity hm1e

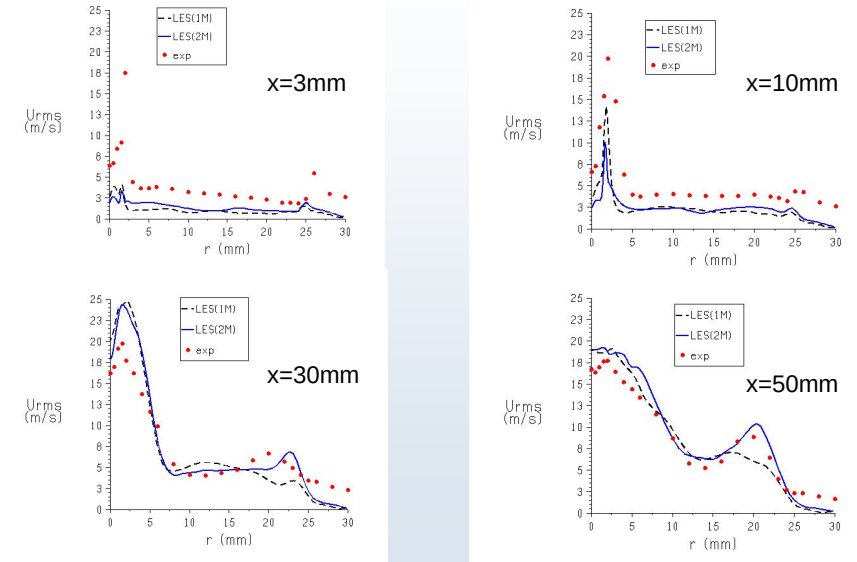

Results: RMS axial velocity hm1e

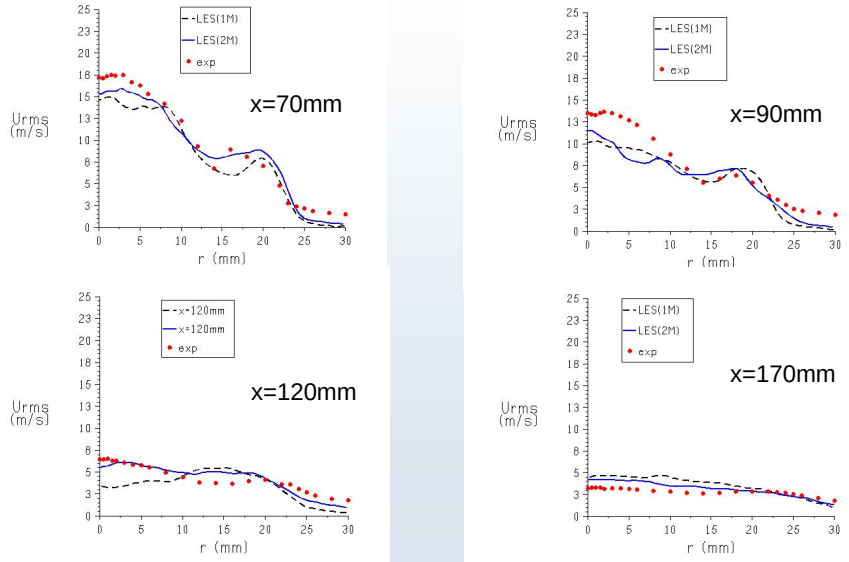

Results: RMS radial velocity hm1e

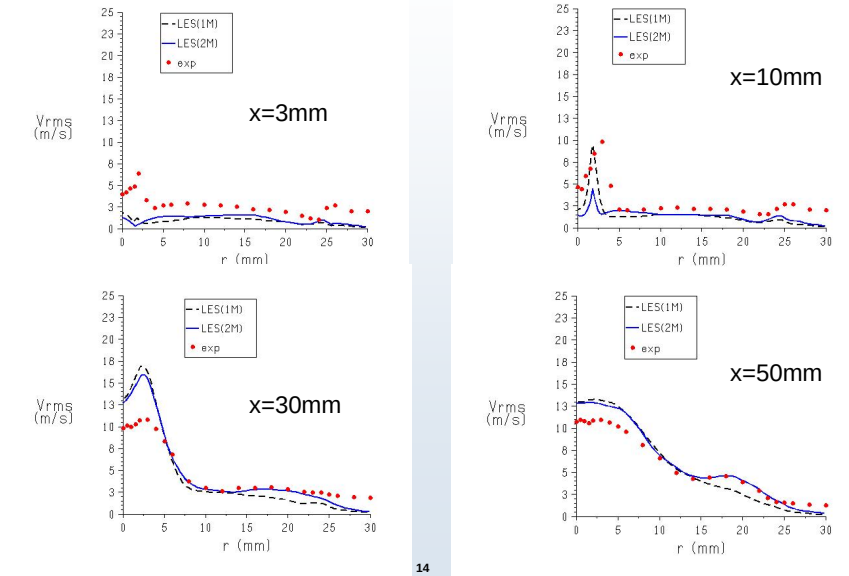

Results: RMS radial velocity hm1e

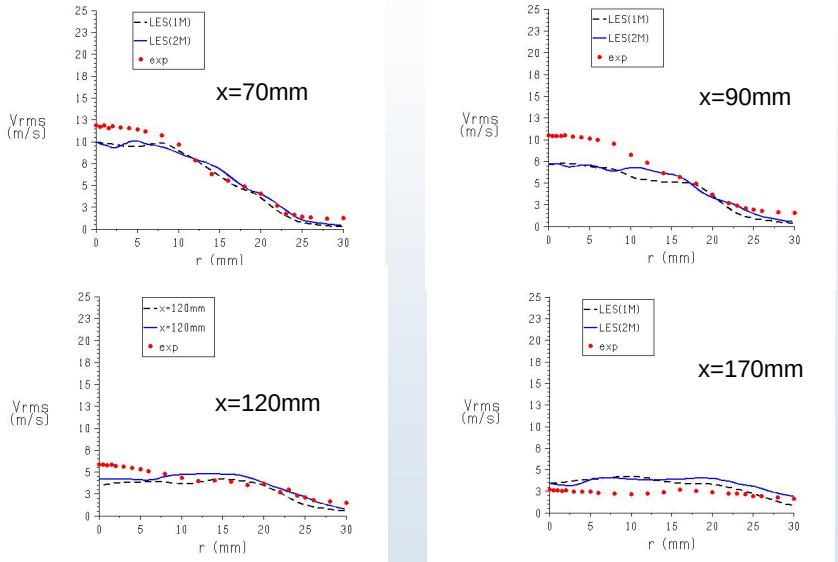

LES Quality: 1. Pope Criterion

- **Fraction of TKE in resolved scales:**

$$M(x) = \overline{\left(\frac{K(x,t)}{K(x,t) + k(x,t)} \right)}$$

- **Means denoted by overbars**
- **Resolved TKE:** $K(x,t) = \frac{1}{2}\left((U - \overline{U})^2 + (V - \overline{V})^2 + (W - \overline{W})^2\right)$
- **sgs TKE:** $k(x,t) = 1.5u'^2 = 1.5\left(\mu_t / (\rho L_{sgs})\right)^2$
- **Typically strive for for M>0.8**

Results: hm1e Pope Criterion

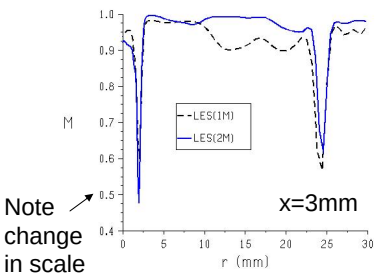

Note change in scale

x=3mm

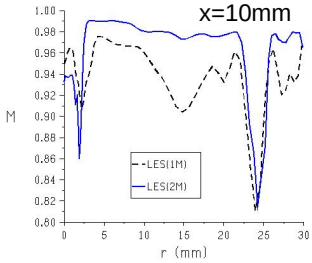

x=10mm

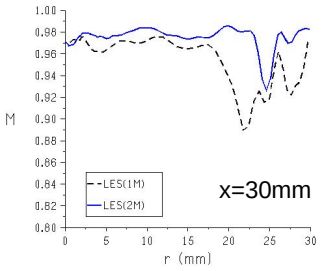

x=30mm

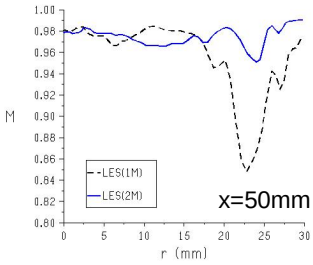

x=50mm

17

Results: hm1e Pope Criterion

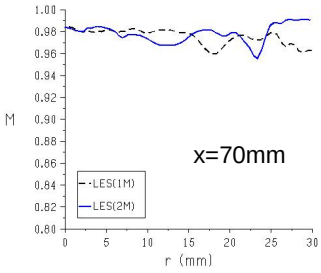

x=70mm

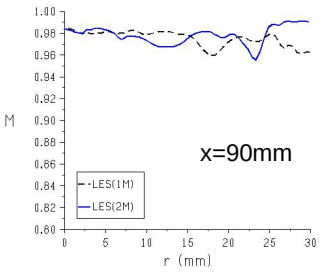

x=90mm

18

LES Quality: 2. LESIQ$_\nu$

- **Celik et al., J. Fluids Eng., 127 (2005)**
- **Single grid index of quality**

$$LESIQ_\nu(x) = \left(1 + 0.05\left(\frac{\nu + \nu_t}{\nu}\right)^{0.53}\right)^{-1}$$

- **Typically strive for LESIQ$_\nu$>0.8**
  - LESIQ$_\nu$>0.95 is considered DNS

Results: hm1e LESIQ$_\nu$

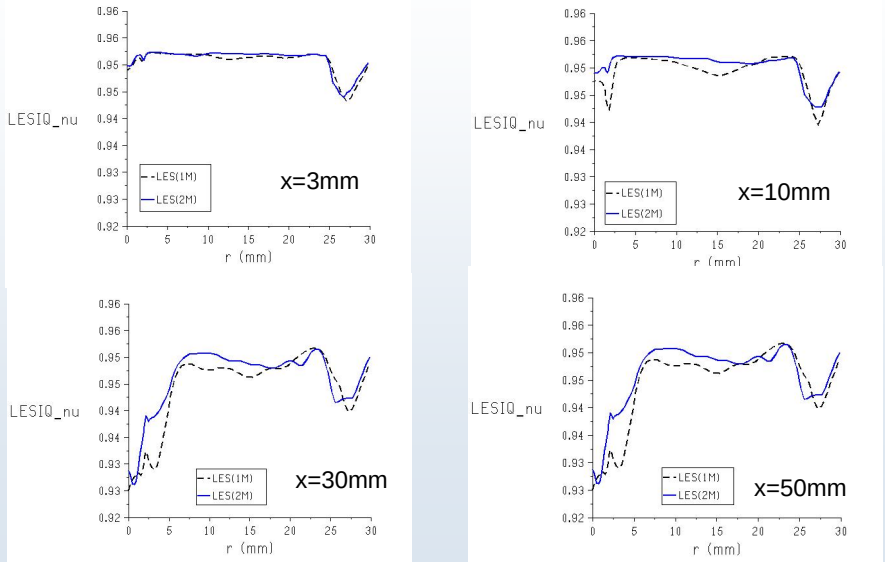

Results: hm1e LESIQ$_\nu$

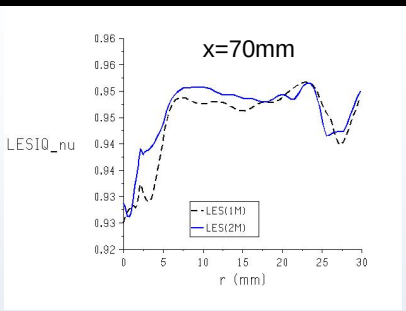

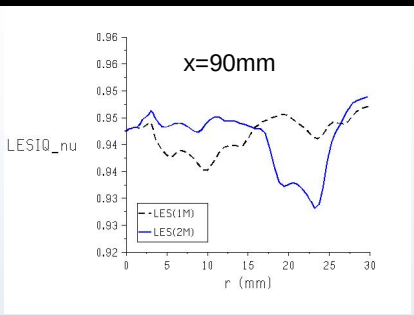

LES Quality: 3. LESIQ$_\kappa$

- **Celik et al., J. Fluids Eng., 127 (2005)**
  - Two grid index of quality
    - Richardson extrapolation
    - More reliable than LESIQ$_\nu$

$$LESIQ_\kappa(x) = \left(1 + \left(1 - \frac{K^c}{K^f}\right) \Big/ \left(\left(\frac{\Delta^c}{\Delta^f}\right)^p - 1\right)\right)^{-1}$$

  - K^c/K^f are resolved TKE on coarse/fine grids
  - Δ^c/Δ^f is coarse/fine grid length = 2
  - p is the discretization order of accuracy = 2
- **Typically strive for LESIQ$_\kappa$>0.8**

Results: hm1e LESIQ$_\kappa$

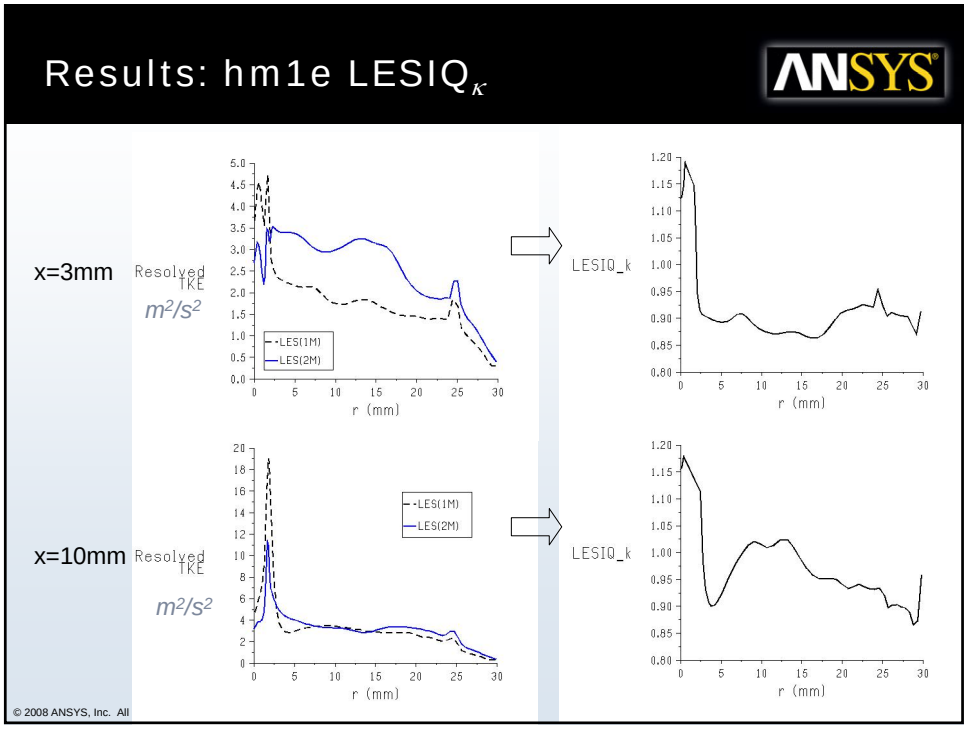

Results: hm1e LESIQ$_\kappa$

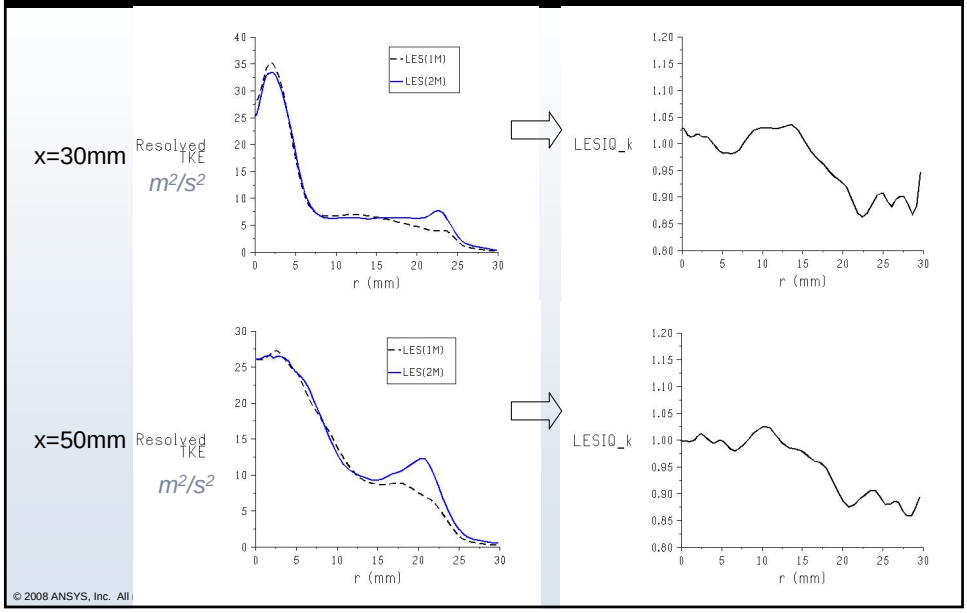

Results: hm1e LESIQ$_\kappa$

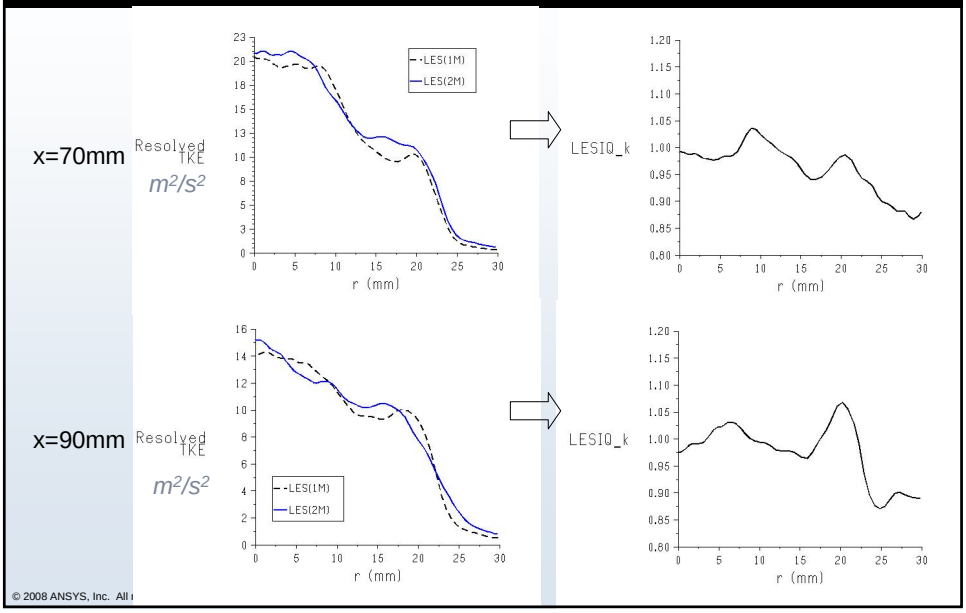

hm1e Quality: Some thoughts

- **For a LES scheme that is too dissipative:**
  - Velocity fluctuations damped
  - Low turbulent viscosity (μ_t) with Smagorinsky
  - All three quality indicators will show good resolution for dissipative codes (small μ_t)
    - Perfect quality for MILES
- **Plan to repeat runs with less dissipative schemes in Fluent**
  - Central Differencing
  - Disable reconstruction limiting

hm2e: Turbulent Viscosity low

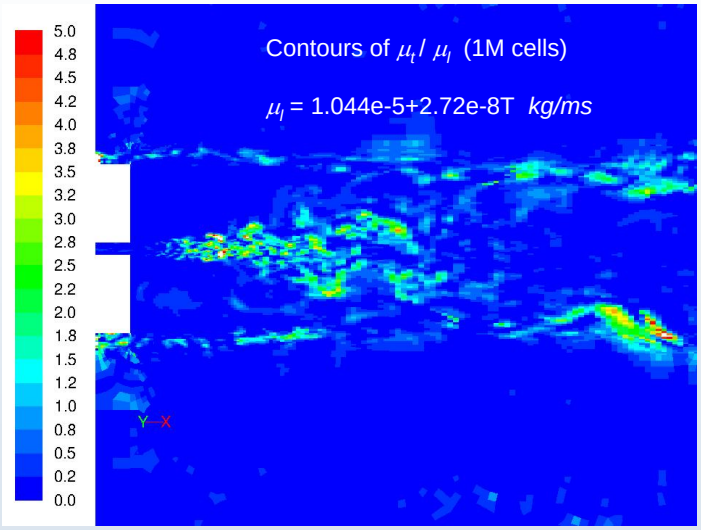

hm1e velocity vectors

Lack of small scale structures?

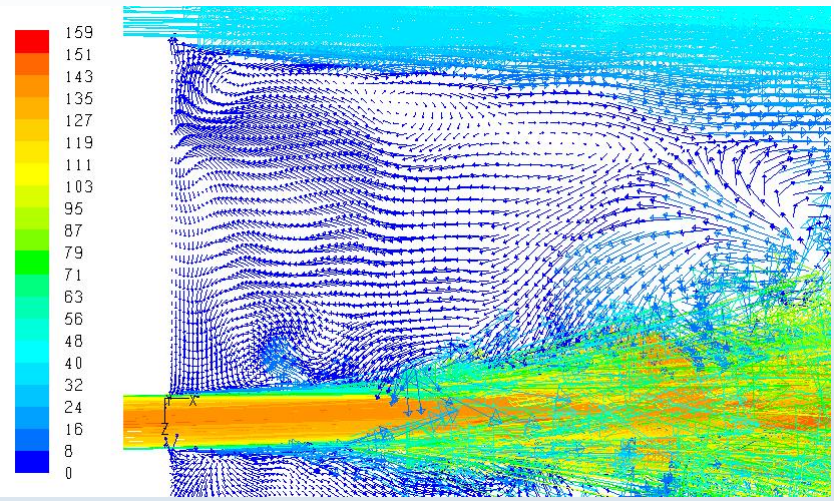

hm1e Smagorinsky constant

C_s<0.1 : is the dynamic model compensating for excessive numerical dissipation?

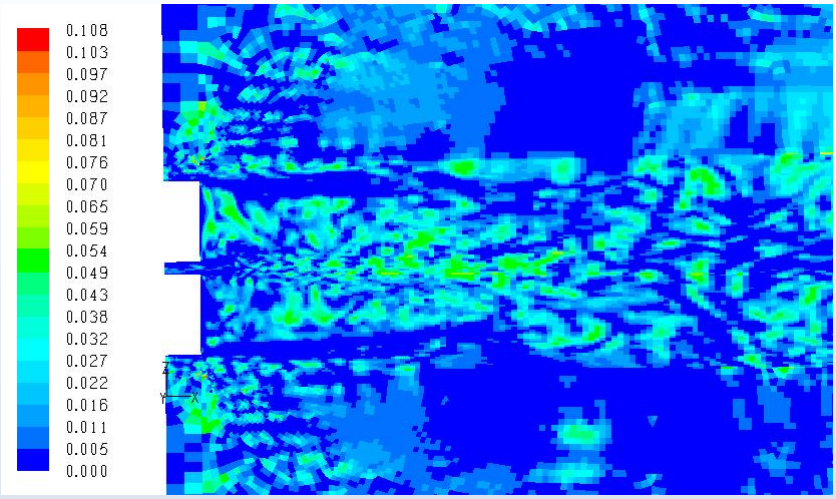

Results: hm1

- ***Ujet = 118 m/s***
- **Uco-flow = *40 m/s***
- **Scalar and velocity measurements**
- **LES statistics collected over 4(3) flow throughs for the 1M(2M) cell cases**

Results: Mean axial velocity hm1

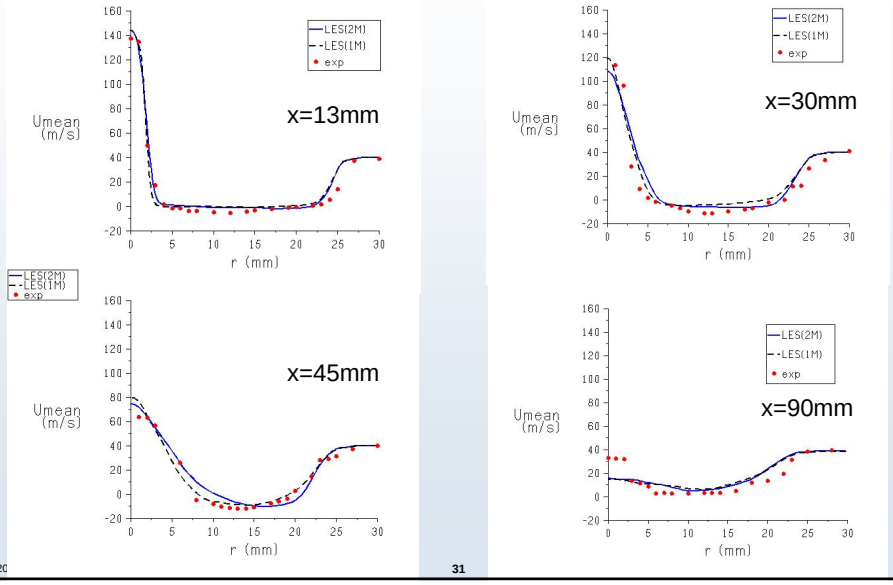

Results: Mean radial velocity hm1

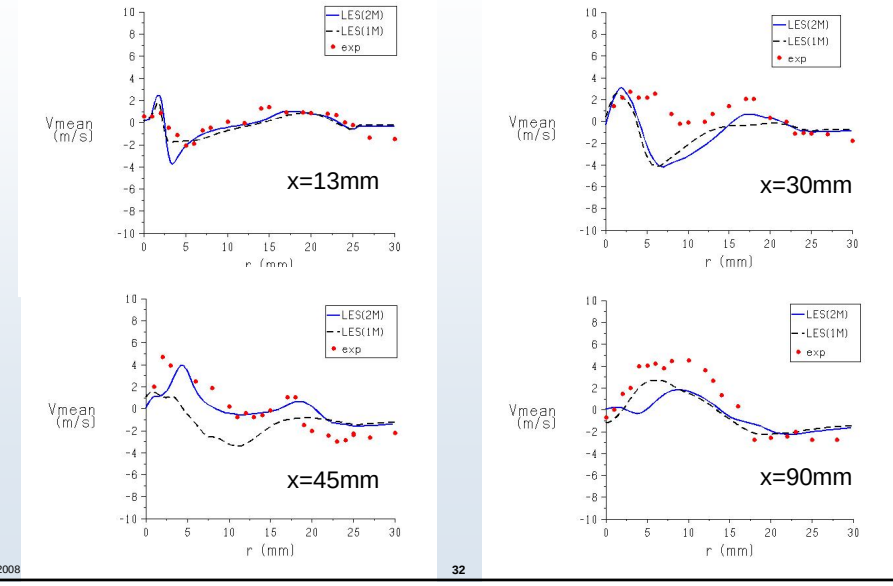

Results: RMS axial velocity hm1

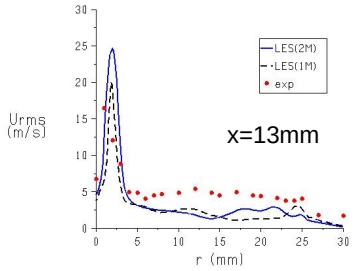

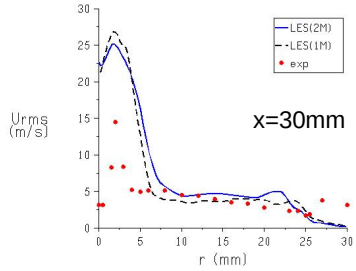

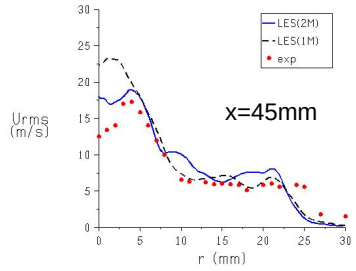

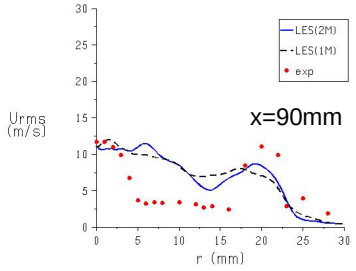

Results: RMS radial velocity hm1

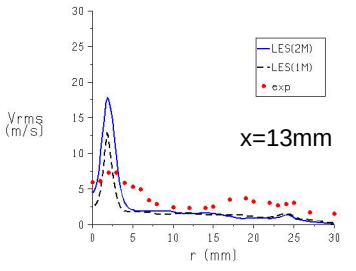

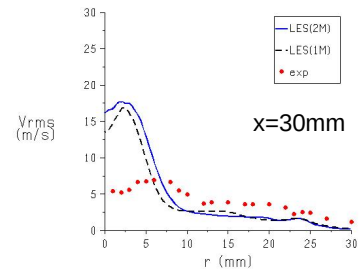

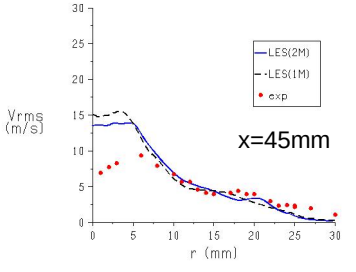

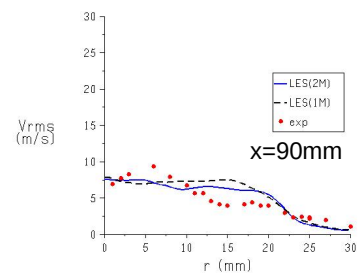

Results: Mean Temperature hm1

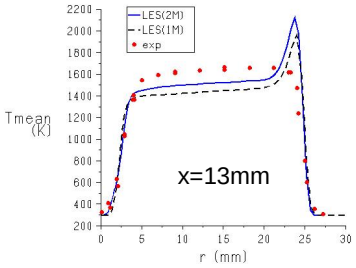

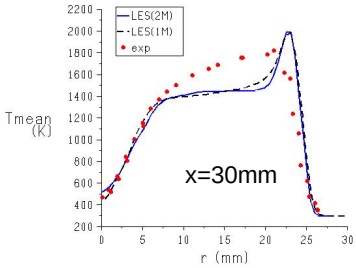

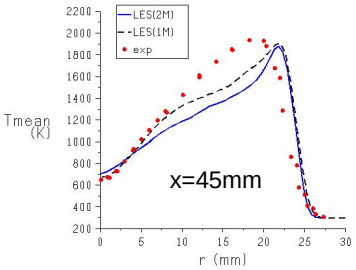

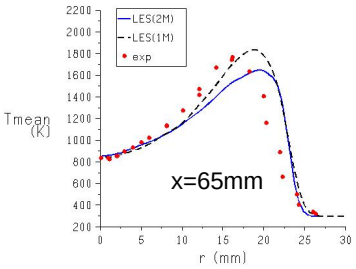

Results: Mean Temperature hm1

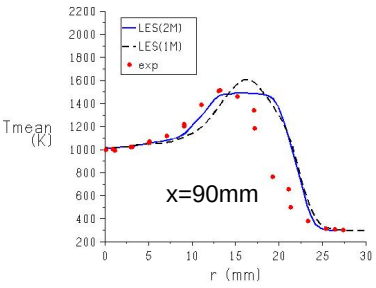

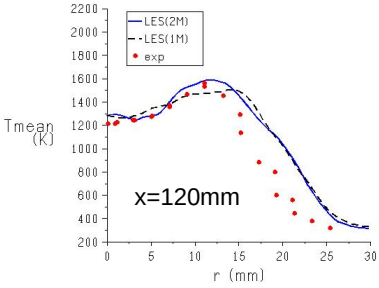

Results: RMS Temperature hm1

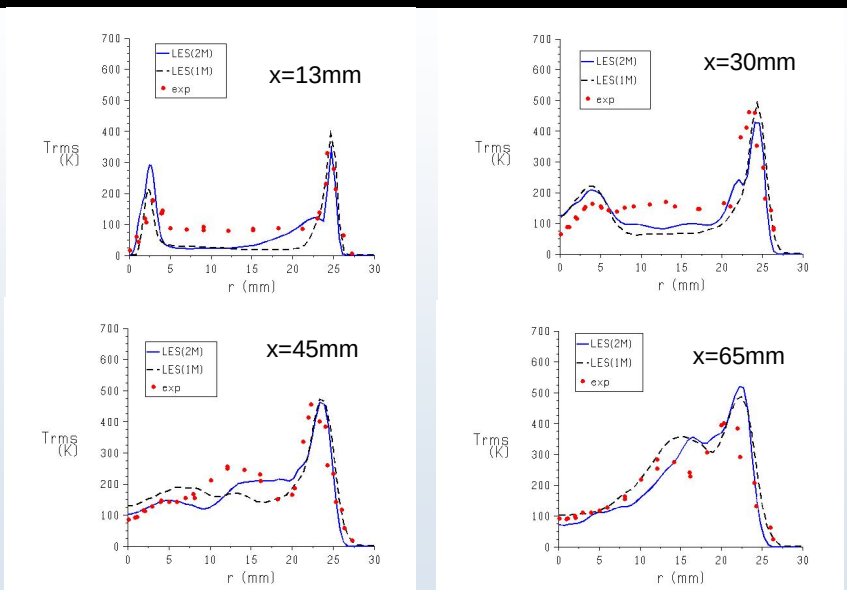

37

Results: RMS Temperature hm1

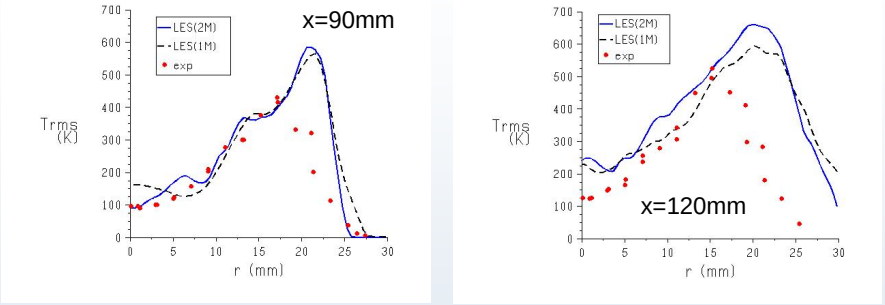

38

Results: Mean Y_{H2O} hm1

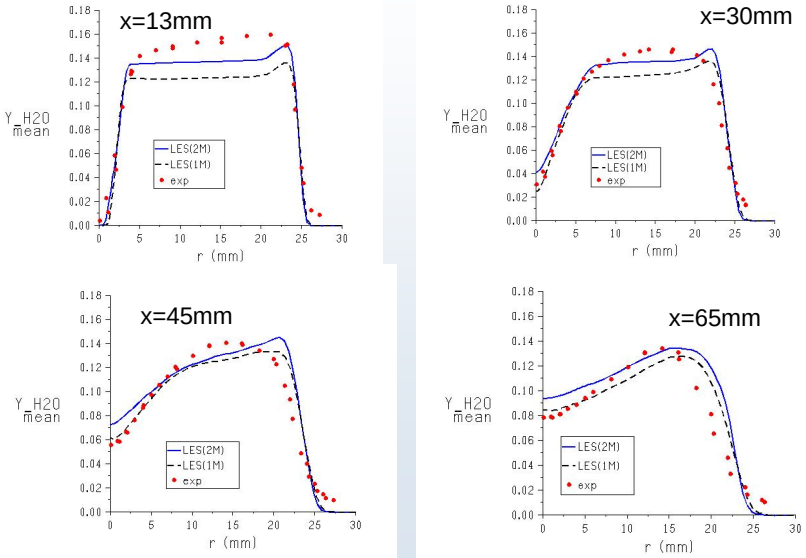

Results: Mean Y_{H2O} hm1

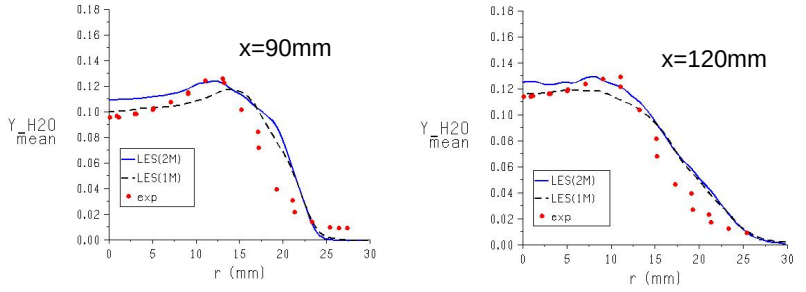

Results: Mean Y_{CO} hm1

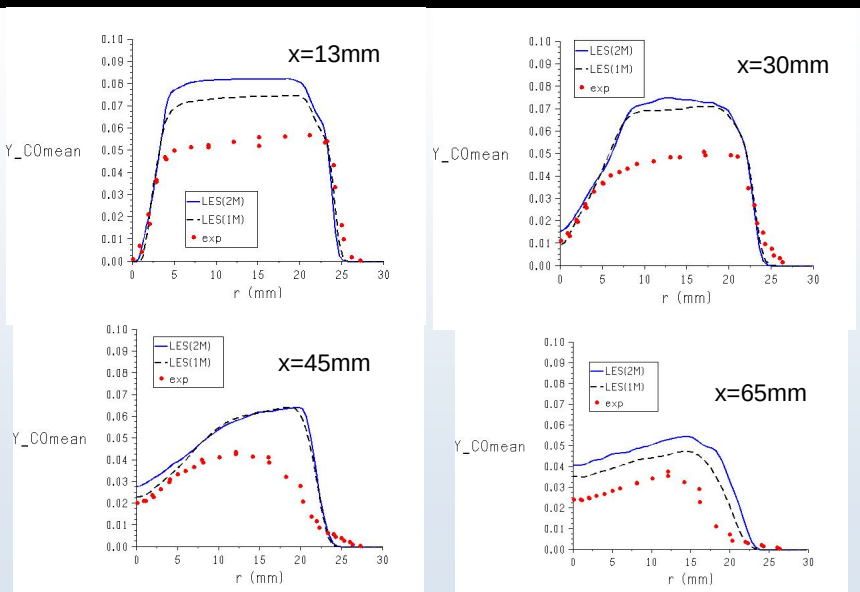

Results: Mean Y_{CO} hm1

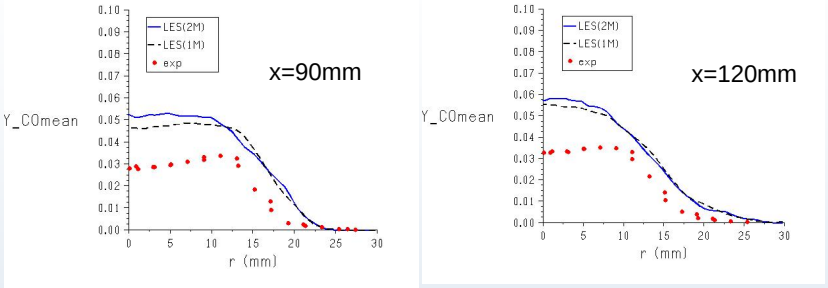

- **Mixture fraction over-predicted behind bluff**
  - Numerics too dissipative?
  - Entrainment from co-flow under-predicted?
- **Small mixture fraction difference but large over-prediction of Y_{CO}**

Results: Mean Y_{OH} hm1

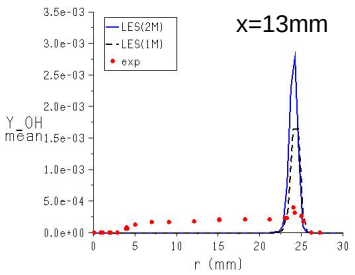

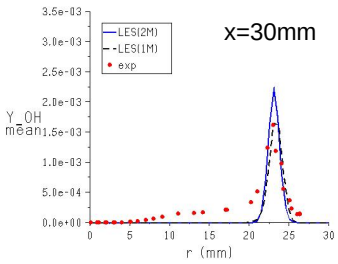

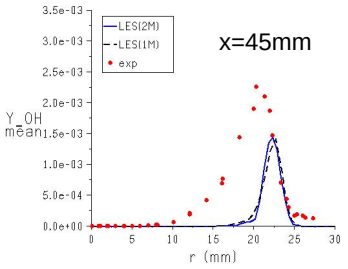

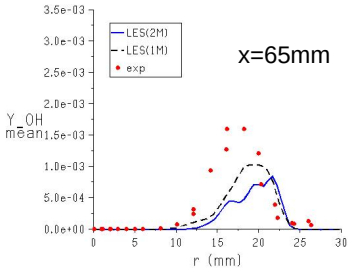

43

Results: Mean Y_{OH} hm1

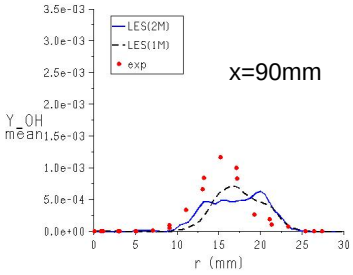

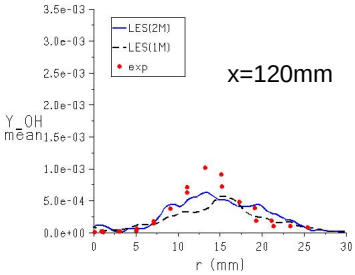

44

Conclusions

- **LES of Sydney bluff body flame hm1 and hm1e**
  - Reasonably good predictions for velocity statistics on 1M and 2M cells
- **Low sgs turbulence (low μ_t/μ_l)**
  - Are Fluent's default settings too dissipative?
  - Quality Indices based on μ_t/μ_l have limitations

Notes

Issues and Examples for Comparing Experiments and LES

Jonathan Frank, Joe Oefelein
Combustion Research Facility
Sandia National Laboratories
Livermore, CA
USA

Andreas Dreizler
Center of Smart Interfaces (CSI) and Energy and Power Plant Technology (EKT)
Mechanical Engineering
Technical University of Darmstadt
Germany

Acknowledgements

Sebastian Kaiser, Guanghua Wang, Rob Barlow (Sandia)
Andreas Kempf (Imperial College)
Michael Renfro (Univ. of Conn.)
Benjamin Böhm, Christof Heeger, Robert Gordon (TU Darmstadt)
Isaac Box, Wolfgang Meir (DLR Stuttgart)
Noel Clemens, O.A. Ezekoye, Mirko Gamba (UT Austin)

Goal: Predictive LES capability for a wide range of conditions

- Subgrid scale model development and validation
  - Measured vs. modeled subgrid scale statistics
- Verification of resolved-scale dynamics
  - Beyond matching mean and rms profiles
  - Consider spatial and temporal correlations

But first, we need…

- Framework for valid comparisons between experiments and LES
- Consistency in spatial and temporal averaging
- Systematic method for choosing LES filter sizes
- Knowledge from LES of non-reacting flows

Progression from Point Measurements to Imaging

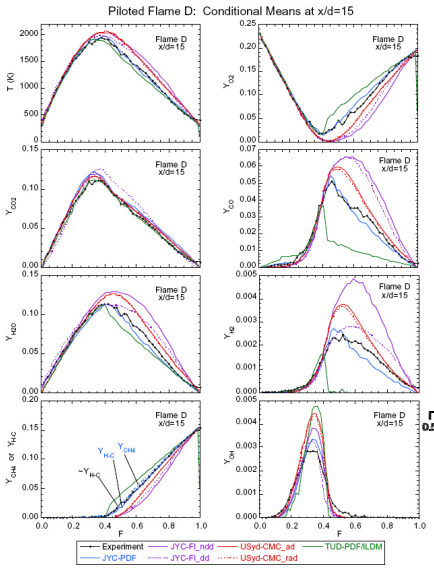

- Significant progress in TNF Workshop using point and line measurements
- Agreement of mean and rms profiles is necessary but not sufficient for validation of LES

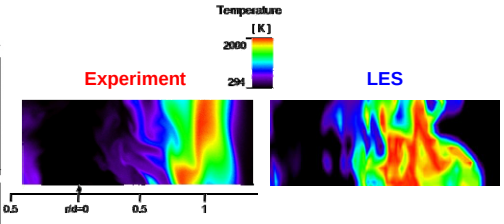

- Develop approaches for quantitative comparisons of physical structures on a statistical basis

- Dissipation length scales in flames
- Effects of filter size on dynamics of scalar mixing
- Time-series measurements
  - Diagnostic capabilities
  - Sampling requirements

Overlap of Dissipation and Energy Scales

Re_L = 1,000
Re_λ = 82

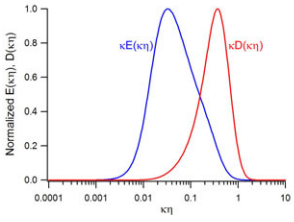

Re_L = 10,000
Re_λ = 260

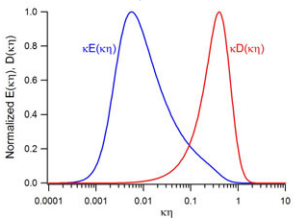

Re_L = 100,000
Re_λ = 820

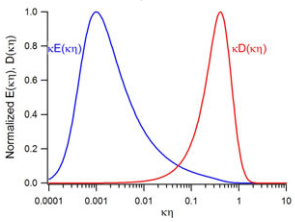

- Small scales on which mixing takes place assumed to be independent of large scale motions
- Lack of scale separation negates this assumption

S.B. Pope, Turbulent Flows, Cambridge University Press, New York, 2000

Overlap of Dissipation and Energy Scales in DLR-A Flame

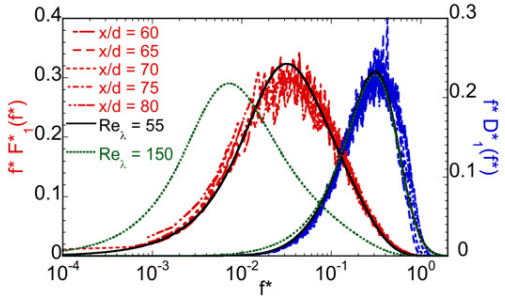

- Significant overlap of dissipation and energy spectra in TNF flames
- Sensitivity of LES results to scale separation – implications for models
- How do we ensure results are relevant at higher Reynolds number?

Wang, Clemens, Varghese, Barlow *Combust. Flame* 152 (2008) 317-335

Laser Rayleigh Imaging of Turbulence Scales in DLR-A

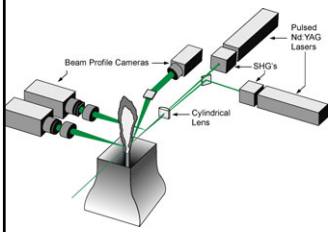

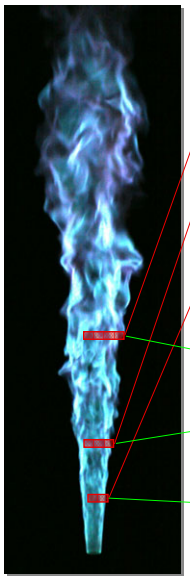

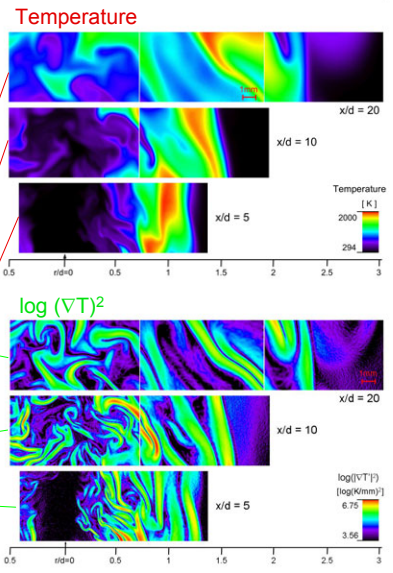

J.H. Frank, S.A. Kaiser, *Exp. Fluids* 44 (2008) 221-233

Measuring the Turbulence Cutoff Length Scale

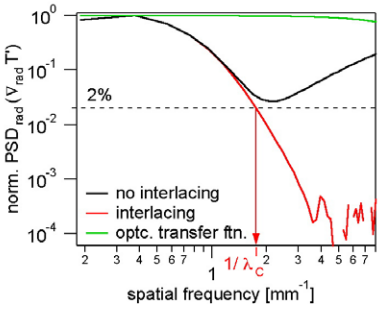

- Estimate minimum length scale for measuring mean dissipation
  - 1/ λ_c = spatial frequency at 2% of peak PSD
  - Analogous to cutoff criteria in 1-D model spectra of non-reacting turbulent flows (S.B. Pope, Turbulent Flows, Cambridge University Press, New York, 2000)

J.H. Frank, S.A. Kaiser, *Exp. Fluids* 44 (2008) 221-233

Wang, Barlow, Clemens, *Proc. Combust. Symp.* 31 (2007)

Spatial Variation of Cutoff Length Scale in DLR-A Flame

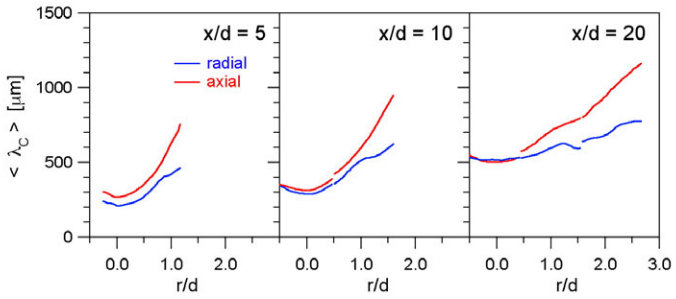

- Cutoff length scale increases monotonically with r/d and x/d
- λ_c gives the resolution requirement for measuring mean dissipation
- Batchelor scale: $\lambda_B = \lambda_c/2\pi$

J.H. Frank, S.A. Kaiser, *Exp. Fluids* 44 (2008) 221-233

Laser Rayleigh Imaging of Turbulence Scales in DLR-A

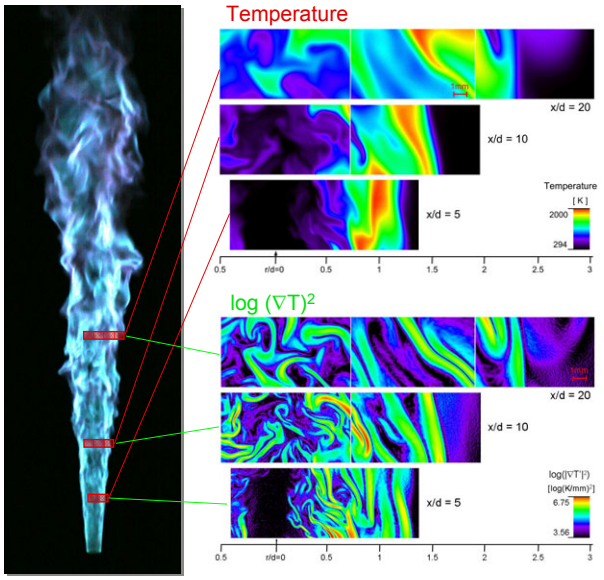

J.H. Frank, S.A. Kaiser, *Exp. Fluids* 44 (2008) 221-233

Temperature Dependence of Dissipation Layer Widths

Dissipation layer widths ~ $7\lambda_B$

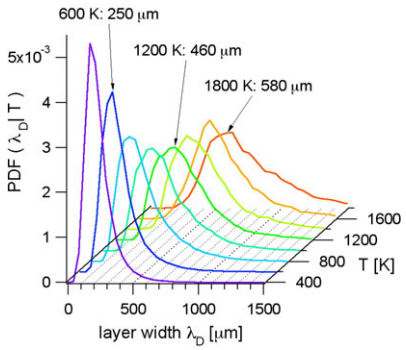

x/d = 10

Probability density functions of layer width, λ_D, conditioned on temperature

Angular Distribution of Dissipation Structures in DLR-A Flame

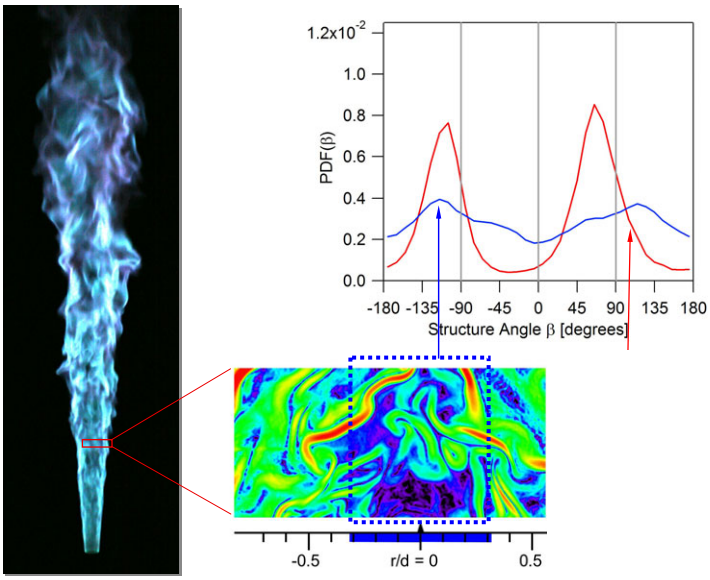

S.A. Kaiser, J.H. Frank, *Proc. Comb. Inst.* 31 (2007) 1515-1523

Challenge of Predicting Extinction with LES

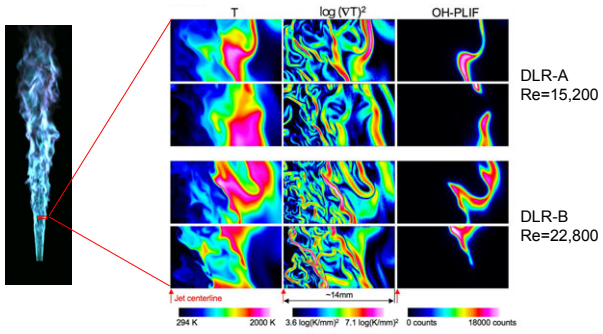

- Quantify size and probability of extinguished regions

See Kaiser & Frank, *Proc. Combust. Inst.* 32 (2009)
doi:10.1016/j.proci.2008.05.082

Turbulent Flames: Coupling Experiments with LES

Advanced Imaging Lab (J. Frank)

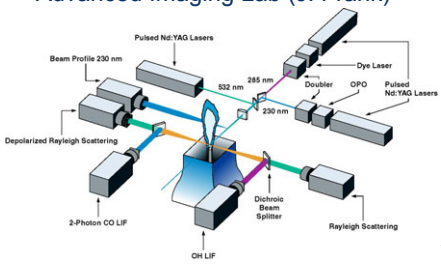

Large Eddy Simulations (J. Oefelein)

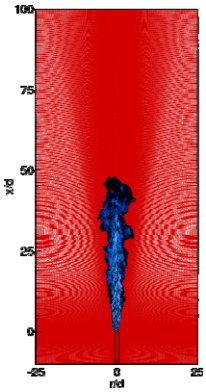

Turbulent Combustion Lab (R. Barlow)

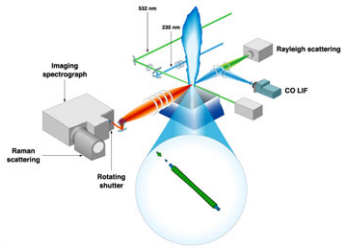

TNF WORKSHOP

LES provides good agreement with mean, RMS values (necessary but not sufficient!)

DLR A Flame: Re_d = 15,200

Fuel: 22.1% CH_4, 33.2% H_2, 44.7% N_2

Coflow: 99.2% Air, 0.8% H_2O

Detailed Chemistry and Transport: 12-Step Mechanism (J.-Y. Chen, UC Berkeley)

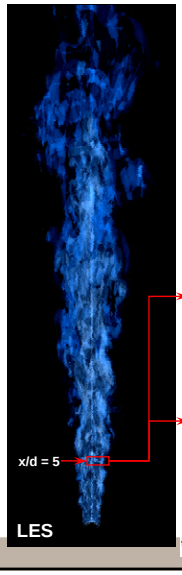

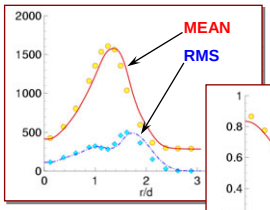

Temperature

Comparisons with 1D Raman/Rayleigh/CO-LIF line images (Barlow et al.)

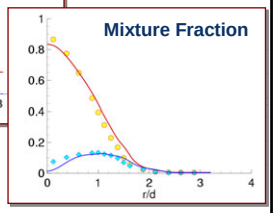

LES (with identical color map)

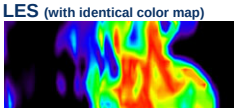

Comparisons of instantaneous spatial structures using 2D Rayleigh images (Frank et al.)

Experiment

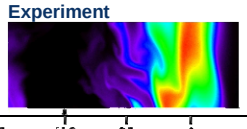

TNF WORKSHOP

- Dissipation length scales in flames
- Effects of filter size on dynamics of scalar mixing
- Time-series measurements
  - Diagnostic capabilities
  - Sampling requirements

Laboratory-Scale Turbulent Flames

Ultra-mild combustion
(a.k.a. non-reacting flow)

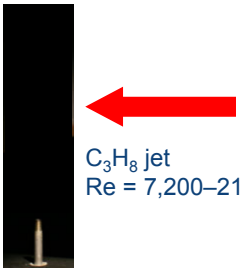

C_3H_8 jet
Re = 7,200–21,700

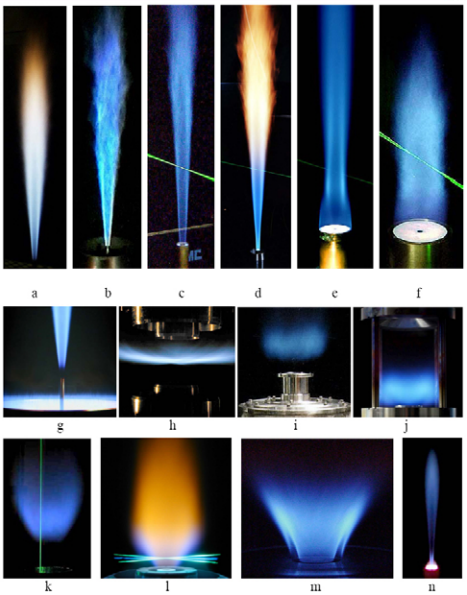

- No messy chemistry
- Very low *Da*
- Amenable to diagnostics
- Isolates scalar mixing

High-Resolution Grid For Testing LES

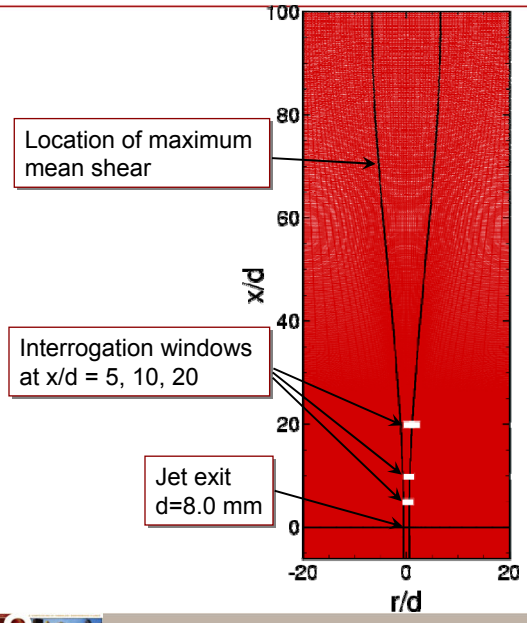

LES Configuration

- Fully-coupled, compressible conservation equations, detailed thermodynamics and transport
- Dual-time stepping integration
  - Fully implicit, 2nd/4th order accurate
  - All Mach number formulation
- Staggered finite volume differencing
  - Body-fitted coordinates, 2nd order-accurate
  - Non-dissipative, discrete conservation
- Mixed dynamic Smagorinsky model

	n_{axial}	n_{radial}	$n_{azimuthal}$	Total
Baseline	2592	144	192	71,663,616
2^3 Coarser	1296	72	96	8,957,952
4^3 Coarser	648	36	48	1,119,744

Cutoff Length Scales and Sequential Coarsening of LES Grid

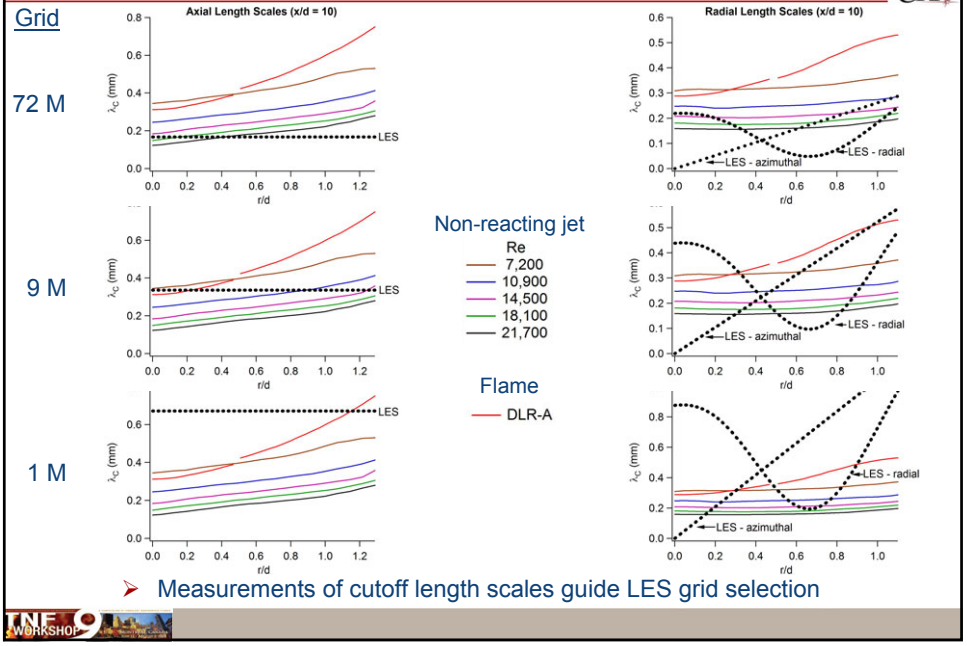

- Measurements of cutoff length scales guide LES grid selection

Understanding Spatial Resolution Issues in Non-reacting Flows

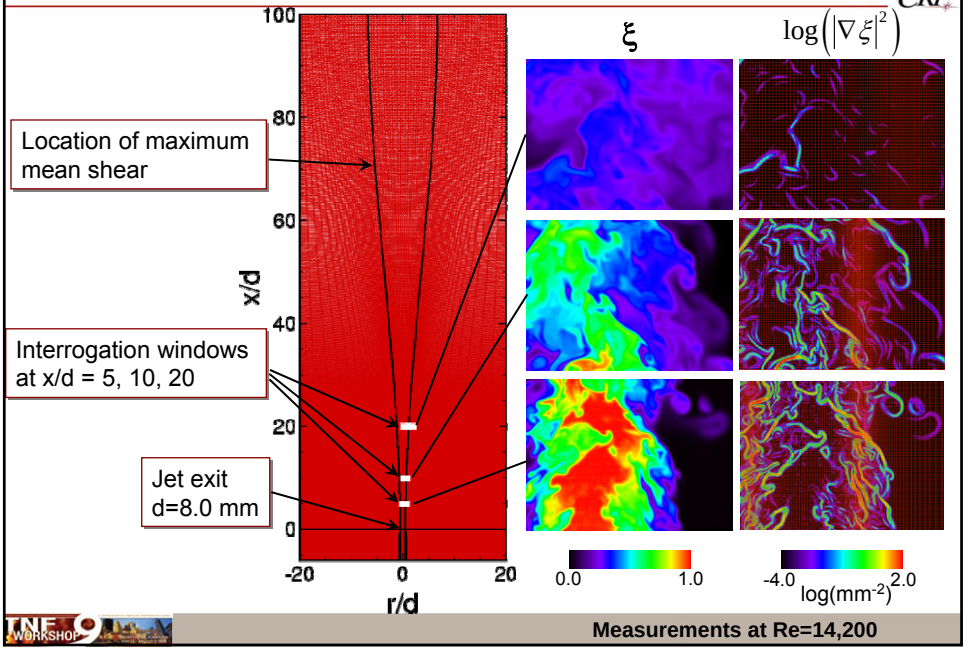

Measured Mixture Fraction & Dissipation in Non-reacting Jet

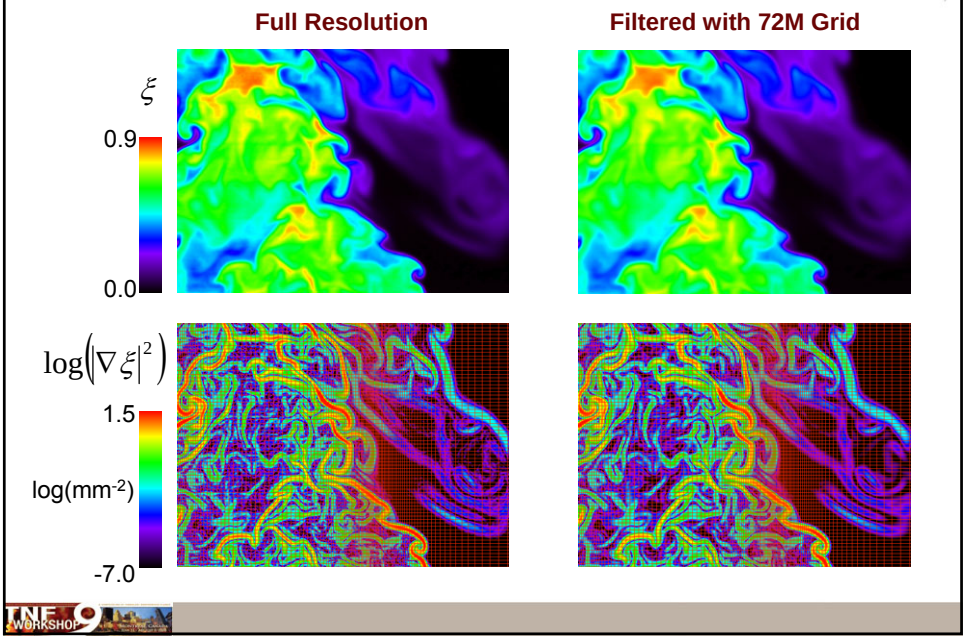

Experiments & LES – Non-reacting Jet (9M Cell Grid)

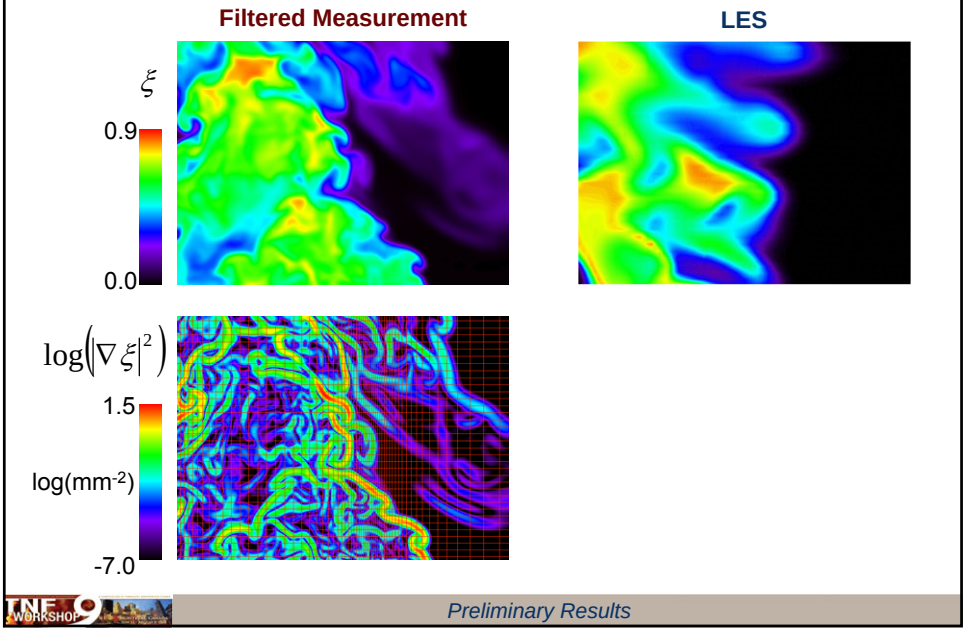

Preliminary Results

Experiments & LES – Non-reacting Jet (1M Cell Grid)

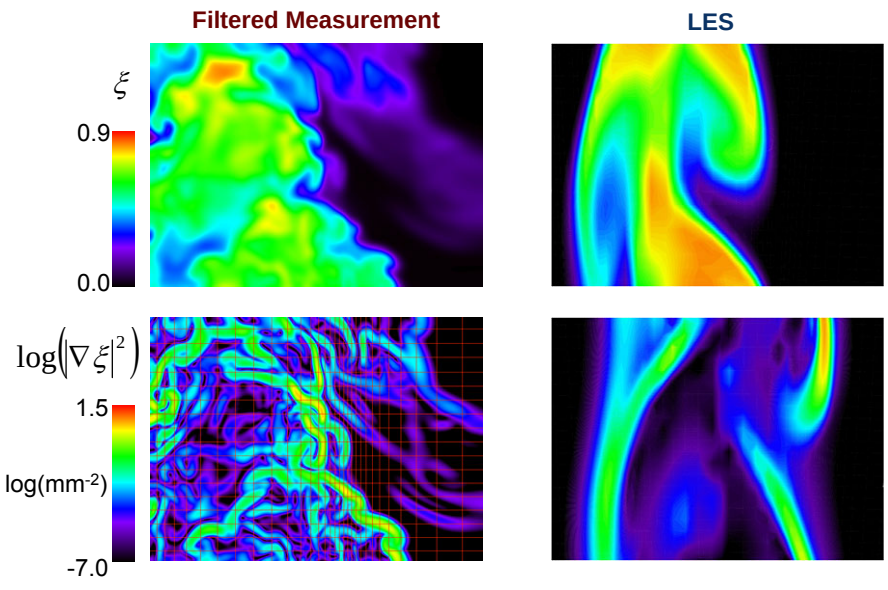

Preliminary Results

- Temporal damping and dispersion significantly alter the spatial evolution and structural similarities of the filtered dissipation layers relative to the actual field.
- Need to understand LES of passive scalar mixing before tackling LES of flames
- Results from 72M cell grid may be useful for understanding damping and dispersion.

- Dissipation length scales in flames
- Effects of filter size on dynamics of scalar mixing
- Time-series measurements
  - Diagnostic capabilities
  - Sampling requirements

Flame luminosity at 15kHz
x/d = 12.5

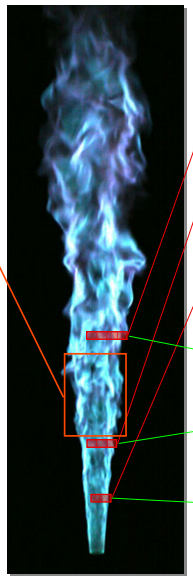

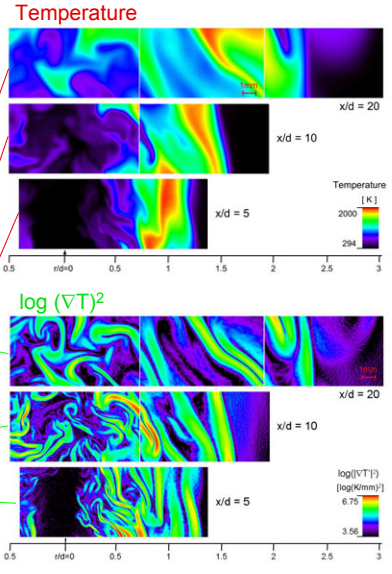

J.H. Frank, S.A. Kaiser, *Exp. Fluids* 44 (2008) 221-233

Planar high-speed diagnostics: Temporal evolution for LES-validation

Benjamin Böhm, Christof Heeger,
Robert Gordon, Andreas Dreizler

Center of Smart Interfaces (CSI) and Energy and Power Plant Technology (EKT)
Mechanical Engineering
TU Darmstadt
Germany
Email: dreizler@ekt.tu-darmstadt.de

Benefits of high repetition rate diagnostics

- Insights into dynamics and time-histories of combustion processes
- Especially valuable for transients such as
  - Extinction
  - Ignition (auto and spark)
  - Flashback
  - Cyclic variation in IC engines
- Benefit for LES
  - Enables comparison of temporal evolution, time-history and dynamics
  - Supplemental validation data to 1- and 2-point statistics
  - ⇨ Discussion needed on details of LES-EXP-comparison

OH Time-series in Hydrogen Jet Flame LES & Experiments

Compare LES to accessible data:

- OH-PITLIF time-series (Renfro)
- LES with steady flamelets (Kempf)
- Quantities
  - Time-series (quantitative)
  - Spectra
  - Integral time-scales

Jet Flame H3 (50% H_2/50% N_2, Re=10,000)

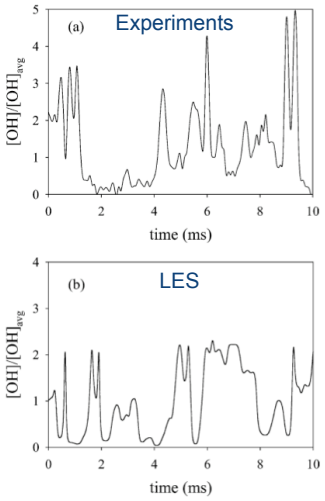

Renfro et al., *Combust. Flame* 139 (2004) 142–151

OH Time-series

- Power-spectrum OH
  - Good fit (but normalised)

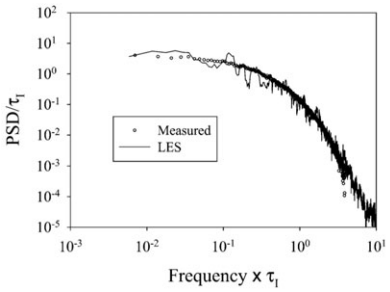

- Integral time scales OH
  - x/D = 20: OK
  - x/D = 30: strong deviation
  - Difference between x/d = 20, x/D = 30: Sensitivity?

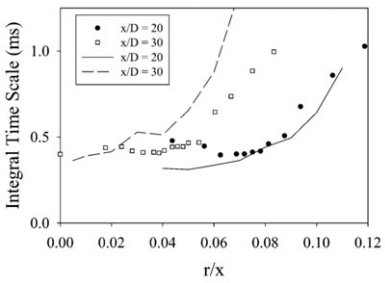

Renfro et al., *Combust. Flame* 139 (2004) 142–151

Dissipation Time Scales in DLR-A Flame

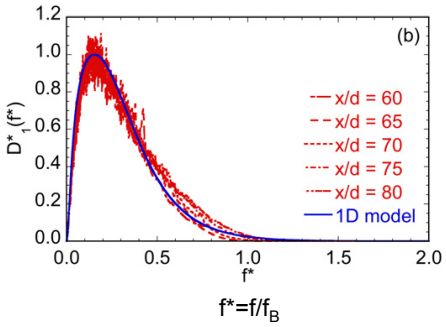

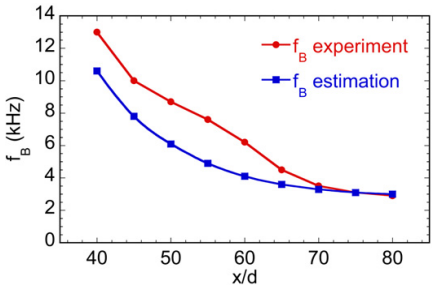

- Resolving Batchelor frequency (f_B) is a challenge

Wang, Clemens, Varghese, Barlow *Combust. Flame* 152 (2008) 317-335

3-D velocity field measurements invoking Taylor's hypothesis

M. Gamba, N. T. Clemens, O.A. Ezekoye – U. T. Austin (TNF Poster)

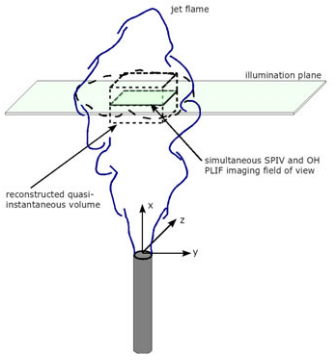

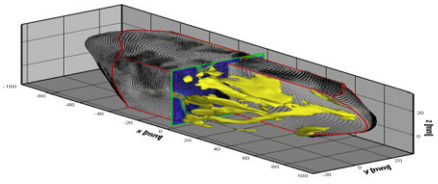

Pseudo-instantaneous volume from a set of high-repetition rate stereo PIV measurements showing the 3-D vector field and an extract of the 3-D rendering of iso-surfaces of enstrophy

State-of-the-art

TECHNISCHE UNIVERSITÄT DARMSTADT

- Time-series of several 1000 frames covering up to 2s
  - Sequences contain hundreds of integral time scales
- Frame-to-frame interval presently 100µs (10 kHz)
  - Typical integral time scales resolvable

⇨ Large temporal dynamic range

- "Post-event-triggering" enables 100%-success rate of capturing unforeseen processes (extinction, flashback,…)
- Demonstrated (Combustion Symposium 4A09, 5C08, 5F04)
  - 2- and 3-component PIV up to 12 kHz
  - Qualitative OH-imaging up to 5 kHz
  - Combined PIV/ OH PLIF up to 5 kHz

Example

TECHNISCHE UNIVERSITÄT DARMSTADT

- Extinction in turbulent opposed jet flame
  - (partially premixed CH4/air, Re=6,650)

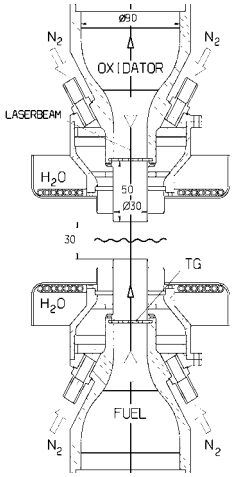

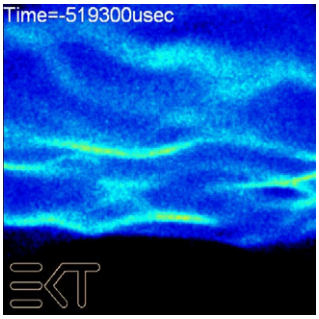

Chemiluminescence 10 kHz

TNF WORKSHOP

Example

TECHNISCHE UNIVERSITÄT DARMSTADT

- Extinction in turbulent opposed jet flame
  - (partially premixed CH4/air, Re=6,650)

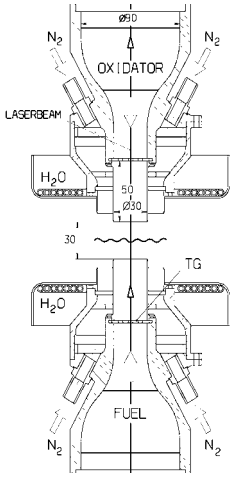

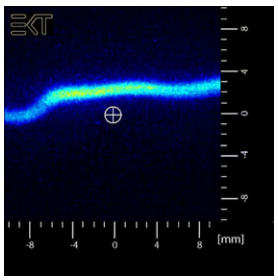

OH PLIF 5 kHz

Example

TECHNISCHE UNIVERSITÄT DARMSTADT

- Extinction in turbulent opposed jet flame
  - (partially premixed CH4/air, Re=6,650)

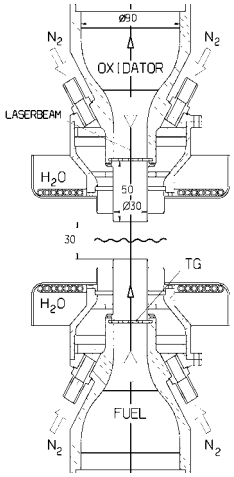

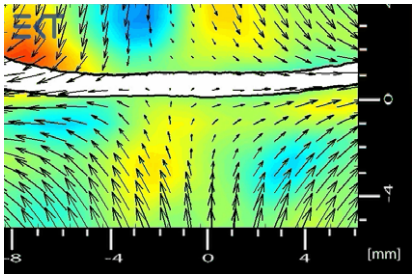

2C-PIVOH PLIF 5 kHz

In collaboration with W. Meier and I. Boxx (DLR-S)

From single events to conditional averages

TECHNISCHE UNIVERSITÄT DARMSTADT

- LES-validation needs averaged temporal evolutions
- ⇨ Conditional averages
- Here:
  - Step 1: definition of t=0ms where flame breached first
  - Step 2: shift radial co-ordinate to location where flame breached
  - Step 3: shift axial co-ordinate for each frame to de-convolute from intermittency

More information and results: visit Combustion Symposium Paper 4A09

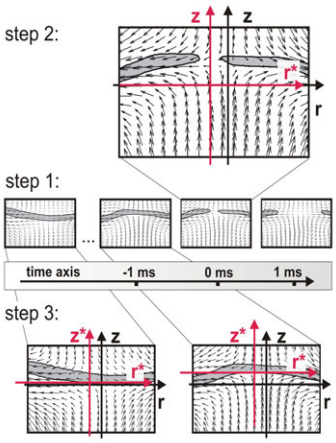

Resolution issues

TECHNISCHE UNIVERSITÄT DARMSTADT

- Area of active pixels in CMOS depends on repetition rate
  - 1024 x 1024 pixels @ 5.4 kHz → 128 x 16 pixels @ 675 kHz
- ⇨ Trade-off between temporal and pixel resolution

- What resolution is required?
  - Integral length scales (mm-range) → resolving dynamics of integral length scales by 10 kHz often feasible
  - Small scales
    - » Limited by PIV interrogation boxes, laser light-sheet thickness
    - » Typical value 300µm in each direction
    - ⇨ Kolmogorov-/Batchelor-scales in general not resolved
    - » Use information from PIV-cross-correlation to estimate temporal resolution necessary to resolve 300µm-sized flow structures
    - » Typical values 10 – 100µs → rep-rates ≥ 10 kHz desired

Work-in-progress

TECHNISCHE UNIVERSITÄT DARMSTADT

- Quantitative scalar imaging
  - Needs careful characterization of IRO-CMOS
  - Example: non-linearity of CMOS

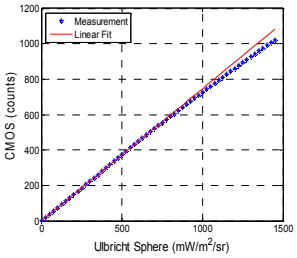

  - Tracer PLIF for mixture fraction imaging
- Quasi-4D-measurements

Discussion on LES – high speed diagnostics

TECHNISCHE UNIVERSITÄT DARMSTADT

- Inclusion of time-history in turbulence-chemistry interaction models
- Statistics of time-sequences spanning few ms
  - Transient event (extinction, flashback etc.) spreads over a few ms
- What temporal resolution (repetition rate) actually is needed?

Discussion Points

- Differences in spatial and temporal averaging for LES and experiments
- Complementary measurements: single-point, 1-D, 2-D, 3-D
  - New opportunity for use of imaging measurements
  - Comparisons with LES on statistical basis
  - Applicability of Taylor's hypothesis
- Sensitivity of models to anisotropy on subgrid scale
- Systematic approach to determining filter size
  - How much of energy spectrum needs to be resolved?
  - Large enough to provide "statistically significant" sample within cells?
  - Computational cost
- Approaches for progressing to higher Reynolds numbers
  - Effects of overlap of energy and dissipation spectra

Focus Group 1

New Target Flames

Desirable Burner/Flame Characteristics

- Well defined boundary conditions
- Easy optical access → more complete data
- Turbulence parameters at appropriate levels (Re, Da, u'/S_L, etc.)
  (what 'appropriate' means is open for discussion)
- Portable and repeatable
  (apply diagnostics in different labs)
- Velocity and scalar measurements with good statistical sample size
  (other measurements to be discussed)
- Variation of one or more parameters to which the flames are sensitive
  (particularly with respect to turbulence-chemistry interaction or a transition between combustion regimes)
- Steady flow (depending on modeling interest in unsteady cases)

New Target Flames: Broad Issues

- One burner for all modes?
  - Not really necessary
  - Opposed flow geometry proposed (Yale)
  - Some benefit to multiple configurations that overlap in mode space
- One mixture fraction
  - Necessary for some methods
  - Includes most of the candidate burners
  - Syndey PPJB will be modeled by some
- Preview calculations
  - Use initial calculations to evaluate candidate burners
  - Better understanding of issues for broad comparisons

Discussion:

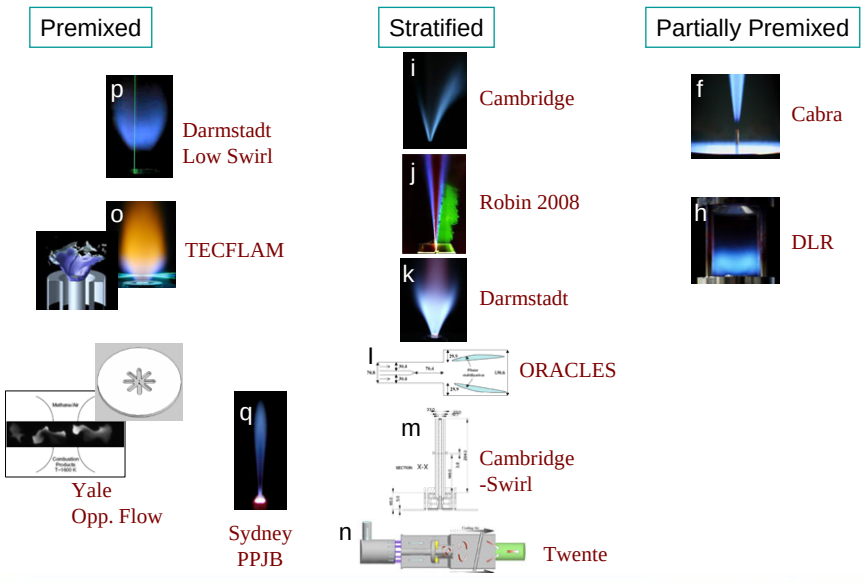

New Target Flames: TU Darmstadt Stratified Burner

- Pros
  - Data ready soon (LDA, Rayleigh, OH PLIF… Raman-later)
  - Relatively complete experiments planned
  - Parametric variations including premixed cases
  - BC's designed for validation
- Cons
  - Limited Da range
  - Some questions about sensitivity to pilot conditions

New Target Flames: Lifted Jet in Hot Coflow (Cabra Burner)

- Pros
  - Already modeled by a few groups
  - Can move across different modes (auto-ignition ←→ flame propagation)
  - Good burner for new fuels
  - Relatively simple geometry but complex turbulence-chemistry issues
- Cons
  - Very sensitive to bc's (pilot temperature), chemistry, and dissipation model
  - Need more well-planned experiments
  - H_2/air in pilot (check sensitivity using calculations)
- Use models in planning experiments
- Consider possible design improvements

New Target Flames: Next Steps

- Stratified
  - Data distribution when available
  - Selection of cases (some initial calculations?)
  - Possible comparisons in 2010
- Cabra
  - Communication (near term) to sort out current state of data
- Other flames
  - Follow development of data set

Fuels Group

- **Gaseous Fuels:**
  - **Near-term recommendation:** move to Methane + Ethane as first step, with to addition of propane subsequently.
  - **Motivation:** C_2 is simplest of higher hydrocarbons, with greater relevance than CH_4, and has well-defined mechanisms
  - **Syngas:** a lot of practical interest, but it is unclear whether there are holes in existing data-sets, since data-bases exist with CO + H2 fuels
- **Transport Fuels:**
  - **Near-term recommendation:** move to oxygenated fuels – ethanol or DME vaporised as first step
  - **Motivation:** simplest of commercially available bio fuels and has well-defined mechanisms
  - **Practical fuel surrogates:** Wait until results from large-chemistry studies become available.

Fuels Group

Soot in turbulent flames:

- **Relevance to TNF?:** Agreed to be of relevance since this encompasses turbulence-chemistry interactions
- **When to incorporate into TNF?:** When sufficiently good data is available
- **Approach:** make incremental modifications to operating conditions of existing TNF flames to produce soot.

Suggestions for new experiments based on

TRANSIENT FLAMES

TNF9

Focus Group 3

Challenges (from yesterday):

1. Combustion mode/regime; common model?

2. New fuels

3. LES-experiment comparison

Additional considerations:

1. Automotive community needs access to validation data with transient phenomena

2. Fast diagnostics can offer new insights

Suggested experiments:

1. Spark ignition of two-stream flows
2. Autoignition of starting jets
(3. More on extinction)

Spark Ignition

Phase 1: kernel generation; quasi-laminar; vulnerable to quenching; stochastic features.
Phase 2: stratified/edge flame propagation;
Phase 3: overall flame stabilization

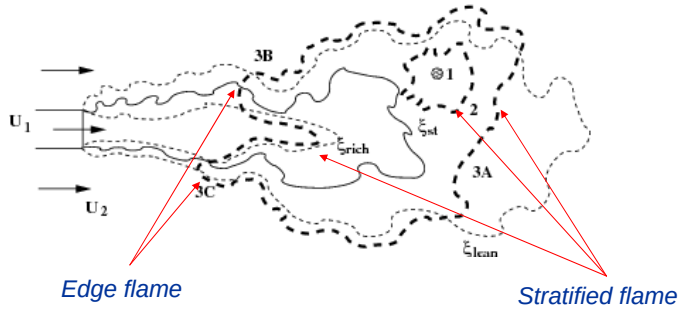

Jets, counterflow, recirculating, swirl etc. can be used, extending existing TNF flames/geometries.

Existing data: Cambridge (methane; TNF9 poster)

Autoignition

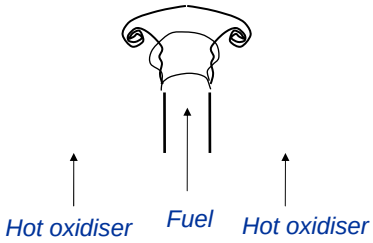

Berkeley/Sandia/Sydney/Cambridge/Delft/Adelaide steady-flow experiments transformed for *transient* fuel injection

Auto-ignition will occur somewhere; subsequent flame evolution; transition to the statistically-steady (and already-studied!) flame

Fuel: H2/CH4/C2H2/C7H16 etc. Oxidiser: vitiated air/pure air

Turbulence may pre-exist in co-flow

Existing data: Nat gas injection: 90's Sandia, U Brit Columbia; DME: Karlsruhe

Advantages

Very suitable for LES

Very suitable for fast diagnostics

New ways to validate LES:
- **based on ensemble averages comparison?**
- **based on individual events?**
- **based on the range of possibilities?**

Easy to set-up in DNS & LES

Relatively easy to alter existing experiment

Includes all combustion modes (premixed / stratified / non-premixed)

Autoignition / flame propagation

Easy to expand to any fuel, including *sprays*

Poster Highlights, Developments and Possible New Burners

A. Masri & D. Roekaerts
TNF 9, Montreal
31st July – 2nd August 2008

Posters: TNF Target Flames:

DLR Flames:

Comparison between LES and imaging experiments:
- **Frank, Kaiser and Oefelein**
- **Non-reacting jets and DLR-A ($CH_4/H_2/N_2$)**

Piloted Flames:

LES for Sandia flame E
- **Ihme and Pitsch**
- **Flamelet/progress variable approach, presumed pdf(ξ,c)**
- **Good predictions of finite rate chemistry**

Piloted Flames:

Filtered Density Function simulations with MMC for Sandia flame E
- **Cleary and Klimenko**
- **Only 10,000 reacting particles used.**
- **Scatter plots show reasonable predictions of local extinction events**

Posters: TNF Target Flames:

Bluff Body and Swirl Flames:

RANS approaches:
- **Claramunt, Anker and Hirsch:**
  presumed pdf and ILDM for flame HM1 (and other combustors)
- **De Meester, Merci and Naud:**
  realizable k-e model, presumed pdf and flamelets for flame SM1

Hybrid FVM/PDF:
- **Lee, Kang, Kim and Muradoglu**
- **IEM mixing model and flamelets for SM1**

LES
- **Olbricht, Hahn, Kuehne, van Oijen, Janicka**
- **Flamelet/progress variable approach**
- **Bluff-body and swirl flames**

TNF9 Montreal, 31 July - 2 August 2008

Posters: Experimental Advances:

High-Speed Laser Diagnostics:
- **Gordon, Heeger, Bohm, Ahmed, Box, Dreizler, Mastorakos, Meier**
- **Joint PIV/OH-LIF at 5kHz and 10kHz**
- **Capabilities to observe transient phenomena in flows and flames**

Time-resolved stereoscopic PIV and 2D OH-PLIF
- **Gamba, Clemens, Ezekoye**
- **3D-SPIV at 3kHz and OH-LIF at 10Hz**

LII: Zhang, Williams, Shaddix and Schefer
LII: Medwell, Chan, Kalt, Alwahabi, Dally and Nathan
- **Two-line atomic fluorescence will be used to obtain temperature**

New Burners:
- **EKT stratified burner (Dreizler et al.)**
- **Counterflow in hot products (Gomez et al.)**
- **Stratified V-flame burner (Hochgreb et al)**
- **Auto-ignition Chamber & forced ignition burner (Mastorakos et al.)**

TNF9 Montreal, 31 July - 2 August 2008

FACULTY OF ENGINEERING

APPLICATION OF LES/CMC METHODOLOGY TO HYDROGEN AUTO-IGNITION IN A TURBULENT CO-FLOW OF HEATED AIR

Ivana Stanković[1], A. Triantafyllidis[2], E. Mastorakos[2], C. Lacor[3] and B. Merci[1]

[1]Ghent University – UGent, Dept. Flow, Heat and Combustion Mechanics
[2]Hopkinson Laboratory, Cambridge University Engineering Department
[3] Vrije Universiteit Brussel, Dept. Mechanical Engineering

Experimental set-up *

- **Fuel**: hydrogen diluted with nitrogen
- **Co-flow**: preheated ambient air

- The burner inner diameter: 25.00 mm
- The jet inner diameter: d = 2.25 mm

- A perforated plate was placed in the outer flow to create turbulence

- The temperature of the air and the jet velocity were varied to obtain different auto-ignition regimes

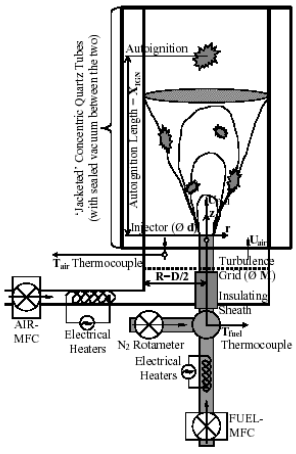

* C.N. Markides and E. Mastorakos, *An experimental study of hydrogen auto-ignition in a turbulent co-flow of heated air*, Proc. Combust. Inst. 30 (2005) 883-891.

Department of Flow, Heat and Combustion Mechanics – www.FloHeaCom.UGent.be
Ghent University – UGent

Chemical mechanism:

- A comprehensively tested H_2/O_2 chemical kinetic mechanism is used:
  - 19 reversible reactions and 13 species *

*J. Li, Z. Zhao, A. Kazakov and F. L. Dryer, *An updated comprehensive kinetic model of hydrogen combustion*, International Journal of Chemical Kinetics, 36 (2004) 566-575.

- LES mesh: 96 x 48 x 48 cells; CMC mesh: 16 x 4 x 4 cells
- Solution domain: 135 mm x 25 mm x 25 mm

Boundary conditions for the simulation (Markides and Mastorakos)		
Region	Item	$U_{fuel} > U_{air}$
Fuel jet	Velocity, U_{fuel} (m/s)	120
	Temperature (K)	691
	Composition	$Y_{H_2} = 0.13$ $Y_{N_2} = 0.87$
Co-flow	Velocity, U_{air} (m/s)	26
	Temperature (K)	962 - 1015
	Composition	$Y_{O_2} = 0.233$ $Y_{N_2} = 0.767$
	Turbulence intensity (%)	15

Instantaneous planar temperature fields in physical space and OH mass fraction profiles in mixture fraction space

T_{air} = 1009 K T_{air} = 970 K

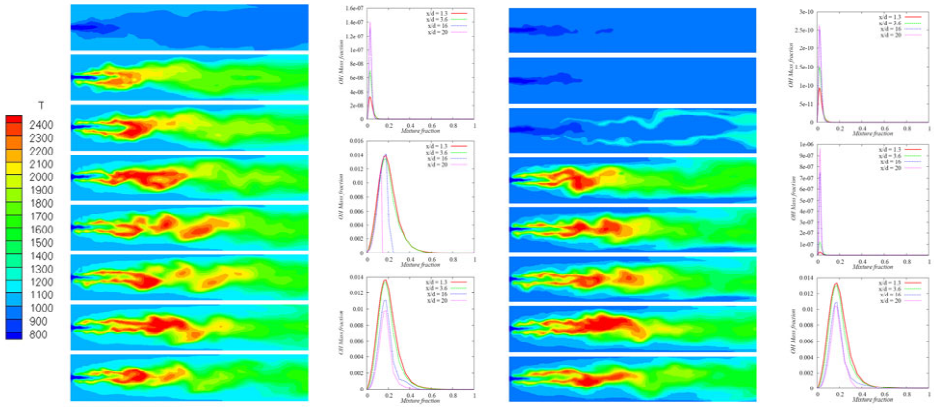

Department of Flow, Heat and Combustion Mechanics – www.FloHeaCom.UGent.be
Ghent University – UGent

Inlet boundary condition – LES pre calculation

- Turbulence enhances mixing of reactants, and therefore formation of radicals, and promotes ignition
- The air is injected through nine separate holes (5x5 mm)
- Ait inflow bulk velocity: 72 m/s

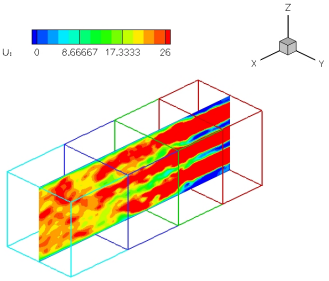

Results without proper inlet turbulence

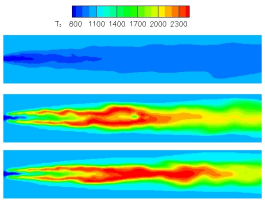

Spark-ignition of turbulent bluff-body flames

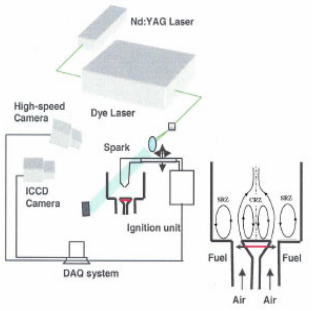

(a)

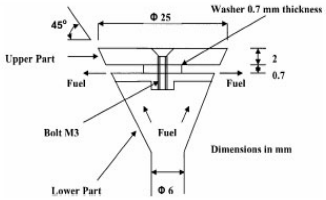

(b)

Measurements: - PLIF of acetone, OH-PLIF, LDA, Ignition probability

Electrical spark, 1mm gap, 0.4ms duration

Methane, atmospheric conditions

Spark-ignition of turbulent bluff-body flames

Photo

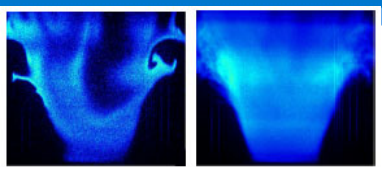

OH-PLIF: instantaneous, average

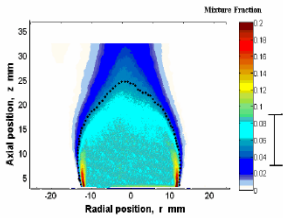

Mean mixture fraction

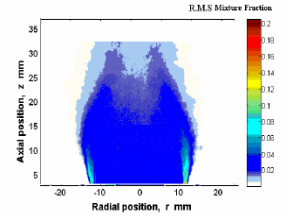

RMS mixture fraction

- Stable flame is blue, short, turbulent
- CRZ of inert flow well-mixed, but rich

UNIVERSITY OF CAMBRIDGE 800 YEARS 1209-2009

Spark-ignition of turbulent bluff-body flames

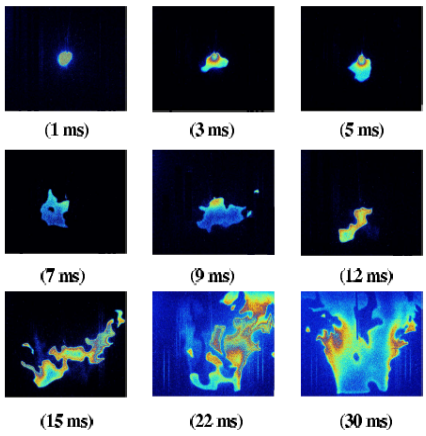

Instantaneous OH-PLIF

(successful events only)

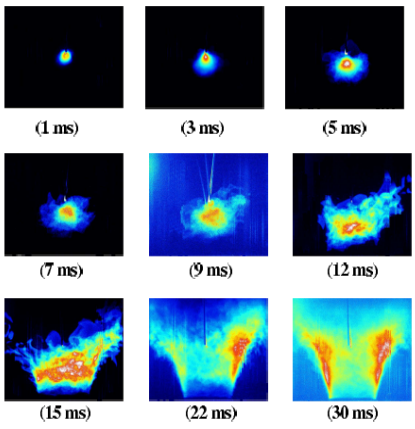

Ensemble-average OH-PLIF

(successful events only)

UNIVERSITY OF CAMBRIDGE 800 YEARS 1209-2009

Spark-ignition of turbulent bluff-body flames

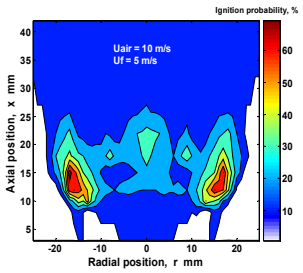

Ignition probability (whole flame)

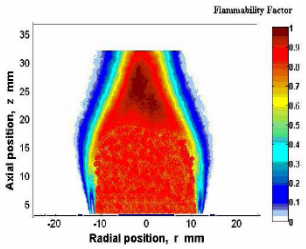

Flammability factor
(prob. of mixture within flammability limits)

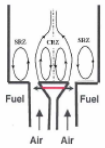

P(ignition) ≠ flammability factor

UNIVERSITY OF CAMBRIDGE 800 YEARS 1209-2009

Spray Combustion

Despite lack of interest by TNF, there is strong interest from modelers to compute such flows:

- **Raman (Texas)**
- **Roekarets (Delft)**
- **Merci (Ghent)**
- **K.Y. Huh (Postech)**
- **Jones (Imperial)**
- **Others?**

The Sydney spray burner

- **Simple flow**
- **Data bank is gradually developed.**

TNF9 Montreal, 31 July - 2 August 2008

Spray Burner

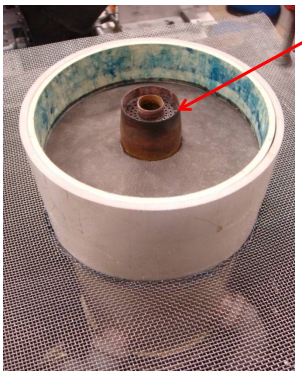

Pilot flame holder

Ultrasonic nebulizer

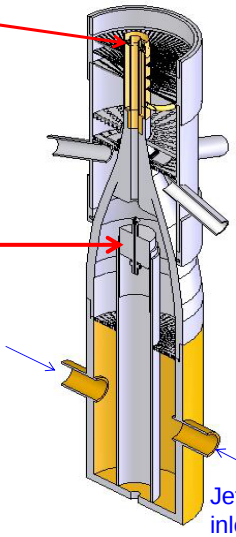

Jet carrier air inlet

Burner coflow assembly mounted in the wind tunnel

Spray Burner

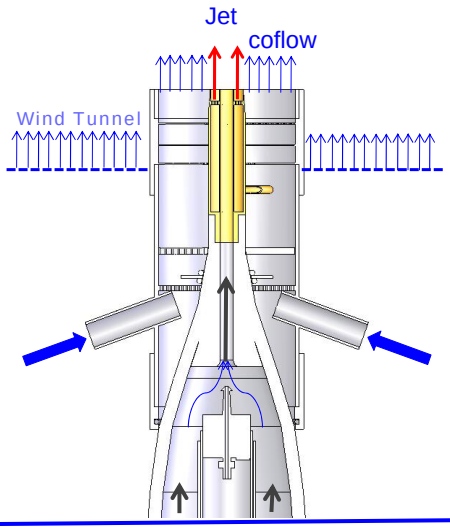

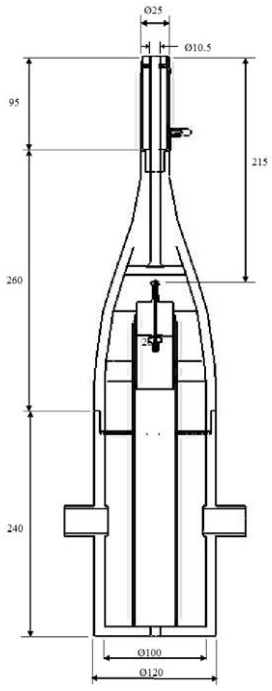

Flame Conditions

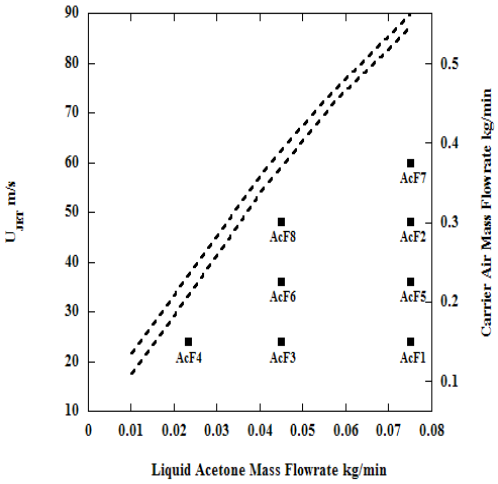

Flame	Bulk Jet Velocity (m/s)	Liquid Acetone Mass Flow Rate kg/min	Carrier Air Mass flow rate Kg/min
AcF1	24	0.0750	0.150
AcF2	48	0.0750	0.301
AcF3	24	0.0450	0.150
AcF4	24	0.0234	0.150
AcF5	36	0.0750	0.225
AcF6	36	0.0450	0.225
AcF7	60	0.0750	0.376
AcF8	48	0.0450	0.301

Boundary Conditions

Pilot Flame
Stoichiometric mixture of Acetylene, Hydrogen and Air.
Carbon to Hydrogen ratio of pilot flame equal to the main fuel.

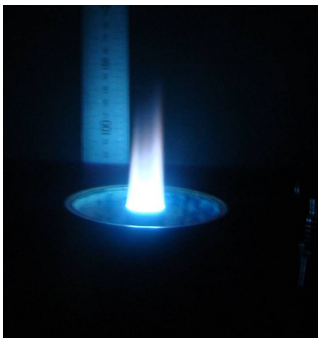

- Pilot unburned velocity 1.5 m/s
- Coflow Velocity 4.5 m/s
- Wind tunnel Velocity 4.5 m/s

Boundary Conditions (ctd)

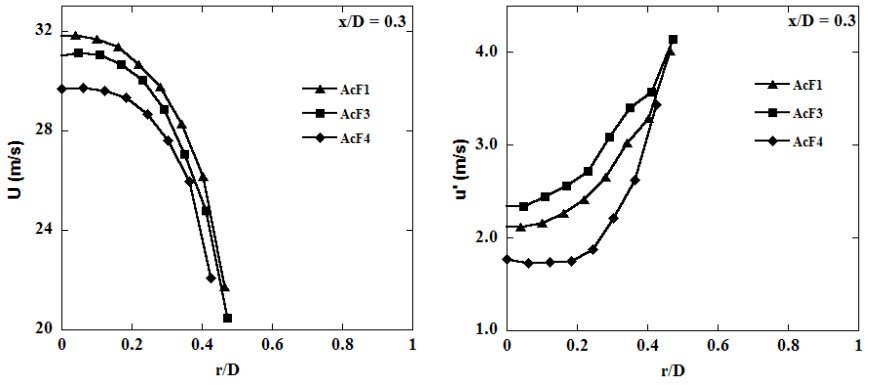

Boundary conditions (ctd)

Flame AcF 1

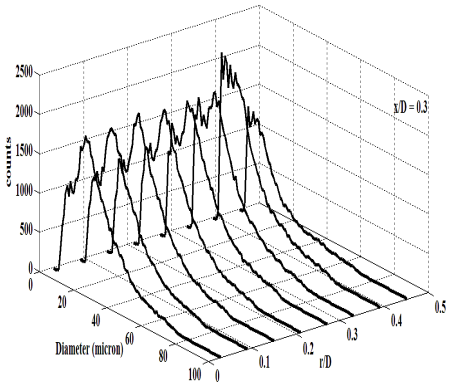

Droplet Distribution at exit plane

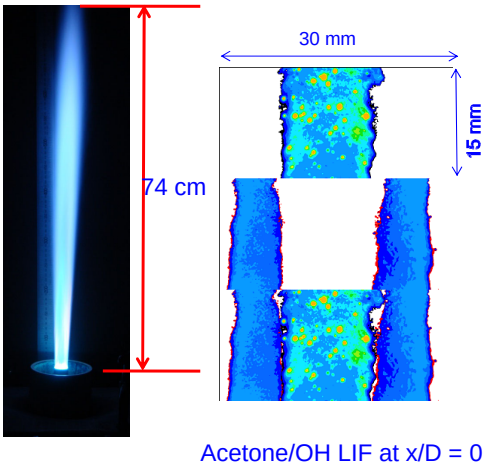

Acetone/OH LIF at x/D = 0

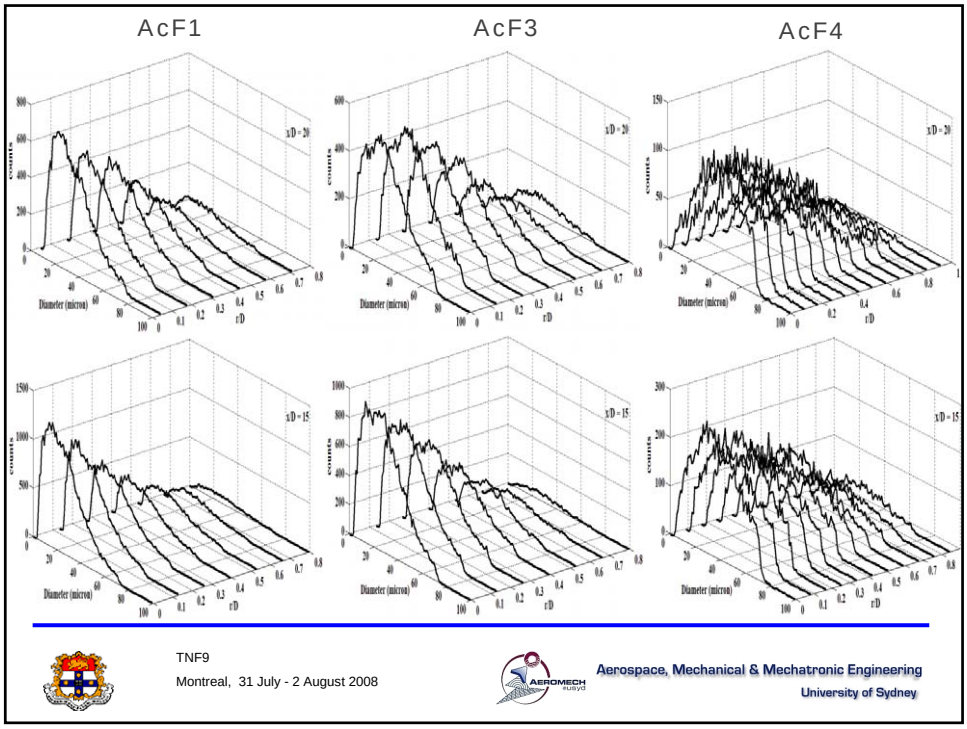
AcF1
AcF3
AcF4
x/D = 20
x/D = 15
counts
Diameter (micron)
r/D
TNF9
Montreal, 31 July - 2 August 2008
Aerospace, Mechanical & Mechatronic Engineering
University of Sydney

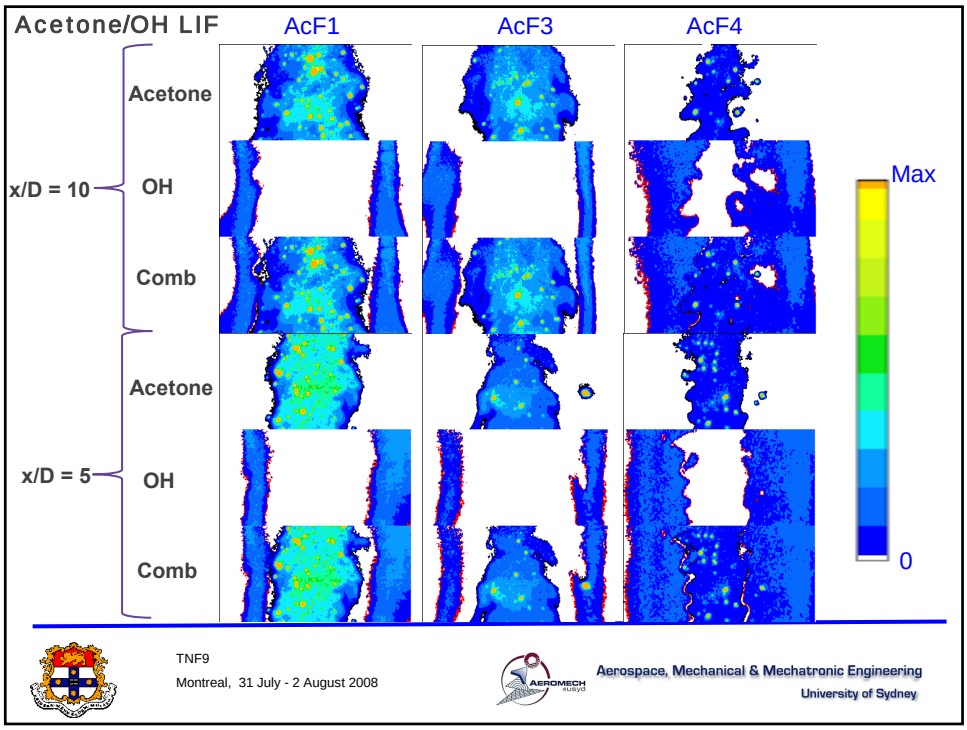
Acetone/OH LIF
AcF1
AcF3
AcF4
Acetone
OH
Comb
x/D = 10
x/D = 5
Max
0
TNF9
Montreal, 31 July - 2 August 2008
Aerospace, Mechanical & Mechatronic Engineering
University of Sydney

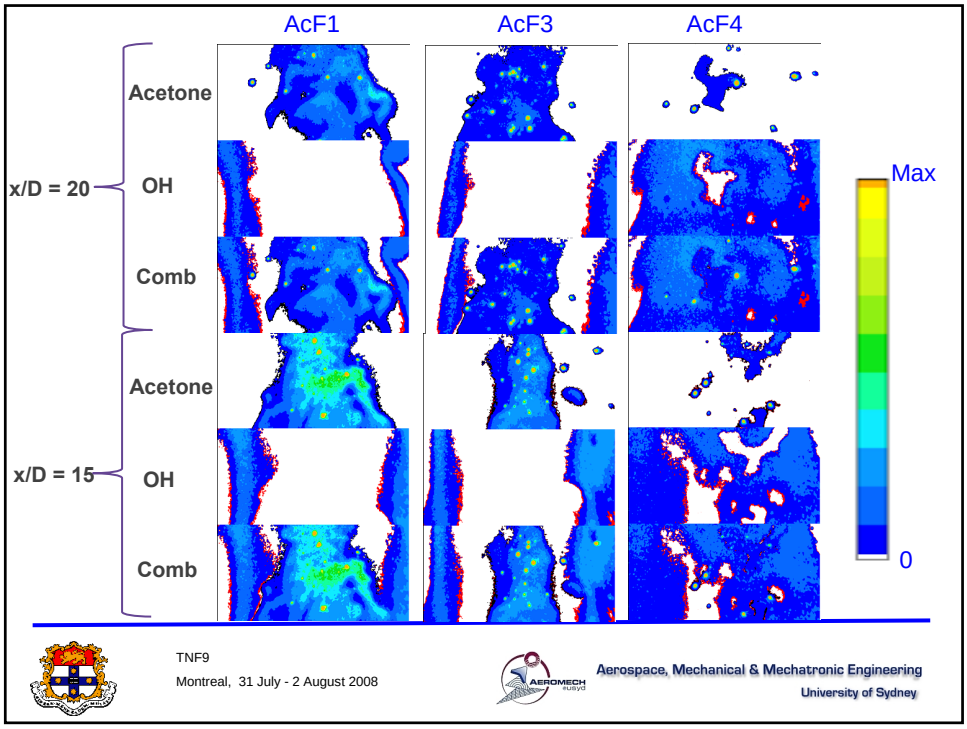
AcF1
AcF3
AcF4
Acetone
OH
Comb
x/D = 20
Acetone
OH
Comb
x/D = 15
Max
0
TNF9
Montreal, 31 July - 2 August 2008
Aerospace, Mechanical & Mechatronic Engineering
University of Sydney

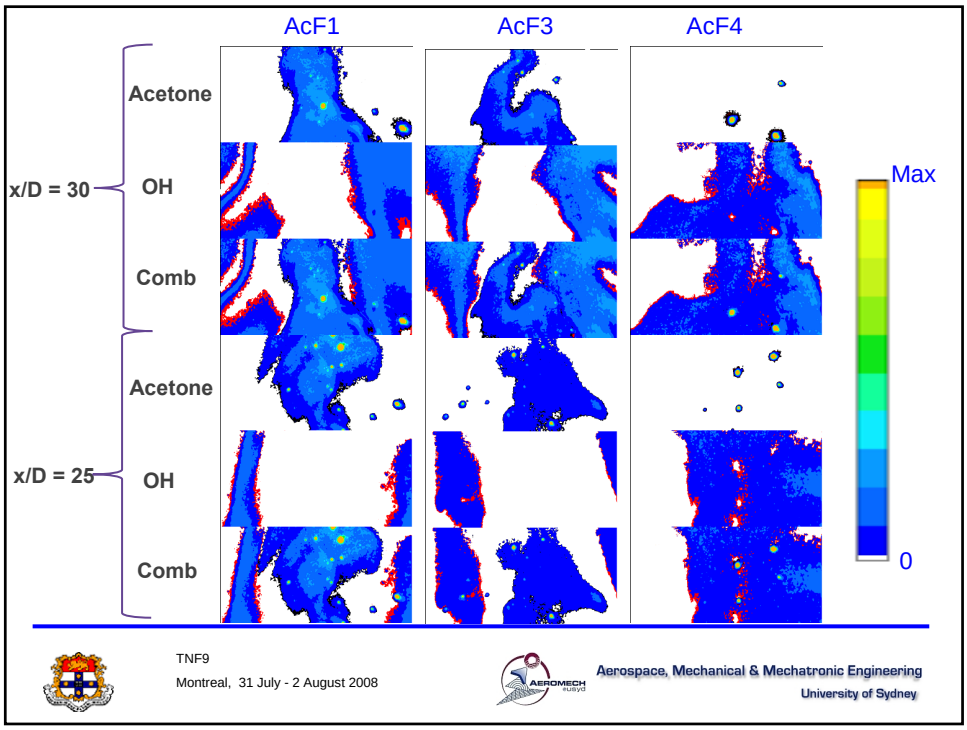
AcF1
AcF3
AcF4
Acetone
OH
Comb
x/D = 30
Acetone
OH
Comb
x/D = 25
Max
0
TNF9
Montreal, 31 July - 2 August 2008
Aerospace, Mechanical & Mechatronic Engineering
University of Sydney

Single droplet combustion

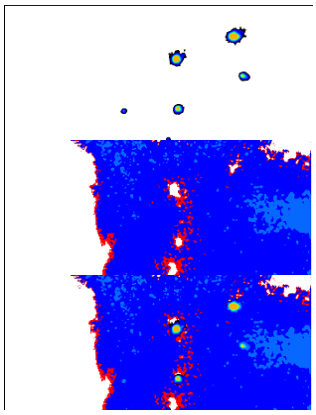

Combustion of droplet clouds

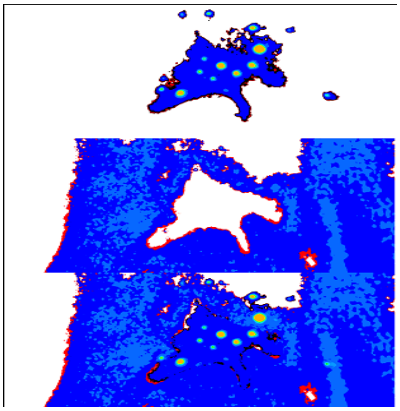

TNF- Existing Target Flames:

Piloted flames

- **Is there a need for measurements of more complex fuels?**

Bluff Body and Swirl Flames:

- **Are LES of swirling flames as sensitive to boundary layer as bluff-body flames?**
- **Is there is need for more detailed measurements of the boundary conditions? What needs to be measured?**
- **Is there a need for measurements of scalar dissipation rates?**

TNF9

August 2008

Future Collaborations and Comparisons

J. Janicka

Institute for Energy and Powerplant Technology

Remarks

- **Model development**
  - **Nice: A2 or N3**
  - **Models: applicable and/or accurate**
  - → **Still far away from regime independent models**
    - → **PDF modelling for premixed combustion?**
  - → **A2 models ok, applicable (in principle) for A3/N3 are sufficient**

Perspective TNF10

TECHNISCHE UNIVERSITÄT DARMSTADT

- **Focal point: multiple calculation for target flames**
- **New Target flames**
  - **Stratified burner: first result 2010**
  - **Cabra burner: systematic comparisons, also flame propagation model**
  - **Yale opposed flow: very interesting, wait for future development**
  - **→ Make simulation first**
- **Complex fuels**
  - **Gaseous fuels: methane + ethane (+ propane)**
  - **Transportatioon fuels: ethanol, DME**
  - **→ Define TNF fuels !!!**
  - **→ Start with jet-flame (D,E,F) series or/and Cabra burner**
- **Unsteady phenomena**
  - **Spark ignition**
  - **→ Different configuration, spark characterisation**
  - **Autoignition**
  - **→ Transient fuel jets**

EKT

Perspective TNF10

TECHNISCHE UNIVERSITÄT DARMSTADT

- **Quality assessment of LES**
  - **Available quality indicators are not sufficient**
  - **Strong sensitivity on boundary conditions**
  - **→ Include nozzle or inlet system into simulation**
  - **→ Additional experimental information helpful**
  - **→ Always show sensitivities**
- **Experiments and LES**
  - **Average procedures**
  - **Passive scalar mixing as testcase for QA?**
  - **Highspeed measurements**
- **Arrange a "definition" meeting in approx. one year**
  - **Complex fuels**
  - **Target flame data**

EKT

Perspective TNF10

TECHNISCHE UNIVERSITÄT DARMSTADT

- **Quality assessment of LES**
  - **Available quality indicators are not sufficient**
  - **Strong sensitivity on boundary conditions**
  - **→ Include nozzle or inlet system into simulation**
  - **→ Additional experimental information helpful**
  - **→ Always show sensitivities**
- **Experiments and LES**
  - **Average procedures**
  - **Passive scalar mixing as testcase for QA?**
  - **Highspeed measurements**
- **Arrange a "definition" meeting in approx. one year**
  - **Complex fuels**
  - **Target flame data**

ET

Acknowledgements

TECHNISCHE UNIVERSITÄT DARMSTADT

- **Local committee**
- **Everybody preparing a lecture or a poster**
- **All discussion contributors**
- **Everybody for joining TNF9**

ET

Auto-ignition test of flame condition of Cabra H_2/N_2 lifted flame

Haifeng Wang, Stephen B. Pope

September, 2008

Our investigations of the Cabra flame strongly suggest that the process controlling stabilization (and hence the lift-off height) is the auto-ignition of very lean mixtures. Hence the ignition delay times of lean mixtures with different co-flow compositions can be used as an indication of the expected behavior of the flames with these different co-flows.

Figure 1 shows the ignition delay time (IDT) against the coflow temperature Tc for different coflow compositions of the Cabra burner, air/H_2 products (equivalence ratio=0.25 [1]) or pure air. For the Cabra H_2/N_2 flame condition [1], the coflow composition is not clear from the literature. In [1], only following species are listed, X_{O2}= 0.1474, X_{N2}=0.7534 and X_{H2O}=0.0989, while in [2], two more are added, X_{H2}=5.E-4, X_{OH}<1.E-6, where X is mole fraction. In figure 1, the influence of the added H_2 and OH on the IDT is compared. An equilibrium condition is also used (the equilibrium condition results in X_{OH}=7.5727E-08 at Tc=980K and X_{OH}=6.5669E-07 at Tc=1100K). Adding the amount of H_2 has negligible effect on IDT, but 1ppm of OH has at least a factor of two effect on the IDT. In our previous calculations [3], OH is not included. Adding H_2 and OH does not change the strong sensitivity of the IDT to the coflow temperature. The radical OH seems another strong sensitivity source in this flame in additional to the coflow temperature (the sensitivity is shown in figure 2).

With the pure air as the coflow of the Cabra burner, the curve of IDT vs. Tc shows a marked change in slope around Tc=970K (IDT=3 ms). For Tc greater than 970K, the sensitivity of IDT to Tc is significantly less for the air co-flow than it is for the vitiated co-flow (at the same IDT); whereas, conversely, for Tc less than 970, the sensitivity of IDT to Tc is significantly greater for the air co-flow than it is for the vitiated co-flow. With air coflow, the strong sensitivity to the coflow temperature remains, and the most sensitive coflow temperature shifts to the left about 50K compared to the Cabra flame (1045K is the reported measurement of the coflow temperature of the Cabra flame). However, the possible strong sensitivity of the lift-off height to the coflow compositions (e.g., OH) in the Cabra flame is eliminated.

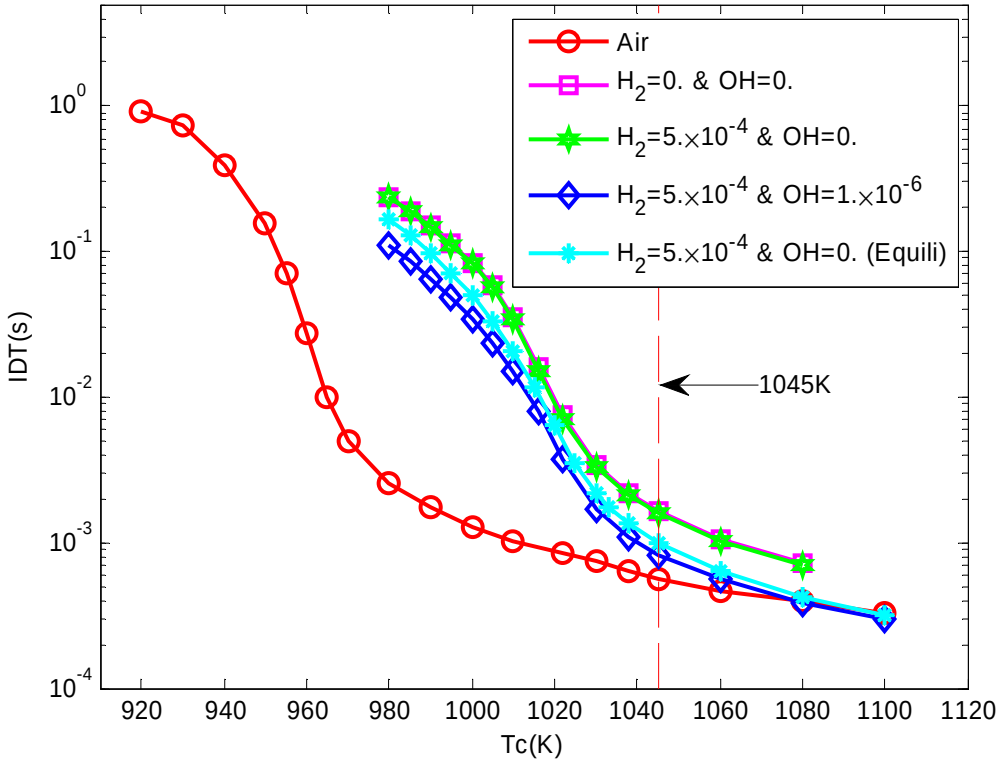

Figure 1 The ignition delay time (IDT) against the coflow temperature for different coflow compositions of the Cabra burner (for the condition of mixture fraction=0.05)

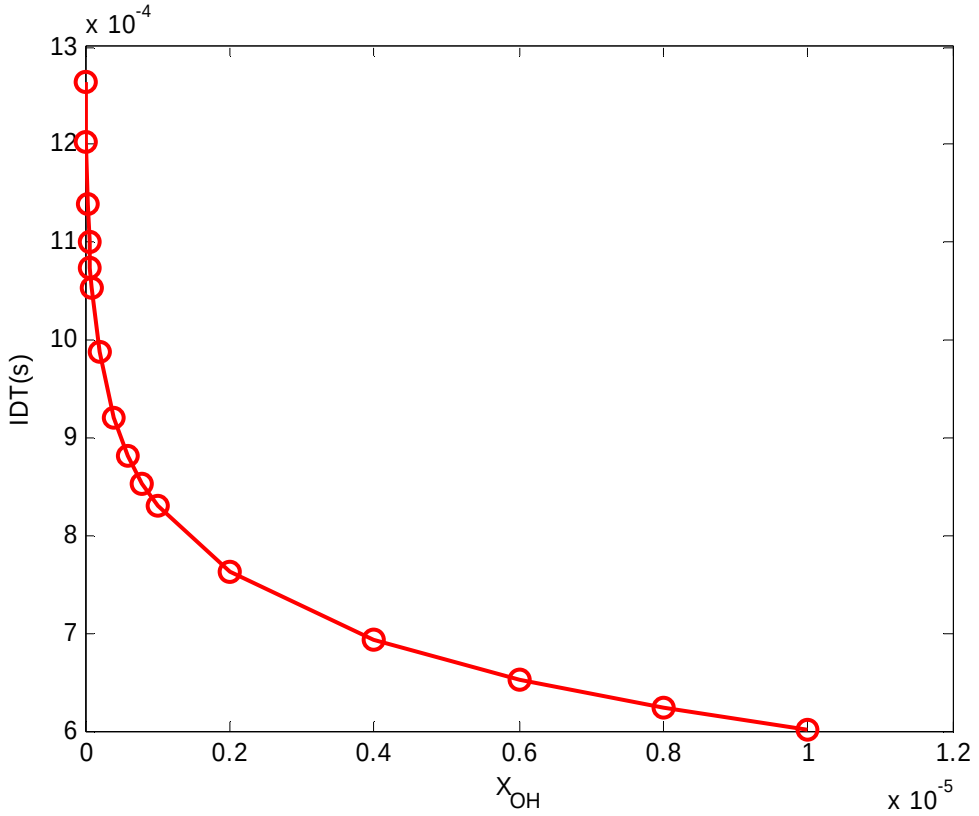

Figure 1 The ignition delay time (IDT) against the OH mole fraction in the coflow (for coflow temperature of 1045K and mixture fraction=0.05)

[1] R. Cabra, T. Myhrvold, J.-Y. Chen, R.W. Dibble, A.N. Karpetis, and R.S. Barlow. Simultaneous Laser Raman-Rayleigh-LIF Measurements and Numerical Modeling Results of a Lifted Turbulent H2/N2 Jet Flame in a Vitiated Coflow. Proc. Combust. Inst. 29 (2002) 1881-1888.
[2] R. Cabra, J.-Y. Chen, R.W. Dibble, A.N. Karpetis, R.S. Barlow. Lifted methane-air jet flames in vitiated coflow. Combust. Flame 143 (2005) 491-506.
[3] R. Cao, S.B. Pope and A.R. Masri. Turbulent lifted flames in a vitiated coflow investigated using joint PDF calculations. Combust. and Flame 142 (2005) 438-453 .

Section Divider – Poster Abstracts

TNF9 Workshop – Poster Abstract Titles and Authors

Holiday Inn Midtown Hotel, Montreal, Canada, July 31–August 2, 2008

1. **Spark Ignition of Turbulent Non-premixed Combustion: A New Benchmark Problem for the TNF Workshop?**
   S.F. Ahmed, E. Mastorakos

2. **Fast Solution of Quasi-Steady State Species by Combination of Fixed-Point Iteration and Matrix Inversion**
   F. Bisetti, Y.-F. Tham, J.-Y. Chen

3. **Development and Validation of an Unstructured, Density-Based Navier-Stokes Solver for Nonpremixed and Partially Premixed Combustion**
   K. Claramunt, J. E. Anker, C. Hirsch

4. **Modelling Local Extinction in Flames E using a Sparse-Lagrangian MMC Model**
   M.J. Cleary, A.Y. Klimenko

5. **Local Extinction and Reignition in a Premixed Turbulent Flame Counterflowing Hot Combustion Products**
   B. Coriton, A. Gomez

6. **Effect of Initial Conditions on the Structure of Turbulent Premixed Jet Flames Propagating in a Hot and Diluted Coflow**
   B.B. Dally, G. Wang, R.S. Barlow

7. **RANS/PDF Simulations of Sydney Swirling Flames**
   R. DeMeester, B. Merci, B. Naud

8. **The Use of High Resolution Experimental Imaging Results for Validation of Large Eddy Simulations Utilizing Proper Orthogonal Decomposition**
   M.J. Dunn, A.R. Masri, R.W. Bilger, R.S. Barlow

9. **Coupling Imaging Diagnostics and LES Simulations in a Turbulent Non-Reacting Jet and a Nonpremixed Jet Flame (DLR-A)**
   J.H. Frank, S.A.Kaiser, J.C. Oefelein

10. **Simultaneous 3-D Volumetric PIV and 2-D OH PLIF in the Far-Field of a Non-Premixed Turbulent Jet Flame**
    M. Gamba, N.T. Clemens, O.A. Ezekoye

11. **Laser Diagnostics for Transient Combustion Phenomena**
    R. Gordon, C. Heeger, B. Böhm, S.F. Ahmed, I. Boxx, A. Dreizler, E. Mastorakos, W. Meier

12. **Towards Predictability of Isothermal and Reacting Flows using LES: From a Simple Test Case to Technically Relevant Swirl burner Configurations**
    F. Hahn, C. Olbricht, J. Kuehne, J. Janicka

13. **LES modeling of extinction and reignition using a flamelet/progress variable formulation: Application to Sandia flame E**
    M. Ihme, H. Pitsch

14. **Numerical Study of n-Heptane Auto-Ignition using LES-PDF Methods**
    W.P. Jones, S. Navarro-Martinez

15. **Numerical Modeling for Structure and Pollutant Formation in Syngas Turbulent Nonpremixed Swirling Flames**
    J. Lee, S. Kang, Y. Kim K.-Y. Ahn

16. **Hybrid FVM/PDF Transport Model for Turbulent Swirling Reacting Flows**
    J. Lee, S. Kang, Y. Kim, M. Muradoglu

17. **A Novel Domain Decomposition Strategy for Low-Speed Hydrodynamics**
    R. McDermott, K. McGrattan, W.E. Mell

18. **Simultaneous Application of Laser-Induced Incandescence and Two-Line Atomic Fluorescence Temperature Measurement to Sooting Turbulent Nonpremixed Flames**
    P.R. Medwell, Q.N. Chan, P.A.M. Kalt, Z.T. Alwahabi, B.B. Dally, G.J. Nathan

19. **Using a Tabulated Flamelet Approach to Simulate a Lifted Methane Jet Flame**
    J.B. Michel, C. Angelberger, O. Colin, D. Veynante

20. **LES of Sydney Flames using Steady Flamelet and Progress Variable Approaches**
    C. Olbricht, F. Hahn, J. Kuehne, J. van Oijen, J. Janicka

21. **Creating a Dataset of Velocities, Temperatures and Minor Species on the Delft Jet in Hot Coflow Flames**
    E. Oldenhof, M.J. Tummers, E.H. van Veen, D.J.E.M. Roekaerts

22. **Particle Advection for Large Eddy Simulation/Filtered Density Function Methods for Turbulent Combustion Simulations**
    P.P. Popov, S.B. Pope

23. **A Stable and Conservative Pressure-Correction Method for Transient Simulations of Reacting Flows**
    P. Rauwoens, J. Vierendeels, E. Dick, B. Merci

24. **Direct Numerical Simulation and Analysis of Stratified Turbulent Methane-Air Flames**
    E.S. Richardson, J.H. Chen

25. **EKT Stratified Burner: A Generic Premixed Jet Flame Series for Model Validation**
    F. Seffrin, F. Fuest, D. Geyer, A. Dreizler

26. **Flame Modeling using Artifcial Neural Networks and Linear Eddy Mixing Model Based Tabulation Strategy**
    B.A. Sen, S. Menon

27. **Application of LES/CMC Methodology to Hydrogen Auto-Ignition in a Turbulent Co-Flow of Heated Air**
    Stankovic, A. Triantafyllidis, E. Mastorakos, C. Lacor, B. Merci1

28. **Investigation of Unsteady Combustion Phenomena in a Gas Turbine Model Combustor**
    M. Stöhr, R. Sadanandan, P. Weigand, W. Meier

29. **Premixed and Stratified Flame Diagnostics Based on 3D Flame Orientation**
    M.S. Sweeney, S. Hochgreb, R.S. Barlow

30. **Large Eddy Simulations - Conditional Moment Closure of Forced Ignition of a Nonpremixed Methane Bluff-Body Stabilised Flame**
    Triantafyllidis, E. Mastorakos, R. Eggels

31. **Hybrid Binomial Langevin-MMC Modeling of a Reacting Mixing Layer**
    A.P. Wandel, R.P. Lindstedt

32. **Second-order Accurate Splitting Schemes for Monte Carlo Particle Methods**
    H. Wang, P.P. Popov, S.B. Pope

33. **Effect of Air-Side vs. Fuel-Side Dilution on NO_x Emissions in Turbulent Hydrogen Jet Diffusion Flames**
    N.T. Weiland, P.A. Strakey

34. **Soot Volume Fraction Imaging in a Turbulent Nonpremixed Ethylene Jet Flame by Quantitative 2D Laser Induced Incadescence**
    J. Zhang, T.C. Williams, C.R. Shaddix, R.W. Schefer

35. **DNS of a Turbulent Lifted Ethylene/Air Jet Flame in an Autoignitive Coflow – Stabilization and Flame Structure**
    C.S. Yoo, E.S. Richardson, R. Sankaran, J.H. Chen

Spark Ignition of Turbulent Non-premixed Combustion: A New Benchmark Problem for the TNF Workshop?

S.F. Ahmed and E. Mastorakos*

Engineering Department, University of Cambridge, UK
* Corresponding author, e-mail: em257@eng.cam.ac.uk

The initiation of a *premixed* flame in a uniform mixture through a spark is one of the most widely combustion phenomena, but surprisingly little attention has been given to this problem when the reactants are *non-premixed*. Spark ignition of turbulent non-premixed combustion is important from a practical (in risk assessment of accidental fuel releases, in gasoline direct-injection engines, in gas turbines) and from a theoretical viewpoint. In particular, many interesting phenomena have been recently revealed, and, broadly speaking, the following characteristics of the problem have been observed, all of which require much further study.

- The ignition process has a strong stochastic nature. After depositing energy at the spark, a kernel may or may not be generated depending on the local mixture fraction [1], the local strain rate and the turbulence level [2-4]. The probability of creating a kernel can be different from the probability of finding flammable mixture at the spark location and from the probability of establishing the whole flame [5-7].
- The kernel will grow into a flame that then propagates in stratified ("partially-premixed") mixture and if this mixture has a wide range of mixture fraction fluctuations, a turbulent non-premixed edge flame propagating along the stoichiometric iso-surface will be created. The propagation speed and quenching of such flames in turbulent flows is little known [8-10] and must be studied more.
- In complicated flows with recirculating or swirl, the best placement of the spark in order to promote ignitability of the whole flame must be better understood, something that can be achieved with studies of the ignition probability and its relation to local flow variables [5-7] and with high-speed laser diagnostics [10].

It is clear that the wide range of fates that a spark or an ignition kernel can have in a turbulent flow, and the complicated nature of the flame propagation processes, in conjunction with the huge practical importance of ignition, can motivate extensive and challenging research. In the references given and in the examples presented at the poster, some of these issues are discussed through recent collaborative work at the Universities of Cambridge, Liverpool and Darmstadt [2-10]. Sufficient quantitative data to initiate modelling efforts already exist from experiments and DNS.

It is proposed that the topic of spark ignition on non-premixed combustion becomes a focal point of the TNF Workshop.

- Examination of ignition would serve as an excellent test-case for LES, especially in the context of sub-grid models for simultaneously occurring premixed and non-premixed combustion.

- The intrinsic transient nature of the problem poses great challenges. New ways by which experimental data and RANS or LES should be compared can be explored; for example, to examine if the simulations can capture the ensemble-averaged behaviour compiled over a large number of realizations of the sparking events and if the whole range of kernel behaviour (quenching, growth, success, failure etc.) can be observed numerically in LES.
- With an extension of this work to various fuels, chemistry more complex than methane can be validated.

An initial step in this direction could be to select one of the Sydney bluff-body configurations, perform measurements on it *without* combustion (e.g. inert velocity, inert mixing), then spark at various positions and monitor the outcome with fast-response laser diagnostics. The advantage of this would be that modellers who have already modelled the Sydney flame could quickly start their efforts. Alternatively, one of the Cambridge flames [5-7] could be used. Further laminar flame simulations and DNS are also necessary, as is the extension of spark-ignition work to turbulent sprays.

References

[1] Birch, A.D., Brown, D.R., Dodson, M. G. and Thomas, J. R. (1978). Studies of flammability in turbulent flows using laser Raman spectroscopy. Proceedings of the Combustion Institute 17, 307-314, 1978.

[2] Richardson, E.S. & Mastorakos, E. (2007) Numerical investigation of forced ignition in laminar counterflow non-premixed methane-air flames. Combustion Science and Technology 179, 21-37.

[3] Chakraborty, N., Mastorakos, E. & Cant, R.S. (2007) Effects of turbulence on spark ignition in inhomogeneous mixtures: a Direct Numerical Simulation (DNS) study. Combustion Science and Technology 179, 293-317.

[4] Chakraborty, N. & Mastorakos, E. (2008) Direct Numerical Simulations of localised forced ignition in turbulent mixing layers: the effects of mixture fraction and its gradient. Flow, Turbulence and Combustion 80, 155-186.

[5] Ahmed, S.F. & Mastorakos, E. (2006) Spark-ignition of lifted turbulent jet flames. Combustion and Flame 146, 215-231.

[6] Ahmed, S.F., Balachandran, R. & Mastorakos, E. (2007) Measurements of ignition probability in turbulent non-premixed counterflow flames. Proceedings of the Combustion Institute 31, 1507-1513.

[7] Ahmed, S.F., Balachandran, R., Marchione, T. & Mastorakos, E. (2007) Spark ignition of turbulent non-premixed bluff-body flames. Combustion and Flame 151, 366-385.

[8] Chakraborty, N. & Mastorakos, E. (2006) Numerical investigation of edge flame propagation characteristics in turbulent mixing layers. Physics of Fluids 18, 105103.

[9] Hesse, H., Chakraborty, N. & Mastorakos, E. (2008) The effects of Lewis number of the fuel on the displacement speed in igniting turbulent mixing layers. Submitted to the Proceedings of the Combustion Institute 32.

[10] Heeger, C., Böhm, B, Ahmed, S.F., Gordon, R., Boxx, I., Meier, W., Dreizler, A. & Mastorakos, E. (2008) Statistics of relative and absolute velocities of turbulent non-premixed edge flames following spark ignition. Submitted to the Proceedings of the Combustion Institute 32.

FAST SOLUTION OF QUASI-STEADY STATE SPECIES BY COMBINATION OF FIXED-POINT ITERATION AND MATRIX INVERSION

F. Bisetti[1,*], Y.-F. Tham[2], J.-Y. Chen[2]

[1]: *Center for Turbulence Research, Stanford University, USA*

[2]: *Department of Mechanical Engineering,University of California at Berkeley, USA*

fbisetti@stanford.edu

In recent years, detailed chemical mechanisms have been developed to describe the combustion chemistry of practical fuels [1-6]. While the large number of species increases computational demands, the wide range of time scales associated with large hydrocarbon molecule combustion also cause numerical difficulties. Thus, reduction of these mechanisms is needed for practical applications. Quasi-Steady State Approximation (QSSA) is a widely used method to construct reduced chemistry [7-14], by assuming that the net production rate of each QSS species is equivalent to the net destruction rate. The underlying non-linear system of balance equations for the QSS species is solved internally with Fixed Point Iterations (FPI). However, such approach can be computationally very intensive at times [15]. Lu and Law [16] approximated the nonlinear QSS system by a set of linear equations, and used this approach for solving a handful of QSS species. For reduced chemistry with a large number of QSS species and strong nonlinear interactions, the linearized approach may become inadequate as the inter-dependence of QSS species becomes strong. In this poster, we explore a new hybrid solution scheme for solving the non-linear QSS system.

By closely examining the form of the QSS system, it was concluded that the root cause of the slow convergence with FPI is the strong coupling among fast reacting isomer QSS species. In order to speed up the convergence of the entire QSS system, strongly coupled species groups are first identified and solved with Matrix Inversion (MI). The QSS species not strongly coupled are solved with the usual FPI. By using this hybrid FPIMI solution scheme, significant speed-up can be achieved for QSS systems for heavy hydrocarbon fuels. Fig. 1 shows the total CPU times with FPIMI normalized by those with FPI versus different QSS species coupling threshold ε for: 1) a 18-species methane reduced chemistry with 17 QSS species, 2) a 63-species isooctane reduced chemistry with 152 QSS species [17], and 3) a 101-species reduced chemistry for Primary Reference Fuel (PRF) of gasoline with 251 QSS species. While there isn't any significant difference in CPU time for the methane QSS system, the isooctane and the PRF QSS systems require much lower CPU time when FPIMI is used. When the isooctane and PRF QSS systems are resolved by the Newton Iterations (NI) method, the CPU times required to reach convergence are much higher than when FPI is used. Despite the quadratic convergence rate from NI, the larger system size of the heavy hydrocarbon mechanisms require more CPU time per iteration, and thus longer overall time. On the other hand, the CPU time required for convergence is 47-57% of the FPI time for isooctane with FPIMI, and 0.5 – 20% of the FPI time for PRF with FPIMI. The potential saving in CPU time increases with the degree of coupling and, to a less extent, with the nonlinear system size. In this poster, the performances of FPIMI are evaluated and analyzed for the following areas during autoignition delay calculations: total number of iterations to reach convergence, total CPU time, CPU time per iteration, and the influence of the coupling

threshold ε .

References

[1] C.K. Westbrook, J. Warnatz, W.J. Pitz, Proc. Comb. Inst. 22 (1998) 22:893-901.

[2] C.E. Roberts, R.D. Matthews, W.R. Leppard, "Development of a Semi-Detailed Kinetics Mechanism for the Autoignition of Iso-Octane," SAE paper 962107, 1996.

[3] E. Ranzi, T. Faravelli, P. Gaffuri, A. Sogaro, A. D'Anna, A. Ciajolo, Combust. Flame 108 (1) (1997) 24-42.

[4] C.K. Westbrook, Proc. Comb. Inst. 28 (2000)1563-1577.

[5] H.J. Curran, P. Gaffuri, W.J. Pitz, C.K. Westbrook, Combust. Flame 129 (3) (2002) 253-280.

[6] J. Warnatz, U. Maas, R.W. Dibble, Combustion 4th Edition, Springer-Verlag, 2006, p. 74.

[7] N. Peters, B. Rogg (Eds) "Reduced Kinetic Mechanisms for Applications in Combustion Systems," Lecture Notes in Physics, Springer-Verlag Berlin, 1993

[8] N. Peters, R.J. Kee, Combust. Flame 68 (1987) 17-29.

[9] J.-Y. Chen, Combust. Sci. Technol. 78 (1991) 127-145.

[10] T. Turanyi, A.S. Tomlin, M.J. Pilling, J. Phys. Chem., 97 (1993) 163-172.

[11] A. Massias, D. Diamantis, E. Mastorakos, D.A. Gousis, Combust. Flame 117 (4) (1999) 685-708.

[12] C.J. Sung, C.K. Law, J.-Y. Chen, Combust. Flame 125 (2001) 906-919.

[13] T. Lovas, D. Nilsson, F. Mauss, Proc. Combust. Inst. 28 (2000) 1809-1815.

[14] T.F. Lu, Y. Ju, C.K. Law, Combust. Flame, 126 (1-2) (2001) 1445-1455.

[15] C.K. Law, C.J. Sung, H. Wang, T.F. Lu, AIAA J. 41 (2003) 1629-1646.

[16] T.F. Lu, C.K. Law, J. Phys. Chem A 110 (49) (2006) 13202-13208.

[17] F. Bisetti, Y.F. Tham, J.-Y. Chen, Journal of Engineering for Gas Turbines and Power, 130 (2008) 042804.

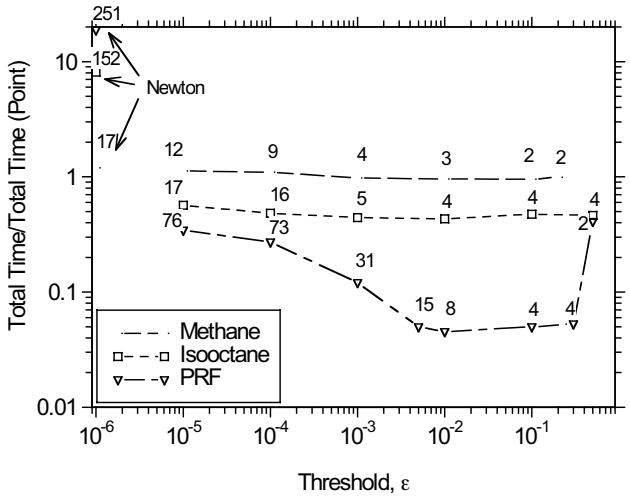

Fig. 1. Normalized total CPU time by fixed-point iteration versus coupling threshold, ε, for three reduced mechanisms with different number of quasi-steady state species: methane 17; isooctane 152, and primary reference fuel 251. CPU saving becomes significantly as the number of QSS increases. The number on each symbol denotes the maximum size of matrix being solved.

Development and validation of an unstructured, density-based Navier-Stokes solver for non-premixed and partially premixed combustion

K. Claramunt, J. E. Anker, Ch. Hirsch*
NUMECA Int., Av. Franklin D. Rooseveltlaan 5
B-1050 Brussels, Belgium
www.numeca.com
*charles.hirsch@numeca.be

Synopsis

The poster describes the implementation and validation of combustion models for non-premixed and partially-premixed combustion in the unstructured hexahedral simulation system FINE™/Hexa. The solution scheme of the flow solver is explained and numerical issues concerning robustness and solution monotonocity are addressed. The flow solver has been assessed on a comprehensible set of test cases ranging from simple verification test cases to geometrically complex, industrially relevant test cases. A key element in the validation procedure is the numerical simulation of TNF target flames. As the various TNF flames feature specific physical aspects, they are suited to assess that the flow solver is able to reproduce fundamental aspects of non-premixed and partially premixed combustion. Results from the simulation of various target flames together with examples from runs of industrial test cases are used to discuss the capabilities and the limitations of the developed numerical approach as well as the implemented combustion models.

Introduction

Combustion accounts for the major part of the energy conversion processes conducted throughout the world. An accurate modeling of combustion processes is thus essential if the current policy objectives of increased efficiency and reduction in emissions of combustion engines and devices are to be realized. Since there is a demand for reliable and accurate simulation tools for reactive flows, NUMECA Int. has incorporated advanced combustion modeling capabilities in its unstructured CFD software system. To ensure the reliability of the developed combustion models, a thorough verification and validation procedure has been applied. The simulation of TNF target flames represents an important part of the validation procedure, as those cases are well defined, have detailed experimental and numerical data available and exhibit specific characteristics of non-premixed and partially premixed flames.

Numerical Method

The FINE™/Hexa integrated CFD solver software package in which combustion models have been implemented consists of HEXPRESS™ for the automatic generation of unstructured fully hexahedral meshes, the flow solver HexStream™, and CFView™ for post-processing and visualization. FINE™/Hexa solves the Reynolds-Averaged Navier-Stokes equations (RANS) for compressible flows on unstructured, hexahedral grids by means of an explicit time-marching finite volume scheme. The solution scheme that is used ensures monotonous solutions and allows thus a robust and accurate resolution of both reactive and inert flow fields. By using agglomeration multigrid, implicit residual smoothing and parallelization with automatized domain decomposition, the solution scheme is highly efficient.

Modeling approaches for non-premixed and partially-premixed combustion

Non-premixed combustion is mainly controlled by the mixing process between the fuel and the oxidizer. This is exploited in the chosen modeling approach, where the mixture fraction approach is used to model non-premixed reactive flows. By using look-up tables based on the chemical equilibrium or the laminar flamelet concept, the flame structure and the thermo-chemical properties can be calculated in a pre-processing step and the computational costs of a reactive simulation can thus be kept low. To account for turbulence-chemistry interaction, RANS-based models are used in conjunction with presumed probability density functions (PDF). This approach forms also the basis of more advanced functionalities like a model for non-adiabatic combustion where radiative heat loss is accounted for, and a post-processing tool for the determination of the thermal NOx formation. For non-adiabatic flow situations, the heat loss is determined via an adequate transport equation for the determination of the enthalpy defect in conjunction with a radiation model. Currently, the Optically Thin Model (OTM) and the first-order spherical harmonics method (P_1 approximation) are used for the computation of the radiative heat transfer in the flow field. The Weighted Sum of Gray Gases method (WSGG) is used to determine the optical properties.

In addition to models for purely non-premixed combustion, a framework for modelling partially premixed combustion has been implemented in FINE™/Hexa. This framework is currently used in conjunction with combustion tables generated by the Intrinsic Low Dimensional Manifolds (ILDM) method [1] where a detailed mechanism is automatically reduced and the combustion processes is parameterized by the mixture fraction and one (or several) progress variables.

Verification and validation procedure

The verification and validation procedure of combustion models developed in FINE^{TM}/Hexa consists of three distinct components. In the first part the consistency of the implemented transport equations for flow, turbulence and combustion is verified by carrying out elementary test cases like the flat diffusing plate, the mixing of two streams, etc. In some instances also the method of manufactured solutions is employed for model verification. This phase of the testing procedure consists also of conducting simulations for non-reacting jets (TNF's propane jet, TNF's inert swirling test cases) and laminar flames. By conducting grid refinement studies and comparing the computational results with analytical data, experiments and detailed simulations, it is verified that the implementation has the expected numerical order of accuracy.

In a second step well-established test cases for turbulent, non-premixed and partially premixed flames are carried out to validate and to calibrate the models for turbulent non-premixed combustion. An important part in this phase is the validation of the flow solver on several of TNF's target flames, as those test cases are well defined and have detailed measurement data available for comparison. As an example for one of the test cases conducted for the validation of the combustion models in FINE^{TM}/Hexa, the computed and measured carbon monoxide mass fractions are plotted in Fig. 1 for the TNF Bluff-body HM1e test case [2]. It should be noted that since each of the various TNF flames feature specific physical phenomena, they are particularly suited to assess that the flow solver is able to reproduce fundamental aspects of non-premixed and partially premixed combustion.

In the last part, the robustness, the reliability and the efficiency of the implemented combustion models are examined by conducting computations of geometrically complex, industrially relevant test cases. In this part of the overall quality assessment procedure, the combustion and radiation models implemented in FINE^{TM}/Hexa were for instance used to simulate the reactive flow field of the IFRF glass-furnace [3], of the industrial combustor of Sandia's Burner Engineering Research Laboratory (BERL) [4], and of the generic gas turbine (GGT) combustor of EKT/TU Darmstadt [5] (cf. Fig. 2).

Outlook

The modelling approach for partially premixed combustion is currently assessed using TNF Flame E, the Cabra flame [6] and the GGT case mentioned above. It is thereby investigated, whether or not it is necessary to account for the turbulent fluctuations in the progress variables in the modelling of the turbulence-chemistry interaction.

The combustion models used in FINE/Hexa are by default used in conjunction with the standard k-ε model. In turbomachinery simulations specialized models like that of Yang-Shih are used to avoid occurrence of the stagnation point-anomaly. It thus is planned to compare the performance of various two-equation turbulence models on several of the TNF target flames (TNF Flame D, Bluff-body and swirl-stabilized flames HM1e/SMH1)

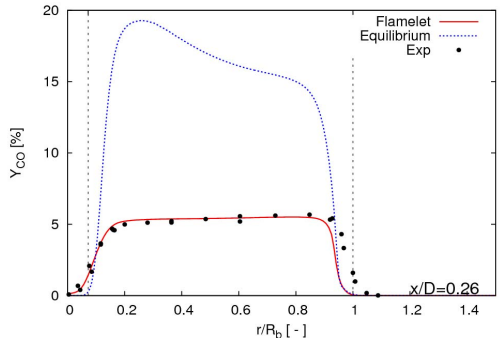

Fig. 1: Simulated and measured CO mass fraction (x/D = 0.26) in the TNF Bluff-body test case

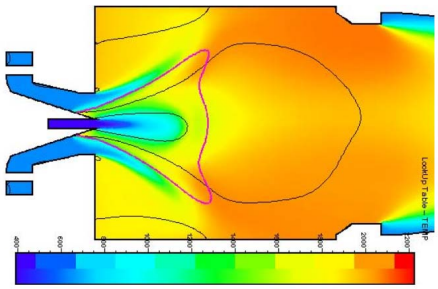

Fig. 2: Computed temperature field in the generic gas turbine combustor

Acknowledgement

A part of this work was accomplished under the EU funded Marie Curie AdComb-CFD project in which NUMECA collaborated with TU Delft (MSP), TU Darmstadt (EKT) and Univ. of Heidelberg (IWR). The authors gratefully acknowledge the guidance of Prof. J. Warnatz, Dr. U. Riedel, Prof. J. Janicka, and Prof. D. Roekaerts in that project.

References

[1] Maas, U.; Pope, S. B. (1992): *Combustion and Flame*, Vol. 88, No. 3, pp. 239
[2] Dally, B. B.; Masri, A. R.; Barlow, R. S.; Fiechtner, G. J. (1998): *Combustion and Flame*, Vol. 114, pp. 119-148
[3] Nakamura, T.; Kamp, W. L. v. d.; Smart, J. P. (1991): *Further Studies on High Temperature Natural Gas Combustion in Glass Furnaces*, International Flame Research Foundation (IFRF), Ijmuiden, The Netherlands
[4] Kaufman, K. C.; Fiveland, W. A.; Peters, A.A.F; Weber, R. (1994): *The BERL 300 kW Unstaged Natural Gas Flames with a Swirl-stabilized Burner*, Babcock & Wilcox's Research and Development Division, Alliance, OH, USA
[5] Janus, B.; Dreizler, A.; Janicka, J. (2004): *ASME Paper GT2004-53340*
[6] Cabra, R.; Chen, J.Y.; Dibble, R. W.; Karpetis, A. N.; Barlow, R.S. (2005): Lifted methane–air jet flames in a vitiated coflow, *Combustion and Flame*, Vol. 143, pp. 491–506

Modelling local extinction in Flame E using a sparse-Lagrangian MMC model

M.J. Cleary* and A.Y. Klimenko
University of Queensland, Australia
* Corresponding author: m.cleary@uq.edu.au

At TNF8 it was noticed that different mixing models tend to converge when operating under localised conditions with a very large number of particles [1]. Under these conditions many mixing models can effectively approach DNS [4] and their satisfactory performance is not surprising. However the quality of a mixing model is demonstrated by its ability to perform with a relatively small number of particles. In principle, an inferior model may perform better if it uses more particles in the simulations. In this work filtered density function (FDF) simulations with a multiple mapping conditioning (MMC) mixing model are performed for Sandia Flame E. The model is tested under extreme conditions where only 10,000 reacting particles are used in the simulations.

Multiple mapping conditioning (MMC) [2] is a modelling framework which becomes a joint PDF model when formulated stochastically. Mixing is controlled so that it is local in a reference space which is chosen to enforce compositional locality. The mixture fraction is the best and simplest example of a reference variable. To ensure that independence and linearity principles are satisfied the mixture fraction reference variable cannot be determined from the stochastic composition but must be produced in some other way. We note that the EMST mixing model [3] also enforces localness but violates independence and linearity. In the original interpretation of MMC [2] reference variables are modelled by Markov processes. However reference variables do not have to be formulated in this way and removing the Markovian restriction corresponds to a generalised understanding of MMC [4,5]. In the present work stochastic Lagrangian particles for the reactive scalar field are transported by an underlying Eulerian LES flow field and the reference variable is given by the filtered mixture fraction. The Eulerian LES is conventional, using a Smagorinsky model for SGS shear stresses and an eddy diffusivity SGS scalar flux model for the filtered mixture fraction.

Particle mixing pairs are selected based on their proximity in physical (x) and reference mixture fraction ($\tilde{f}$) spaces. We define the normalised mean square distance between two particles (p and q) as

$$\hat{d}^2_{(p,q)} = \frac{1}{1+\lambda^2}\left[\sum_{j=1}^{3}\left(\frac{x_j^{*(p)} - x_j^{*(q)}}{L_x}\right)^2 + \lambda^2\left(\frac{\tilde{f}^{*(p)} - \tilde{f}^{*(q)}}{L_f}\right)^2\right] \tag{1}$$

Here L_x and L_f are characteristic scales set to the stoichiometric flame length and $(1 - Z_{st})$ respectively. The parameter λ determines the relative localisation in physical and reference mixture fraction spaces; in the present simulations $\lambda = 1$. Particle pairs are determined by minimising $\hat{d}^2_{(p,q)}$ for all particles in the domain. At each time step all particles mix by relaxing to the two-particle scalar average

$$\Delta\phi_n^{*(p)} = \frac{1}{\tau}\left(\hat{\phi}_n^{*(p,q)} - \phi_n^{*(p)}\right) \tag{2}$$

where the mixing time is given by

$$\tau = C_L^{-1}\left(\frac{\Delta_L}{\Delta_E}\right)^{2/3}\frac{C_\chi \Delta_E^2}{2(D + D_t)} \tag{3}$$

In Eq.(3) C_L is a tunable constant, Δ_L is the distance between mixing particles, Δ_E is the LES grid size, D and D_t are the molecular and SGS diffusivities respectively and $C_\chi = 0.1$ [6].

In the Eulerian LES there are 2 million grid cells while the sparse-Lagrangian particle scheme employs 35,000 particles and of these only 10,000 are within a mixture fraction range where reactions occur. With fewer particles than LES cells we do not intend to model the finest details of the sub-filter fluctuations and do not predict the filtered reacting species at each time step. However as each particle represents a single sub-filter turbulent realisation we are able to predict the steady-state joint scalar distributions. The LES in this case is simply a tool to provide the Lagrangian scalar scheme with a high quality velocity and reference mixture fraction field.

Figure 1 shows experimental and predicted scatter plots of CO and OH at x/d = 15. Predictions are sensitive to the choice of C_L. Low C_L increases the mixing time and reduces the extent of mixing between particles resulting in greater sub-filter fluctuations and by association greater conditional fluctuations. The results shown here are for $C_L = 5$ and the level of conditional fluctuations is over-predicted by about 20 or 30%. Global extinction occurs when C_L is reduced below three. We have also run simulations with C_L as large as 25 and this produces results with almost no local extinction at all. These results are preliminary and more work is need to determine the best choice of parameters for given flame conditions. In general it may be necessary to use greater numbers of particles to model the detailed structure in complex flames, and this option is of course available for MMC. However, as these results show, even with extremely low particle density the MMC mixing model captures the major features of Flame E reasonably well.

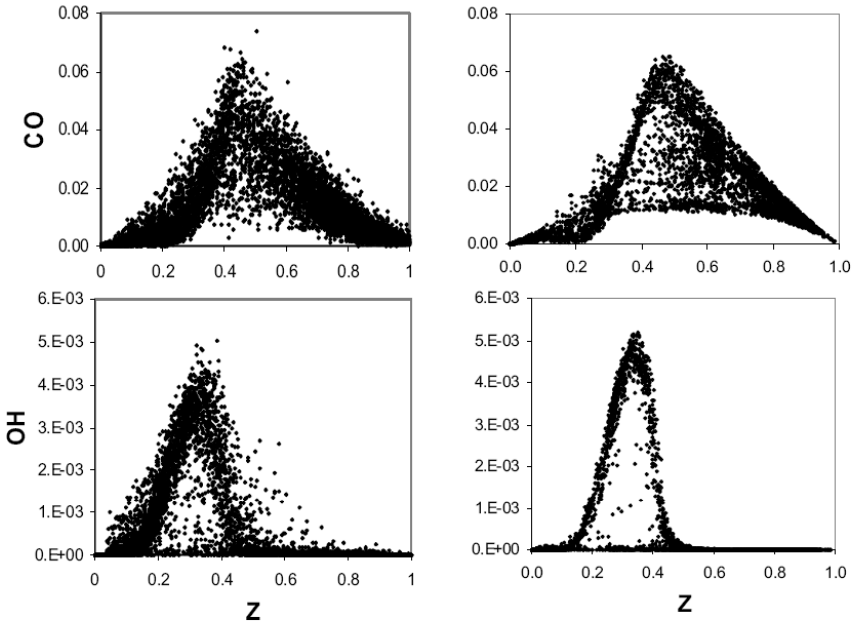

Fig 1. Scatter plots of CO and OH versus mixture fraction at x/d = 15.

References

1. F. Bisetti, J.Y. Chen, A. Kempf, J. Janicka, in TNF-8 (Turbulent Non-premixed Flames) Workshop, Heidelberg, 2006.
2. A.Y. Klimenko and S.B. Pope, *Phys. Fluids* 15 (7) (2003) 1907-1925.
3. S. Subramaniam and S.B. Pope, *Combust. Flame* 115 (1998) 487-514.
4. A.Y. Klimenko, *Phys. Fluids* 19 (2007) 31702.
5. M.J. Cleary, A.Y. Klimenko, *Flow, Turbulence and Combustion* DOI 10.1007/s10494-008-9161-3 (2008).
6. S. Navarro-Martinez, A. Kronenburg and F. Di Mare, *Flow, Turbulence and Combustion* 75 (2005) 245-274.

Local extinction and reignition in a premixed turbulent flame counterflowing hot combustion products

Bruno Coriton and Alessandro Gomez
Department of Mechanical Engineering
Yale Center for Combustion Studies
Yale University, New Haven, CT 06520-8286, USA
alessandro.gomez@yale.edu

Introduction

In turbulent premixed combustion, experimental investigation of the non-flamelet regime, often called broken reaction zone regime or distributed reaction zone regime, still remains an open challenge [1]. The non-flamelet regime corresponds to a situation of discontinuous flame sheets locally extinguished by turbulent eddies and is expected in very intense turbulence, at turbulent Karlovitz number greater than 100, of relevance to practical applications such as industrial furnaces and supersonic combustors. Conditions of strong turbulence and chemistry interaction are particularly hard to reproduce in a laboratory-scale burner and rare evidence of the non-flamelet regime under such conditions has been reported to date [2]. In other practical combustors and engines, where turbulence intensity is more modest, several additional factors can contribute to reduce the heat release rate, which eventually may lead to local extinction and reignition by turbulence. These factors can be: volumetric heat loss in the vicinity of walls, an intense strain rate imposed by the mean convective flow field or local mixing of the reactants with combustion products. In this context, Poinsot et al [3] showed that the limit of the flamelet regime could be lowered to much smaller Karlovitz numbers in the presence of volumetric heat loss.

We plan to study local flame extinction/reignition in a premixed turbulent environment at elevated (O(1000)) turbulent Reynolds number and at Karlovitz number in the 1-10 range, where a well-controlled volumetric heat loss and mean strain rate are applied to the flame. To that end, we designed a counterflow turbulent burner where one jet of fresh reactants is opposed to a second jet of hot combustion products. The temperature of this second jet and the separation between the nozzles define the volumetric heat loss and the bulk strain rate, respectively.

Experimental setup

The counterflow burner consists of two axisymmetric nozzles mounted on electrical translational stages to control accurately their alignment and separation. The top nozzle is suitable to discharge a highly turbulent jet of reactants, whereas the bottom nozzle emits hot combustion products. Turbulence in the top jet is generated by a properly designed blockage plate [4], to achieve a large turbulent intensity, while preserving a uniform and axisymmetric mean velocity profiles at the nozzle outlet and ensuring the absence of peculiar frequencies within the inertial range of turbulence. The turbulence generator plate is made with a star-shaped opening at the center (Fig. 1). The plate is located between 50 mm and 75 mm upstream of the nozzle outlet measuring 12.5 mm in diameter. The counterflowing jet of combustion products is produced by a turbulent premixed torch-flame enclosed within a ceramic cylindrical chamber measuring 50 mm in inner diameter and terminated by a contraction to an outlet diameter measuring 12.5 mm, as for the reactant jet. Two sizes of torch burner are used for small and large flow rates ranging from 20 SLPM to 120 SLPM. The size of the torch-flame does not exceed 100 mm. The temperature of the hot product jet, changed by varying equivalence ratio and dilution of the torch-flame, can be as large as 1800 K. Hot-wire anemometry is used to measure the performance of the turbulence generator plate. The flow field is characterized by PIV under cold and burning conditions. Flame front location and structure are observed by OH-PLIF.

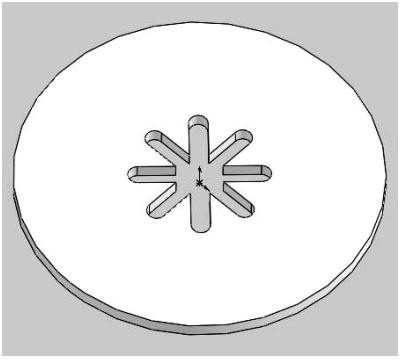

Figure 1 - Turbulence generator plate.

Results

The Performance of the turbulence generator plate was examined over a large range of flow rates corresponding to mean exit velocities between 9 and 21 m/s. The size of the integral length scale was estimated by applying the Taylor hypothesis for statistically independent 1D velocity measurements. The turbulent Reynolds number and the integral length scale are proportional to the flow rate (Fig. 2). The turbulent intensity is independent of the flow rate varying from 10% to 25% at the nozzle outlet, depending on the position of the plate with respect to the nozzle outlet. The Taylor scale, estimated at 0.5 mm, could not be resolved with our hot-wire probe measuring 1.2 mm in sensor length. The Kolmogorov scale was estimated at 25 um.

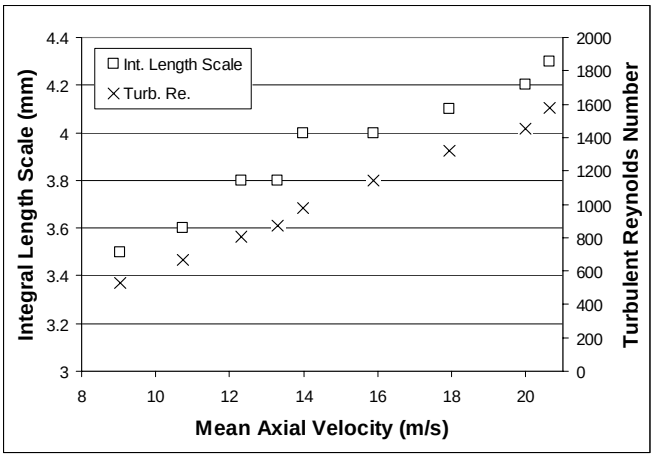

Figure 2 - Integral length scale and turbulent Reynolds numbe as a function of the mean exit velocity.

Depending on the combustion product jet temperature, stoichiometric methane/air flames could be stabilized between the two counterflowing jets at bulk strain rates ranging from 300 s^{-1} and 2000 s^{-1}. At low strain rate, OH-PLIF images show that the flame front varies from a singly connected structure with a hot product jet temperature of 1800 K (Fig. 3, left), to broken reaction zones with the occurrence of extinction holes and reignition, when such a temperature is lowered to 1600 K (Fig. 3, right). At an elevated bulk strain rate of 2000 s^{-1}, combustion happens in an unstable regime where low intensity flashes of blue light are emitted from the burner. Under these conditions, OH appears in very thin and distributed sheets. Additional work will be presented in the poster, including high-speed photographic sequences of the relevant phenomenology.

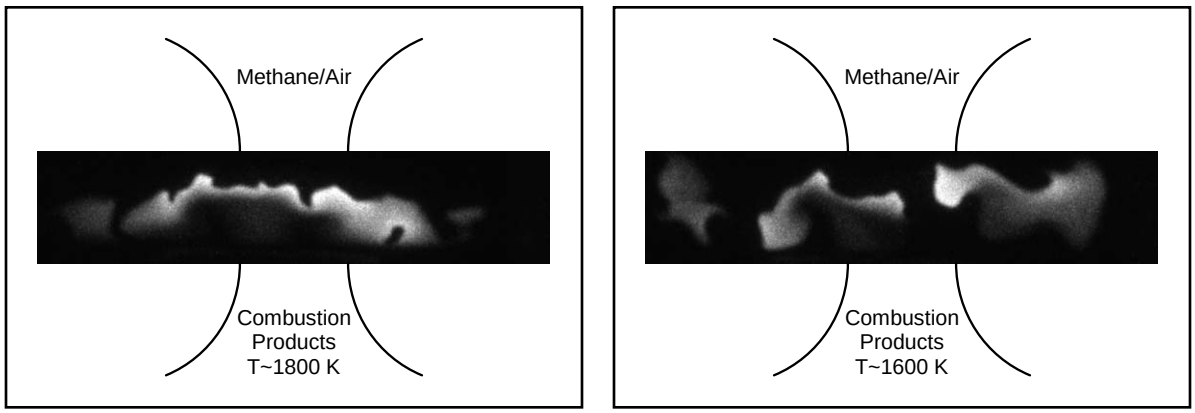

Figure 3 – Instantaneous OH-PLIF images of a stoichiometric CH_4/air flame counterflowed to hot combustion products at 1800 K (left) and 1600 K(right) and a bulk strain rate of 300 s^{-1}.

References

[1] – Peters, N. Cambridge Monographs on Mechanics, Cambridge University Press, 2000.
[2] – Mansour, M.S., Peters, N., Chen, Y.-C., Proc. Combust. Inst. 22 (1998) 767-773.
[3] – Poinsot, T., Veynante, D., Candel, J. Fluid Mech. 228 (1991) 561-606
[4] – Coppola, G., Gomez, A., *submitted to* Exp. Fluids (2008),

Effect of Initial Conditions on the Structure of Turbulent Premixed Jet Flames Propagating in a Hot and Diluted Coflow

B.B. Dally[1], G. Wang[2], R.S. Barlow[2]
[1]School of Mechanical Engineering, The University of Adelaide, Australia
[2]Combustion Research Facility, Sandia National Laboratories, Livermore, CA, USA
bassam.dally@adelaide.edu.au

The Jet in Hot Coflow, JHC burner is used in this study. Premixed turbulent flames of methane-air issuing from a variety of jets with different diameter and reactants inlet temperatures are investigated. The jets propagate into and products of a premixed flame of similar or different equivalence ratio to that of the jet. Figure 1 shows a sketch of the burner assembly. Table 1 shows the different cases investigated in this study.

Table 1 Details of the Methane Flames Measured in This Study

Flame	Reynolds No.	ϕ_{Jet}	ϕ_{Coflow}	Inlet Temp. (K)
MT-J19A	13,000	0.6	0.6	300
MT-J19B	37,000	0.6	0.6	300
MT-J19C	51,000	0.6	0.6	300
MT-J19D	49,000	0.8	0.8	300
MT-J19E	49,000	0.6	0.7	300
MT-J19F	49,000	0.6	0.8	300
MT-J19G	37,000	0.6	0.7	500
MT-J19P3A	51,000	0.6	0.6	300
MT-J19P3B	91,000	0.8	0.8	300
MT-J10A	51,000	0.6	0.6	300
MT-J10B	51,000	0.8	0.8	300
MT-J15P08A	98,000	0.7	0.7	300
MT-J15P08B	49,000	0.7	0.7	300
MT-J15P08C	24,500	0.7	0.7	300
MT-J15P08D	31,000	0.7	0.7	500
MT-J15P08E	46,000	0.7	0.7	800
MT-J15P08G	50,300	0.785	0.8	300

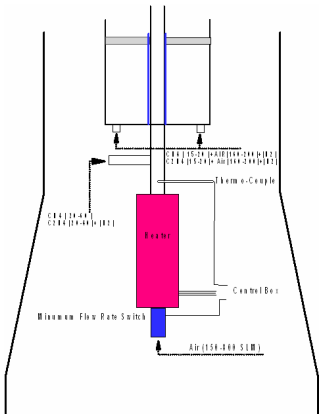

Figure 1 Sketch of Burner Setup

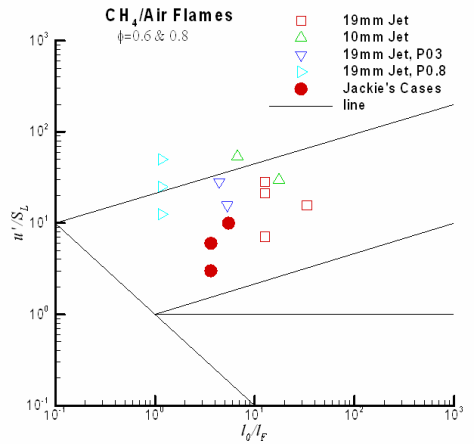

Figure 2 Estimated Flames' Position on Borghi's Diagram

Figure 2 shows the estimated position of the flames measured on the Borghi Diagram. It is clear that the operating conditions will allow us to have a clearer picture of effect of the initial conditions on the flames behaviour. Figure 3 and 4 show the measured radial profiles of temperature at 10mm above the jet exit and for two jet diameters 10mm and 19mm respectively. Both jets are blocked by a perforated plate with a 3mm hole diameter and blockage ratio of 49%. The figures show for the 19-mm case the flame front is wider and the equivalence ratio seems to have more influence over the flame thickness.

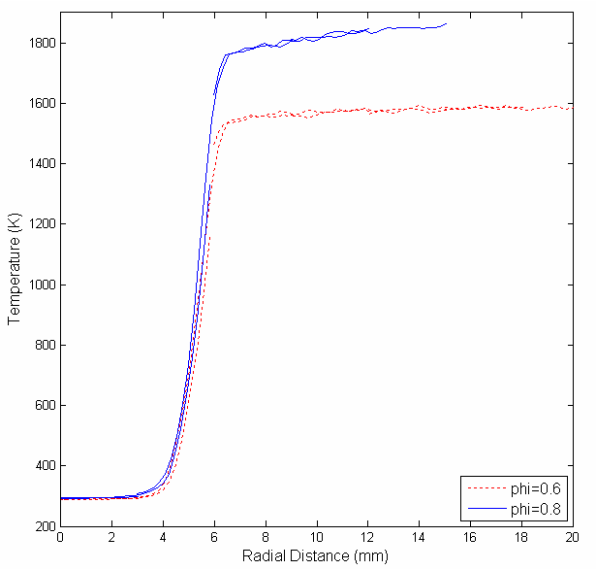

Figure 3 Radial Profile of Temperature for a 10mm jet with a perforated plate with 3mm hole diameter

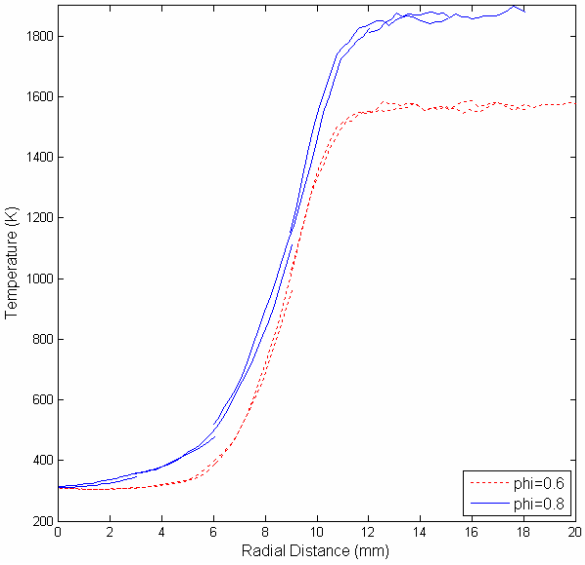

Figure 4 Radial Profile of Temperature for a 19mm jet with a perforated plate with 3mm hole diameter

Figures 5 and 6 show the effect of jet Reynolds number and inlet temperature respectively. The interaction of the jet with the hot coflow at low Reynolds number flame is more apparent that high Reynolds number flames. The increase in the reactants temperature seems to have reduced effect on the flame temperature but stronger effect on the flame front thickness.

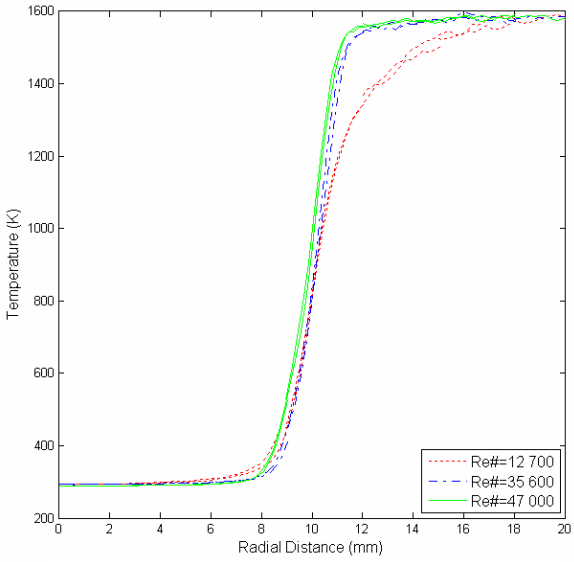

Figure 5 Radial Profile of Temperature for a 19mm jet. Reynolds Number Comparison.

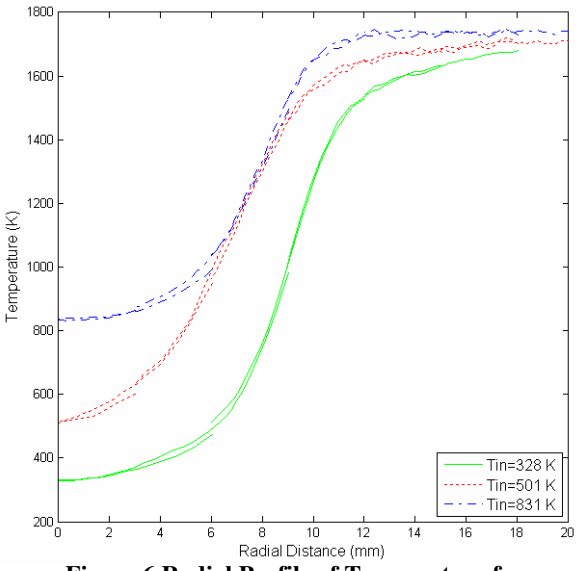

Figure 6 Radial Profile of Temperature for a 15mm jet. Inlet Temperature Comparison.

RANS/PDF SIMULATIONS OF SYDNEY SWIRLING FLAMES

R. De Meester[1], B.Merci[1], B.Naud[2]
[1] *Ghent University, Belgium;* [2] *CIEMAT, Spain;*
reni.demeester@ugent.be

Swirling flames have a lot of industrial applications, e.g. gasturbines, because of their specific advantages. The swirling flow in these flames for example enhances mixing and stabilizes the flame, leading to better combustion efficiency and less pollutant formation. However, swirl flames are quite complex and not yet totally understood. One of the complex phenomena involved in swirl flames is vortex breakdown which leads to flow instability, i.e. precessing vortex core and periodically expanding/shrinking recirculation zone. Our research aims to investigate the ability of RANS to qualitatively and quantitatively predict the specific flow phenomena involved in swirling flames. This will be done for the case of Sydney Swirl flame SM1 (CH_4) [1], because it has a smaller amount of flow instability and is thus more suitable for RANS simulations. The experimental setup for both flames consists of a wind tunnel containing a bluff body with a central fuel jet (3.6mm diameter,) surrounded by a swirling air annulus(50mm inner and 60mm outer diameter). The flow field of SM1 has a second recirculation zone due to vortex breakdown, which is a commonly found feature in swirling flows.
Assessment of unsteady RANS in predicting swirl flow instability in inert flows has been done in [2], where is concluded that 3D Unsteady RANS with a Reynolds Stress model is able to capture the flow instability, i.e. precessing vortex core, to some extent. Our research extends this to swirling flames and focuses on the use of preassumed and transported probability density functions (PDF) in the modeling of turbulence chemistry interactions. The validity of 2D axisymmetric steady RANS simulations is assessed by comparing these simulations with 3D unsteady RANS simulations.

Case	Composition Jet	U_{jet}	$U_{annulus}$	$W_{annulus}$	U_{coflow}
N29S054	air	66m/s	29.7m/s	16m/s	20m/s
SM1	CNG or CH_4	32.7m/s	38.2m/s	19.1m/s	20m/s

Table1: Flow conditions of N29S054 and SM1

First, 2D steady and 3D unsteady RANS simulations have been done for the inert swirling flow N29S054[3],because the flowfield of N29S054 is qualitatively similar to that of SM1.This way the predicted flow field can be investigated without the influence of the chemistry. For reacting flows (like SM1) the flow field must be well predicted in order to have a correct representation of the mixture fraction field, which will influence the shape of the flame.
In 2D, RANS simulations are done with the realizable k-ε model and with LRR Reynolds stress model.
With the realizable k-ε model, the flowfield is predicted quite well qualitatively: the second recirculation zone is predicted to extend from x=0.05m to x=0.135, while in experiments the 2nd recirculation extends from x=0.05m to x=0.110m.

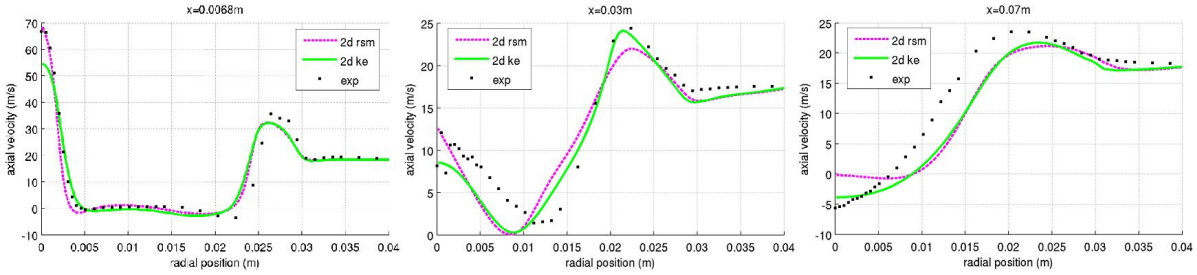

Figure 1:radial profiles of axial velocity for 2d simulation of N29S054 (rsm-ke)

With rsm , there is no steady 2D axisymmetric solution. This is most likely due to instability in the flow, causing a precessing vortex core.

In 3D, the flowfield of the steady k-ε simulation is very similar to that of the 2D k-ε simulation, but the 2nd recirculation zone, extending from x=0..05 to x=0.125, is predicted even better.
The unsteady 3D rsm simulation however does not give a good representation of the flowfield: the 2nd recirculation zone extends to the end of the calculation field at x=0.3m. Though the flow field and mixture fraction field up to x=0.1m is predicted quite well and is similar to that of the k-ε simulations. The precessing of the vortex core can be seen.
For the N29S054 case, one can conclude that a steady 2d axisymmetric simulation with the realizable k-ε model gives a good qualitatively and reasonable quantitatively representation of the flowfield. A 3D k–ε simulation is less attractive, because it gives slightly better results but with a much higher computational cost.

For SM1 steady 2d axisymmetric and unsteady 3d simulation with the realizable k-ε model and the LRR Reynolds stress model have been done. The steady laminar flamelet model and a preassumed β–PDF for composition describe respectively the chemistry and the chemistry-turbulence interaction.
In 2D, the steady simulation with the realizable k-ε model gives a good qualitative representation of the flow: the 2nd recirculation zone is predicted to extend from x=0.0625m to x=0.1m, while in the experiment it extends form x=0.7 to x=0.1. The reasonable qualitative prediction of the flow field results in a reasonable representation of the mixture fraction field and the flame shape as can be seen in figure 2.
The steady 2D rsm simulation of SM1 does not converge, due to the precessing vortex core.

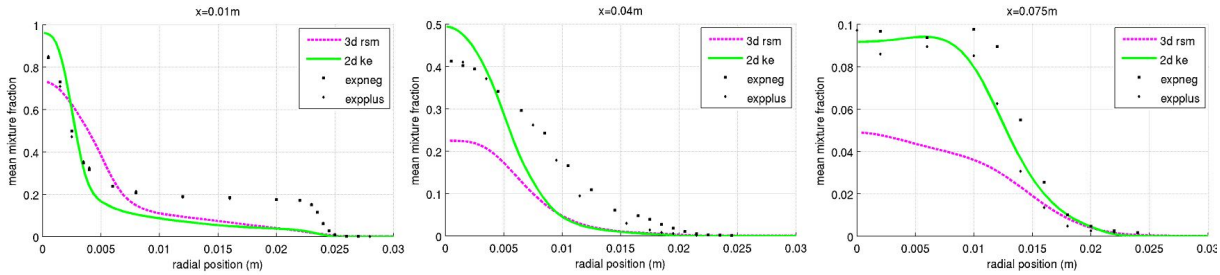

Figure 2:radial profile of the mean mixture fraction for SM1 (2d ke-3d rsm)

In 3D, the flow field of the simulation with the k–ε model is similar to the one in 2D.
The unsteady 3D rsm simulation however does not give a good qualitative representation of the flow field: there is no second recirculation zone. Though the flow field up to x=0.07 is predicted reasonably well and the precessing vortex core can be seen.
One can conclude that also for SM1 a steady 2d axisymmetric simulation with a k-e model is the best option for RANS simulations.
The next step in the research is a steady 2d axisymmetric simulation with the k-ε model , but with REDIM to account for finite kinetics and with a transported composition PDF.
The influence of different mixing models (C/D, EMST) is investigated.

REFERENCES

1Al-Abdeli, Y.M., and Masri, A.R., 'Recirculation and Flow Field Regimes of Unconfined Non-Reacting Swirling Flows', Experimental Thermal and Fluid Sciences, 27(5):655-665 (2003).

2Wegner, Maltsev, Schneider, Sadiki, Dreizler, Janicka, 'Assessment of unsteady RANS in predicting swirl flow instability based on LES and experiments', Int. Journal of Heat and Fluid Flow 25, pp.528-536 (2004)

3Al-Abdeli, Y.M., and Masri, A.R., 'Stability Characteristics and Flow Fields of Turbulent Swirling Jet Flows', Combust. Theory and Modeling, 7:731-766 (2003).

The use of high resolution experimental imaging results for validation of large eddy simulations utilizing proper orthogonal decomposition

Matthew J. Dunn[1*], Assaad R. Masri[1], Robert W. Bilger[1] and Robert S. Barlow[2]

*Corresponding author: *m.dunn@usyd.edu.au*
[1]*School of Aerospace, Mechanical and Mechatronic Engineering, The University of Sydney, NSW 2006, Australia.*
[2]*Sandia National Laboratories, Livermore, CA,94551-0969 USA*

The validation of Large Eddy Simulations (LES) from experimental data is a challenging prospect that has not yet been adequately addressed beyond spatial and conditional statistics of mean and RMS scalar and or velocity fields. Recent advances in computer storage, camera, optics and laser technologies have enabled measurements of high resolution line or 2D images resulting in very large data sets (>1e4 realizations). The challenge is how to utilize this information to develop a better understanding of the physics of the flow and for validation of LES in a meaningful way that exploits the large amount of data collected.

LES for reacting flows can also produce enormous amounts of information if all of the variables are stored at every grid point on the three dimensional grid at a specified time interval. The ratio of the largest fluid stream flow through time (eg. the air coflow in the piloted TNF flame series) to the smallest resolved eddy turn over time can be very large for current state of the art highly resolved LES simulations. This leads to a large amount of data that needs to be stored if all significant modes including the lowest are to be analyzed. It needs to be noted that a single realization in a LES cannot be directly compared with a single experimental realization of say a 2D scalar image, as a single LES realization is a filtered realization in both the spatial co-ordinate and time co-ordinates. Typically the equations solved for LES for reacting flow simulations are the Favre filtered equations, complicating the comparison further. For current state of the art high resolution measurements, the realization is an instantaneous image (no temporal filtering) and typically in well designed experiments there are negligible spatial filtering effects.

One possible method to bridge the gap from large experimental datasets to LES validation is to use the method known as Proper Orthogonal Decomposition (POD). POD is known in literature as under many names such as Karhunen–Loéve Decomposition and Principal Component Analysis. The discretized version of the integral equation involved in continuous POD is commonly known as Singular Value Decomposition (SVD). All data that is analyzed from LES and experiments are ensembles of single realizations, thus the discretized form of POD, SVD, is utilized. Essentially, POD aims to obtain a low-rank (low-dimensional) decomposition of the data, hence revealing from very large data sets significant modes and flow structures. POD analysis is based around a decomposition of a continuous flow variable $\boldsymbol{I}$ (scalar or vector) possibly temperature or velocity. If $\boldsymbol{I}$ is a continuous function of space (S) and time (t), $\boldsymbol{I}(S,t)$. S can be a function of one variable $S(x)$, for example in line imaging, two variables $S(x,y)$, that occurs in 2D sheet imaging or three variables $S(x,y,z)$ such as a multi sheet imaging experiments or an LES realization. A decomposition of $\boldsymbol{I}(S,t)$ under the assumption that I is separable in S and t, maybe expressed as:

$$I(S,t) \simeq \sum_{i=1}^{n} a_i(t)\varphi_i(x)$$

This is the familiar stating point for Fourier series, Galerkin Finite element formulation, Legendre polynomials and Chebyshev polynomials depending on the choice of the basis functions. If an orthogonal basis function is selected, then by definition of orthogonality at the $i=j^{\text{th}}$ term $a_j(t)$ depends only on the $\varphi_j(x)$ term. As an addition to orthogonality, a further desire is to construct the basis functions such that the least mean square error is minimized. The use of SVD to compute the non-unique basis functions satisfies both the orthogonality condition and the least mean square error criteria [1].

The experimental data to be analyzed may be organized into an n_rxn_s matrix A, where n_s is the number of spatial locations in each measurement, noting that $n_s = n_x, n_x \times n_y$ or $n_x \times n_y \times n_z$, depending on the problem dimensionality. n_r is taken to be the number of realizations of the measurement that are recorded. The common notation for the SVD of the matrix A is: $A = U\sum V^T$, where the columns of the orthogonal matrix $\boldsymbol{V}$ are the 1st n_r POD modes of the data embedded in the matrix A. The diagonal elements of the matrix $\boldsymbol{\Sigma}$, are the relative mode weightings of the 1st n_r POD modes. The computation of the SVD of A to yield $\boldsymbol{U}$, $\boldsymbol{\Sigma}$ and $\boldsymbol{V}$ is possible using standard linear algebra routines available in LAPACK [2].

One of the strengths of POD applied to LES and large experimental datasets is the ability to identify the various mode shapes of the flow, producing plots of the particular POD modes in the dimensional space of the original dataset, for instance for 2D imaging experiments a set of n_r images will be produced representing images the 1st n_r modes of the flow. The identification and classification of these modes based on their shape can be quite difficult in the 1D case, in the 2D case spatial ambiguity in the third dimension that can occur in any 2D imaging experiment can complicate analysis. 3D datasets are the easiest to interpret in terms of plots of the mode shapes. Spiral or helical modes that are inherently three dimensional and difficult to identify in 2D imaging are easily identified in 3D mode plots. As well as identifying the POD mode shapes, POD also gives an indication of the relative contributions or weights of the POD modes.

An example POD analysis from the experimental data in Dunn *et al.* [3] is given in Fig. 1. The first six mode shapes in Fig. 1a)-c) are presented in sequential POD mode pairs to exploit identification of any symmetrical modes that might be expected to occur in the axisymmetrical configuration of the burner. Examination of Figs. 1a)-c) reveals that the first two mode pairs a),b) are approximately symmetrical, whilst the third mode pair c) exhibit some symmetry but not with the same degree of correlation as the first two. This can also be seen in the mode weightings presented in Fig. 1d), the fist two pairs of modes have approximately the same contribution to the variance where as for the third pair this identification is not as obvious. A comparison of these mode weightings with those obtained for the LES results would be extremely revealing about how faithfully the calculations are resolving the flows.

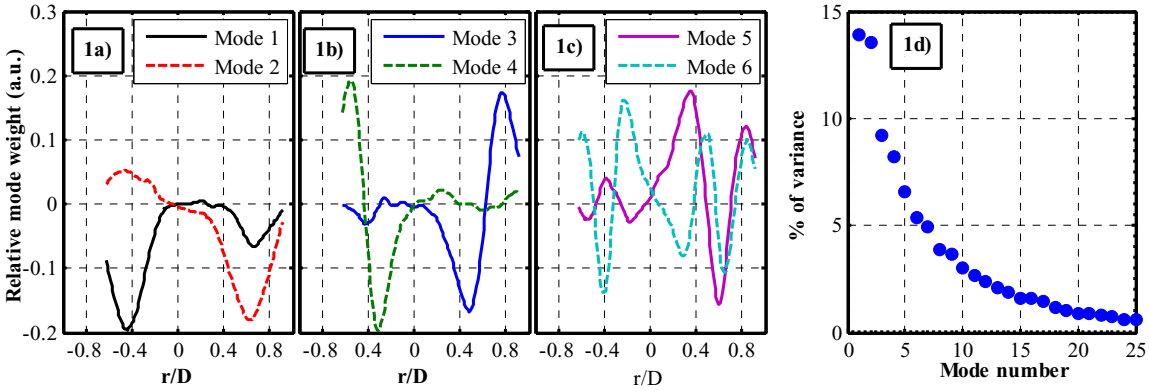

Figure 1a)-c) plots of the first six POD 1D radial POD modes of temperature in the PPJB for the PM1-50 flame at x/D =7.5 (D=4mm). Figure 1d) presents the relative weights of the computed POD modes to the variance, note the abscissa is truncated in this plot for clarity.

In summary, POD is an invaluable technique in analyzing experimental data from large data sets. Areas such as PIV analysis [4], facial recognition, vibration analysis and many other applications have already benefited from this powerful technique. POD could provide a valuable link between experiments and LES to utilize the large data sets being generated in both of these arenas. Work is in progress analyzing 2D experimental imaging results and comparing these with results obtained from a large eddy simulation of the same configuration. Preliminary results of this analysis will be presented in the poster on display.

References

[1] C. Eckart and G. Young., "*The approximation of one matrix by another of lower rank*", *Psychometrika*, 1:183–187, 1936.

[2] E. Anderson, , Z. Bai, C. Bischof, S. Blackford, J. Demmel, J. Dongarra, J. Du Croz, A. Greenbaum, S. Hammarling, A. McKenney, and D. Sorensen, LAPACK User's Guide (http://www.netlib.org/lapack/lug/lapack_lug.html)

[3] M.J. Dunn, A.R. Masri, R.W. Bilger, R.S. Barlow, G.-H. Wang., "*The Compositional Structure of Highly Turbulent Piloted Premixed Flames Issuing into a Hot Coflow*", *accepted for publication in: Proc. Combust. Inst.* 32, (2008).

[4] G. Berkooz, P. Holmes and J.L. Lumley., "*The proper orthogonal decomposition in the analysis of turbulent flows*", *Annu. Rev. Fluid Mech.* 1993.25: 539-75.

Coupling Imaging Diagnostics and LES Simulations in a Turbulent Non-reacting Jet and a Non-premixed Jet Flame (DLR-A)

Jonathan H. Frank, Sebastian A. Kaiser, Joseph C. Oefelein

Combustion Research Facility, Sandia National Laboratories, Livermore, CA 94551 USA
Corresponding Authors: jhfrank@sandia.gov, oefelei@sandia.gov

The coupling of imaging diagnostics and large eddy simulations (LES) provides an opportunity to improve our understanding of the physical structures in turbulent flames. As a first step in this process, we are developing a systematic approach for comparing imaging measurements and simulations, which have inherently different spatial and temporal resolutions. Our present effort focuses on these issues in simple jet flames. Laser Rayleigh imaging of turbulent jet flames and non-reacting jets are coupled with high-fidelity large eddy simulations (LES) to study the effects of filter size on the evolution of turbulent jets with and without heat release. High-resolution laser Rayleigh imaging measurements are performed in the near field (x/d=5-20) of a $CH_4/H_2/N_2$ jet flame with Re=15,200 (DLR-A) and in non-reacting propane jets with Reynolds numbers ranging from 7,200 to 21,700. The same 8-mm diameter nozzle is used for the flames and non-reacting flows. A detailed description of the experimental configuration and an analysis of the jet flame measurements are given by Frank & Kaiser [1-3]. The resolution of the measurements is sufficient to resolve the dissipation structures on the subgrid scale of the LES.

The theoretical-numerical framework used for the LES provides a general treatment of the governing equations. Details related to the theoretical formulation are given by Oefelein [4]. We solve the fully-coupled compressible form of the conservation equations using a numerical framework that provides a fully-implicit all-Mach-number time-advancement via a fully explicit multistage scheme. A unique dual-time approach is employed with a generalized preconditioning methodology that treats convective, diffusive, geometric, and source term anomalies in an optimal manner. The algorithm is massively-parallel and has been optimized to provide excellent parallel scalability attributes. The baseline closure is obtained using the mixed dynamic Smagorinsky model by combining the models of Erlebacher et al. [5] and Speziale [6] with the dynamic modeling procedure [7-9] and the Smagorinsky eddy viscosity model [10]. There are no tuned constants employed anywhere in the closure.

Fig. 1 illustrates the differences in resolution for experiments and simulations by comparing the spatially filtered mixture fraction with the LES results. Fig. 1a shows the fully-resolved measurements. In Fig. 1b, the measurements are filtered by smoothing with a Gaussian filter kernel whose width varies according to the LES grid. Fig. 1c shows the mixture fraction from the LES results. The differences between the spatial structures in the filtered measurements and the LES results are quantified by statistical analysis. To understand the effect of filter size on the spatial and temporal evolution of the flow, we will analyze the structures in the mixture fraction and dissipation fields with grids that are successively refined by factors of two in each direction. The finest resolution that we will use approaches the order of magnitude of the cutoff lengthscale determined from measured dissipation spectra.

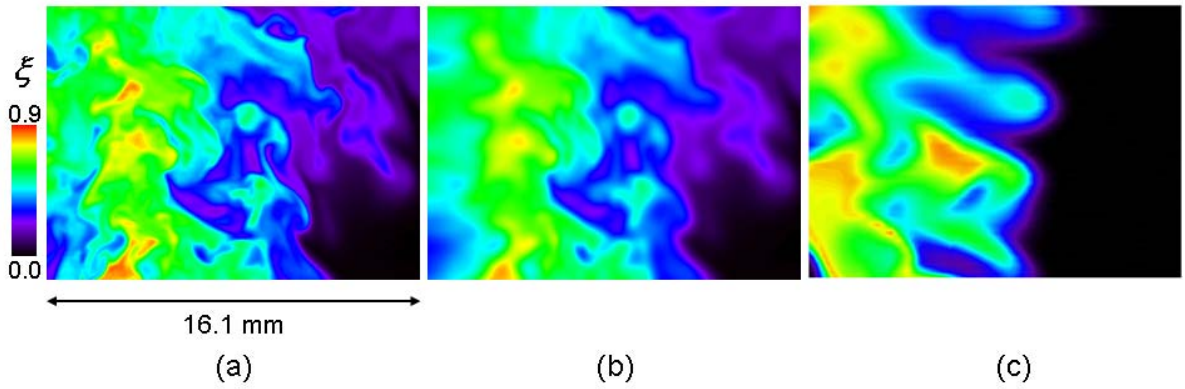

Fig. 1 Comparison of measurements and LES simulation of a turbulent non-reacting propane jet (Re=14,500) at x/d=10. a) Fully-resolved measurements of mixture fraction, b) Measurements smoothed with LES filter, c) Corresponding LES simulation.

References

1. J. H. Frank, S. A. Kaiser, *Exp. Fluids* 44 (2008) 221-233.
2. S. A. Kaiser, J. H. Frank, *Proc. Combust. Inst.* 31 (2007) 1515-1523.
3. S. A. Kaiser, J. H. Frank, *Proc. Combust. Inst.* 32 (2008) in press.
4. J. C. Oefelein, *Progress in Aerospace Sciences* 42 (2006) 2-37.
5. G. Erlebacher, M. Y. Hussaini, C. G. Speziale, T. A. Zang, *Journal of Fluid Mechanics* 238 (1992) 155-185.
6. C. G. Speziale, *Journal of Fluid Mechanics* 156 (1985) 55-62.
7. M. Germano, U. Piomelli, P. Moin, W. H. Cabot, *Physics of Fluids a-Fluid Dynamics* 3 (1991) 1760-1765.
8. P. Moin, K. Squires, W. Cabot, S. Lee, *Physics of Fluids a-Fluid Dynamics* 3 (1991) 2746-2757.
9. D. K. Lilly, *Physics of Fluids a-Fluid Dynamics* 4 (1992) 633-635.
10. J. Smagorinsky, *Monthly Weather Review* 91 (1963) 99-164.

Simultaneous 3-D Volumetric PIV and 2-D OH PLIF in the Far-Field of a Non-Premixed Turbulent Jet Flame

Gamba, M.[1], Clemens, N. T.[2], and Ezekoye, O. A.[3]

[1]Department of Aerospace Engineering and Engineering Mechanics, The University of Texas at Austin, mirkog@mail.utexas.edu
[2]Department of Aerospace Engineering and Engineering Mechanics, The University of Texas at Austin, clemens@mail.utexas.edu
[3]Department of Mechanical Engineering, The University of Texas at Austin, dezekoye@mail.utexas.edu

Introduction

In the present work space-time volumes of the velocity field are acquired in a turbulent nonpremixed jet flame at a Reynolds number of 7,800. The space-time volumes are generated by using cinematographic stereoscopic PIV (SPIV) in a plane perpendicular to the jet axis. By invoking Taylor's frozen flow hypothesis the velocity field in a neighboring region of the plane is reconstructed by transforming the temporal coordinate to a spatial one (Matsuda and Sakikabara, 2005; Ganapathisubramani et al., 2008). With this approach quasi-instantaneous three-dimensional information is obtained, providing volumetric knowledge of the three-dimensional velocity gradient tensor.

Experimental Considerations

The nonpremixed jet flame issued into a slow co-flow, and the fuel used was a mixture composed of 22.1% CH_4/ 33.2% H_2/ 44.7% N_2 by volume. The SPIV measurements were acquired at 3 kHz, in a plane perpendicular to the jet axis, and at an axial downstream location of 40 diameters (see Fig. 1), which corresponds to approximately half of the visible flame length. The field of view was approximately 43 mm by 48 mm. The velocity vector fields were extracted from the raw particle images using a single pass on an interrogation window of size $4.4\eta \times 4.4\eta$ (where $\eta = 0.65\ mm$ is the Kolmogorov scale based on the local Reynold number Re_δ of about 1,600). A median filter and interpolation scheme was then applied to remove spurious vectors (typically less than 4%). The vector fields were then filtered with a moving average filter on a $3 \times 3 \times 3$ window.

The time-resolved 3-component planar velocity field measurement is complemented by simultaneous 10 Hz OH PLIF acquired on the same plane. The OH PLIF signal yields the approximate location of the instantaneous reaction zone and the time-resolved velocity field enables the computation of the full 3D velocity gradient tensor, which in turn enables the computation of the 3D strain field and the spatial structure of important kinematic quantities in the vicinity of the reaction zone.

Volumetric Reconstruction and Fine-Scale Turbulence Structures

The time-resolved SPIV planar measurements were used to directly compute the in-plane components of the velocity gradient tensor $\nabla\vec{u}$. The remaining three out-of-plane components were then computed by applying Taylor's hypothesis as $\partial(\cdot)/\partial x = -\langle u(y,z)\rangle^{-1}\partial(\cdot)/\partial t$. The data were then reorganized in a three-dimensional grid constructed by computing the out-of-plane spacing as $\Delta x(y,z) = \langle u(y,z)\rangle\Delta t$, where Δt is the temporal separation between frames and $\langle u(y,z)\rangle$ is the in-plane average profile of the out-of-plane velocity component. The OH PLIF image is then inserted in the appropriate location of the three-dimensional grid. An example of a reconstructed volumetric field is presented in Fig. 2. The figure shows a cut-view of the 3D vector field reconstructed in the corresponding quasi-instantaneous pseudo-volume. The OH PLIF image is shown at the central plane of the reconstructed volume. The 3D kinematic quantities were then computed from knowledge of $\nabla\vec{u}$. Structures of intense vorticity are also visualized in the figure by rendering iso-surfaces of large-magnitude enstrophy (three times the mean measured value) around the central planar view of the OH distribution.

Figure 3 shows 3D structures of intense enstrophy and intense dissipation, together with a plane of OH. Unlike non-reacting turbulent jets, the present data suggest that for this reacting case regions of intense vorticity do not exhibit the typical tube-like structure but tend to closely correspond to regions of high dissipation that are mostly sheet-like.

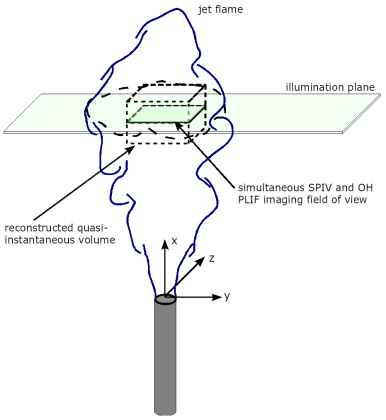

Figure 1: Schematic diagram of the turbulent flame and imaging location.

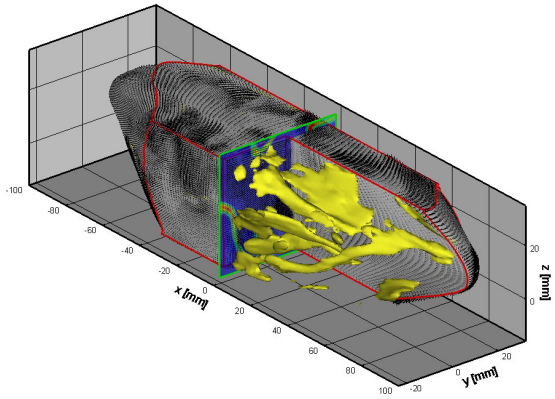

Figure 2: Example of a quasi-instantaneous pseudo-volume reconstructed from a set of cinematographic SPIV measurements.

Moreover, these sheet-like structures are oriented along the thin OH layers. The reason for these features is believed to be due to the stabilizing effect of heat release on the relatively low Reynolds number jet flame under consideration. It is further observed that both positive and negative dilatation (not shown for brevity) are present and tend to be associated with the oxidizer and fuel sides of the OH zones, respectively. These dilatation features are believed to be mainly due to convection of regions of varying density rather than to instantaneous heat release rate.

This technique shows promise for obtaining important information of the effects of heat release on the 3D turbulence structure and may be useful for LES validation purposes.

References

Ganapathisubramani, B., Lakshminarasimhan, K., Clemens, N. T., 2008. Investigation of three-dimensional structure of fine scales in a turbulent jet by using cinematographic stereoscopic particle image velocimetry. J. Fluid Mech. 598, 141–175.

Matsuda, T., Sakikabara, J., 2005. On the vortical structure in a round jet. Phys. Fluids 17 (2).

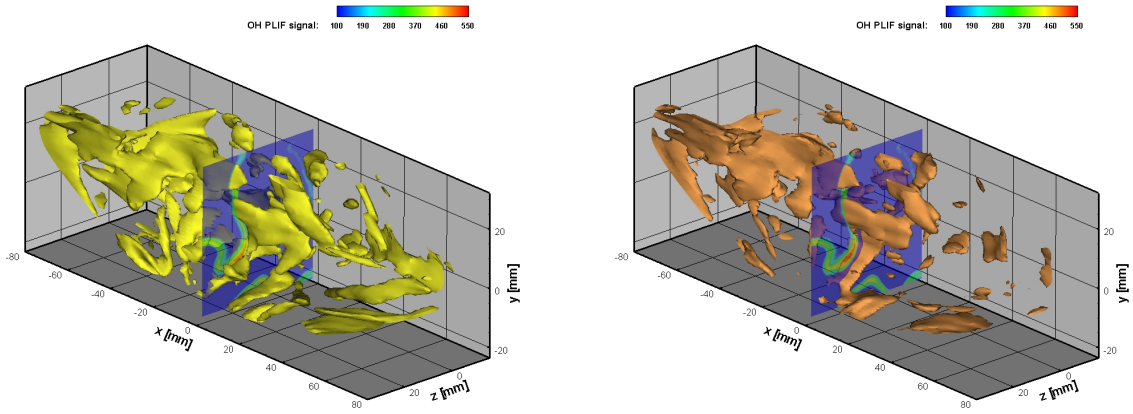

(a) (b)

Figure 3: 3D rendering in probed pseudo-volume of iso-surfaces of (a) enstrophy ($\xi_{thr} = 750\ s^{-1}$) and (b) dissipation ($\varepsilon_{thr} = 375\ m^2 s^{-3}$).

Laser Diagnostics for Transient Combustion Phenomena

R. Gordon[1,*], C. Heeger[1], B. Böhm[1], S.F. Ahmed[2], I. Boxx[3],
A. Dreizler[1], E. Mastorakos[2], W. Meier[3]

1: Mechanical Engineering, TU Darmstadt, Germany
2: Engineering Department, University of Cambridge, UK
3: German Aerospace Center, Stuttgart, Germany
* Corresponding author, e-mail: gordon@ekt.tu-darmstadt.de

Analysis of transient combustion phenomena such as ignition, extinction and flashback requires not only sampling rates that resolve the critical time scales of these events, but also sampling of the conditions leading up to the event. Recent advances in all-solid-state diode-pumped laser- and CMOS-camera technology have made kHz application of common laser diagnostic techniques such Mie scattering, PIV and PLIF achievable. The structure of the CMOS on-board memory allows one to release a trigger after an event (such as flame extinction or auto-ignition of flammable mixtures) has occurred, storing data-sequences prior to the trigger. In contrast to previous technology, the success rate of recording essential time-intervals is increased to virtually 100% and data-sequences consist of up to several thousand frames.

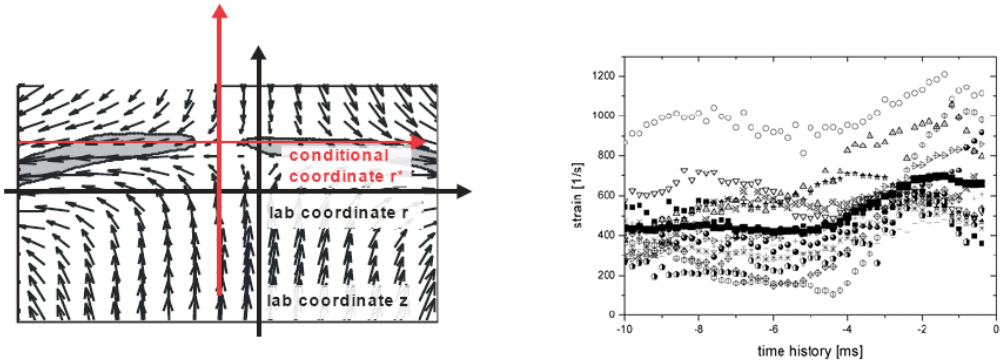

Figure 1: Multi-dimensionally conditioned data of strain at the location of extinction in an opposed-flow partially-premixed flame [6].

The long-term goal of these techniques is to provide quasi-4D simultaneous data on the flow-field and scalar fields in reacting flows. Transient events can be tracked in a cinematographic manner over sufficiently long periods to study temporal evolutions in turbulent flames from a new perspective [1-3]. Milestones in the development process include (i) 2-D qualitative scalar imaging (e.g. OH at 5kHz [4], 10kHz) (ii) 2-D flow field imaging with 2 and 3 velocity components (2C-PIV [5, 6], 3C-PIV [7]) (iii) quantitative mixture fraction and scalar dissipation imaging (iso-thermal, reacting cases) (iv) qualitative volume scanning techniques (quasi-4D imaging) (v) volume application of quantitative techniques. Simultaneous application of these methods is also a key goal.

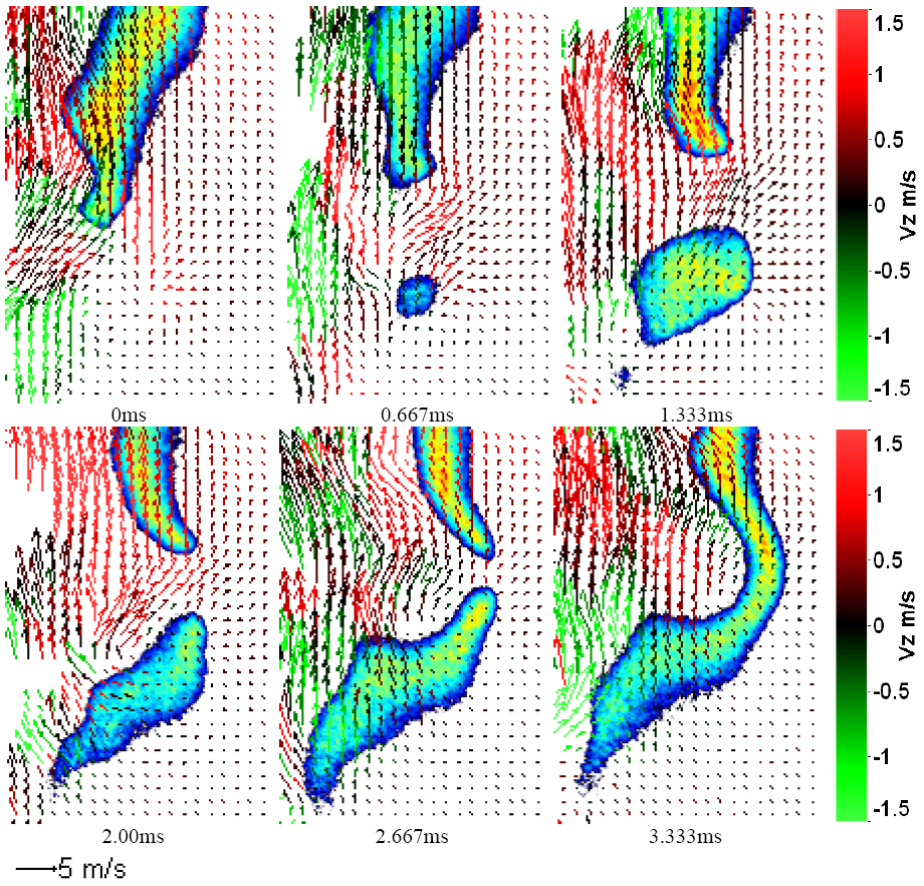

Figure 2: image sequence from simultaneous 3C-PIV/OH-PLIF of a turbulent lifted diffusion flame [7].

In this poster, preliminary results of the application of simultaneous 5kHz OH-PLIF and 10 kHz chemiluminescence imaging of flashback events in the TECFLAM [8, 9] burner are reviewed. This burner simulates swirl-stabilised flows typical of modern lean premixed gas turbine combustors. Insights into the dominant mechanisms of flashback in this geometry are postulated from review of the time history of joint flame-front and flame-visualisation imaging. This combined technique provides greater confidence not only in interpreting the results of the 2-D imaging technique, but also in confirming of the location of the region of interest for the experiment.

Further work is being undertaken to develop techniques for high repetition rate quantitative mixture fraction imaging for application to ignition research. This will involve not only accessing higher energy densities, but quantification of the CMOS camera response and sensitivities.

[1] Fajardo, C. M., Smith, J. D., Sick, V., *Appl. Phys. B*, 85 (2006) 25–30.
[2] Upatnieks, A., Driscoll, J., Ceccio, S., *Proc. Combust. Inst.*, 29 (2002) 1897–2003.
[3] Smith, J. D., and Sick, V., *Appl. Phys. B*, 81 (2005) 579–584.
[4] Kittler, C., Dreizler, A., *Appl. Phys. B*, 89 (2007) 163-166.
[5] Heeger, C., Böhm, B., Ahmed, S.F., Gordon, R., Boxx, I., Meier, W., Dreizler, A., Mastorakos, E., *Proc. Comb. Symp.* 32 (2008, to appear)
[6] Böhm, B., Heeger, C., Boxx, I., Meier, W., Dreizler, A., *Proc. Comb. Symp.* 32 (2008, to appear)
[7] Boxx, I., Kittler, C., Gordon, R., Böhm, B., Aigner, M., Dreizler, A., Meier, W., *Proc. Comb. Symp.* 32 (2008, to appear)
[8] A. Nauert, P. Petersson, M. Linne, A. Dreizler, *Exp. Fluids,* 43 (2007) 89-100.
[9] M. Freitag, M. Klein, M. Gregor, D. Geyer, C. Schneider, A. Dreizler, and J. Janicka, *Int. J Heat Fluid Flow*, 27 (2006) 636-643.

Towards predictability of isothermal and reacting flows using LES: From a simple test case to technical relevant swirl burner configurations

F. Hahn, C. Olbricht, J. Kuehne, J. Janicka

hahn@ekt.tu-darmstadt.de, olbricht@ekt.tu-darmstadt.de

Fachgebiet Energie– und Kraftwerkstechnik,Technische Universität Darmstadt

Petersenstr. 30, 64287 Darmstadt, Germany

Mixing processes are of fundamental relevance in various technical applications, e.g. chemical engineering, process engineering or combustion applications. The importance of density variation in such applications is great, while acoustic effects can be neglected. Especially for combustion devices in addition to the scalar transport the impact of the resulting density field distribution is strong due to its interaction with the velocity field, via buoyancy and continuity. Such cases can strongly benefit from a low Mach number based formulation, highly reducing the computational effort compared to fully compressible variable density approaches. The majority of mixing dependent applications are designed to benefit from turbulence, to increase the efficiency of the mixing process. It has been shown that Large Eddy Simulation (LES) has great potential predicting mixing processes under constant density conditions. In case of time dependent variable density flows, additionally the time derivative of the density has to be included into the pressure correction equation.

Implementing this additional term straight forward leads to crucial oscillations for all of the widespread low Mach number approach based pressure correction methods. Damping of these oscillations is contrary to accuracy and predictability, independent of wether it is done by numerics or adopted models. It has to be highlighted that generally it is not trivial, in this context, to ensure the physical constraint of conservation.

The present work introduces an approach which handles mixing and combustion phenomena with density ratios up to ten and more. This technique is based on a fractional step formulation. The method is implemented and tested in the finite volume method based flow solver FASTEST-ECL. Several mixing configurations are simulated covering the range from a simple test case of a convected density jump to a reacting model gas turbine combustor.

FASTEST-ECL is a three-dimensional CFD code, which uses geometry flexible, block-structured, boundary fitted grids. Therefore, the used code is able to reproduce the investigated complex geometries. The grid is collocated with a cell-centered variable arrangement. The accuracy of the flow solver is of fully second order, by using a specialized central-differencing scheme for spatial discretization. Boundedness of the mixture fraction is assured by discretizing the convective term within the scalar transport equation by a non oscillatory TVD scheme. A mainpoint of FASTEST-ECL is a modified flux limiter function. In order to prevent unphysical values of the scalars, the gradient ratio within the flux limiter function has been changed. For time stepping a second order accurate three-stages Runge-Kutta scheme is used. In order to satisfy continuity, a momentum correction is made by using a fractional step formulation in each stage. Therefore a Poisson equation is solved iteratively with multigrid and successive over-relaxation (SOR). FASTEST-ECL is parallelized by domain decomposition using the MPI libraries.

For validation of the implemented numerical schemes a simple one-dimensional test case is simulated. Here, a convected density jump with a density ratio up to ten is performed. This configuration is dedicated to testing the scheme for conservation, accuracy, stability and robustness. It completely neglects turbulence and geometrical effects.

A step further into more complex configurations is the second simulated test case. Therefore, a LES of a spatially evolving non-reacting helium-nitrogen mixing layer [1] is performed. This case includes three-dimensional turbulence and mixing effects but does not show a higher level of complexity regarding the geometry. Anyway, it is a challenging configuration not only due to its high density ratio (≈ 7) but also because of the high density difference between helium and nitrogen ($\approx 4\,kg/m^3$).

The following flow cases aim on more complex geometries. Here, three different swirl configurations have been simulated in order to show the code's ability to handle with such almost technically relevant flows. The first one is an unconfined swirl burner with a double-concentric swirler nozzle. This burner has been designed and investigated by Habisreuther et al. [2]. In the following, non-reacting operation conditions of a premixed operation mode are investigated. Therefore, the fuel has been substituted by air. The complexity of the nozzle, consisting of both axial as well as radial swirlers, offers an excellent test case to investigate the impact of the inflow conditions on the flow patterns inside the numerical domain. This work shows comparisons of experimental data of the velocities and fluctuations with the simulated ones. Here, the simulation shows very good agreement with the experiments.

The second complex test case is the so called TECFLAM burner, [3]. Here, again the isothermal configuration is calculated. The swirler nozzle of this burner follows a movable block design. Due to this fact, the theoretical swirl number can be adjusted between 0 and 1.98. For all simulations presented in this work this

swirl number is 0.75 and the resulting Reynolds number based on the axial bulk velocity is approximately $10,000$. For numerical investigation of this burner, simulations with a successively increased number of grid points are performed. Here, the mesh size is varied from $0.75 \cdot 10^6$ over $1.76 \cdot 10^6$ and $3.75 \cdot 10^6$ up to $6.25 \cdot 10^6$ control volumes. An example of the resulting swirl nozzle grid is shown in Figure 1. For this TECFLAM burner comparisons between experiments and simulations of the three velocity components as well as the turbulent kinetic energy are provided.

As a confined configuration, a model gas turbine combustor is investigated. This configuration shows complexity comparable to realistic technical applications. Although this burner is generic, the geometry is sophisticated. Like real combustors the test rig is pressurized and hence the resulting flow has to be confined. An impression of the geometry can be drawn from Figure 2, where a cross section through the numerical domain is shown. Geometrical complexity arises not only due to the included swirler device but also because the shape of this configuration is partly assymmetric to allow for optical accessibility. The configuration has been experimentally investigated by our group [4], [5]. The applied numerical grid for this case is based on the 3D O-grid technique, with refined resolution in regions of high shear, leading to a mesh size of approximately $3.1 \cdot 10^6$ control volumes. For this configuration isothermal as well as reacting simulations are performed. In Figure 3 results for the mean velocity profiles are depicted for both cases and are compared with experimental results. The isothermal results show good agreement with the experiments in all velocity components, while the reacting simulation overpredicts the length of the jet penetration. Further results of this burner configuration can be shown and discussed.

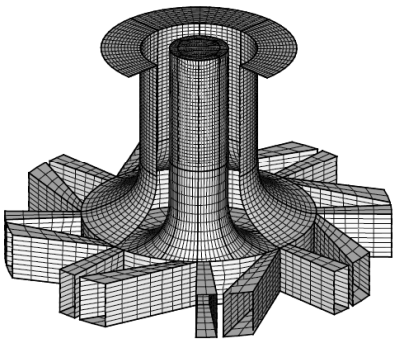

Figure 1: Computational domain of the TECFLAM swirl nozzle. The mesh is coarsened for visualization purpose.

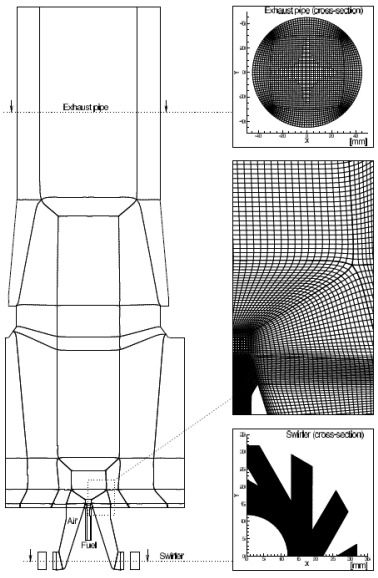

Figure 2: Numerical domain and blocking of the model gas turbine combustor, including grid details

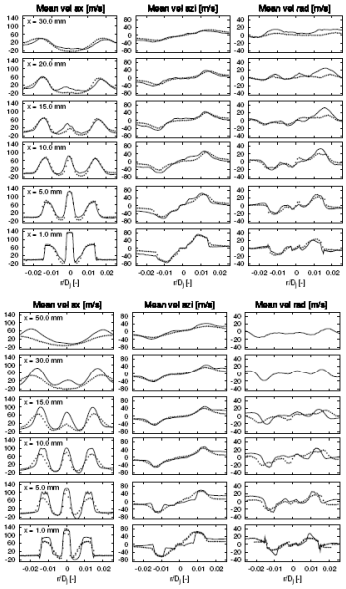

Figure 3: Comparison of radial mean velocity profiles at different axial positions, top: isothermal; bottom: reacting case; symbols: experiments, solid line: simulation

[1] Rebollo,R.M.: *PhD thesis, California Institute of Technology, 1973*

[2] Habisreuther, P. and Petsch, O. and Büchner, H.: *Gas-Wärme International, Vol.53(6) (2004), 326–331*

[3] Schneider, C. and Dreizler, A. and Janicka, J.: *Flow. Turb. Combust., 74 (2005), 103–127*

[4] Janus, B. and Dreizler, A. and Janicka, J.: *Flow. Turb. Combust., 75 (2005), 293–315*

[5] Janus, B. and Dreizler, A. and Janicka, J.: *ASME Turbo Expo GT2004-53340, Vienna (2004)*

LES modeling of extinction and reignition using a flamelet/progress variable formulation: Application to Sandia flame E

Matthias Ihme*
Department of Aerospace Engineering, University of Michigan, Ann Arbor, MI 48109
and Heinz Pitsch
Department of Mechanical Engineering, Stanford University, Stanford, CA 94305

In the present work a flamelet/progress variable (FPV) model [1] was extended for the prediction of extinction and reignition in turbulent non-premixed flames [2, 3]. In this model all thermochemical species are expressed in terms of the mixture fraction and the reaction progress parameter, and a presumed PDF model is employed to express the unclosed chemical source term and other Favre-filtered quantities in terms of the moments of these two scalars. While a beta-PDF is used for the mixture fraction, the reactive scalar distribution in the extended FPV model is represented by a so-called statistically most-likely distribution (SMLD) [4]. The key idea of SMLD is to approximate the true distribution from a reduced set of known moments subject to the constraint that the resulting PDF contains a minimum of statistical information. The significant advantages of SMLD over other presumed shape distributions are that (i) an arbitrary number of moment information can be incorporated into the presumed PDF; (ii) time scale information which characterizes the turbulence-chemistry interaction can be incorporated [4]; and (iii) arbitrarily complex shaped PDFs for the reactive scalar distribution can be represented. The SMLD closure model for application in the extended FPV model was analyzed in an *a priori* study [2] using direct numerical simulation results and experimental data from Sandia flames D, E, and F. Particularly for cases which are characterized by strong local extinction and reignition, it was shown that the extended model leads to improved predictions over previous PDF closure models employing a delta function or beta distribution for the reactive scalar.

Following this *a priori* model analysis the extended FPV formulation was applied in LES of Sandia flame E [3]. In this model, information about the first two moments of mixture fraction and progress variable is used to construct the presumed joint PDF, and all Favre-averaged thermochemical quantities are tabulated in a flamelet library. In addition to the solution of conservation equations for mass and momentum, the extended FPV model requires also the solution of transport equations for the mean and variance of mixture fraction and progress variable. This set of equations is solved in a cylindrical coordinate system employing a low Mach-number, finite volume code, which has been developed by Pierce & Moin [1]. The computational mesh contains 256 cells in axial direction, 160 in radial direction, and 64 grid points in circumferential direction on a computational domain $80 \times 26.5\ D$ in axial and radial direction, respectively.

Results obtained from the simulation (solid red lines) are compared with experimental data (symbols) in Figs. 1-3. In addition, the black dashed lines show computational results that are obtained from the FPV model in which a Dirac function was used as PDF closure model for the flamelet parameter. Conditional data for temperature and methane mass fraction are presented in Fig. 1. The predictions with the extended FPV model show significant improvements over the FPV-model employing a delta function closure model at $x/D = 7.5$, where local flame extinction is largest. With increasing downstream distance some over-prediction on the fuel-rich side of the flame is evident. Conditional PDFs for the CO_2 mass fraction are shown in Fig. 2. The large tail at the first measurement location is an indication for flame extinction. This is accurately predicted with the extended FPV model (solid red line). The burning indices, evaluated for the temperature and CO_2 mass fraction, are shown in Fig. 3. The stabilizing effect of the pilot flame is evident around $x/D = 2.5$ which is reflected by the local maximum in the burning indices. Compared with the delta function FPV closure model, results from the extended FPV model accurately predict local flame extinction and reignition in Sandia flame E.

*Corresponding author: mihme@umich.edu

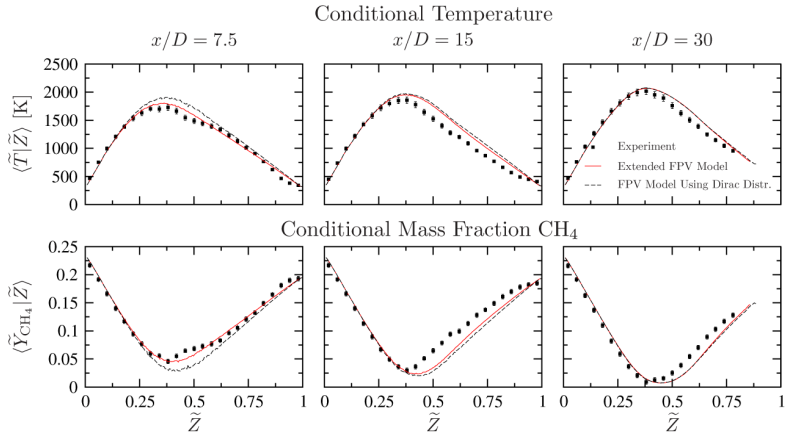

Figure 1: Comparison of measured (symbols) and calculated (lines) conditional date for temperature and CH_4 mass fraction at $x/D = 7.5, 15, 30$ for Sandia flame E. Experimental data are plotted with estimated uncertainties.

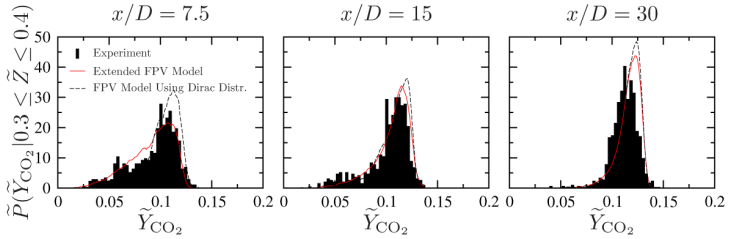

Figure 2: Comparison of conditional PDFs of CO_2 mass fraction at three axial locations in Sandia flame E.

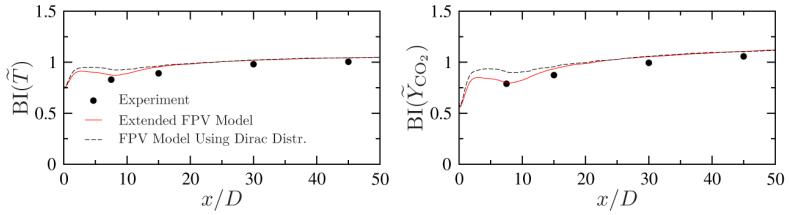

Figure 3: Comparison of burning indices for temperature and CO_2 mass fraction between simulations and experimental data for Sandia flame E.

References

[1] C. D. Pierce and P. Moin. Progress-variable approach for large-eddy simulation of non-premixed turbulent combustion. *J. Fluid Mech.*, 504:73–97, 2004.

[2] M. Ihme and H. Pitsch. Prediction of extinction and reignition in non-premixed turbulent flames using a flamelet/progress variable model. 1. A priori study and presumed PDF closure. *Combust. Flame*, 2008. in press.

[3] M. Ihme and H. Pitsch. Prediction of extinction and reignition in non-premixed turbulent flames using a flamelet/progress variable model. 2. A posteriori study with application to Sandia flames D and E. *Combust. Flame*, 2008. in press.

[4] S. B. Pope. The statistical theory of turbulent flames. *Phil. Trans. Roy. Soc. London*, 291(1384):529–568, 1979.

Numerical study of *n*-heptane auto-ignition using LES-PDF methods

W. P. Jones and S. Navarro-Martinez*

Department of Mechanical Engineering
Imperial College, London SW7 2AZ, UK
** Email: s.navarro@imperial.ac.uk*

Introduction

This work deals with *n*-heptane auto-ignition in turbulent flows. The paper applies the Eulerian Stochastic Field method to the solution of the sub-grid joint-scalar probability density function (PDF) of the reacting scalars in the Large Eddy Simulations (LES) context. A reduced mechanism of 22 species and 18 reactions is used to model n-heptane chemical kinetics.

Ignition problems are particularly difficult due to the fact that fluid mechanics and chemical time scales are of the same magnitude. Current understanding of auto-ignition in turbulent flows is limited by the ability of present numerical models to simulate turbulence-chemistry interactions at realistic Reynolds numbers. In particular, for large molecule hydrocarbons, a large number of species need to be considered, which vastly increases the computational cost. Crucial "slow" reactions are important in the formation of a pool of reactants, particularly radicals R-HO_2 and R-H_2O_2, which act as "combustion-triggers". This type of configuration often exhibits behaviour midway between premixed and non-premixed flames, often called "partially" premixed, and therefore specific models of the two regimes are not *a-priori* appropriate. N-heptane is widely used as a research fuel due to its similarities to diesel fuel, as they have similar cetane number. The current work seeks to provide a better understanding of transient *n*-heptane auto-ignition, especially the effects of temperature and turbulence.

Modelling

A powerful approach to obtain the time and spatially varying statistics of reacting scalars is LES combined with solution of a modelled form of the evolution equation of the *joint sub-grid scale PDF* of the complete set of scalars. This approach is only feasible if stochastic methods are used, the practical advantage is that highly non-linear reaction terms appear in closed form. In this work the PDF is represented by an ensemble of continuous fields [1], which followed a set of Stochastic Partial Differential equations. The Eulerian character of the *stochastic fields* method makes it very attractive compared with particle–based methods as typical Eulerian transport solvers can be used and complex interpolation issues are avoided. The model combined with LES has been successfully applied to methane and hydrogen combustion [2-4].

The configuration considered in the present work corresponds to the studied experimentally by Markides *et al.* [5]. A central jet of gaseous fuel (vaporised n-heptane/nitrogen) is injected into a stream of pre-heated turbulent air in a duct flow. The turbulent co-flow is generated by a grid with 3 mm holes, the integral turbulent scales of the inflow turbulence were measured L_{turb}=3-4 mm and τ_{turb}=1 ms. The central jet has a diameter of 2.25 mm and the considered test section is 250 mm. Auto-ignition was detected by chemiluminescence of the hydroxyl radical.

The calculations were performed using a grid of 256 × 72 × 48 cells with 8 stochastic fields. A database of turbulent velocity was generated using the digital filters approach [6] using L_{turb} and τ_{turb}. Two approaches were used to detect numerically the ignition process: OH mass fraction greater than 0.001 and a temperature increase greater than 1% of co-flow temperature. Three co-flows temperature were tested: 1150 K, 1155 K and 1165 K.

Results

The auto-ignition process can be divided into two separate phases: First, the large carbon chains of n-heptane are broken down in a series of endothermic reactions (see Fig. 1 upstream). After the pool of radicals, HO_2, H_2O_2 and heptylperoxil, built up, exothermic reactions dominate and triple flames appear which are convected and merged to form the "flame front". The time and length scale of these events are dominated by the inflow turbulence. The

resultant flame is largely a non-connected flame with extinction pockets, whose size is determined by the integral turbulent scale of the co-flow. The results show an auto-ignition process very sensitive to air temperature. At the lowest temperature examined, there is not enough heat release to sustain combustion as the kernels are extinguished or are convected outside the domain. At the largest temperatures (1160 K), an unstable flame is formed which propagates upstream (see Fig 2 left). Temperature fluctuations were introduced to mimic experimental noise and were found to have a several impact on ignition. Moderate fluctuations of 15 K (or ~1%) quickly damped the oscillations and reduce maximum temperatures in more than 50 K.

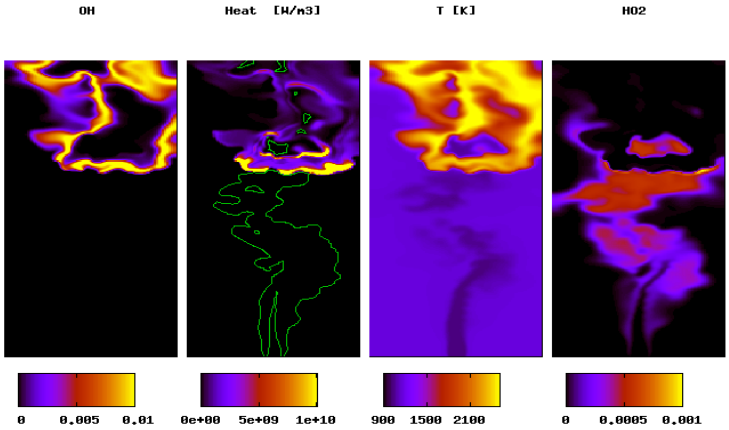

Figure 1: From left to right, instantaneous distribution of filtered OH mass fraction, heat release due to combustion, temperature and HO_2 mass fraction. The green line indicates negative heat release. The dimensions of each plot are 10 x 60 jet diameters.

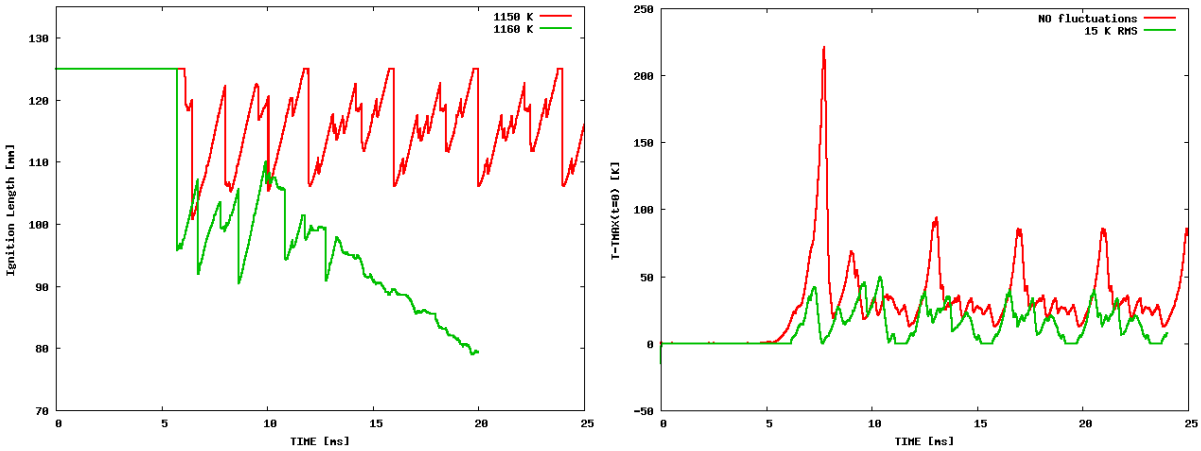

Figure 2: On the left side, ignition length as a function of time for two temperatures 1150 K and 1160 K .On the right, maximum temperatures versus time for two different co-flow temperature fluctuations.

References

[1]L. Valiño, *Flow, Turb. and Combustion* 60 (1998) 157-172
[2] R. Mustata, L. Valiño, C. Jimenez, W. P. Jones and S. Bondi, *Comb. and Flame* 145 (2006) 88-104.
[3] W. P. Jones, S. Navarro-Martinez and O. Röhl, *Proc. Comb. Inst.* 31 (2007), 1765-1771
[4] W. P. Jones and S. Navarro-Martinez, *Computers & Fluids* 37 (2008), 802-808
[5] C. N. Markides, G. De Paola and Mastorakos, *Exp. Therm. and Fluid Sci.* (2006)
[6] L. di Mare, M. Klein, W. P. Jones and J. Janicka, *Phys. of Fluids* 18 (2006) 025107

NUMERICAL MODELING FOR STRUCTURE AND POLLUTANT FORMATION IN SYNGAS TURBULENT NONPREMIXED SWIRLING FLAMES

[1]Jeongwon Lee, Sungmo Kang, Yongmo Kim; [2]Kook-Young Ahn
[1]Hanyang University, KOREA; [2]KIMM, KOREA
e-mail : ymkim@hanyang.ac.kr

The internal composition of syngas fuels can vary greatly depending on the source and the processing technique; the volumetric H2/CO ratio usually varies from 0.33 to 40, diluent gases range from 4% to 51%, and water too can vary from 0% to 40%. Since the caloric heating value of the syngas used in the IGCC gas turbine combustor is relatively low, the syngas flames with the high volumetric flow rate in IGCC gas turbine combustor could be susceptible to local extinction process. The proper kinetic characterization of the H2/CO system is also of great importance in the development of advanced combustion technologies. The present study numerically investigate the effects of the Syngas chemical kinetics on the basic flame properties and the structure of the Syngas diffusion flames. In order to realistically represent the turbulence-chemistry interaction and spatial inhomogeneity of scalar dissipation rate. the Eulerian Particle Flamelet Model(EPFM) with multiple flamelets has been applied to simulate the combustion processes and NOx formation in the syngas turbulent nonpremixed flames. Validation cases include the Syngas turbulent nonpremixed jet and swirling flames[1]. Based on numerical results, the detailed discussion has been made for the sensitivity of the Syngas chemical kinetics as well as the precise structure and NOx formation characteristics of the turbulent Syngas nonpremixed flames.

Figure 1 shows the geometry of burner and inlet conditions. In this Lab-scale gas turbine combustor, the flame is stabilized by the strong swirling flows induced by axial swirl vane at the fuel jet nozzle and radial swirler at the oxidizer nozzle. In Figure 2, the predicted OH contours and measured OH PLIF[1] are compared for two power loads. In terms of the OH distribution, the agreement between prediction and measurement[1] is reasonably good. However, the noticeable deviations exist at the proximity of the annual injector mainly due to the shortcomings of the Eulerian Particle Flamelet Model as well as the neglect of heat transfer between the flame field and the injector region. In Figure 3, the predicted conditional profiles of temperature, OH, NO and PDF are displayed along the stoichiometric line at the strong shear region and the recirculating region for the different power loads. Numerical results clearly indicate that the shear-layer flame regions with the much higher scalar dissipation rate and shorter residence time have the flame structure with the higher OH formation and lower NOx formation due to the much stronger non-equilibrium effects.

References:

1. T. Kretschmer et al., 2006,"Numerical Simulation of A Lab-scale Syngas Burner Using Complex Chemistry", 13th Int. Conference on Fluid Flow Technology, Budapast, Hungary

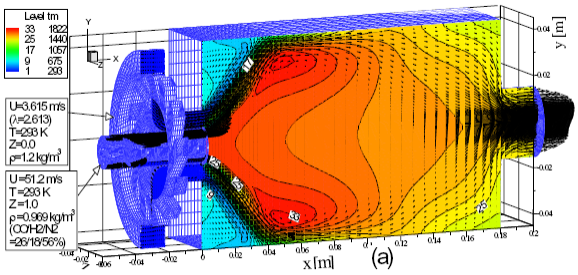

Fig. 1 DLR HEGSA swirl combustor : (a) geometry and inlet condition

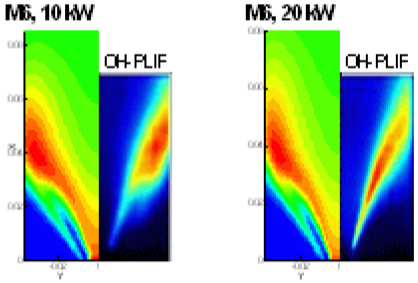

Fig. 2 Comparison of prediction and OH-PLIF for M6

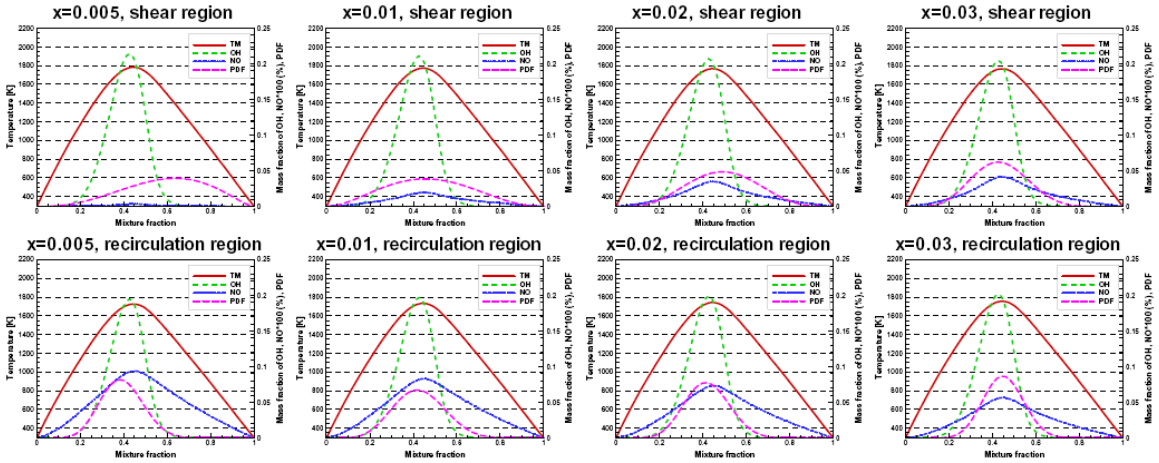

(a) 10 kW

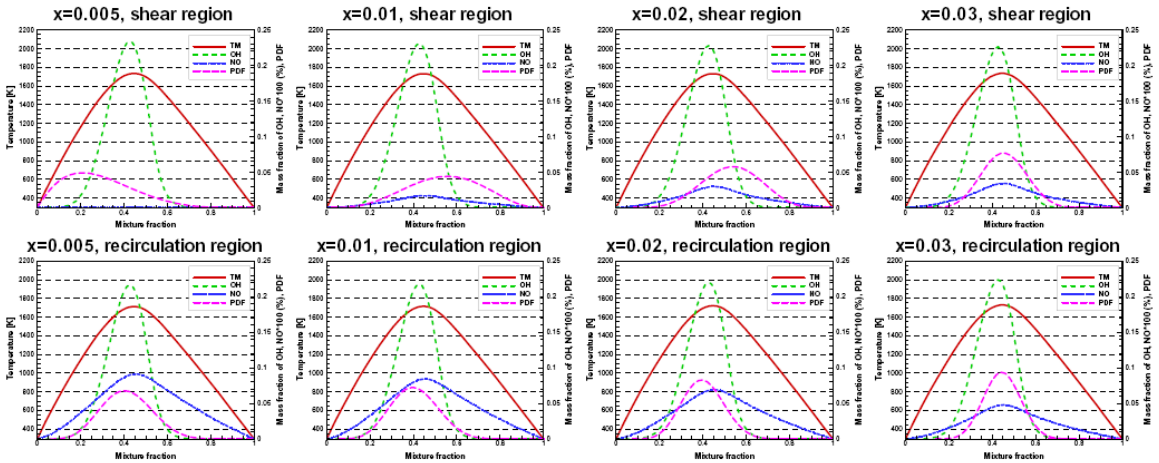

(b) 20 kW

Fig. 3 Conditional profiles of Temperature and mass fraction of OH and NO for M6

HYBRID FVM/ PDF TRASPORT MODEL FOR TURBULENT SWIRLING REACTING FLOWS

[1]Jeongwon Lee, Sungmo Kang, Yongmo Kim; [2]Metin Muradoglu,
[1]Hanyang University, KOREA; [2]KOC University, TURKEY
e-mail : ymkim@hanyang.ac.kr

In general, the presumed PDF models have severe limitations to accurately predict local extinction and reignition especially in the highly stretched swirling flame field. In the present study, to improve the predicative capability of the turbulent combustion model for the complex turbulent reactive flows, the hybrid PDF Monte Carlo method combined with the pressure-based finite volume method(FVM) has been developed and applied to simulate the turbulent swirling isothermal and reacting flows. The algebraic Reynolds stress model has been employed to realistically account for the non-isotropic turbulence effects in the swirling turbulent flows with the vortex breakdown and the strong flow reversal while maintaining computational efficiency. To realistically account for the turbulence-chemistry interaction and enhance computational robustness, in the swirling turbulent flows with the vortex breakdown and the strong flow reversal, the present PDF formulation is based on the composition PDF Monte Carlo method. In this transported probability density function method, the effects of molecular diffusion are represented by the interaction by exchange with the mean (IEM) model.

In this hybrid FVM/ PDF transport approach, the non-equilibrium chemistry is based on the flamelet library with the wide range of the scalar dissipation rates to efficiently handle the practical flame fields. The efficient particle tracking procedure with the adaptive time-step control has been devised for this hybrid PDF Monte Carlo method. Moreover, to minimize statistical errors, a new particle splitting and combination procedure has been utlized. To validate the present hybrid PDF transport model, the SM1 swirl flame with $S = 0.5$, $Re = 7200$ and the fuel jet velocity, 32.7m/s has been chosen. The numerical results are precisely compared with measurements of Masri et al.[1] for the turbulent bluff-body swirling isothermal and reacting flows in terms of the velocity field, turbulent transport properties, unconditional and conditional means. The predicted unconditional and conditional means shown in Figures 1 and 2 are reasonably well agreed with the experimental date[1]. However, there exist the noticeable discrepancies in the profiles of mean axial and circumferential velocity and the conditional scatter plots. These discrepancies could be mainly attributed to the shortcomings of algebraic Reynolds stress model and IEM mixing model, as well as the limitation of the flamelet-based chemistry to deal with the local extinction encountered in the swirling flame.

References:

1. TNF Workshop. Website: http://public.ca.sandia.gov/TNF/swirlflames.html

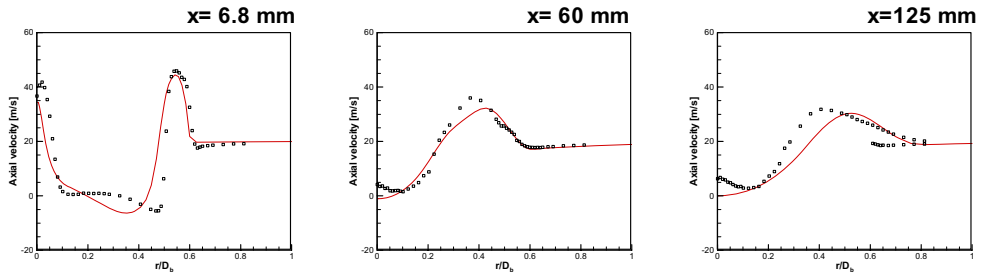

(a) axial velocity

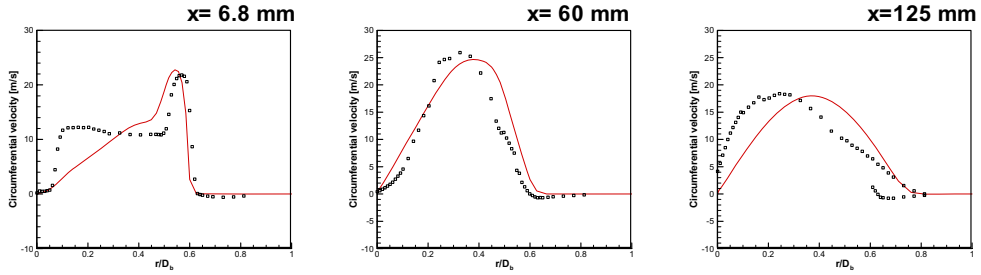

(b) circumferential velocity

Fig. 1 radial profiles of mean (a) axial velocity and (b) tangential velocity at three axial locations. (symbol-measured, line-calculation)

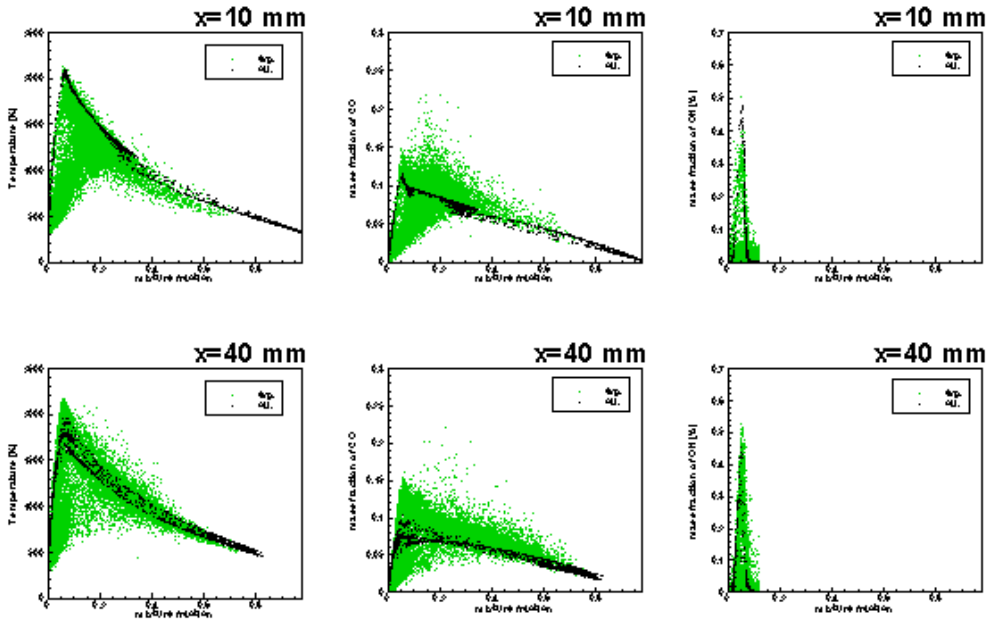

(a) temperature (b) CO2 mass fraction (c) OH mass fraction

Fig. 2 Conditional scattered plots of (a) temperature, (b) mass fraction of CO2 and (c) mass fraction of OH at two axial locations. (green dot-measured, black dot-calculation)

A novel domain decomposition strategy for low-speed hydrodynamics

R. McDermott†, K. McGrattan, and W. E. Mell

Building and Fire Research Laboratory
National Institute of Standards and Technology
Gaithersburg, MD 20899-8663, USA

In this work we develop a new method for time advancement of the velocity field in distributed-memory low-Mach flow solvers such as the NIST Fire Dynamics Simulator (FDS) [3]. Conventional additive Schwarz techniques for enforcing the global elliptic constraint are too costly for CFD-based fire models, requiring around 80% of the computational effort, whereas the FDS linear solve requires less than 5%. Further, most of the research in this area focuses on the development of scalable linear solvers for massively parallel architectures, resulting in methods which are highly scalable but which often yield poor serial performance. For fire modeling, we require methods which run efficiently on a relatively small number of processors. The new method presented here is a two-stage projection scheme imbedded within a two-stage Runge-Kutta time integration. In this projection scheme, the hydrodynamic pressure is decomposed into a fine-scale fluctuating component, which obeys a Poisson equation and enforces the divergence constraint locally, and a mesh-scale pressure correction, which obeys Laplace's equation and enforces volume conservation from mesh to mesh (here a "mesh" refers to the domain assigned to a particular process in a parallel calculation). Additional key components of the method are: (1) the averaging of the coincident staggered velocity components at a mesh interface which enforces symmetry of the stress tensors, (2) the specification of a Dirichlet condition for the fine-scale pressure fluctuation at a mesh interface which maintains continuity of the pressure field, and (3) the specification of a Neumann condition for the mesh-scale "pressure correction" at a mesh interface which is ultimately responsible for volume conservation across meshes. We demonstrate the performance and scalability of the algorithm by simulating the Sydney bluff-body-stabilized flame HM1a [1] (see Figure 1: left and lower-right), and we demonstrate time accuracy using a 2D analytical solution [2] (Figure 1: upper-right). As can be seen, the current implementation reverts to first-order accuracy due to the mesh boundary approximation. Our current work is focussed on improving this accuracy to second order.

The basic idea behind the scheme is the following. First, we break up the hydrodynamic pressure into a fluctuating component $\mathcal{H}$ and a small correction $\mathcal{H}'$. We may then write the momentum equation as

$$\frac{\partial \mathbf{u}}{\partial t} = -\left[\mathbf{F} + \nabla\mathcal{H} + \nabla\mathcal{H}'\right] , \tag{1}$$

where $\mathbf{u}$ is velocity and $\mathbf{F}$ accounts for all other body forces. Equation (1) is integrated in time under the constraints that the fluctuating pressure satisfies the Poisson equation,

$$\nabla^2\mathcal{H} = -\left[\frac{\partial}{\partial t}\left(\nabla\cdot\mathbf{u}\right) + \nabla\cdot\mathbf{F}\right] , \tag{2}$$

and the pressure correction satisfies Laplace's equation,

$$\nabla^2\mathcal{H}' = 0\,. \tag{3}$$

As opposed to conventional domain decomposition techniques where boundary conditions are prescribed only along the global boundary of the problem domain and the PDEs (2) and (3) are supposed to apply across mesh interfaces, in the FDS multiple mesh algorithm we impose a Dirichlet condition on $\mathcal{H}$ and

†Corresponding author.
Email: randall.mcdermott@nist.gov

a Neumann condition on $\mathcal{H}'$ at mesh boundaries. The Dirichlet condition for the pressure fluctuation is designed to provide stability, accuracy, and continuity and the Neumann condition for the (ideally small) pressure correction field is designed to enforce volume conservation from mesh to mesh. Once these boundary conditions are prescribed, calculations on each mesh may proceed independently, resulting in an algorithm which is embarrassingly parallel.

Acknowledgements

This research was performed while the first author held a National Research Council Research Associateship Award at the National Institute of Standards and Technology.

References

[1] Turbulent Nonpremixed Flame Workshop URL. http://public.ca.sandia.gov/TNF/abstract.html, 2008.

[2] R. McDermott. A nontrivial analytical solution to the 2-d incompressible navier-stokes equations. http://randy.mcdermott.googlepages.com/NS_exact_soln.pdf, 2003.

[3] K. McGrattan, S. Hostikka, J. Floyd, H. Baum, R. Rehm, W. Mell, and R. McDermott. Fire Dynamics Simulator (Version 5) Technical Reference Guide. NIST Special Pub. 1018-5, http://fire.nist.gov/fds/, 2008.

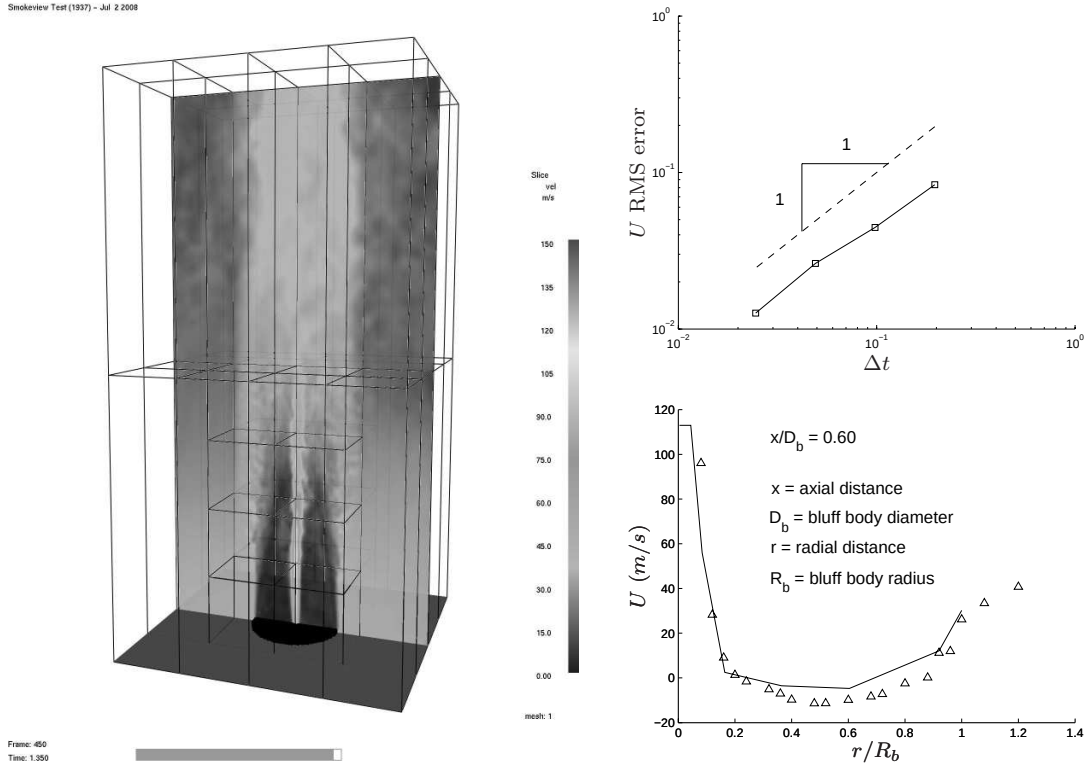

Figure 1: (Left) Velocity contours from a 44 mesh case for flame HM1a with block-structured grid refinement. (Lower-right) Comparison of axial velocity U at $x/D_b = 0.60$; symbols are HM1a data and lines are FDS results. (Upper-right) Convergence of RMS velocity error.

SIMULTANEOUS APPLICATION OF LASER-INDUCED INCANDESCENCE AND TWO-LINE ATOMIC FLUORESCENCE TEMPERATURE MEASUREMENT TO SOOTING TURBULENT NONPREMIXED FLAMES

P.R. Medwell[1], Q.N. Chan[1, 2], P.A.M. Kalt[1], Z.T. Alwahabi[2], B.B. Dally[1] & G.J. Nathan[1]
Fluid Mechanics, Energy and Combustion Group
Schools of [1]Mechanical and [2]Chemical Engineering, The University of Adelaide, Australia
paul.medwell@adelaide.edu.au, schan@chemeng.adelaide.edu.au, pkalt@mecheng.adelaide.edu.au,
zalwahab@chemeng.adelaide.edu.au, bassam.dally@adelaide.edu.au, gnathan@mecheng.adelaide.edu.au

The role of soot in combustion is important due its environmental and health impact, in addition to its role in radiative heat transfer. In order to understand the complex soot formation process, there is a need for the parallel application of accurate measurements and modelling to produce adequate models that are rigorously tested by reliable data sets that consist of parameters prevalent in sooting and fuel-rich flames. A multitude of interdependent parameters are of fundamental importance to soot production; however, temperature remains one of the most significant parameters in understanding and describing the chemical reactions and physical processes in combustion systems.

Producing experimental data sets in sooting flames using non-intrusive laser-based techniques has been problematic. Absorption, scatter and other interferences due to the presence of soot and its precursors in such flame prevents common laser diagnostics techniques from being applied reliably to such flames. These issues lead to the application of laser diagnostics often being limited to idealised clean flames, thus excluding comprehensive data sets of many practical flame situations.

The recent advent of laser-induced incandescence (LII), a laser-based soot diagnostic technique which is based on the laser heating of soot particles, has allowed good temporal and spatial measurements to be carried out on soot laden turbulent flames. Although LII is a complicated process and its details are still under investigation [1], LII has proven to be a powerful tool for particle-concentration measurement in practical combustion system [e.g. 2, 3, 4].

Successful application of LII within our group has revealed a number of interesting findings towards the soot volume fraction distribution in a turbulent nonpremixed flame. “Delft Flame III” produced using Delft burner from TNF workshop [5] was investigated and a number of interesting findings regarding the soot volume fraction distribution in the flame, which includes the time-averaged soot volume fraction distribution (Fig. 1) and probability density function (Fig. 2), has since been revealed.

The probability density function of maximum instantaneous soot volume fraction shows that the values of the instantaneous soot volume fraction spanning across the sooting region of the flame are generally lower that 0.33ppm, which is close to the values in strained laminar flames as reported in literature [6]. It is also clear that the concentration of the soot increases from the bottom of the flame, but remains relatively high at the tip of the flame, when present. This,

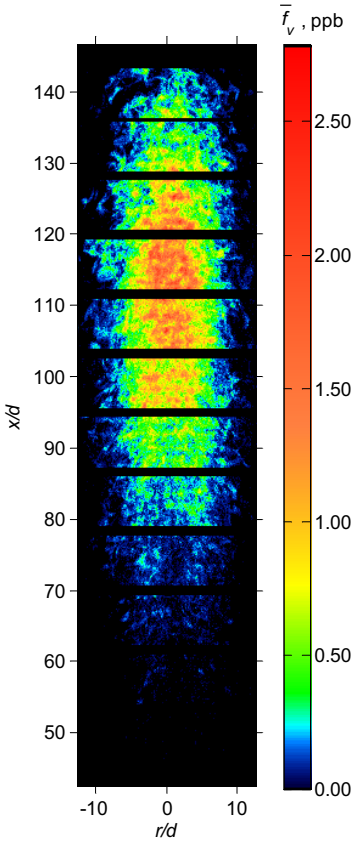

Figure 1: Time-averaged LII images of soot volume fraction spanning the sooting region of “Delft Flame III”

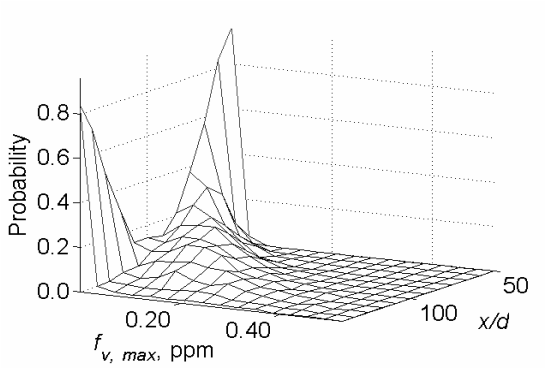

Figure 2: Probability density function of maximum soot volume fraction as a function of axial distance from burner.

along with the bi-modal distribution at the tip of the flame suggests that the burnout occurs primarily by the reduction of the number of soot sheet within the flame, rather than the values of the soot volume fraction within the sheet.

To complement the soot volume fraction data, measurements of temperature will be included into the experiment in the near future. Two-line atomic fluorescence (TLAF) will be used to image temperature simultaneously with the LII to provide great insight into the interrelationship between temperature and soot. The non-elastic nature of TLAF has the advantage of enabling optical filtering to reduce interferences from spurious scattering. Recent feasibility studies [7, 8] have also shown that TLAF, with indium as the thermometry species, holds promise for measurement in a highly sooting environment.

The experimental arrangement which is currently used to perform TLAF is shown in Fig. 3. Two Nd:YAG pumped dye lasers are fired simultaneously (~100ns separation) to produce the 410 & 450nm excitation beams, which are combined into a coplanar light sheet. The frequency-shifted fluorescence is detected through narrowband interference filters using two intensified CCD (ICCD) cameras. A tank containing fluorescing dye is included in the imaging field-of-view to facilitate correction of laser energy variation.

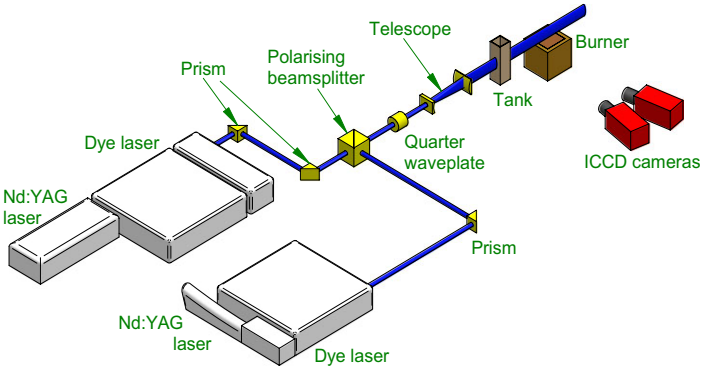

Figure 3: Experimental setup for TLAF.

Whilst still in the development stage, this work shows significant potential to advance our understanding soot and its formation. The ability to collect single-shot temperature images using TLAF, in conjunction with soot volume fraction, in sooting turbulent nonpremixed flames will form an invaluable data set for future studies on soot. This will, for the first time, enable instantaneous and simultaneous two-dimensional imaging of soot and temperature in turbulent nonpremixed flames.

References:

[1] C. Schulz, B.F. Kock, M. Hofmann, H. Michelsen, S. Will, B. Bougie, R. Suntz, G. Smallwood (2006) *App. Phys. B* **83**, pp. 333–354.
[2] H. Geitlinger, T. Streibel, R. Suntz, H. Bockhorn (1998) *Proc. Combust. Inst.* **27**, pp. 1613–1621.
[3] H. Bockhorn, H. Geitlinger, B. Jungfleisch, T. Lehre, A. Schön, T. Streibel, R. Suntz (2002) *Phys. Chem. Chem. Phys.* **4(15)**, pp. 3780–3793.
[4] N.H. Qamar, G.J. Nathan, Z.T. Alwahabi, K.D. King (2005) *Proc. Combust Inst* **30**, pp. 1493–1500.
[5] Available at: http://www.ca.sandia.gov/TNF.
[6] C.R. Shaddix, K.C. Smyth (1996) *Combust. Flame* **107**, pp. 418–452.
[7] J. Engström, J. Nygren, M. Aldén, C.F. Kaminski (2000) *Optics Letters* **25**(19), pp. 1469–1471.
[8] J. Nygren, J. Engström, J. Walewski, C.F. Kaminski, M. Aldén, (2001) *Meas Sci & Tech* **12**, pp. 1294–1303.

USING A TABULATED FLAMELET APPROACH TO SIMULATE A LIFTED METHANE JET FLAME

J.B. Michel[1*], C. Angelberger[1], O. Colin[2], D. Veynante[3]
[1] *IFP, France;* [2] *Air Liquide, France;* [3] *CNRS et Ecole Centrale Paris, France*
J-Baptiste.MICHEL@ifp.fr

The ADF-PCM model (Approximated Diffusion Flame Presumed Conditional Moment) has been developed by Michel et al. [1] for simulating non premixed or partially premixed turbulent flames. This model is based on a coupling between the FPI tabulation method [2], the flamelet equation by Peters [3] and the PCM model [4]. Indeed approximate diffusion flames are computed by solving the flamelet equation for the progress variable only. All chemical terms such as reaction rates or mass fractions are directly read from a FPI-type look up table. The latter is built from auto-igniting PSR calculations which, in contrast with laminar diffusion flames or premixed flames, enable the use of very detailed chemical mechanisms with low CPU requirements. In addition this approach ensures that auto-ignition delays are correctly reproduced. The approximate diffusion flames are then used for generating a turbulent look up table where mean values are estimated by integration over a P(Z) function, which is assumed to be a β-function. In this sense the model could be seen as a pre-tabulated version of the RIF model [5]. Two different formulations of ADF-PCM are tested with two corresponding probability density functions of the stoichiometric scalar dissipation rate: a Dirac function centered on the mean value, or a log normal function as proposed by Effelsberg and Peters [6], leading to an improved model referenced ADF-PCMχ. The turbulent look up table is read in the CFD code in the same manner as for the PCM model.

The developed models have been implemented into the IFP-C3D RANS CFD code and applied to the simulation of the Cabra et al. [7] experiment of a lifted methane flame. The GRI-MECH 3.0 is used for generating the chemical database. A k-epsilon turbulence model was used with a modified $C\varepsilon_2$ constant and allowed to accurately retrieve the experimental mean and RMS values of the mixture fraction. The results obtained with the two proposed model formulations show that the PDF of the stoichiometric scalar dissipation rate has a major impact on the lift-off height. Indeed, the ADF-PCM model underpredicts the experimental value, leading to important errors on the chemical composition. In contrast ADF-PCMχ allows a very accurate prediction. Fig. 1 displays the radial evolution of the mean and RMS values of the CO_2 mass fraction at three downstream locations. The agreement of the ADF-PCMχ predictions with experimental results is found to be much better than with the original formulation terms of mean and RMS values.

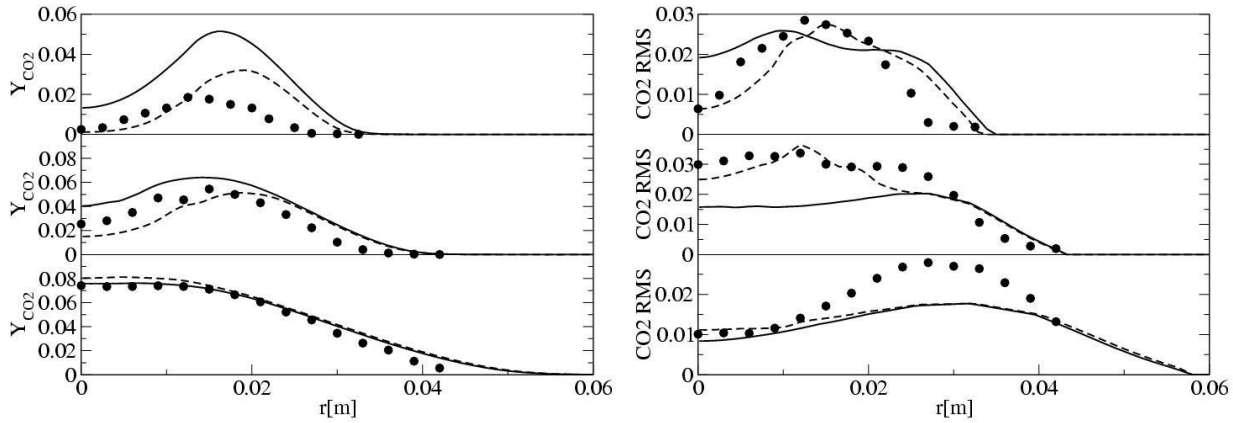

Figure 1: Radial evolution of the mean and RMS values of the CO_2 mass fraction at z=40D (top), z=50D (middle) and z=70D (bottom) for experiments (symbols), ADF-PCM (solid line) and ADF-PCMχ (dotted line).

References:

[1] J.B. Michel, O. Colin, and D. Veynante, Combust. Flame 158 (2008) 80-99
[2] O. Gicquel, N. Darabiha, and D. Thevenin, Proc. Combust. Inst. 28 (2000) 1901-1908
[3] N. Peters, Prog. Energy Combust. Sci. 10 (1984) 319-339
[4] L. Vervisch, R. Haugel, P. Domingo, and M. Rullaud, J. Turbulence 5 (4) (2004) 1-36
[5] H. Barths, C. Hasse, G. Bikas and N. Peters, Proc. Combust. Inst. 28 (2000) 1161-1168
[6] E. Effelsberg, and N. Peters, Proc. Combust. Inst. 22 (1988) 693-700
[7] R. Cabra, J.-Y. Chen, R.W. Dibble, A.N. Karpetis, and R.S. Barlow, Combust. Flame 143 (2005) 491-506

LES of Sydney Flames using Steady Flamelet and Progress Variable Approaches

C. Olbricht[1], F. Hahn[1], J. Kuehne[1], J. van Oijen[2], J. Janicka[1]

olbricht@ekt.tu-darmstadt.de, hahn@ekt.tu-darmstadt.de

[1]Fachgebiet Energie– und Kraftwerkstechnik, Technische Universität Darmstadt

Petersenstr. 30, 64287 Darmstadt, Germany

[2]Department of Mechanical Engineering, Eindhoven University of Technology

Den Dolech 2, 5600 MB Eindhoven, The Netherlands

Understanding mixing and combustion dynamics becomes increasingly important, particularly for achieving high efficiency and low emissions. In gas turbine combustion the prevention of global extinction is of significant importance. Therefore, stability of the reaction is ensured by using geometrical flame holders or by aerodynamic flame holding approaches. Such stabilization methods are applied within the Sydney bluff-body configuration which was experimentally investigated at the University of Sydney and the Sandia National Labs, [1] and [2]. To stabilize the flame the un-swirled case takes advantage of the bluff-body geometry. Some swirling cases of this series are characterized by a vortex breakdown mechanism which induces recirculation above the bluff-body wake which serves as a second stabilization zone. In this work several, tabulated chemistry based, combustion models are applied to Large-Eddy Simulation (here: LES with Germano's dynamic approach). Simulations of selected isothermal flow cases provide a basis for further studies of reacting, un-swirled and swirled bluff-body configurations. A detailed overview of the investigated cases is shown in Table 1. The sensitivity of several parameters, like the used SGS model, grid resolution or combustion model is studied in detail.

Flame	u_e (ms^{-1})	u_s (ms^{-1})	w_s (ms^{-1})	u_j (ms^{-1})	Re_s $(-)$	Re_{jet} $(-)$	S_g $(-)$	L_f (m)
NRFC	20.0	-	-	61.0	-	11 900	-	-
N29S054	20.0	29.7	16.0	66.0	59 000	15 700	0.54	-
N16S159	20.0	16.3	25.9	66.0	32 400	15 700	1.59	-
HM1E	35.0	-	-	108.0	-	15 800	-	-
HM3	35.0	-	-	195.0	-	28 500	-	-
SM1	20.0	38.2	19.1	32.7	75 900	7 200	0.50	0.12
SMA2	20.0	16.3	25.9	66.3	32 400	15 400	1.59	0.23

Table 1: Flame and flow conditions of the investigated cases.

The Sydney bluff-body configuration with all dimensions and the coordinate system, is shown in Figure 1. Here, the rotationally symmetric bluff-body nozzle (diameter $D_{bb} = 50\,mm$) is located in a square duct. Gas is fed through the centered pipe (diameter $D_j = 3.6\,mm$) at a bulk velocity of u_j at ambient conditions. The secondary airstream (ambient conditions, co-flow) between the duct and the burner is fixed at u_e. Swirled air is injected through an annular gap (primary air flow, $u_s, w_s, l_s = 5\,mm$). The swirl numbers S_g are evaluated with the mean bulk velocities (w_s/u_s) within the gap flow. All velocities and velocity fluctuations were measured through Laser Doppler velocimetry (LDV). Scalar measurements were carried out using Raman/Rayleigh/LIF. The measurements were conducted by Al-Abdeli and Masri [1] and Dally et al. [2].

Three different non-swirling bluff-body flow cases have been considered, the non-reacting NRFC, and the reacting cases HM1E and HM3. For the NRFC excellent results have been obtained. Jet penetration, bluff-body wake etc. matched with the experimental data. The reacting HM-cases use a mixture of CNG and H_2 $(1:1)$ as fuel. Both HM-cases are simulated with different elliptically smoothed, multi-block meshes (up to $6.6 \cdot 10^6$ grid points) and different PDF/chemistry models. Here, a variation of the used chemistry library is carried out, which utilizes steady flamelets (SF) with one or multiple strain rates ($a = 10, ..., 1662s^{-1}$). Additionally, a progress variable approach (PVA) similar to [3] has been used which applies non-premixed (NPGM) and premixed (PGM) generated manifolds, respectively. Results of the temperature and the concentrations of CO and OH conditioned at the mixture fraction for HM1E are shown in Figure 2. It can be identified that this flame (50% from extinction) is in principle well described with a multiple strain rate SF approach. Applying PVA with NPGM improves the results of minor species like CO and OH. Conceptual CO is far to high at the rich side using PGM. Deviations of the temperature, which arise for PGM, are caused by linear extrapolation beyond the burning limits. At Figure 3 radial temperature, CO and OH-concentration profiles and their fluctuations at different axial positions are shown for the same case and model combination. The spatial plots allow to assess the interplay of the CFD code and the three combustion models. Temperature and OH are predicted with excellent accuracy by all models; even the fluctuations are captured with good accuracy. For CO the best

results succeed with the NPGM approach, while the trend to overestimate CO with PGM is confirmed.
The simulations of HM3 (90% of blow-off velocity) using SF and PVA approaches provided good agreement of the velocities and their fluctuations to experimental data at all positions. The main flow features like recirculation and jet penetration are predicted with good accuracy. Within the sphere of the recirculation zone scalar and species predictions succeed; above this zone local extinction is present. With the PVA the local extinction is too high. Consequently the temperature and species are under predicted in this region.

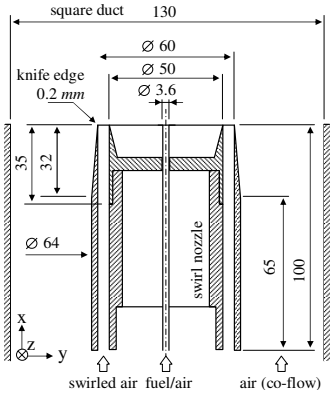

Figure 1: Sketch of the Sydney bluff-body configuration.

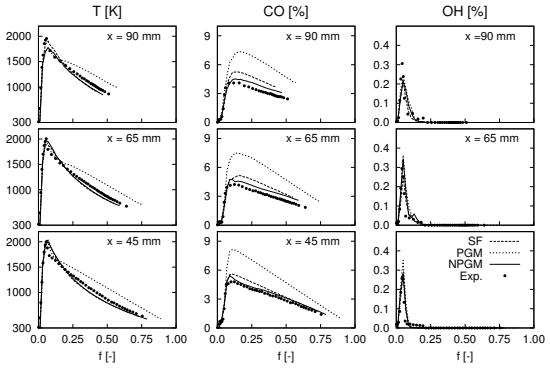

Figure 2: Conditional means of the temperature, CO and OH concentrations of HM1E burner.

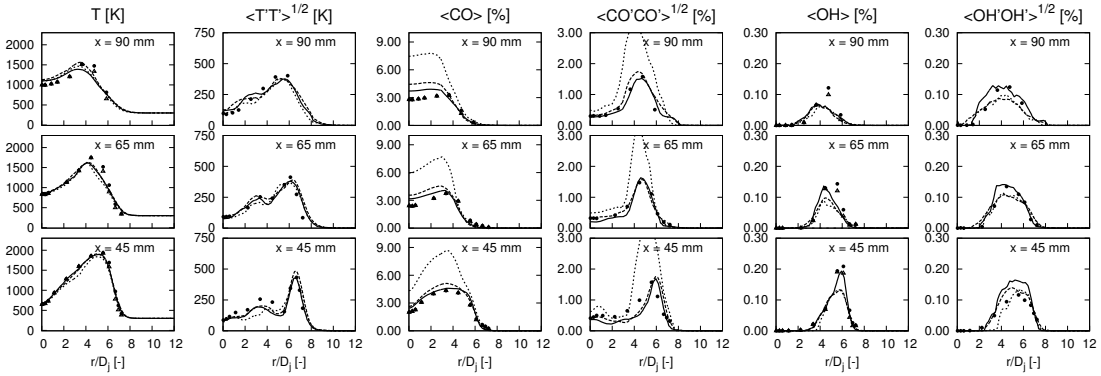

Figure 3: Comparison of the time-averaged temperature <T> , <CO> and <OH> concentration and their fluctuations for flow case HM1E (Legend: see Figure 2).

Both isothermal swirling cases N29S054 and N16S159 with and without vortex breakdown were predicted excellently by LES. Lengths and positions of the recirculation zone exhibit only a minimal shift to measured data. Shape and levels of the velocities and their fluctuations match with the experiments.
For the simulations of the swirled bluff-body methane-air flame SM1 single and multiple strain rate SF approaches on two different grids ($1.1 \cdot 10^6$ and $2.2 \cdot 10^6$ grid points) were used. Best results were achieved by inclusion of multiple strain rates. Here, opening angle, vortex breakdown and jet penetration are predicted with good accuracy; much better than with a single Flamelet. Correct species concentration levels have been achieved only by including strain rate effects.
The results of LES/SF calculations for the diluted methane-air flame SMA2 (no vortex breakdown mechanism present) revealed that standard steady Flamelet approaches are insufficient to describe the burning behavior correctly; especially the flame front location. Main problems consist in predicting the backward convection of fuel and momentum driven by the recirculation zone.
The LES/SF approach has been successfully applied to complex bluff-body flows. For the un-swirled cases the PVA approach provided improved results for species concentrations. The application of PVA to swirl flames promises improved results; especially for SMA2 where partially premixing is present.

References

[1] Al-Abdeli, Y., Masri, A.: *Comb. Theory Modelling, vol.7 (2003), 731–766*

[2] Dally, B., Fletcher, D., Masri, A.: *Comb. Theory Modelling, vol.2 (1998), 193–219*

[3] Vreman, A.W., Albrecht, B.A., van Oijen, J.A.,de Goey, L.P.H., Bastiaans, R.J.M.: *Comb. Flame, in print*

CREATING A DATASET OF VELOCITIES, TEMPERATURES AND MINOR SPECIES ON THE DELFT JET-IN-HOT-COFLOW FLAMES

E. Oldenhof, M.J. Tummers, E.H. van Veen, D.J.E.M. Roekaerts
Multi-Scale Physics, Faculty of Applied Sciences, Delft University of Technology, The Netherlands
e.oldenhof@tudelft.nl

Flameless Combustion

Flameless oxidation is a combustion technique that combines reduction of fuel consumption in industrial furnaces with low NO_x emissions. These environmental and economical benefits are realized by the utilization of a heat recovery system (recuperators of regenerators) combined with an injection system that forces mixing of products into the fuel and/or combustion air stream before reaction takes place [1,2]. The reaction rates in this type of combustion are lower due to the low temperatures, posing a modelling challenge for turbulence-chemistry interaction in these flames.

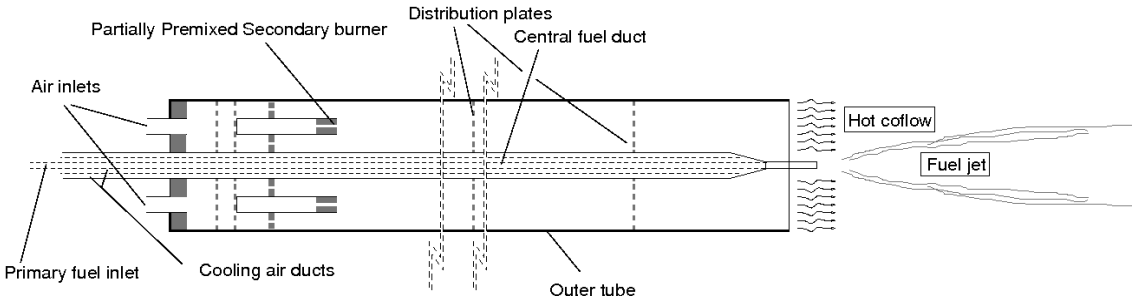

Figure 1: *Schematic design drawing of the Delft JHC burner*

The Delft Jet-in-Hot Coflow burner

The goal of the experimental work is to investigate the detailed flame structure of the produced flames of the Delft Jet-in-Hot-Coflow burner and to generate a detailed dataset of statistics of velocities, temperatures and species of flames relevant to flameless combustion, to be used for validation of turbulence-chemistry interaction models. The DJHC burner is therefore designed to deliver a flame that mimics the important characteristics of flameless combustion. It is unconfined, giving full optical access, and its axi-symmetry allows for detailed measuring and modelling. The design is based on that of the Adelaide JHC burner [3], differing however in two aspects. Firstly, cooling of the flame is achieved only by heat loss of the coflow, so no nitrogen is added. This process is explained in the next section. Secondly, the secondary burner allows the addition of seeding particles, making LDA and PIV measurements possible. The design is illustrated in Figure 1. A natural gas jet, emerging from a 4.5 mm diameter tube, develops in a coflow of hot and diluted air. The coflow is generated by a secondary burner inside an annulus. This partially premixed secondary burner also operates on natural gas in an overall lean condition. Due to the enthalpy deficit of the coflow (the coflow loses heat to the environment via radiation and convection of the outer tube) the peak temperature in the flame is lower than that of a natural gas flame in normal air. This results in flames with reduced luminosities ("flameless").

Relation between secondary burner, coflow properties and jet flame temperatures

The cooling effect of the hot coflow on flame temperature can be explained making use of the Burke-Schumann flame structure assumptions. In the secondary burner products are created with a mixture fraction equal to the injected fuel mass fraction, $\xi^O = Z_{fuel}$.

The amount of enthalpy loss can be normalized by the available sensible enthalpy, $h_{sens\,;\,max}(\xi^O) = \xi^O Q$, with Q the calorific value of the fuel, valid for $\xi^O \le \xi_{st}$. Here, the insulation value α has been chosen, such that α=1 implies perfect insulation and α=0 implies full heat loss. The enthalpy loss in the coflow is then:

$$\Delta h(\xi^O) = (\alpha - 1)\xi^O Q \qquad (1)$$

As the coflow itself is the oxidizer stream for the fuel, the original mixture fraction can be rescaled to be between zero and one for mixtures of coflow and fuel:

$$\xi' = \frac{\xi - \xi^O}{1 - \xi^O} \quad , \quad \xi^O \le \xi \le 1 \qquad (2)$$

Under certain assumptions (Lewis numbers equal to 1, adiabatic conditions), enthalpy is a passive scalar with the same transport equation as mixture fraction. Therefore, the enthalpy loss at stoichiometry in the jet flame, normalized with the available sensible enthalpy in combustion of fuel in a fresh air stream can be expressed as a function of mixture fraction alone. Combining (1) and (2) yields the following expression for the normalized effective enthalpy deficit at stoichiometry, valid for a coflow mixture fraction ξ^O smaller than or equal to stoichiometry:

$$\frac{\Delta h_{sens}(\xi'_{st})}{h_{sens\,;\,max}(\xi_{st})} = \left(\frac{1-\xi_{st}}{\xi_{st}}\right)\left(\frac{\xi^O}{1-\xi^O}\right)(\alpha-1) \qquad (3)$$

Equation 3 shows that the enthalpy loss in the coflow directly influences the maximum flame temperature, and that this influence is greater for coflow mixture fractions closer to stoichiometry. By operating the secondary burner with less excess air, the relative heat loss will be greater (due to the non-linearity of radiation loss vs. temperature) and a colder jet flame will be formed.

DJHC-1 and DJHC-2 flames

Two specific flames, differing by their coflow properties, have been chosen as study objects: DJHC-1 and DJHC-2. Their properties are summarized in Table 1. The average coflow temperature in this table is obtained from CARS measurements, and is mass flux weighted. The difference in coflows is achieved as described in the previous section, namely by operating the burner with less excess air for the DJHC-2 flame, resulting in effective enthalpy deficits (see Equation 3) of -0.13 and -0.21, and maximum adiabatic jet flame temperatures of 2040 K and 1920 K, respectively. For comparison, Özdemir [4], finds maximum instantaneous flame temperatures of around 1900 K. Finite rate effects will further diminish the actual peak temperatures to a certain extent, making DJHC-2 a suitable study flame for flameless combustion. A clear visual difference between the flames is also observed, the jet flame of DJHC-2 is hardly visible at the base.

		DJHC-1	**DJHC-2**
Sec. Burner	Power [W]	8600	8600
	Air input [l/s]	3.42	3.02
Coflow	$T_{\_ave}$ [K]	1520	1550
	YO_2	7.6 %	5.1 %
Jet	Re	5,000	5,000
	Fuel	Dutch Natural Gas	Dutch Natural Gas

Table 1: *Properties of the coflow and jet streams of the DJHC-1 and DJHC-2 flames*

Measurements

LDA measurements of radial profiles at different axial locations are currently in progress. These will be followed by CARS measurements on a similar grid to provide single point temperature data. PLIF measurements will complement the data with instantaneous 2-D fields of minor radicals in the flame zone.

[1] Wünning J.A. & Wünning J.G. *Flameless oxidation to reduce thermal NO-formation*, Progress in Energy and Combustion Science, 1997, 23, 81-94

[2] Tsuji, H. Gupta, A. Hasegawa, T. Katsuki, M. Kishimoto, K. & Morita, M. *High temperature air combustion*, CRC Press, 2003

[3] Dally B.B., Karpetis A.N. & Barlow RS. *Structure of turbulent non-premixed jet flames in a diluted hot coflow*, Proceedings of the Combustion Institute, 2002, 29, 1147-1154

[4] Özdemir, I.B. & Peters, N. *Characteristics of the reaction zone in a combustor operating at mild combustion* Experiments in fluids, 2001, 30, 683-695

[5] Oldenhof E., Tummers M.J., van Veen E.H. & Roekaerts, D.J.E.M. *The turbulent flowfield of the Delft jet-in-hot-coflow burner,* Proceedings 5th European Thermal-Sciences Conference, Editors: G.G.M. Stoffels, T.H. van der Meer and A.A. van Steenhoven, ISBN 978-90-386-1274-4, Eindhoven, 2008

Particle Advection for Large Eddy Simulation/Filtered Density Function Methods for Turbulent Combustion Simulations

Pavel P. Popov†, Stephen B. Pope

Sibley School of Mechanical and Aerospace Engineering, Cornell University

Here, we present new developments in Lagrangian particle advection which are to be incorporated into the LES/FDF code currently being developed by the Turbulence and Combustion Group in Cornell University. In Large Eddy Simulation/Filtered Density Function (LES/FDF) methods, we solve for a joint composition filtered density function (FDF), which is represented by an ensemble of particles. The particle positions follow a standard diffusion process whose drift and diffusion coefficients are determined by the filtered velocity and subgrid-scale velocity fluctuations of an LES solution. The back-coupling of the FDF into the LES solution occurs though the filtered density, which is determined from the FDF and used in the LES solution.

As pointed out by Muradoglu *et al.* [1], an important aspect of particle advection for an LES/FDF code is the consistency between the LES filtered density and the particle mass density. Briefly put, this means that the total mass of particles within a given region should be consistent with that region's volume and the density of the particles within it. In order to implicitly satisfy this consistency condition, Jenny et al. [2] and McDermott and Pope [3] introduce a new velocity interpolation scheme, called the Parabolic Edge Reconstruction Method (PERM), which, similarly to standard bi- and tri-linear velocity interpolation schemes, yields a second-order accurate velocity, but has the added advantage that the divergence of the velocity field is second-order accurate as well (whereas with multilinear interpolation it is first-order accurate).

The original version of PERM was designed for Cartesian grids – here we present a modified version, called Polar PERM (PPERM), which has the same properties but enables interpolation on polar and cylindrical grids, which are better suited for the simulation of many canonical turbulent reactive flows. Figure 1 demonstrates, in 2D, the advantage of using PPERM to using standard bilinear velocity interpolation in the r-θ parameter space.

In addition to introducing a new velocity interpolation scheme, we also examine the accuracy of the time integration scheme used to integrate the stochastic differential equation (SDE) which the particle positions evolve by. A second-order accurate SDE integration scheme has been proposed by Cao and Pope [4]. This scheme is particularly well-suited for the LES/FDF code developed by the Turbulence and Combustion Group because it uses values of the drift and diffusion terms at the midpoint of a time-step, which is ideal for the implementation of a staggered position-advance time step.

In Cao and Pope [4], the authors show that their scheme is second-order accurate (with respect to the time step), provided that the drift and diffusion coefficient fields are known exactly. Here, we demonstrate a stronger form of convergence, namely that the Cao and Pope scheme is second-order accurate even if the drift and diffusion coefficient fields are accurate up to second-order errors, and their derivatives are accurate up to first order errors. This stronger form of convergence is more relevant in an LES/FDF setting, because the drift and diffusion coefficient fields are not known exactly, but rather are interpolated from discrete data onto the particle positions.

References:

† Corresponding author. Email address: ppp7@cornell.edu

1/ M. Muradoglu, S. B. Pope, and D. A. Caughey, *The Hybrid Method for the PDF Equations of Turbulent Reactive Flows: Consistency Conditions and Correction Algorithms*, Journal of Computational Physics **172**, 841-878 (2001)

2/ P. Jenny, S. B. Pope, M. Muradoglu, and D. A. Caughey, *A Hybrid Algorithm for the Joint PDF Equation of Turbulent Reactive Flows*, Journal of Computational Physics **166**, 218-252 (2001)

3/ R. McDermott and S. B. Pope, *The Parabolic Edge Reconstruction Method (PERM) for Lagrangian Particle Advection*, Journal of Computational Physics **227** 5447-5491 (2008)

4/ R. Cao and S. B. Pope, *Numerical Integration of Stochastic Differential Equations: Weak Second-Order Mid-Point Scheme for Application in the Composition PDF Method*, Journal of Computational Physics **185**, 194-212 (2003)

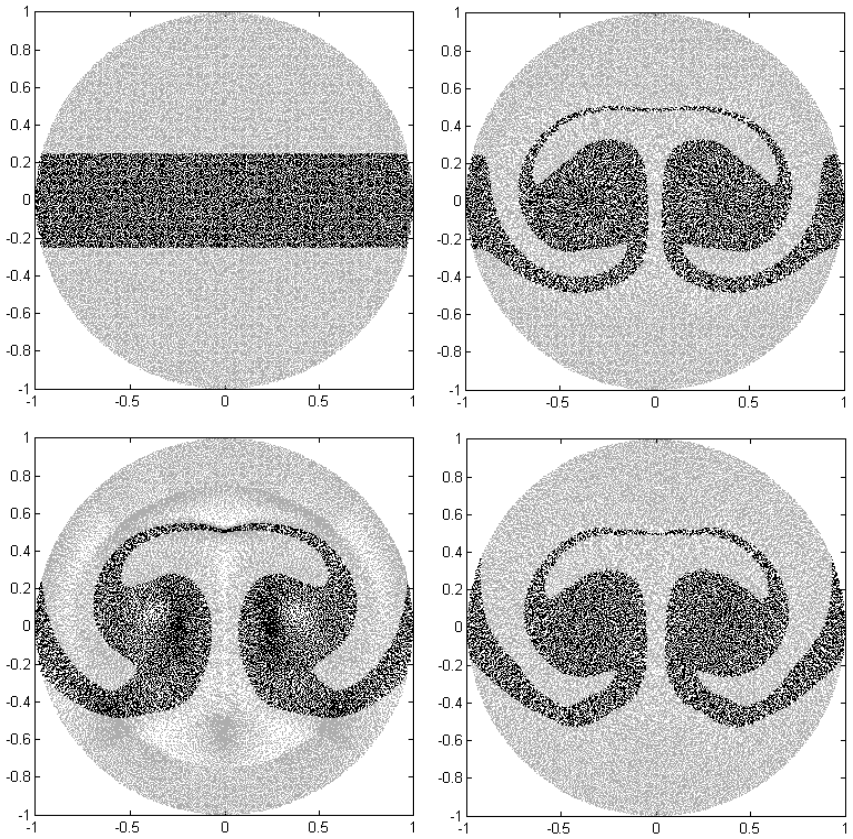

Fig. 1: Particle advection results with zero diffusion (particle positions evolve by an ODE instead of an SDE). Top left: initial positions of particles within a 2D circular domain – each dot represents a single particle, and the particles in the middle of the domain are darker for visualization purposes. Top right: final particle positions using an exact divergence-free velocity field and exact time advancement – since the velocity field is divergence-free and the particles are initially uniformly spaced, they remain so. Bottom left: final particle positions using a bilinearly interpolated velocity field on a 4-by-16 polar grid – it can be seen that the particles do not remain uniformly spaced. Bottom right: final particle positions using a PPERM interpolated velocity field on the same 4-by-16 polar grid – because PPERM yields a second-order accurate velocity divergence, the final particle positions are more uniform than those yielded by the bilinearly interpolated velocity field.

A Stable and Conservative Pressure-Correction Method for Transient Simulations of Reacting Flows

Pieter Rauwoens*, Jan Vierendeels, Erik Dick and Bart Merci[1]

Ghent University – UGent, Department of Flow, Heat and Combustion Mechanics,
Sint-Pietersnieuwstraat 41, B-9000 Ghent, Belgium

Pieter.Rauwoens@UGent.be

[1]Postdoctoral Fellow of the *Fund of Scientific Research - Flanders (Belgium) (FWO-Vlaanderen)*

Because of reported algorithmic stability problems [1, 2, 3] in turbulent combustion simulations, making use of the LES-approach, we present a novel algorithmic strategy that guarantees a stable solution. Since, for low-Mach number flows, a segregated solution procedure is believed to be more efficient, the algorithm is of a pressure-correction type method. The coupling between the equations is retained in the correction step, that accounts for the pressure influence. The pressure follows from a constraint on the velocity field. A consistent choice of this constraining equation was found to be the key to obtain stable results. This conclusion, originally drawn for non-reacting flows in [4], was later extended [5, 6] towards non-premixed combustion simulations, making use of the mixture fraction as a conserved variable. A pressure-correction algorithm was obtained which (1) conserves mass, (2) conserves fuel mass, (3) predicts states that exactly match the equation of state, (4) respects time-accuracy, as required for LES and (5) is stable and robust, without the need of (unphysical) rescaling factors. These properties are obtained by introducing a chemical operator $\mathcal{H}_C$ as $\rho = \mathcal{H}_C(\rho\xi)$ (ρ: density, ξ: mixture fraction). In case of combustion, $\mathcal{H}_C$ is highly nonlinear, which is incorporated in the algorithm. The resulting pressure-correction scheme is called *discrete compatibility-constraint pressure-correction*. For further details upon the algorithm, we refer to [5, 6, 7].

Results for test cases involving simple Burke-Schumann flamesheet chemistry for non-premixed flames are presented (fig. 1). Comparison is made with commonly applied pressure-correction methods, of a *continuity-constraint* type [1, 2] and of an *analytical compatibility-constraint* type [8]. From these test cases, we prove the superior properties of the novel algorithm in terms of conservation, fulfillment of the equation of state and stability. Furthermore, it is shown that only a minor extra cost is involved, compared to existing algorithms, such that more reliable results can be obtained in transient simulations, such as LES, with only a minimal decrease in efficiency. Also, the method is easily extendable to other types of chemistry models, also including turbulence effects. In that case, more scalars are involved in the chemical operator and the algorithm is adopted in a straightforward manner.

[1] A.W. Cook and J.J. Riley. 'Direct numerical simulation of a turbulent reactive plume on a parallel computer'. *J. Comput. Phys.*, 129:263–283, 1996.

[2] H.N. Najm, P.S. Wyckoff, and O.M. Knio. 'A semi-implicit numerical scheme for reacting flow, I. Stiff chemistry'. *J. Comput. Phys.*, 143:381–402, 1998.

[3] F. Nicoud. 'Conservative high order finite difference schemes for low-Mach number flows'. *J. Comput. Phys.*, 158:71–97, 2000.

[4] P. Rauwoens, K. Nerinckx, J. Vierendeels, E. Dick, and B. Merci. , 'A stable pressure-correction algorithm for low-speed turbulent combustion simulations'. In *'ECCOMAS European Conference on Computational Fluid Dynamics'*, Egmond aan Zee, The Netherlands, 2006. Delft University of Technology.

[5] P. Rauwoens, J. Vierendeels, and B. Merci. 'A stable pressure-correction scheme for variable density flows involving non-premixed combustion'. *Int. J. Numer. Methods Fluids*, 56(8):1465–1471, 2008.

[6] P. Rauwoens, J. Vierendeels, E. Dick, and B. Merci. 'A conservative discrete compatibility-constraint low-Mach pressure-correction algorithm for time-accurate simulations of variable density flows'. *J. Comput. Phys.* submitted.

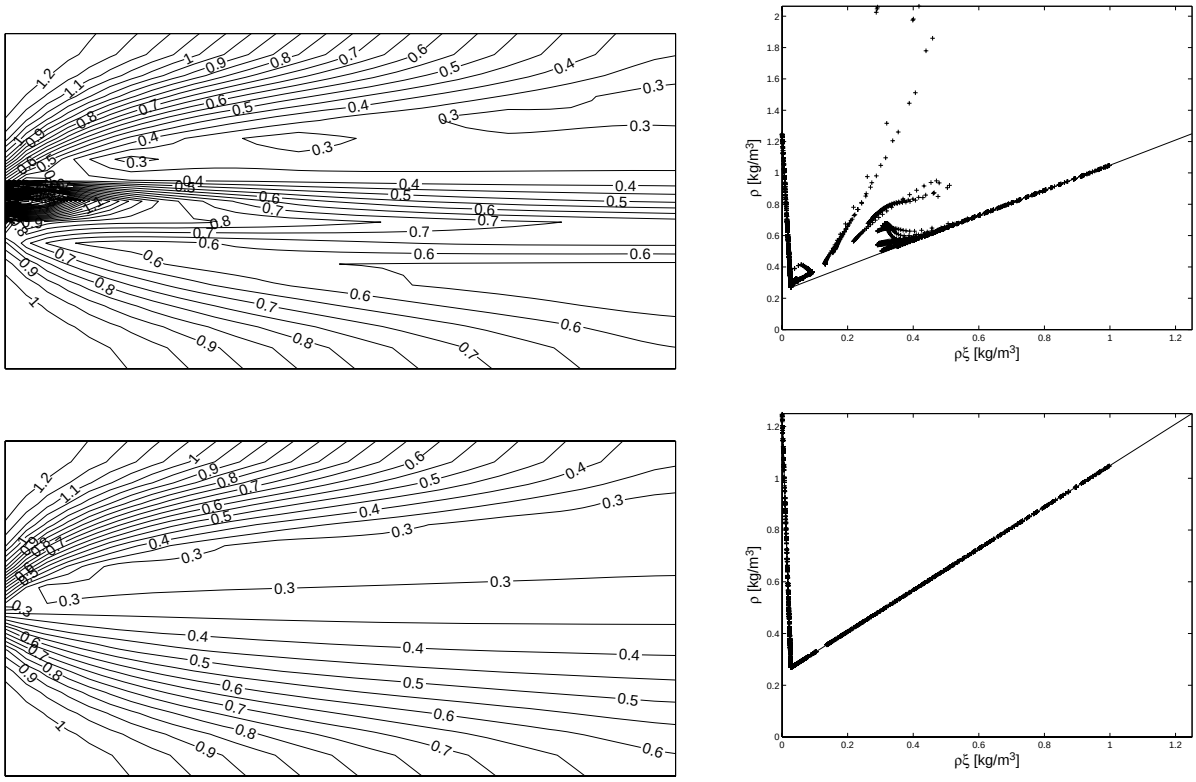

Figure 1: Results for the test case of a 2D reacing mixing layer: fuel and oxidizer enter the domain at the left; two slip-walls block the flow at the top and bottom; flue gases leave the domain at the right. A transient simulation is performed untill a steady-state solution is found. The inlet velocity is uniform ($10m/s$) and species diffusivity is $\rho D = 0.015625Pa.s$. The computational domain of $1m \times 0.5m$ is discretized on a 32×16 collocated vertex centered grid. For this test case, the continuity-constraint pressure-correction method did not result in a stable solution, irrespective of the time step size. A stable solution could be obtained with the compatibility-constraint types. However, using the analytical compatibility-constraint algorithm (top), results are predicted that do not match with the equation of state (full line, top left), yielding also a strange density field (top left). The use of the compatibility-constraint pressure-correction algorithm does result in reasonable field predictions (bottom left), with states that exactly match the equation of state (bottom right0.

[7] P. Rauwoens, J. Vierendeels, and B. Merci. 'A stable pressure-correction scheme for time-accurate non-premixed combustion simulations'. *Flow, Turbulence and Combustion*. submitted.

[8] M.S. Day and J.B. Bell. 'Numerical simulation of laminar reacting flows with complex chemistry'. *Combust. Theory Model.*, 4:535–556, 2000.

Direct numerical simulation and analysis of stratified turbulent methane-air flames.

E.S. Richardson[1] and J.H. Chen
Combustion Research Facility, Sandia National Laboratories, Livermore, CA, USA

Introduction

Flame response to equivalence ratio gradients has been studied previously in simulations of laminar, for example Ref. [1], and two dimensional turbulent [2] configurations. Current experimental diagnostic developments for stratified flows [3] have now given access to fully resolved composition information at low turbulence levels. This work introduces new fully resolved three-dimensional direct numerical simulation data for turbulent stratified methane Bunsen flames with a jet Reynolds' number of 2100. The flame series displays three levels of equivalence ratio (φ) stratification: premixed, φ=0.70; low stratification, 0.41<φ <1.0; and high stratification, 0.0<φ <1.46. Spanning from premixed to partially-premixed combustion modes, and extending beyond the thickened flame regime, this set of data permits investigation of turbulence-flame interactions relevant to modern multi-mode combustion devices, and their modeling. In particular we examine the effects of differing equivalence ratio and of equivalence ratio gradients on the propagation and structure of the flame.

Configuration

The two stratified cases are an extension of an existing series of premixed Bunsen DNS data [4]. In the premixed case, reactants heated to 800K issue from a 1.8mm wide slot at 100ms^{-1} into a co-flow of products moving at 25ms^{-1}, with the variation of composition from the jet to the co-flow prescribed by a profile of progress variable, and a tabulated premixed flame solution.

The stratified cases, shown schematically in Fig. 1, have a variation of mixture fraction in the periodic spanwise *z* direction between the equivalence ratio limits given above. The equivalence ratio limits were selected and the coflow velocity profiles calculated to give the same global equivalence ratio as the premixed case (φ =0.7). The inlet compositions for the stratified cases are specified as a function of mixture fraction and progress variable with reference to two-dimensional, laminar flame solutions with the corresponding range of equivalence ratios. The premixed and low stratification cases are solved with a non-stiff reduced mechanism for lean methane-air combustion [4], and the high stratification case uses a reduced methane-air mechanism based on GRI –Mech 3.0 applicable to the full range of stoichiometry encountered [5].

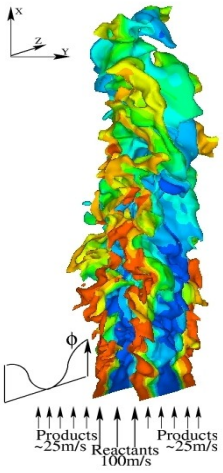

Figure 1. Stratified flame configuration. The 1200K temperature isosuface is colored by equivalence ratio from blue at φ=0.41 red at φ=1.0.

Analysis

Characterizing the turbulence by the velocity fluctuations and length scales evaluated at one quarter of the domain height [4], and evaluating the laminar flame properties for the range of equivalence ratio in each case gives a range of Karlovitz numbers ($Ka = (\alpha/S_L l_k)^2$) seen in the simulations. Here α is the thermal diffusivity, S_L is the laminar flame speed and l_k is the Kolmogorov length scale. Previous analysis [4] has illustrated that the premixed case, with Ka=5.2, sees turbulent eddies penetrating the flame's preheat layer, placing that case in the thin reaction zone

1 esrich@sandia.gov

regime. Scaling the Karlovitz number by the ratio of the full width half maximum heat release thickness (δ_H) to the flame's thermal thickness (δ_L), $Ka^*=Ka.(\delta_H/\delta_L)^2$, gives a value of 1.9 for the premixed case, but gives a range of 17.7-1.0 for the low stratification case, suggesting that the flow will perturb the reaction zone in the leaner mixtures of the stratified cases leading to combustion in the broken reaction zone regime.

Employing a partially premixed progress variable *c,* which varies between zero and one at all mixture fractions, profiles of progress variable gradient through the flame conditioned on φ=0.5 and φ=0.7, Fig. 2, show thickening of the flame's preheat zone relative to the laminar flame profiles. However, when conditioning on φ=0.5 the reaction zone structure also deviates from the laminar profile close to the peak heat release (c=0.65) where turbulence acts to reduce flame thickness.

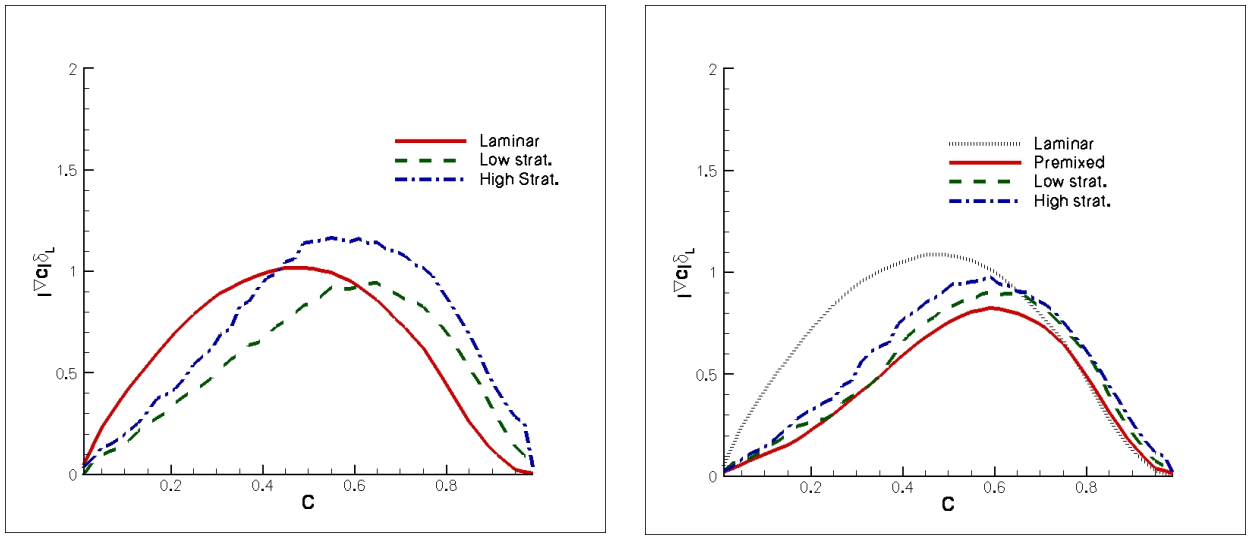

Figure 2. |∇c| conditionally averaged on progress variable *c* and equivalence ratio φ=0.5 (left) and φ=0.7 (right) compared to the laminar flame profile for the three simulations. The means are obtained at an axial position of ½ of the flame height.

Analysis of the flame surface density equation and the contributions of equivalence ratio gradients to the flame's displacement speed will be presented in order to aid further discussion of stratification effects on flame structure and propagation statistics.

[1] Y. M. Marzouk, A. F. Ghoniem and H. N. Najm, Dynamic response of strained premixed flames to equivalence ratio gradients. *Proceedings of the Combustion Institute.* Vol.28 (2000) pp.1859-1866.
[2] C. Jiménez, B. Cuenot, T. Poinsot and D. Haworth, Numerical simulation and modeling for lean stratified propane-air flames, *Combustion and Flame* 128:1-21 (2002)
[3] R.S. Barlow, G.H. Wang, P. Anselmo-Filho, M.S. Sweeney, S. Hochgreb, Application of Raman/Rayleigh/LIF diagnostics in turbulent stratified flames, submitted to *Proceedings of the Combustion* Institute. 2008.
[4] R. Sankaran, E. R. Hawkes, C.S. Yoo, J.H. Chen, T. Lu, C.K. Law, Direct numerical simulation of stationary lean premixed methane-air flames under intense turbulence. 5th US combustion meeting, San Diego, March 2007.
[5] T. Lu and C.K. Law. A CSP-Based Criterion for the Identification of QSS Species: A Reduced Mechanism for Methane Oxidation with NO Chemistry. In preparation (2008).

EKT Stratified Burner: a Generic Premixed Jet Flame Series for Model Validation

F. Seffrin, F. Fuest, D. Geyer & A. Dreizler*
**dreizler@ekt.tu-darmstadt.de*
TU Darmstadt, FG Energie- und Kraftwerkstechnik
Petersenstrasse 30, D – 64287 Darmstadt, Germany

1. Introduction

The stratified lean premixed burner was developed to study the effects of shear and stratification on reacting flows in the scope of experiments for model validation. The generic burner addresses combustion phenomena relevant to technological applications, where flames are often turbulent, lean premixed, and stratified. As there are only a few comprehensive data sets available for premixed [1] or stratified [2,3] combustion the aim of this project is to provide detailed information about velocity and scalar fields for a set of turbulent flames with variations in Re number, stratification, shear, and fuel. The intentionally simple burner design accounts for practical aspects in the process of numerical setup (e.g. a simple flow field, rotational symmetry) and for the application of advanced laser diagnostics for scalar and velocity field measurements.

2. Design & Operational Conditions

The burner was already presented at TNF8 [4]. In brief, it consists of three staged concentric tubes with inner diameters of 16, 37, and 60 mm, respectively, resulting in almost constant hydraulic diameters for the inner tube and the two annular slots. The minimal tube length of the slots is about L = 500 mm according to 25 hydraulic diameters. The flame is stabilized by a premixed pilot flame in the ceramic center tube burning 40 mm upstream the exit plane on a centered flame holder ring. The two surrounding annular slots can be operated independently (flow rate / equivalence ratio Φ / fuel) of the pilot and of each other.
Six methane flow configurations with diversified Re-numbers, shears, and stratifications, as well as two ethene configurations (addressing aspects of fuel flexibility) and their corresponding isothermal configurations (see *Tab. 1*) were investigated with 2-component Laser Doppler Velocimetry (LDV) to generate radial profiles of the axial and radial velocity. For selected configurations and positions time series were measured in order to determine correlations and time scales.
LDV measurements will be soon compared to Highspeed Particle Imaging Velocimetry. Planar Rayleigh Scattering will gain first insight into temperature fields.

3. Selected Results

a Velocity Profiles

Radial profiles of the axial and radial velocity were measured at different axial heights between 25 and 250 mm. *Fig. 1* shows selected results for the reacting basic configuration TSF_A_r as well as for configurations with increased Re number (TSF_B_r), increased shear (TSF_D_r), and alternative fuel (ethene, TSF_I_r).

b Velocity Correlations

For selected configurations and positions time series were measured to provide additional information as correlations of the axial velocity, energy density spectra, and integral length scales. *Fig. 2* shows typical results for the basic configuration TSF_A_r.

Config	Φ_{Pilot}	v_{Pilot} [m/s]	Φ_{Slot1}	v_{Slot1} [m/s]	Re_{Slot1}	Φ_{Slot2}	v_{Slot2} [m/s]	Re_{Slot2}	P_{total} [kW]
TSF_A_r	0.9	1	0.9	10	13800	0.6	10	13300	72
TSF_A_i1	0.9	1	0	10		0	10		
TSF_A_i2	0	10	0	10		0	10		
TSF_B_r	0.9	1.5	0.9	15	20700	0.6	15	20000	109
TSF_B_i1	0.9	1.5	0	15		0	15		
TSF_B_i2	0	15	0	15		0	15		
TSF_C_r	0.9	1	0.9	10	13800	0.6	5	6700	53
TSF_D_r							20	26600	111
TSF_C_i1	0.9	1	0	10		0	5		
TSF_D_i1							20		
TSF_E_r	0.9	1	0.9	10	13800	0.9	5	6700	64
TSF_F_r	0.9	1	0.9	10	13800	0.75	10	13300	83
TSF_G_r						0.9			94
TSF_H_r	0.9	0.6	0.6 *(ethene)*	10	14000	0.9 *(ethene)*	5	6800	53
TSF_I_r	0.9	0.6	0.6 *(ethene)*	10	14000	0.6 *(ethene)*	10	13500	63
TSF_J_r	0.9	0.6	0.6	10	13700	0.9	5	6600	52
TSF_J_i1	0.9	0.6	0	10		0	5		
TSF_J_i2	0	6	0	10		0	5		
TSF_K_r	0.9	0.6	0.6	10	13700	0.6	10	13300	61

Tab. 1 – Configurations of the **T**urbulent **S**tratified **F**lame series.

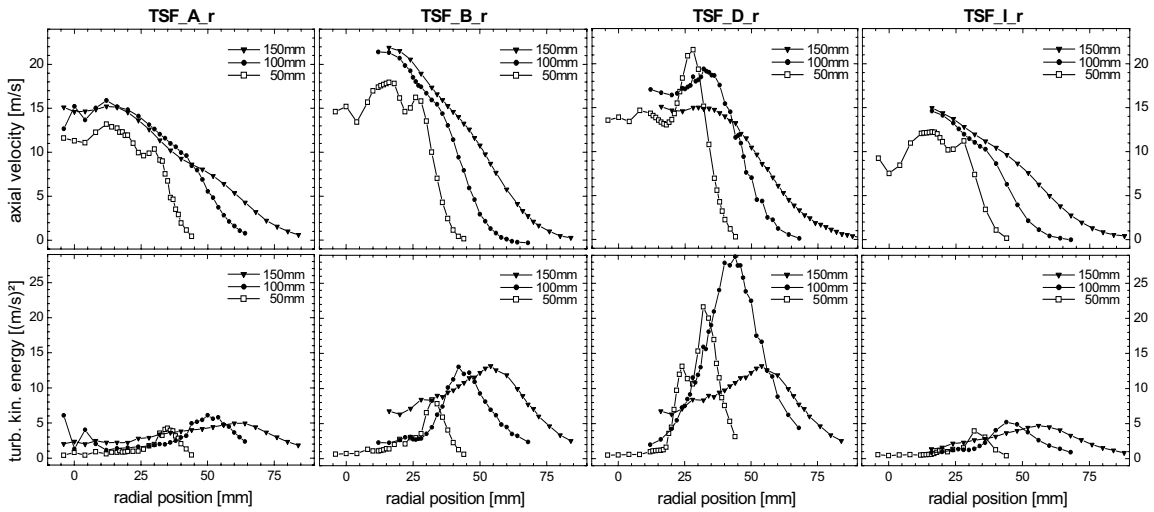

Fig. 1 – Selected radial profiles of the axial velocity and the turbulent kinetic energy for different axial heights.

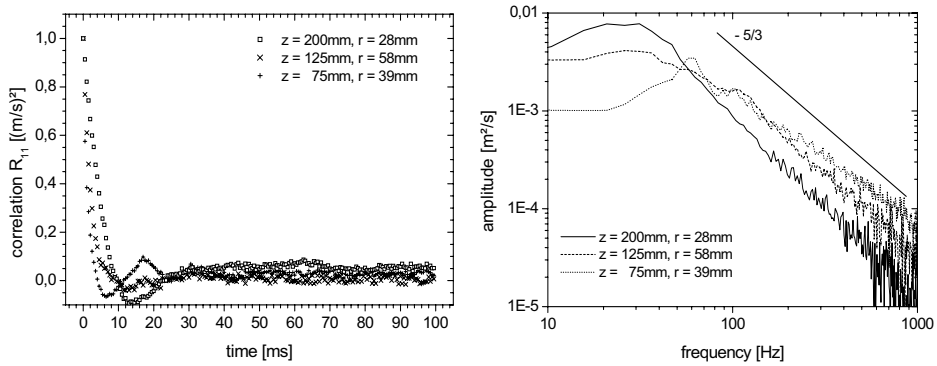

Fig. 2 – Auto correlation and energy density spectrum for TSF_A_r at different axial heights z each at its radial maximum of the turbulent kinetic energy. The corresponding integral length scales for increasing z are 1.1, 2.0, and 3.7 ms, respectively.

4. Outlook

Planar OH Laser induced Fluorescence and Raman Scattering will provide information on temperatures and species concentrations. Additional exhaust analysis (unburned fuel, NOx) will be performed.

Acknowledgements

This work is funded by the DFG, project DR 374/5-1. We benefited greatly from discussions with R.S. Barlow. LDV and PIV measurements performed by A. Ludwig and C. Beyer are greatly acknowledged.

References

[1] M.A. Gregor, F. Seffrin, F. Fuest, D. Geyer, A. Dreizler, "Multi-scalar measurements in a premixed swirl burner using 1D Raman/Rayleigh scattering", Proc. Combust. Inst. 32 (accepted for oral presentation).

[2] P. Anselmo-Filho, R. S. Cant, S. Hochgreb, and R. S. Barlow, "Experimental Measurements of Geometric Properties of Turbulent Stratified Flames", Proc. Combust. Inst. 32 (accepted for oral presentation).

[3] R.S. Barlow, G.H. Wang, P. Anselmo-Filho, M.S. Sweeney, S. Hochgreb, "Application of Raman/Rayleigh/LIF Diagnostics in Turbulent Stratified Flames", Proc. Combust. Inst. 32 (accepted for oral presentation).

[4] D. Geyer et al, TNF8 Workshop Proceedings, 298-299 (web version).

Flame Modeling Using Artificial Neural Networks and Linear Eddy Mixing Model Based Tabulation Strategy

Baris A. Sen, Suresh Menon
baris.sen@gatech.edu, suresh.menon@ae.gatech.edu
School of Aerospace Engineering, Georgia Institute of Technology
Atlanta, GA, 30332-0150, USA

1. Introduction

The focus of the current study is to generate multi-dimensional look-up tables based on the 1-D Linear Eddy Model (LEM) calculations of turbulent non-premixed and premixed flames, and use them in Artificial Neural Networks (ANN) for Large Eddy Simulation (LES). Table generation based on stand alone LEM computations would yield a better description of the interaction between the small scale turbulent processes and the combustion, since they are fully resolved at their respective time and length scales in the LEM formulation [1]. This feature is absent in most of the flamelet based tabulation strategies, as they inherently assume a laminar flame front with respect to the flow field [2]. ANN eliminates the use of a look-up table during LES with substantial reduction of computational time and memory [3].

Direct Numerical Simulation (DNS) has been used to investigate scalar mixing in temporally evolving jet flames up to a Reynolds number of 9000 with a detailed CO/H_2 reaction mechanism [4]. The current study aims to study the same problem with LEMLES in a much computationally affordable way. The numerical code used in this work solves the fully compressible and unsteady form of the Navier-Stokes equations. An eddy viscosity closure with dynamic coefficients [6] is employed for the subgrid scale (sgs) momentum closure and LEM model [7–9] is used for the sgs combustion modeling. A multi-layer perceptron type of ANN is developed using a back-propagation algorithm based on the gradient descent procedure together with a momentum coefficient for data training [3].

2. Results and Discussion

The LES is initialized with a laminar flamelet solution at an initial scalar dissipation rate χ =1646 1/s [5]. Also, the current computation uses the same detailed mechanism as the original study [5]. The OH mass fraction surface plot and the velocity vectors are given in Fig. 1 at t^* =12 and 16, respectively. Here, $t^* = t/t_j$, with t_j transient jet time [4]. As shown in the figure, the turbulent structures interact with the flame front and the OH mass fraction exhibits broken regions in the shear layer. This feature is more evident at t^* =16. A stand alone LEM code is used to investigate the same flame on a 1-D line across the flame front. As turbulent stirrings are modeled as a stochastic process within the LEM, several realizations of the same computation is performed. The instantanous LEM realizations are later filtered with a filter size equal to the LEMLES grid size and used to extract the instantanous chemical reaction rates (RRANN,hereafter) and the LEM reaction rates (LEMANN, hereafter) of the given parameters. For RRANN, the species composition and the temperature are selected for parameterization and each entry on the table exhibits a unique state. This is not the case for LEMANN since it represents dominantly the effect of the small scale turbulence on the resolved scale, thus a PDF construction strategy is employed. The PDF is parameterized by using the lower moments $\widetilde{Y_{H2}}$, $\widetilde{Y_{OH}}$, $\widetilde{Y_{CO_2}}$, $\widetilde{T}$ and Re_t, with Re_t denoting the sgs turbulent Reynolds number. PDF's obtained by using this methodology are shown in Fig. 2 for two different parameterizing lower moments. The effect of the Re_t can be seen clearly on the figures. For a high Re_t, turbulent stirring is more dominant, and the PDF dominates the molecular diffusion and heat release. Thus, the PDF is more spread around the possible states. The RRANN is used to replace the reaction rate calculations in the LEMLES computation. The comparison of the OH mass fraction profile across the flame front at 4 different x locations is shown in Fig. 3. As seen the profiles are almost identical with a minimal value of error. The look-up table size is 60 MB which is saved by the RRANN and a speed-up of 3.1 is achieved. Further analysis of the results will be reported at the workshop.

References

[1] G. Goldin, S. Menon *Combust. Flame* 113 (3) (1998) 442–453.
[2] N. Peters *Turbulent Combustion*, Cambridge Monographs on Mechanics, 2000.
[3] B. A. Sen, S. Menon *Proc. Combust. Inst.*, (2009)
[4] E. R. Hawkes, R. Sankaran, J. C. Sutherland, J. C. Chen *Proc. Combust. Inst.* 31 (2007) 1633–1640.
[5] E. R. Hawkes *Private Communication* 2008.
[6] W. W. Kim, S. Menon, H. C. Mongia *Combust. Sci. Technol.* 143 (1999) 25–62.
[7] A. R. Kerstein *Combust. Sci. and Technol.* 60 (1988) 391–421.
[8] S. Menon, N. Patel *Combust. Flame* 153 (1-2) (2008) 228–257.
[9] H. El-Asrag, S. Menon *Proc. Combust. Inst.* 31 (2) (2007) 1747–1754.

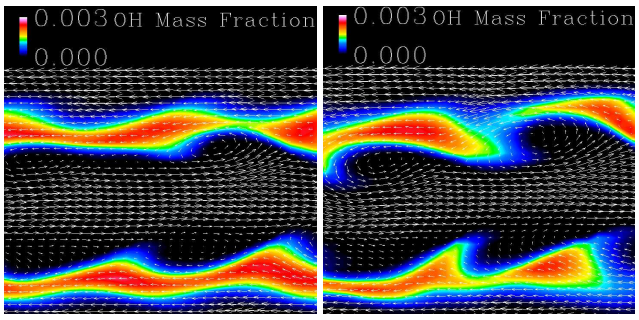

(a) t^* =12 (b) t^* =16

Fig. 1: OH mass fraction and velocity vectors at t^* =12 and 16.

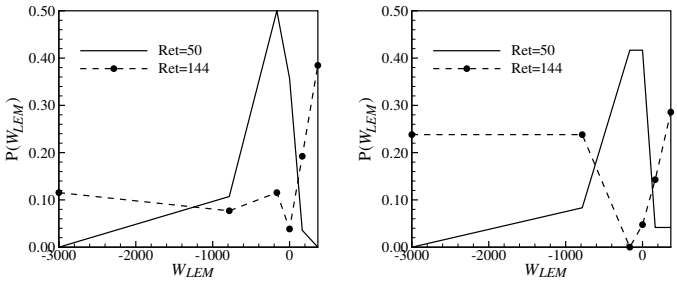

(a) $\widetilde{Y_{H2}}$=0.0044, $\widetilde{Y_{OH}}$=0.00021, $\widetilde{Y_{CO_2}}$=0.0581, $\widetilde{T}$=821 K

(b) $\widetilde{Y_{H2}}$=0.0051, $\widetilde{Y_{OH}}$=0.00014, $\widetilde{Y_{CO_2}}$=0.0525, $\widetilde{T}$=791 K

Fig. 2: Comparison of the $P(W_{LEM}|\widetilde{Y_{H2}}, \widetilde{Y_{OH}}, \widetilde{Y_{CO_2}}, \widetilde{T}, Re_t)$ for different lower moments.

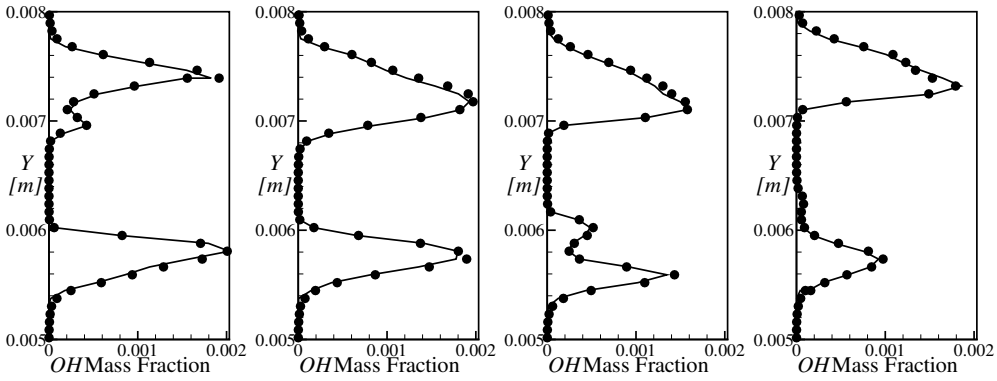

(a) x =0.00384 m (b) x =0.00576 m (c) x =0.00768 m (d) x =0.0096 m

Fig. 3: Comparison of the instantaneous OH mass fraction profiles obtained by using DVODE (•) and ANN (–) at t^*=16.

APPLICATION OF LES/CMC METHODOLOGY TO HYDROGEN AUTO-IGNITION IN A TURBULENT CO-FLOW OF HEATED AIR

I. Stanković[1]*, A. Triantafyllidis[2], E. Mastorakos[2], C. Lacor[3] and B. Merci[1, 4]
[1]*Ghent University, Belgium;* [2]*Cambridge University, UK;* [3]*Vrije Universiteit Brussel, Belgium*
[4]*Postdoctoral Fellow of the Fund of Scientific Research – Flanders (Belgium) (FWO-Vlaanderen)*
*Ivana.Stankovic@UGent.be

The case considered corresponds to the configuration studied experimentally by Markides and Mastorakos [1]. The aim of this work is better understanding of the auto-ignition in the random spots regime. This is the regime where auto-ignition kernels appear randomly in space and time with frequency depending on the inlet velocity and temperature. The auto-ignition kernels are subsequently transported out of domain.

Figure 1 illustrates the set-up. Hydrogen, diluted with nitrogen, is used as a fuel. The fuel is injected into an air co-flow through a 2.25 mm internal diameter at ambient pressure. The burner inner diameter is 25 mm. Air velocities up to 35 m/s, with air temperature up to 1015 K, have been achieved. Fuel velocity ranged from 20 to 120 m/s, with fuel temperature between 650 K and 930 K. Different auto-ignition regimes (no ignition, random spots, flashback and lifted flame) are obtained by varying the temperature of the air and the inlet jet velocity. In the observed configuration all major turbulence effects are expected to be dominated by the inflow conditions.

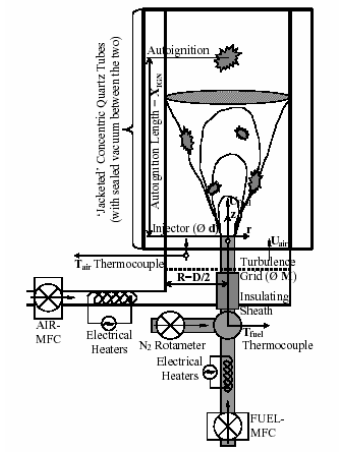

Fig. 1. The experimental set-up.

Region	Item	Ujet > Uair
Fuel jet	Velocity, Ujet (m/s)	120
	Temperature (K)	691
	Composition	$Y_{H_2} = 0.13$ $Y_{N_2} = 0.87$
Co-flow	Velocity, Uair (m/s)	26
	Temperature (K)	962 - 1015
	Composition	$Y_{O_2} = 0.233$ $Y_{N_2} = 0.767$

Table 1. Boundary conditions for the simulation [1]

We apply the Large-Eddy Simulation (LES) approach for the simulation of the turbulent flow and mixing field. Focus is on turbulence-chemistry interaction. We use a first order Conditional Moment Closure (CMC) [2].

As flow field solver, we use an in-house LES code, developed at VUB [3], with standard Smagorinsky sub-grid scale modeling (with $C_s = 0.1$). In the CMC code, species and energy equations are solved, using velocity and mixing field from the flow field solver. Conditional moments are computed at a fixed location x and time t within the flow field. The CMC code has been developed at Cambridge University [4]. In order to obtain mean density, required for the flow calculations, the conditional averaged values obtained from the CMC calculations are weighted by the mixture fraction probability density function (PDF) for computation of the unconditional mean values. We use pre-assumed β-PDF shapes. Due to weaker spatial dependence of the conditional quantities a coarse spatial grid can be used in CMC [4]. A detailed chemical mechanism for hydrogen [5] is used.

The results are still preliminary, in the sense that no sensitivity study has been performed yet. We use a CFD mesh of 96 x 48 x 48 cells, covering a domain of 135 mm x 25 mm x 25 mm. The CMC mesh consists of 16 x 4 x 4 cells. The implementation is parallel, with 4 blocks in the axial direction. The boundary conditions for the simulations (Table 1) are taken from Markides and Mastorakos [1]. First studies confirm that it is very important to apply proper turbulence at the inlet boundary of the CFD mesh in order to obtain realistic results. We confirm the experimental observation that there are notable differences when the temperature of the co-flow air is varied (see Fig. 2 and Fig. 3). Fig. 2 and 3 have been obtained as follows: first, a developed turbulent mixing field is computed, by de-activating the chemical source term in the CMC equations; then, chemistry is activated and instantaneous snapshots of planar temperature field are presented at different times after activation of chemistry. The results look reasonable, but in-depth analysis and comparison to experimental data is still required.

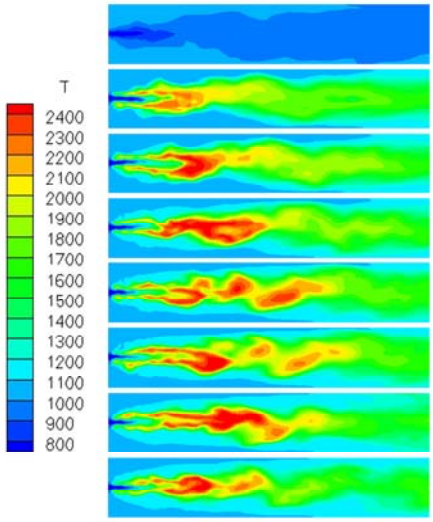

Fig. 2. Instantaneous planar temperature fields (T air = 1009 K) in physical space at different times after activation of chemistry.

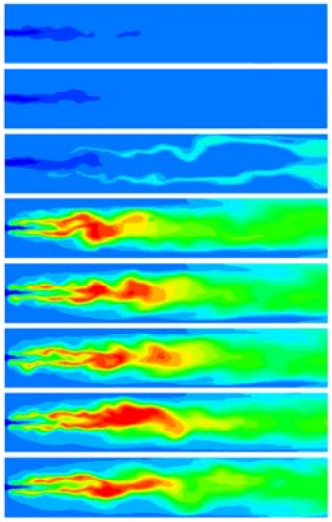

Fig. 3. Instantaneous planar temperature fields (T air = 970 K) in physical space at different times after activation of chemistry.

Figure 4 reveals the result when random white noise is imposed at the inlet of the CFD mesh instead of proper turbulence. Results are clearly substantially different from what is presented in Fig. 2 (where proper turbulence is imposed and all other settings are identical to the simulations of Fig. 2).

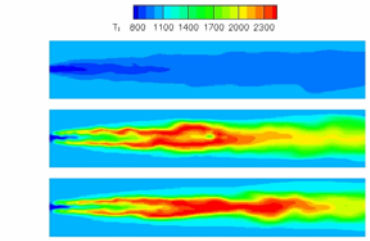

Fig. 4. Instantaneous planar temperature fields (T air = 1009 K) in physical space at different times after activation of chemistry, with random white noise as turbulence at the inlet.

[1] C.N. Markides and E. Mastorakos, *An experimental study of hydrogen auto-ignition in a turbulent co-flow of heated air*, Proceedings of the Combustion Institute, 30 (2005) 883-891.
[2] A.Y. Klimenko and R.W. Bilger, *Conditional moment closure for turbulent combustion,* Progress in Energy Combustion Science, 25 (1999) 595-687.
[3] T. Broeckhoven, *LES of Turbulent Combustion: Numerical Study and Applications*, PhD Thesis, VUB, 2007, http://mech.vub.ac.be/thermodynamics/phd/list_lacor.htm
[4] Y. M. Wright, G. De Paola, K. Boulouchos and E. Mastorakos, *Simulations of spray auto-ignition and flame establishment with two-dimensional CMC*. Combustion and Flame, 143 (2005) 402-419.
[5] J. Li, Z. Zhao, A. Kazakov and F. L. Dryer, *An updated comprehensive kinetic model of hydrogen combustion*, International Journal of Chemical Kinetics, 36 (2004) 566-575.

Investigation of Unsteady Combustion Phenomena in a Gas Turbine Model Combustor

M. Stöhr, R. Sadanandan, P. Weigand, W. Meier

DLR-Institut für Verbrennungstechnik, Pfaffenwaldring 38, 70569 Stuttgart, Germany
E-mail: michael.stoehr@dlr.de

The gas turbine model combustor from the German Aerospace Center (DLR) for confined swirling, partially premixed CH_4/air flames has been presented in a previous TNF Workshop and can serve as a test case for the validation of numerical simulations. The burner is operated with swirling air and CH_4 at atmospheric pressure in a range of thermal powers from 5 to 40 kW. The flames are confined by a squared combustion chamber with an inner diameter of 85 mm and a height of 114 mm, equipped with 4 quartz windows for almost unrestricted optical access. Three flames have been investigated in detail using various laser measuring techniques (LDV, PIV, laser Raman scattering, PLIF, and chemiluminescence imaging). The results have been published [1, 2] and the data sets are available on request. The current investigations aim at the identification and understanding of periodic unsteady combustion phenomena, which occur under certain operating conditions. One of the flames investigated (Φ=0.75, P=10 kW, Re=10000) exhibits self-excited thermoacoustic oscillations at a frequency of around 290 Hz. In order to correlate the pulsed laser measuring techniques with the phase angle of the acoustic pressure oscillation, microphone probes have been installed at different positions in the combustion chamber and plenum. In this way, the phase-angle of the thermoacoustic oscillation could be determined for each individual measurement, revealing the phase-dependant variations of the flame. Further, a hydrodynamic instability in the form of a precessing vortex core (PVC) was identified. The PVC rotates with a frequency different from the acoustic frequency and generates only a weak pressure oscillation. Both periodic instabilities have a significant influence on the flow field, mixing and flame shape and their understanding is of fundamental importance for a correct numerical simulation of the flames.

The Raman measurements for the simultaneous determination of the major species concentrations, mixture fraction and temperature revealed strong effects of turbulence-chemistry interaction in the form of local flame extinction and mixing without reaction. The thermo-chemical state of the flame varied significantly with the phase angle of the pressure oscillation. Simultaneously acquired 2D velocity and OH distributions by particle image velocimetry (PIV) and planar laser induced fluorescence (PLIF), respectively, gave an insight into the interaction between the vortical structures of the flow field and the reaction zones. The structure of the flame exhibits considerable changes during the thermoacoustic oscillation, which is shown in Fig. 2 for measurements in a transverse cross-section. In the OH-PLIF images, the reaction zone usually corresponds to the border between unburned gas (black) and 'young' OH (light gray to white). When pressure and accordingly heat release are near the minimum (Fig. 2a), chemical reaction takes place mostly in the inner recirculation zone. During times of high heat release (Fig. 2b), reaction zones are located along a large-scale spiral that extends over the entire cross-section. Similar structural changes are found in the velocity fields.

The main goals of the investigations were to gain a deeper understanding of the phenomena of periodic combustion and flow field instabilities in swirling flames and the establishment of a comprehensive data base for the validation of numerical combustion models.

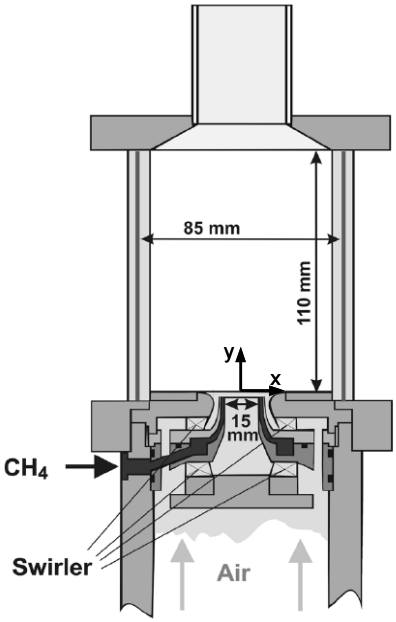

Fig.1: Schematic drawing of the gas turbine model combustor. Gaseous fuel (here CH_4) is injected into the swirler passages.

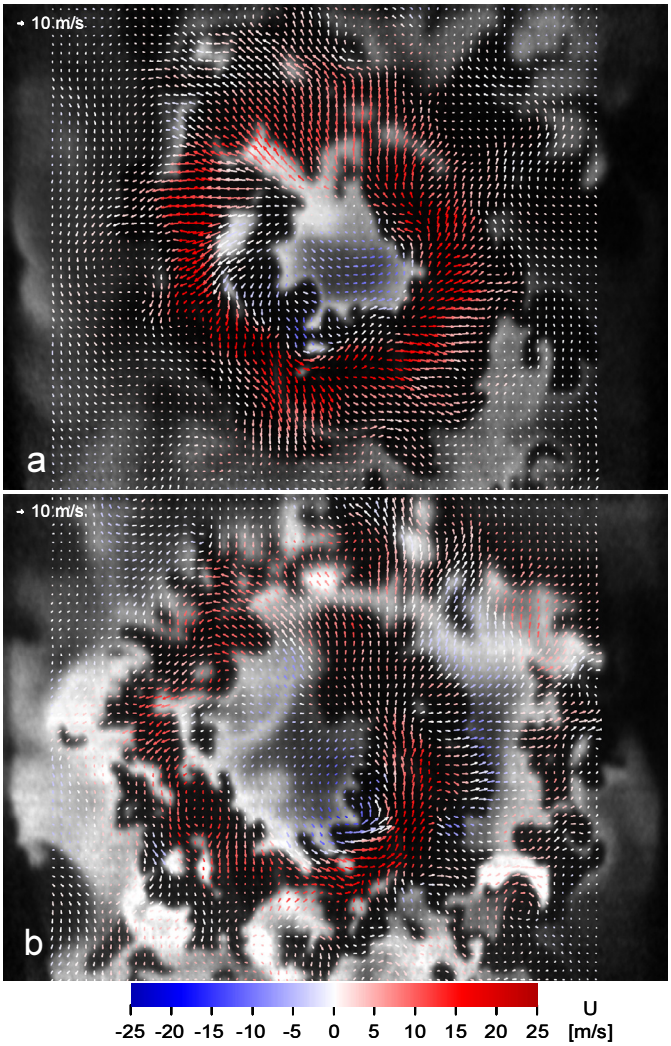

Fig. 2: Simultaneous Stereo-PIV and OH-PLIF measurements in the transverse cross-section at y=10 mm shown for 2 different phase angles of the thermoacoustic oscillation, corresponding to (a) low and (b) high rate of heat release. Vector colors represent the axial velocity. The field of view is 85×60 mm².

[1] P. Weigand, W. Meier, X.R. Duan, W. Stricker, M. Aigner; Investigations of Swirl Flames in a Gas Turbine Model Combustor. Part I: Flow Field, Structures, Temperatures and Species Distributions, Combust. Flame 144, 205-224 (2006)

[2] W. Meier, X.R. Duan, P. Weigand; Investigations of Swirl Flames in a Gas Turbine Model Combustor. Part II: Turbulence-Chemistry Interactions, Combust. Flame 144, 225-236 (2006)

Premixed and Stratified Flame Diagnostics Based on 3D Flame Orientation

Mark Sweeney[*+], *Simone Hochgreb*[+], *Robert Barlow*[§]
[+]Department of Engineering, University of Cambridge, UK
[§]Sandia National Laboratories, California, USA
[*]marksweeney@cantab.net

Stratified flames are common in many practical combustion applications, including gas turbines and IC engines. Despite this there remain many questions regarding the fundamental properties and behaviour of such flames. An investigation of the properties of turbulent premixed and stratified CH_4/air flames stabilized over a rectangular channel burner (Fig. 1) is presented. The data are obtained from multiscalar laser diagnostics (Fig. 2), consisting of simultaneous line imaging of Raman scattering, Rayleigh scattering, and two-photon laser induced fluorescence (LIF) of CO. The scalar information is combined with crossed-plane imaging of OH-PLIF to investigate the statistics of the progress of reaction c, the surface density function $|\nabla c|$, and the scalar dissipation $\chi_c = \alpha(T)|\nabla c|^2$.

A V-flame is stabilized by placing a rod parallel to the rectangular channels, just offset from the centreline. The flame front, defined as the location of maximum gradient in the OH profile normal to the flame front, is detected in each of the two intersecting images, using an augmented Canny edge detection routine with autonomous parameter selection. The parameter selection is performed using chi square tests to determine the smoothing and threshold levels which give the closest match to the physical flame front. This method gives increased robustness and accuracy over the use of a single parameter set chosen "a priori".

The crossed plane flame fronts are used to determine the 3D flame normal, and this is used to bin flame images based on the solid angle made between the normal and the axis of intersection of the planes. Two experimental cases are considered here: a premixed flame (fs1) at equivalence ratio 0.73 and a stratified flame (fs6) with equivalence ratios 0.37 and 1.1 in adjacent slots. The ratio u'/S_L in these flames is of the order unity, which is typical of V-flame experiments. Measurements were taken across the flame brush at different axial distances.

Preliminary findings are presented using distributions of curvature, temperature and progress variable for near-normal flames, defined as those flames with 3D normal angle of within 25° of the intersection axis (see Fig. 3). The progress variable is obtained for each set of line measurements as $c = (T - T_o) / (T_{eq}(\phi) - T_o)$, where T is the temperature at a given point, T_o is the minimum temperature found in the line measurements, and $T_{eq}(\phi)$ is the equilibrium temperature for CH_4/air at the locally measured equivalence ratio. $|\nabla c|$ and $|\nabla c|^2$ are obtained using central differencing to determine the gradient. The multiscalar line measurements have 104 μm spacing, and spatial averaging effects will be quantified and corrected as part of future work.

Figure 3 shows the distribution of values of the progress variable at the location of the detected flame front in the premixed and stratified flames at two downstream locations, 25 mm and 30 mm from the burner surface. These bracket the location where the centre of the flame brush crosses the centre of the mixing layer in flame fs6. The distributions of c at the detected flame front (maximum OH gradient) are nearly symmetric, with the stratified case demonstrating a positive shift in mean value with increasing downstream distance. The pdfs for both cases show similar mean values at the location nearer to the burner mouth. The stratified distributions are notably broader than the premixed counterparts. The mean equivalence ratio of the stratified flame brush decreases with downstream distance, and the observed shift of the intersection to higher c is qualitatively consistent with laminar premixed flame calculations, which show that the c value at the maximum OH gradient increases as the equivalence ratio of the flame decreases below 1.0.

The relationship between the surface density function $|\nabla c|$ and c is shown in Fig. 5. The conditional mean curves are plotted to give a clearer impression of the behaviour of the scatter data. Conditional means in the premixed and the stratified cases show similar trends. It is worth noting however that there is significantly more scatter in $|\nabla c|$ for a given c value in the stratified case. The results are presented using the uncorrected $|\nabla c|$ calculated along a line as well as an angle-corrected 3D flame-normal value, which is obtained by applying a 1/cosine factor. The general effect of the angle correction is to increase the mean value of $|\nabla c|$ at each c value, particularly in the range $0.1 < c < 0.8$. The mean premixed results (corrected and uncorrected) are shown against the results of laminar unstrained premixed CH_4/air flame calculations, using Chemkin with GRI-Mech 3.0. The experimental results for these low-turbulence-level flames show values very close to those expected from laminar (flamelet) calculations.

References:

P. Anselmo-Filho, S. Cant, S. Hochgreb, R. S. Barlow, *Experimental measurements of geometric properties of turbulent stratified flames*, 32nd International Symposium on Combustion, Montreal, Canada, 2008
R. S. Barlow, G. Wang, P. Anselmo-Filho, M. S. Sweeney, S. Hochgreb, *Raman/Rayleigh/LIF diagnostics in turbulent stratified flames*, 32nd International Symposium on Combustion, Montreal, Canada, 2008

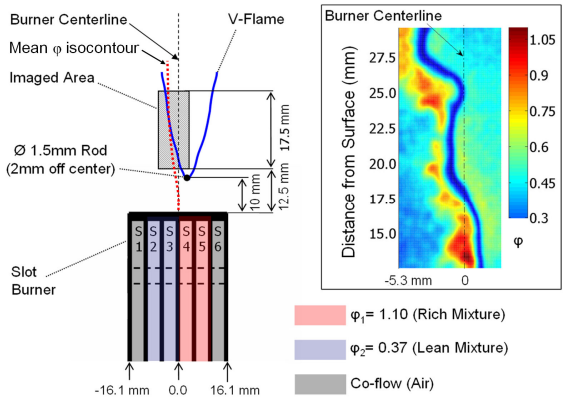

Fig. 1. Stratified V-flame configuration.

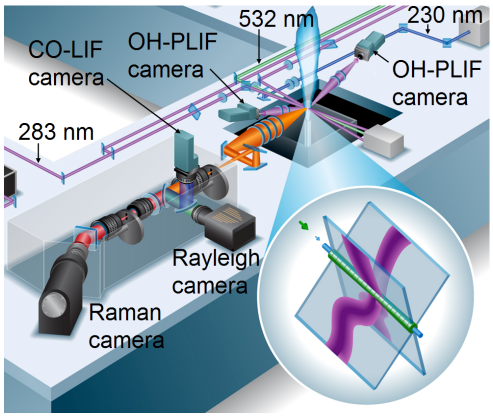

Fig. 2. Multiscalar diagnostic setup.

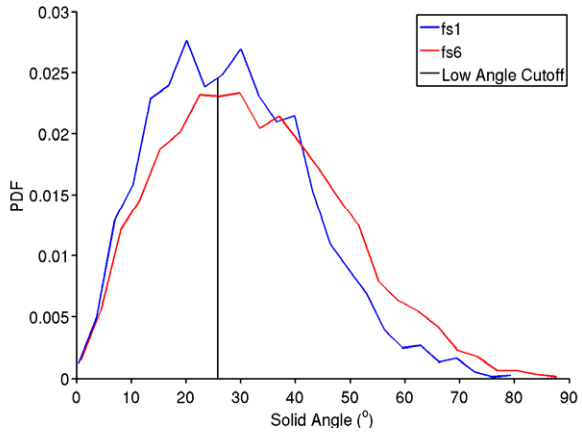

Fig. 3. Pdf of angle between 3D flame normal and the intersection axis, with low angle cutoff marked.

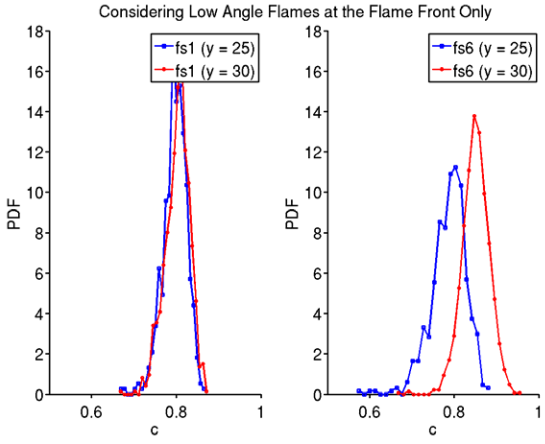

Fig. 4. Pdf of progress variable c for the premixed (fs1) and stratified (fs6) cases at y = 20 mm, 30 mm.

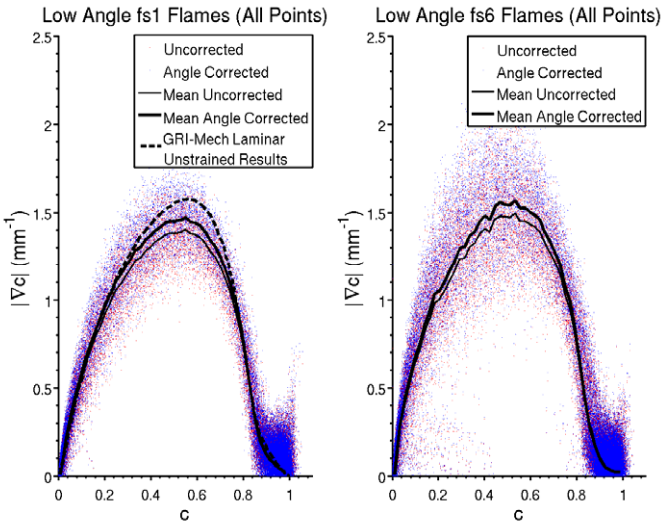

Fig. 5. Scatter plots and conditional means of $|\nabla c|$ vs. c for premixed (fs1) and stratified (fs6) cases. Red points are 1D uncorrected results, and blues points are angle-corrected 3D results.

Large Eddy Simulations - Conditional Moment Closure of forced ignition of a non-premixed methane bluff-body stabilised flame

A. Triantafyllidis[1*], E. Mastorakos[1], R. Eggels[2]
[1]*Cambridge University, UK;* [2]*Rolls Royce, Germany*
at419@cam.ac.uk

Introduction

Predicting the success or failure of a spark ignition event in a combustion chamber is of great importance in many engineering applications, such as industrial gas turbines and jet engines. The speed at which the flame propagates and the way the flow-field is influenced by the presence of the flame can greatly influence the design of a combustor, the size of which is determined by its ignition performance.

Large Eddy Simulations (LES) promise to offer accurate predictions of complicated transient phenomena. LES of an ignition sequence in a helicopter combustor has been performed by Boileau et al (2008). The Conditional Moment Closure (CMC) approach, proposed by Klimenko and Bilger (1999), has been formulated for LES by Navarro-Martinez et al (2005) who studied a steady jet flame. The main assumption in this model is that the sub-grid scale fluctuations of the reacting scalars can be directly correlated with those of a conserved scalar (the mixture fraction). The unsteady nature of the CMC model makes it a good candidate for the study of transient phenomena, such as ignition and flame propagation.

Here, the ignition process of a bluff-body burner, for which experimental results are available from Ahmed et al (2007), is assessed using LES combined with CMC. The fuel (pure methane) is injected radially through a $0.7mm$ slit which is situated $2mm$ before the exit of the bluff body. The full three-dimensional CMC equations are solved on a coarser grid than the LES, while a detailed chemical mechanism, introduced by Smooke et al (1986) involving 16 species and 25 reactions is used. The LES are performed using the Rolls-Royce in-house CFD code PRECISE, which has been used by James et al (2006) in studies of gas turbine combustion systems, while an in-house code is used to solve the CMC equations. This code is based on a RANS CMC code and has been used by Kim and Mastorakos (2006) to investigate an opposed-jet flame, as well as by De Paola et al (2008) in diesel engine simulations. The purpose of this work is to investigate whether it is possible to capture the qualitative behaviour of an igniting non-premixed flame, as well as to study the effects of the flame on the flow-field.

Results

Due to the importance of the mixing field in the success of ignition and the behaviour of the flame, simulations of the inert flow were performed first. Figure 1(a) shows radial profiles of the mean axial velocity at different distances from the bluff-body, obtained using three different grids, compared with experimental data, obtained by Laser Doppler Velocimetry (LDV). The agreement of the predictions with the experimental data is good, independently of the grid used, which implies that the velocity field is not sensitive to the resolution of the grid. Similar agreement has been observed for the mean radial velocity and for the fluctuations of the axial and radial velocities.

The mixing field is best characterised by the distribution of the mixture fraction ξ. Comparison of the radial profiles of the mean and the rms of its fluctuations with experimental data show that the distribution of the mixture fraction is more sensitive to the resolution of the grid than that of the velocity. The key structures of the flow were captured (size of re-circulation zone and small mixture fraction fluctuations inside it), but the peak value of the mixture fraction in the exit of the bluff-body is over-estimated which causes an over-estimation of the value inside the re-circulation zone. This implies that the break-up of the fuel jet, which takes place in a very thin region before the exit of the bluff-body and is crucial for the correct simulation of the flow, is not captured correctly. This could be due to the lack of resolution, lack of a wall function since the fuel jet flows next to the bluff-body wall or lack of realistic turbulence levels. In order to improve the results of the simulation, the degree of mixing before the exit of the bluff-body was artificially increased by decreasing the value of the mixture fraction at the fuel inlet and increasing the velocity, thus maintaining the same total fuel-to-air ratio. It must be stressed that this was done because the focus of this work is the study of the combustion phenomena behind the bluff body and not the break-up of the fuel jet. Figure 1(b) shows radial profiles of the mean mixture fraction using a value of $\xi = 0.30$ at the inlet of the fuel jet. It can be seen that the agreement with the experimental data has improved, especially in the re-circulation zone.

The ignition simulations are performed on the normal grid, with $\xi = 0.30$ in the inlet of the fuel jet. Figure 2 shows preliminary results from an ignition simulation with the spark located in the shear layer. Initially it follows

the stoichiometric contour, while later (30ms) it appears that the flame has moved, mostly by convection towards the re-circulation zone. A similar behaviour has been observed in the experiment.

References

Ahmed, S. F. & Balachandran, R. & Marchione, T. & Mastorakos, E. (2007). Spark ignition of turbulent non-premixed bluff-body flames. *Combustion and Flame.* **151**, 366–385.

Boileau, M. & Staffelbach, G. & Cuenot, B. & Poinsot, T. & Berat, C. (2008). LES of an ignition sequence in a full helicopter combustor. *Combustion and Flame.* **152**, to appear.

De Paola, G & Mastorakos, E. & Wright, Y. M. & Boulouchos, K. (2008). Diesel engine simulations with multi-dimensional Conditional Moment Closure. *Combustion Science and Technology.* **180**, to appear.

James, S. & Zhu, J. & Anand, M. S. (2006). Large-eddy simulations as a design tool for gas turbine combustion systems. *AIAA Journal.* **44**, 674–686.

Kim, I. S. & Mastorakos, E. (2006). Simulations of turbulent non-premixed counterflow flames with first-order conditional moment closure. *Flow, Turbulence and Combustion.* **76**, 133–162.

Klimenko, A. Y. & Bilger, R. W. (1999). Conditional Moment Closure for turbulent combustion. *Progress in Energy and Combustion Science.* **25**, 595–687.

Navarro-Martinez, S. & Kronenburg, A. & Di Mare, F. (2005). Conditional Moment Closure for Large Eddy Simulations. *Flow, Turbulence and Combustion.* **75**, 245–274.

Smooke, M. D. & Puri, I. K. & Seshadri, K. (1986). A comparison beween numerical calculations and experimental measurements of the structure of a counterflow diffusion flame burning diluted methane in diluted air. *Proceedings of the Combustion Institute.* **21**, 1783–1792.

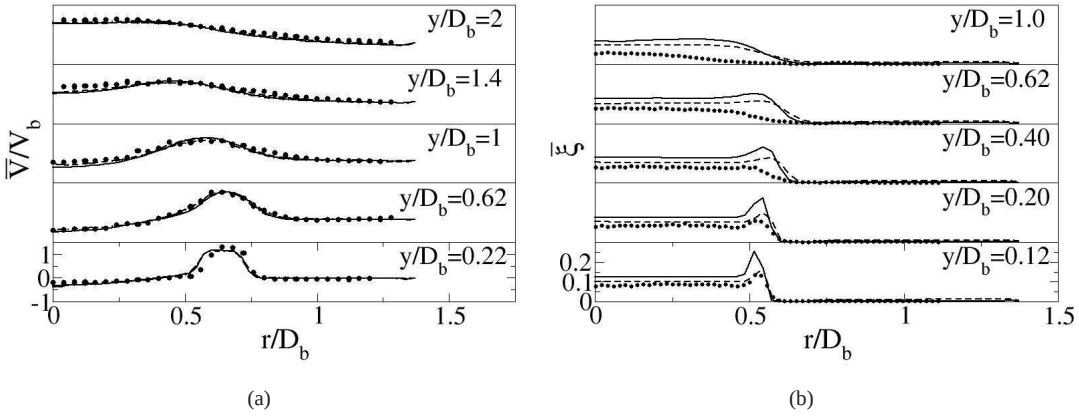

(a) (b)

Figure 1: Radial profiles of (a) the mean axial velocity at different axial distances bluff-body. Dots: experimental data, dashed line: coarse rid, solid line: normal grid, dot-dashed line: fine grid, (b) the mean mixture fraction at different axial distances from the bluff-body using the normal grid. Dots: experimental data, dashed line: $\xi = 0.3$ at the fuel inlet, solid line: $\xi = 1$ at the fuel inlet.

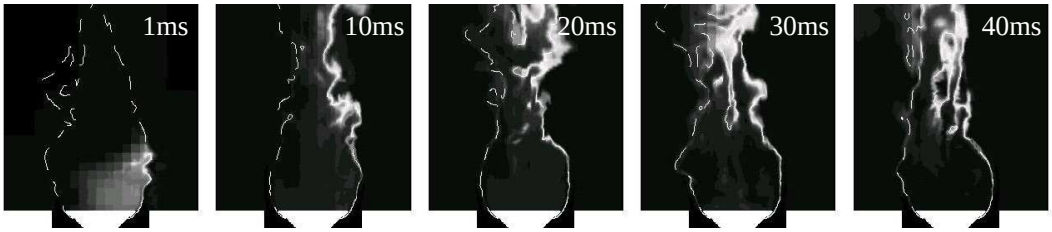

Figure 2: Time evolution of the unconditional temperature. Contour: black:300K, white: 2100K, dashed line: stoichiometric mixture fraction.

Hybrid Binomial Langevin-MMC Modeling of a Reacting Mixing Layer

Andrew P. Wandel, R. Peter Lindstedt
a.wandel@imperial.ac.uk, p.lindstedt@imperial.ac.uk
Department of Mechanical Engineering, Imperial College of Science, Technology and Medicine,
Exhibition Road, London SW7 2BX, United Kingdom

A new hybrid model has been devised combining the strengths of the binomial Langevin [1] and Multiple Mapping Conditioning (MMC) [2] closures. In the binomial Langevin model, the joint velocity-scalar Probability Density Function (PDF) is solved, accounting for velocity-scalar interactions. The MMC model transports all reactive scalars, avoiding the difficulties involved with specifying non-trivial bounds in the binomial Langevin model. Interactions between the two components are as follows. The velocity in MMC is set to be the velocity from the binomial Langevin solution, necessary for self-consistency of both. The velocity is used to determine the reference variable for MMC, obviating the need for some closures. The scalar mixing in the MMC model (using the Modified Curl's model [3, 4]) keeps the mixture fraction in the MMC model as close as possible to the pseudo-mixture fraction in the binomial Langevin model. Finally, feedback to the binomial Langevin component comes via the usual means—the new density field post-combustion. This model is tested in comparison to a reacting shear layer [5].

H̊ulek and Lindstedt [6] developed a generalized form of the binomial Langevin model [1] for the joint-PDF of velocity and multiple scalars. The model for velocity (u_i) transport (including the turbulent kinetic energy dissipation ε, the return-to-isotropy of the Reynolds stresses and dispersion in velocity space) is given for a stochastic particle p:

$$du_i^p = (\alpha_1\delta_{ij} + \alpha_2 b_{ij})\left(u_j^p - \langle u_j\rangle\right)\frac{dt}{\tau_u} + (C_0\langle\varepsilon\rangle)^{1/2} dw_i \,. \tag{1}$$

The turbulent kinetic energy is k, $\tau_u = \langle k\rangle/\langle\varepsilon\rangle$, w_i is a Wiener process, b_{ij} is the Reynolds stress anisotropy tensor and the constants are α_1, α_2 and $C_0 = 2.1$. The modeled stochastic differential equation for the pseudo-mixture fraction η is

$$d\eta^p = \frac{G_\eta}{2\tau_\eta}\left(\eta^p - \langle\eta\rangle\right)dt + \left(B_\eta\langle\varepsilon_\eta\rangle\right)^{1/2} dw_{\text{bin}} \tag{2}$$

where dw_{bin} is a binomial Wiener process and the mean scalar dissipation is modeled as $\langle\varepsilon_\eta\rangle \equiv \left\langle\eta'^2\right\rangle/\tau_\eta$, with the scalar timescale modeled as $\tau_\eta = \frac{1}{2}\tau_u$. The drift and diffusion coefficients are G_η and B_η [6]. It is well known that the solution of Eq. (2) is difficult for scalars with non-trivial bounds. This is avoided in the current implementation by only solving a pseudo-mixture fraction.

The MMC transport equations for mixture fraction Z, its reference variable ξ and reactive scalar Y are:

$$d\mathbf{x}^p = \mathbf{U}dt; \qquad d\xi^p = Adt + (2B)^{1/2}dw \tag{3}$$

$$dZ^p = Sdt; \qquad dY^p = (S+W)dt \tag{4}$$

where A and B are drift and diffusion coefficients, dw is a Wiener process, S is a micro-mixing model, and W the source term. The velocity is modeled as [2]:

$$\mathbf{U} = \langle\mathbf{u}\rangle + \left(\langle\mathbf{u}'Z'\rangle/\langle\xi'Z'\rangle\right)\xi \,. \tag{5}$$

The following is a summary of the hybrid model [7]. To ensure self-consistency, $\mathbf{U} = \mathbf{u}$. The reference variable may be modeled as the inverse of Eq. (5):

$$\xi^p = \left(u_2^p - \langle u_2\rangle\right)\left\langle u_2'^2\right\rangle^{-1/2} \,. \tag{6}$$

Only component 2 is important in the current flow.

The Modified Curl's model [3, 4] was applied for S and pairs of particles selected so that they are close in reference space (thereby maintaining locality):

$$|\Delta\xi^{pq}| \le (B\Delta t)^{1/2} \tag{7}$$

where $\Delta\xi^{pq}$ represents the difference in ξ between particles p and q. This process mimics the diffusive term of a stochastic differential equation [e.g. Eq. (2)], where the average diffusion distance is of the order of $(B\Delta t)^{1/2}$ and the particles interact at the new location. The conventional model for B is used [2].

All particles mix and a least-squares analysis was used to set the amount of mixing to minimize

$$|Z^p - \eta^p| + |Z^q - \eta^q| \,, \tag{8}$$

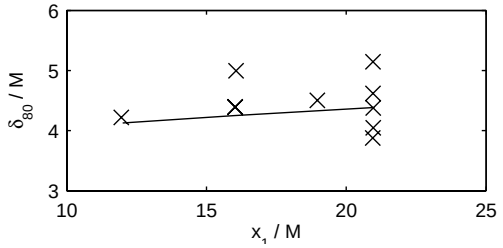

Figure 1: Spread of mean mixture fraction profile. Hybrid, —; experiment [5], ×

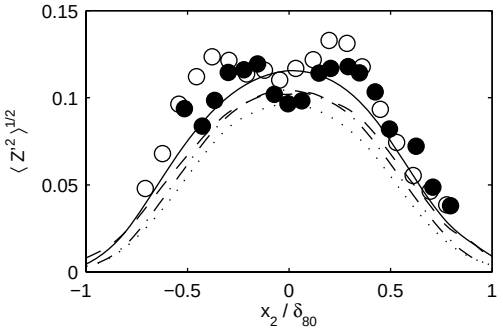

Figure 2: Mixture fraction standard deviation profiles. Hybrid: Da = 2.56: $x_1/M = 16$, —; 21, – –; Da = 0.42: $x_1/M = 16$, – ·; 21, · · ·. Experiment [5]: $x_1/M = 21$, ○; Da = 2.56, empty; Da = 0.42, filled

keeping the mixture fractions from the two component models as close to each other as possible.

The experiment chosen for comparison is a chemically-reacting scalar mixing layer behind a turbulence-generating grid [5]. The streamwise direction is denoted by x_1, with the cross-stream direction x_2 and the origin at the end of the splitter plate. The spreading rate is within the experimental scatter (Fig. 1) as is the mean mixture fraction [7].

The mixture fraction standard deviation is shown in Fig. 2 and it can be seen that the hybrid model is similar to the experiment, but lower and without the central dip. Trends with Damköhler number (Da) and downstream location are reproduced.

The mean mole fractions of the reactants are shown for $x_1/M = 21$ in Fig. 3, where it can be seen that the mean values are predicted quite accurately.

The values of the covariance of the reactants are reported in Fig. 4. The modeled results are narrower than the experiment, but the peaks are estimated well as are the trends with varying parameters.

The relatively simple Modified Curl's model implemented in this hybrid binomial Langevin-MMC model provided encouraging results.

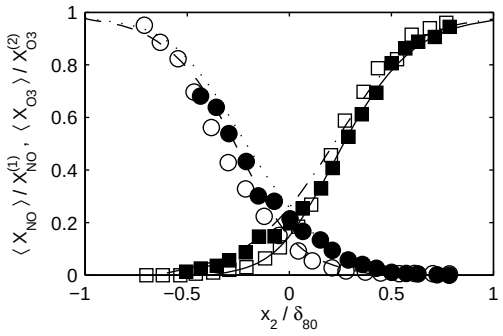

Figure 3: Species mole fraction mean profiles at $x_1/M = 21$. Hybrid: Da = 2.56: — and – –; Da = 0.42: – · and · · ·. Experiment [5]: Da = 2.56, empty; Da = 0.42, filled

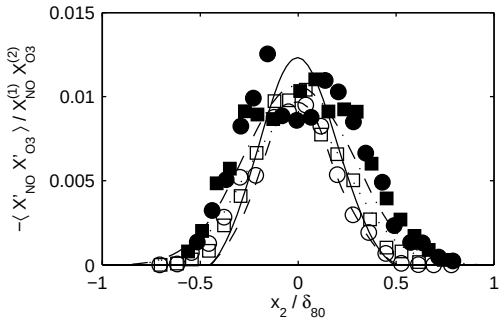

Figure 4: Species mole fraction covariance profiles. As per Fig. 2 with experiment [5] $x_1/M = 16$, □

EPSRC grant GR/T22766 funded this work.

References

[1] L. Valiño and C. Dopazo, Physics of Fluids A **3**, 3034 (1991).

[2] A. Y. Klimenko and S. B. Pope, Physics of Fluids **15**, 1907 (2003).

[3] C. Dopazo, Physics of Fluids **22**, 20 (1979).

[4] J. Janicka, W. Kolbe, and W. Kollmann, J. Non-Equilib. Thermodyn. **4**, 47 (1979).

[5] R. W. Bilger, L. Saetran, and L. Krishnamoorthy, Journal of Fluid Mechanics **233**, 211 (1991).

[6] T. H̊ulek and R. P. Lindstedt, Combustion Science and Technology **136**, 303 (1998).

[7] A. P. Wandel and R. P. Lindstedt, Submitted to Physics of Fluids (2008).

Second-order Accurate Splitting Schemes for Monte Carlo Particle Methods

Haifeng Wang*, Pavel P. Popov, Stephen B. Pope

Sibley School of Mechanical and Aerospace Engineering,
Cornell University, Ithaca, NY 14853, USA

Lagrangian Monte Carlo particle methods [1] have been extensively used for solving the PDF transport equation (or FDF transport equation in the context of LES) in turbulent combustion. In the composition PDF or FDF method, the following set of stochastic differential equations (SDEs) is integrated for each particle

$$d\mathbf{X}(t) = \mathbf{D}\left(\mathbf{X}[t],t\right)dt + \sqrt{2B\left(\mathbf{X}[t],t\right)}d\mathbf{W} \tag{1}$$

$$d\phi(t) = S\left(\phi[t],\mathbf{X}[t],t\right) \tag{2}$$

where $\mathbf{X}(t)$ and $\phi(t)$ are the particle position vector and compositions, $\mathbf{D}\left(\mathbf{X}[t],t\right)$ and $B\left(\mathbf{X}[t],t\right)$ are the drift velocity and diffusivity of particles, respectively, $S\left(\phi[t],\mathbf{X}[t],t\right)$ denotes source terms for compositions (e.g., reaction rate, mixing rate), and $\mathbf{W}$ is an isotropic vector-valued Wiener process. The numerical integration of Eq. (1) is much more difficult than that of ordinary differential equations (ODEs). All the well used second-order integration schemes for ODEs degrade to low order of accuracy when used in SDEs, and even worse lead to inconsistent schemes because (most) ODE schemes violate the non-anticipatory property of Ito SDEs. Cao and Pope [2] developed a second-order integration scheme for Eq. (1). In this work we consider the coupling of Eqs. (1) and (2), and develop different weak second-order splitting schemes for the coupled system. To the authors' knowledge, no second-order splitting schemes have previously been developed for solving the above SDEs, and have been applied in RANS/PDF or LES/FDF practice.

Monte Carlo particle methods converge slowly (the statistical error scales as $1/\sqrt{N}$, where N is the number of particles), so a large number of particles are required to reduce the statistical error to the specified level. It is estimated that, in order to demonstrate the numerical convergence with respect to time, the number of particles required is on the order of Δt^{-5}, where Δt is the time step size, so it is not feasible to perform calculations at very small time steps. To facilitate the tests in this work, the parallel computation is conducted to reduce the overall simulation time.

In order to demonstrate weak p-th order accuracy of a given scheme, we need to show the following asymptotic behavior of the numerical error ε

$$\varepsilon = \left|\left\langle f\left(\mathbf{Y}[t],\psi[t],t\right)\right\rangle - \left\langle f\left(\mathbf{X}[t],\phi[t],t\right)\right\rangle\right| \le C\Delta t^p \tag{3}$$

where f is a function (f is chosen to be ϕ and ϕ^2 in this study), $\mathbf{Y}[t]$ and $\psi[t]$ are numerical solutions to $\mathbf{X}[t]$ and $\phi[t]$, respectively, and C is a constant independent of Δt. $\left\langle f\left(\mathbf{Y}[t],\psi[t],t\right)\right\rangle$ can be estimated from the numerical simulation, while $\left\langle f\left(\mathbf{X}[t],\phi[t],t\right)\right\rangle$ is unknown. In this work, we developed a method of manufactured solution (MMS) [3] for the Monte Carlo particle methods. Manufactured solutions to the (augmented) transport equations of scalar mean $\overline{\phi}$ and scalar square mean $\overline{\phi^2}$ are specified. Extra source terms are required in these transport equations so that they admit the specified

* Corresponding author. Email: hw98@cornell.edu

solutions. The particle scalar equation (2) is modified to account for the extra source terms from the manufactured solutions. The modified SDEs are solved numerically and the manufactured solutions are used as exact solutions to estimate the numerical errors in Eq. (3). The advantage of MMS is that it retains sufficient complexity of the problem so as to be representative and still the exact solution is available. MMS is very useful for the verification of code development and validation of different numerical algorithms.

Different splitting schemes are discussed and compared in [4]. The straightforward combination of the Cao & Pope second-order scheme [2] to Eq. (1) and Strang splitting to scalar Eq. (2) leads to only weak first order convergence (as shown in Fig. 1(a)) although each equation is integrated with weak second-order schemes. As shown in [4], weak second-order splitting can be achieved by performing two full transport steps in one time step (Fig. 1(b)), by putting transport in the middle of Strang splitting (Fig. 1(c)), or by obtaining a modified transport predictor for scalar evolution.

[1] S.B. Pope (1985) ``PDF methods for turbulent reactive flows," *Progress in Energy and Combustion Science*, 11, 119-192.

[2] R. Cao and S.B. Pope (2003) ``Numerical integration of stochastic differential equations: weak second-order mid-point scheme for applications in the composition PDF method," *J. Comput. Phys.*, 185, 194-212.

[3] P.J Roache (2000) ``Code verification by the method of manufactured solutions," *Transactions of the ASME*, 124, 4-10.

[4] H. Wang, P.P. Popov, S.B. Pope (2008) ``Second-order splitting schemes for Monte Carlo particle methods," *J. Comput. Phys.*, (in preparation)

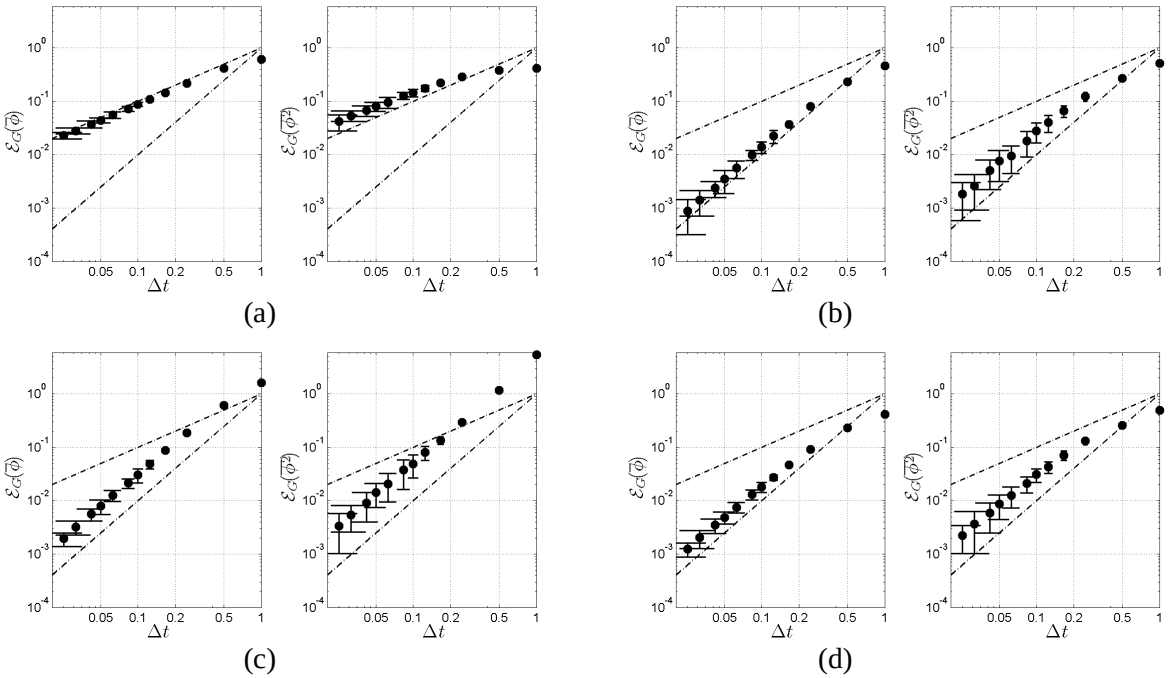

Fig. 1 Convergence of different splitting schemes (the slopes of the reference lines are 1 and 2). (a) PRED-SCALAR-CORR; (b) PRED / CORR - SCALAR - PRED / CORR; (c) SCALAR - PRED / CORR - SCALAR; (d) PRED / PRED2 - SCALAR - CORR, where PRED and CORR are the predictor and corrector steps of Cao & Pope Scheme, SCALAR denotes Strang splitting of scalar step, PRED2 is a modified predictor step of Cao & Pope scheme to achieve weak second-order convergence.

Effect of Air-Side vs. Fuel-Side Dilution on NOx Emissions in Turbulent Hydrogen Jet Diffusion Flames

Nathan T. Weiland – National Energy Technology Laboratory, Pittsburgh, PA
Peter A. Strakey* - National Energy Technology Laboratory, Morgantown, WV
** corresponding author e-mail: peter.strakey@netl.doe.gov*

Lean-Direct-Injection (LDI) style combustion [1] is being considered at NETL as a means to attain low NOx emissions in a high-hydrogen gas turbine combustor. IGCC plant designs can create this high-hydrogen fuel with a water-gas shift reactor and subsequent separation and storage of the CO_2, while producing a roughly equal volume of byproduct nitrogen in the gasifier's air separation unit to help reduce peak flame temperatures and NOx in the diffusion flame combustor [2]. Placement of this diluent in either the air or fuel streams is a matter of practical importance, and has not been studied to date for LDI combustion. Current practice in swirl-based syngas diffusion flame combustors, however, is to place the diluent in the air stream to avoid adding to the already large fuel manifold requirements brought about by the low specific heating value of the syngas fuel [3]. The current work in progress discusses how diluent placement affects diffusion flame temperatures, residence times, and stability limits. In each case, it is shown that dilution of the fuel stream in LDI-style combustion is more preferable to air-side dilution from a NO_x emissions perspective.

Calculated adiabatic flame temperatures for different types of flames and dilution scenarios are presented as a function of overall combustor equivalence ratio in Figure 1. For each level of nitrogen diluent available, premixed flame temperatures also represent fully mixed diffusion flame combustor exit temperatures, where the peak diffusion flame temperatures, which control thermal NOx formation, are also shown for air- and fuel-side nitrogen dilution. In order to achieve the desired turbine inlet temperatures, the combustor must operate at an overall equivalence ratio of $\Phi \approx 0.5$, so that there is twice as much air as is needed for complete combustion. Thus, if the diluent is added to the combustion air, only half of it will arrive at the flame front compared to the fuel-dilution case, where all of the diluent must pass through the flame front with the fuel, thereby reducing flame temperature and hence NOx formation. If the diluent is injected separately into the combustor, there are no guarantees that all of it will arrive at the flame front, and higher flame temperatures may result. From a flame temperature perspective then, greater NOx reduction should be attainable with fuel-dilution rather than air- or independent-dilution in any diffusion flame combustor. However, as the equivalence ratio increases towards unity, it becomes irrelevant whether the fuel or air is diluted, as all of the diluent must arrive at the flame front in either case. This is why, in swirl-based syngas diffusion flame combustors operating near stoichiometric conditions, it has been found that the effects of air or fuel-side dilution are irrelevant [4].

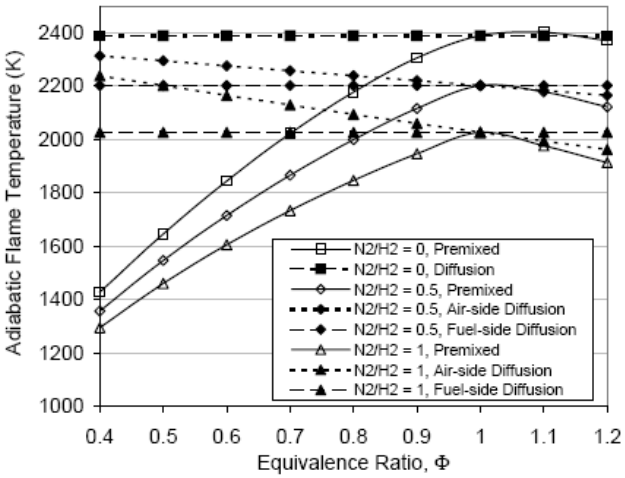

Figure 1: Adiabatic flame temperatures for premixed and diffusion flames with varying N_2/H_2 dilution ratios

A basic LDI combustor can be modeled as an array of simple jet flames in which residence time NO_x scaling relationships apply. A characteristic residence time for a simple jet flame is $L_f^3/U_0 d_0^2$, where the flame length cubed, L_f^3, is proportional to the flame volume, U_0 is the jet exit velocity and d_0 is the jet exit diameter [5]. Gabriel et al. have shown that for pure and diluted hydrogen jet flames, the NO_x emission index ($EINO_x$), normalized by this residence time, is proportional to the square root of the global strain rate of the flame, $(U_0/d_0)^{1/2}$ [5]. The flame length for a momentum-dominated jet flame can be expressed as $L_f \propto d_0(\rho_0/\rho_a)^{1/2}/f_s$, where ρ_0 is the jet exit density, ρ_a is the air density, and f_s is a stoichiometric mixture fraction [6]. Substitution yields the following scaling for the NO_x emissions from a simple jet flame:

$$EINO_x \propto \left(d_0/U_0\right)^{1/2}\left(\rho_0/\rho_a\right)^{3/2}/f_s^3 \tag{1}$$

The stoichiometric mixture fraction for a pure hydrogen fuel burning in ambient air is $f_s = 0.03$. Adding an equal part of nitrogen to the fuel stream yields $f_s = 0.30$, while adding this same quantity of nitrogen to the air stream yields $f_s = 0.02$. Substituting these numbers into Eq. (1) clearly shows that NO_x production for fuel-side dilution is much smaller than for air-side dilution. This is essentially a stoichiometry effect, where dilution of the fuel jet results in less air entrainment required for complete combustion and hence a smaller flame, whereas dilution of the air means a larger air entrainment requirement and a subsequently larger flame, with longer residence times and higher thermal NO_x generation.

In a more realistic LDI combustor, the air flow can used to increase mixing and reduce the flame volume, residence time, and hence thermal NOx generation in various configurations. In addition, with staged air combustion, dilution of the primary combustion air at $\Phi \geq 1$ should result in full use of the diluent for purposes of reducing the peak flame temperature, as shown in Figure 1. Indeed, preliminary experimental results show that for a simple coaxial air arrangement, movement of the nitrogen diluent from the coaxial air stream to the hydrogen fuel stream results in at most a 10% reduction in NO_x, as shown in Figure 2.

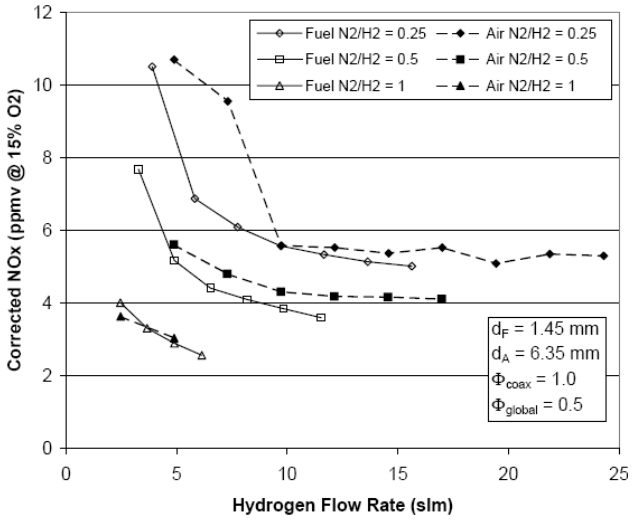

Figure 2: Effect of air- vs. fuel-side nitrogen dilution on global NO_x emissions in a coaxial air flame

However, differential diffusion of hydrogen out of a diluted hydrogen/nitrogen fuel jet creates regions of higher hydrogen content in the immediate vicinity of the fuel injection point than can be attained with dilution of the air stream. In the case of the coaxial air flame, the lip thickness of the fuel tube provides a recirculation region for flameholding, in which hydrogen preferentially diffuses out of the fuel jet to provide a hydrogen-rich flame anchoring point on the outside rim of the fuel tube. Since these low diluent concentration regions cannot be attained with coaxial air dilution, fuel dilution is found to extend the operating envelope to areas with higher coaxial air velocity, where faster mixing rates further reduce flame residence times and NOx emissions with fuel-side dilution.

References

1. Marek, C. J., Smith, T. D., and Kundu, K., "Low Emission Hydrogen Combustors for Gas Turbines Using Lean Direct Injection," AIAA-2005-3776, 41st Joint Propulsion Conference and Exhibit, Tuscon, Arizona, July 10-13, 2005.
2. Chiesa, P. Lozza, G., and Mazzocchi, L., "Using Hydrogen as Gas Turbine Fuel," Journal of Engineering for Gas Turbines and Power, 127:73-80, 2005.
3. Todd, D. M., "Gas Turbine Improvements Enhance IGCC Viability," Gasification Technologies Conference, San Francisco, California, October 8-11, 2000.
4. Cook, C. S., Corman, J. C., Todd, D.M., "System Evaluation and LBTU Fuel Combustion Studies for IGCC Power Generation," *ASME J. Eng. Gas Turbines and Power*, 117:673-677, 1995.
5. Gabriel, R., Navedo, J. E., and Chen, R.-H., "Effects of Fuel Lewis Number on Nitric Oxide Emission of Diluted H_2 Turbulent Jet Diffusion Flames," *Combust. Flame*, 121:525-534, 2000.
6. Delichatsios, M. A., "Transition from Momentum to Buoyancy-Controlled Turbulent Jet Diffusion Flames and Flame Height Relationships," *Combust. Flame*, 92:349-364, 1993.

DNS of a Turbulent Lifted Ethylene/Air Jet Flame in an Autoignitive Coflow – Stabilization and Flame Structure

C. S. Yoo[1,*], E. S. Richardson[1], R. Sankaran[2], and J. H. Chen[1]
[*]Corresponding author: csyoo@sandia.gov

[1]Combustion Research Facility, Sandia National Laboratories, Livermore, CA94551-0969, USA
[2]National Center for Computational Sciences, Oak Ridge National Laboratories, Oak Ridge, TN 37831-6008, USA

Introduction

In many modern combustion systems such as diesel engines or direct injection stratified gasoline engines and gas turbines, fuel is injected into an environment of hot gases such that a flame may be stabilized through the recirculation of hot air and combustion products. Under such conditions, this leads to a turbulent lifted flame, and the hot environment admits the possibility of auto-ignition as a mechanism contributing to the stabilization of the flame base. In addition to auto-ignition, flame propagation and the role of large eddies have been considered as possible mechanisms for stabilization of the lifted flame base[1]. In our previous 3-D direct numerical simulation (DNS) study of a turbulent lifted hydrogen/air jet flame in an autoignitive coflow, it was found that the lifted flame base forms a cycle with the passage of large-scale jet structure and the stabilization is determined by the competition between local axial velocity and auto-ignition that occurs in fuel-lean mixtures[2]. We have recently performed 3-D DNS of a turbulent lifted ethylene/air jet flame in an autoignitive heated coflow to examine the stabilization mechanisms and flame structure of a hydrocarbon fuel jet flame.

Problem configuration

The spatially-developing turbulent lifted jet flame simulation was performed in a 3-D slot-burner configuration. Fuel issues from a central jet, which consists of 18% ethylene (C_2H_4) and 82% nitrogen by volume at an inlet temperature of T_j = 550K. The central jet is surrounded on either side by co-flowing heated air streams at T_c = 1,550K and atmospheric pressure. The fuel jet and coflow velocities are specified as U_j = 204 m/s and U_c = 20 m/s, and the fuel jet width, H, is 2 mm such that the jet Reynolds number, Re_j (= HU_j/ν), is approximately 10,000. The computational domain is $15H \times 20H \times 3H$ in the streamwise, x, transverse, y, and spanwise, z, directions with 2025 × 1600 × 400 grid points. A uniform grid spacing of 15μm is used in the x- and z-directions, while an algebraically stretched mesh is used in the y-direction.

The compressible Navier-Stokes, species continuity, and total energy equations were solved using the Sandia DNS code, S3D, with a 4th-order Runge-Kutta method for time integration and an 8th-order central differencing scheme for spatial discretization. We adopted a reduced ethylene/air kinetic mechanism which consists of 22 species and 18 global reaction steps (T. Lu and C. K. Law, private communication, 2007). Nonreflecting inflow/outflow boundary conditions[3] were used in the x- and y-directions and periodic boundary conditions were applied in the homogeneous z-direction. Based on the fuel jet velocity and the streamwise domain length, a jet time, $\tau_j = L_x/U_j$, is approximately 0.15ms. To obtain a stationary lifted flame while saving computational cost, a simulation with a grid resoution of 40μm was first performed through $10\,\tau_j$. The solution from that simulation was then interpolated to 15μm and used as an initial condition for the fully resolved simulation. The solution was advanced at a constant time-step of 5ns through $1.0\,\tau_j$. The fine-mesh simulation was performed on the Cray XT4 at Oak Ridge National Laboratories and required 2.0 million CPU-hours running for approximately 3 days on 30,000 processors.

Results and Discussion

Figure 1 shows isocontours of temperature, heat release rate, and OH mass fraction on the stoichiometric mixture fraction isosurface, ξ_{st} = 0.2741. Downstream of the high scalar dissipation region, temperature starts to increase at x/H = 6, following the increase in the heat release rate. The downstream development of the reacting planar jet flame is manifested in the profiles of the Favre mean axial velocity and the axial evolution of the jet half-width, $\delta_{1/2}$, the Favre mean temperature, and the centerline axial velocity presented in Fig. 2. Note that the axial velocity profile becomes self-similar downstream of x/H = 7, and $\delta_{1/2}$ increases faster than the rate at which the centerline axial velocity decreases. This is because $\delta_{1/2}$ increases as the shear layer develops right after the fuel jet nozzle, but the mean velocity does not change significantly due to thermal expansion and turbulent mixing. Global characteristics of the lifted flame represented by the Favre mean temperature and heat release rate are presented in Figure 3. Unlike the

hydrogen/air lifted jet flame[1], the mean heat release rate starts to increase in the middle of the shear layer. This is attributed not only to the large stoichiometric mixture fraction of the present flame relative to the hydrogen flame, but also to differences in the ignition characteristics of an ethylene/air mixture.

The stabilization mechanism of the present ethylene/air lifted jet flame is further investigated by tracking Lagrangian fluid particles for several flow through times. Tracer particle methods are commonly used to gain fundamental understanding of intermittent flow and flame physics[4]. The particles will provide the time history of the aero-thermo-chemical conditions that a given fluid parcel undergoes while being advected through the domain. In particular, it will provide the temporal trajectory of a given localized ignition site as it traverses oncoming turbulence intermittency, thus providing valuable lagrangian velocity-scalar statistics for models of autoignitive flows.

References

1. K. M. Lyons, *Prog. Energy Combust. Sci.* **33**, 211–231, 2007.
2. C. S. Yoo, R. Sankaran, and J. H. Chen, *J. Fluid Mech*., submitted, 2008.
3. C. S. Yoo and H. G. Im, *Combust. Theory Modelling* **11**, 259–286, 2007.
4. P. Sripakagorn, G. Kosaly, and J. J. Riley, *Combust. Flame* **136**, 351-363, 2004.

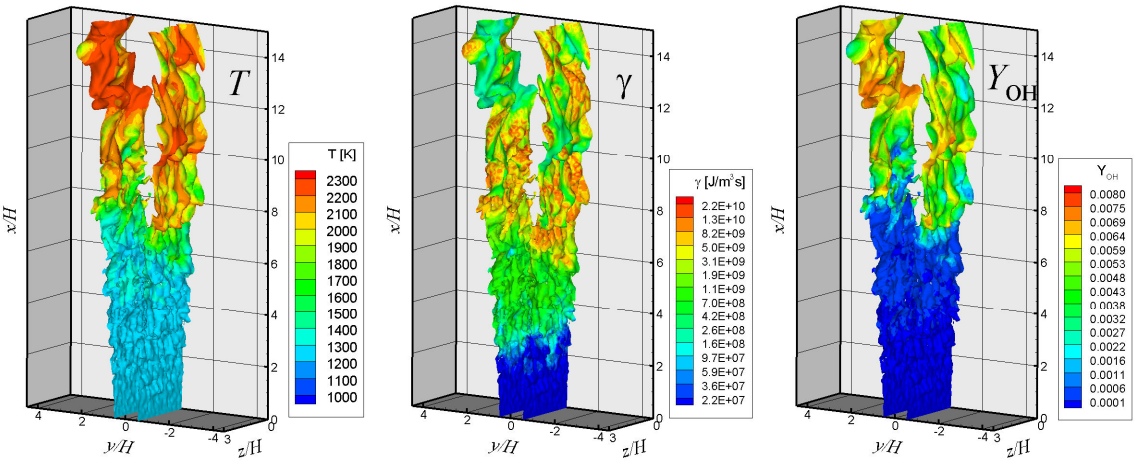

Figure 1. Instantaneous isocontours of temperature, heat release rate, and OH mass fraction on the stoichiometric mixture fraction isosurface, ξ_{st}.

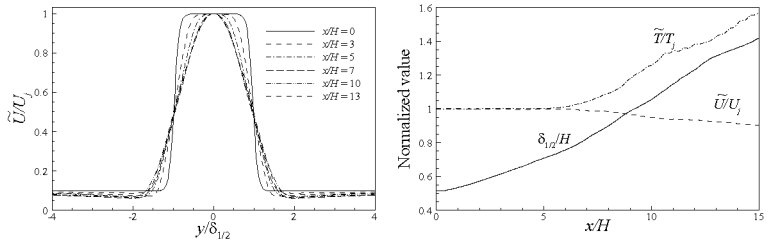

Figure 2. Profiles of the Favre mean axial velocity at different axial locations (left), and axial evolution of the jet half-width and Favre means of temperature and axial velocity at the centerline (right).

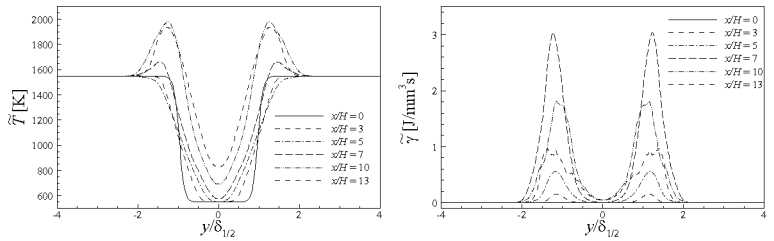

Figure 3. Profiles of the Favre means of temperature (left) and heat release rate (right) at different axial locations.

SOOT VOLUME FRACTION IMAGING IN A TURBULENT NONPREMIXED ETHYLENE JET FLAME BY QUANTITATIVE 2D LASER-INDUCED INCANDESCENCE

J. Zhang*, T.C. Williams, C.R. Shaddix, R.W. Schefer
Combustion Research Facility, Sandia National Laboratories, Livermore, CA 94550 USA
jzhang@sandia.gov

Introduction

Turbulent sooting flames are important in several practical applications, most notably diesel engine and aviation gas turbine combustion, where the soot influences heat transfer processes as well as fine particulate emissions. In addition to the challenges involved in "normal" turbulent combustion with non-sooty flames, soot formation and oxidation involve complex chemical reactions and physical processes operating over relatively long timescales. In addition, thermal radiation from soot modifies the local flame temperature, with coupled effects on the gas-phase chemistry. There have been several past modeling efforts in which simplified gas chemistry and soot dynamics were applied to simulations of turbulent sooting flames [1-3]. Unfortunately, the lack of reliable experimental data has precluded a complete evaluation of these models.

The aim of the work presented here is to produce high-quality experimental data in turbulent nonpremixed sooty jet flames with well-controlled boundary conditions, which can be used for further development and validation of coupled models of gas-phase chemistry and soot formation and oxidation. As a first step, we have applied 2D laser-induced incandescence (LII), which characterizes the soot concentration, and simultaneous planar UV laser-induced fluorescence (PLIF) detection of OH radicals and/or polycyclic aromatic hydrocarbons (PAH). This PLIF-LII approach sheds light on flame-soot interactions.

Experimental

The experimental configuration is shown in Fig. 1. For OH and/or PAH LIF imaging, a 2-mJ/pulse UV laser is used, which is produced from a YAG-pumped dye laser and a subsequent frequency doubling crystal. For OH excitation, the laser wavelength is tuned to 283.55 nm, corresponding to the relatively temperature-insensitive $Q_1(8)$ transition of the (0-1) band in the (A-X) electronic system. For LII imaging, the fundamental output at 1064 nm from a second YAG laser is used. The IR laser sheet has a fluence of 0.5 J/cm^2. The laser sheets pass through the jet axis and the resultant signals are collected by two opposing intensified CCD cameras using full frame 512×512 CCD arrays. The IR and UV laser pulses are separated by 1.6 μs to avoid mutual interferences.

The LII images are converted to soot volume fraction by calibrating against laser extinction measurements that are collected together with LII images in a laminar nonpremixed ethylene jet flame established on the same burner that is used for the turbulent flame studies. A dimensionless extinction coefficient of 9.3 is used for interpreting the extinction measurements [4].

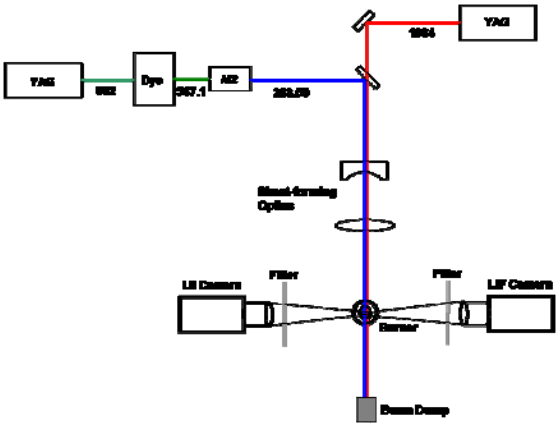

Fig. 1: Experimental setup of simultaneous LII and PLIF imaging. The wavelengths of the different laser beams are indicated in nm.

The burner is a half-size version of the well-known Sydney piloted turbulent nonpremixed jet burner. The central nozzle has an inner diameter of 3.8 mm, and is surrounded by a row of holes for supporting pilot flamelets. A turbulent ethylene jet flame with Re = 10,000 was investigated in this study, with ethylene exiting the central nozzle at a mean velocity of 23.2 m/s and the premixed pilot flame burning a stoichiometric mixture of ethylene and air. This flame has a visible length of 680 mm. A vertical wind tunnel provides co-flowing air at 0.6 m/s to minimize room-air disturbances and provide well-established boundary conditions for flame modeling. The burner is supported on a platform with XYZ translation.

Results and Discussion

Fig. 2 shows the mean soot volume fraction as a function of height above the burner nozzle and Fig. 3 shows three instantaneous realizations of the flame sheet and soot layer structures at a midflame location. The mean soot volume fraction reaches a peak near the top of the flame of just over 1 ppm. As one interrogates the planar images moving from the burner tip upwards, soot-containing regions first appear as localized streaks and pockets, in an annular region close to the OH layer and the stoichiometric flame surface. Approaching the flame tip, the sooty regions are characterized as stacked and occasionally merged sheets that partially overlap the OH zone, indicating regions of active soot oxidation. In contrast, PAH is formed near the jet nozzle and well before any sooty region.

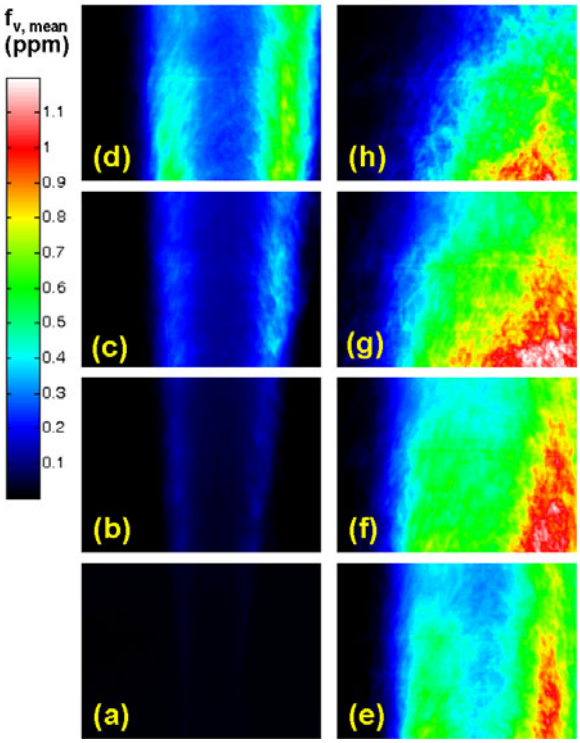

Fig. 2: Time-averaged soot volume fraction (f_v) measured by 2D LII. The vertical extents of these images (in x/d) as measured from the jet exit are as follows: (a) 14.3 – 25.9, (b) 27.6 – 39.2, (c) 40.9 – 52.5, (d) 54.1 – 65.7, (e) 67.4 – 79.0, (f) 80.7 – 92.3, (g) 107.2 – 118.8, (h) 133.7 – 145.3.

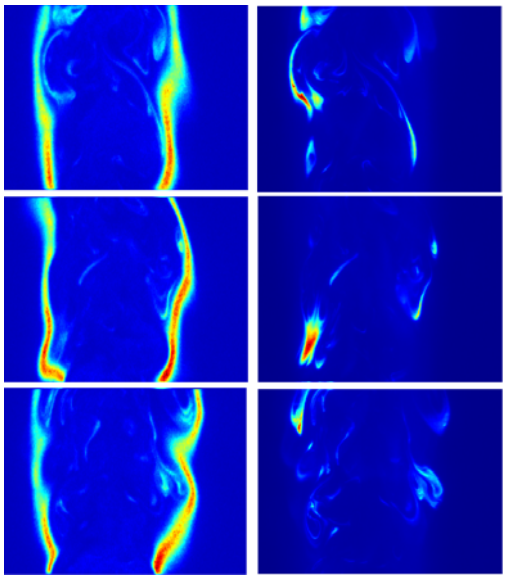

Fig. 3: False-color images of simultaneous OH PLIF (left) and LII (right). The vertical extent of each image is x/d = 40.9 to 52.5. Soot is also evident in the PLIF images due to LII excitation by the UV laser.

References

1. K.M. Leung, R.P. Lindstedt, W.P. Jones, *Combustion and Flame* 87 (1991) 289-305.
2. R.P. Lindstedt, S.A. Louloudi, *Proceedings of the Combustion Institute* 30 (2005) 775-783.
3. D.O. Lignell, J.H. Chen, P.J. Smith, T. Lu, C.K. Law, *Combustion and Flame* 151 (2007) 2-28.
4. T.C. Williams, C.R. Shaddix, K.A. Jensen, J.M. Suo-Anttila, *Int. J. Heat Mass Trans.* 50 (2007) 1616-1630.

Notes